Design and control optimization of an open-type radiant ceiling panel system for thermal comfort and energy saving
(オープンタイプ凹型天井放射パネルシステムの設計と制御の最適化に関する研究)

Supervisor　Prof. Katsunori Nagano

2024

Division of Human Environmental System
Graduate School of Engineering
Hokkaido University

Minzhi Ye

Abstract

Buildings are responsible for a significant portion of global energy consumption, accounting for approximately 34% of the total energy use. There is a pressing need to reduce energy consumption in the building sector. The radiant ceiling panel (RCP) system is an energy-efficient alternative to conventional heating and cooling systems. The open-type RCP system is defined as the radiant panels suspended from the ceiling with an open area above the panels. This system enables the use of higher inlet water temperatures in summer and lower inlet water temperatures in winter to prevent surface condensation and ensure the efficient operation of the integrated energy system. Nevertheless, the open-type RCP system still faces practical challenges such as adverse effect from the solar radiation through windows, long response time, and lack of knowledge regarding efficient operation settings. A novel open-type RCP with curved and segmented structure was proposed to enhance the convective heat transfer, aiming to improve the system efficiency. The main targets of this thesis are to (1) verify the thermal performance of this novel RCP system under different operating conditions, (2) optimize the design of this novel RCP system to improve the cooling capacity and reduce the effect from building envelopes, and (3) optimize the operation of this novel RCP system in terms of both thermal comfort and energy saving.

Chapter 1 is an introduction that presents the research background, describes the motivation and target of this study, and presents the thesis structure.

Chapter 2 explains the radiant ceiling panel system, along with an overview of the research hotspots in this field. The optimization of the RCP system is reviewed, covering aspects of panel structure and arrangement, integrated system design, and control strategies. The introduction of the novel open-type RCP system and the optimization methods applied in this thesis is also presented.

In Chapter 3, a series of laboratory experiments under different operating conditions were carried out to investigate the cooling performance of the novel RCP system. The results indicate that the curved and segmented structure enhances both radiation and convection, especially the convective heat transfer coefficient obtained with this panel was larger than other panel types. Subsequently, a field study was conducted in an office building to examine this novel RCP system throughout a year in practice. The experimental measurement illustrates that the application of the novel RCP system can achieve a comfortable indoor thermal environment. More than 70% of the staff selected the neutral level in the thermal sensation votes (TSV). In addition, the energy performance of the integrated RCP and groundwater heat pump (GWHP) system were investigated, and the intermittent and continuous operation methods were compared during winter. Compared with intermittent operation, the continuous operation could improve both the system performance and indoor thermal comfort.

In Chapter 4, A three-dimensional CFD simulation model was developed to simulate the thermal process of the novel RCP system used in an enclosed space and validated with the measurements provided in laboratory experiments. Firstly, the design of the novel open-type RCP was optimized to maximize the cooling capacity. Panel structure was determined based on six design parameters. The sensitivity analysis was conducted based on the simulations and concluded that void distance plays the most crucial role in influencing cooling performance. Secondly, an integrated the novel open-type RCP with a wall-attached ventilation (WAV) system was proposed to prevent the warm air stream that floats from the window. The result indicated that applying the ventilation system with the ceiling inlet and the ceiling outlet is more effective than installing the ceiling inlet and the floor outlet. After that, the surface response and sensitivity analysis of the operating condition are carried out to optimize the integrated system.

In Chapter 5, a simplified thermal resistance and capacity (RC) network model was developed for the open-type RCP

system. The model was validated using measurements from the field study. The results demonstrate that the model accurately predicts indoor thermal conditions, and parameter identification by the Least-Square Method (LSM) is effective for this system. Following the optimization based on the RC-network model, the system operation was improved with the objective of achieving the desired room temperature while minimizing energy consumption. The optimization addressed issues such as the temperature not reaching the target in the morning due to long response time, and it eliminated problems like overheating and overcooling. In addition, the life cycle cost was calculated to show the benefits of optimization.

In Chapter 6, the research concludes with a summary of key findings, and potential future research directions are outlined.

In summary, this thesis demonstrated that the novel RCP system with curved and segmented structure can enhance heat transfer efficient. The novel RCP are optimized to achieve better indoor thermal condition, energy savings and cost reduction using advanced methodologies. This thesis contributes to the widespread adoption of the radiant ceiling panel system. The results of this thesis also have significant practical implications for reducing building energy consumption while maintaining the indoor thermal comfort and moving toward a zero-emission society in the future.

Contents

Chapter 1

Introduction

1.1 Background

1.1.1 Greenhouse gas emission reduction target

Energy is a crucial foundational element for the survival and progress of humanity. Greenhouse gases (GHG), such as carbon dioxide, methane, and nitrous oxide, are emitted into the atmosphere as a result of energy utilization and human activities, including the burning of fossil fuels (coal, natural gas, and oil), treatment of waste, and agricultural practices. Recently, the energy consumption is increasing significantly with the rapid development of the industrialization and improved of living [1-3]. As shown in Fig. 1-1 [4], greenhouse gas emissions have experienced an explosive trend in the past century.

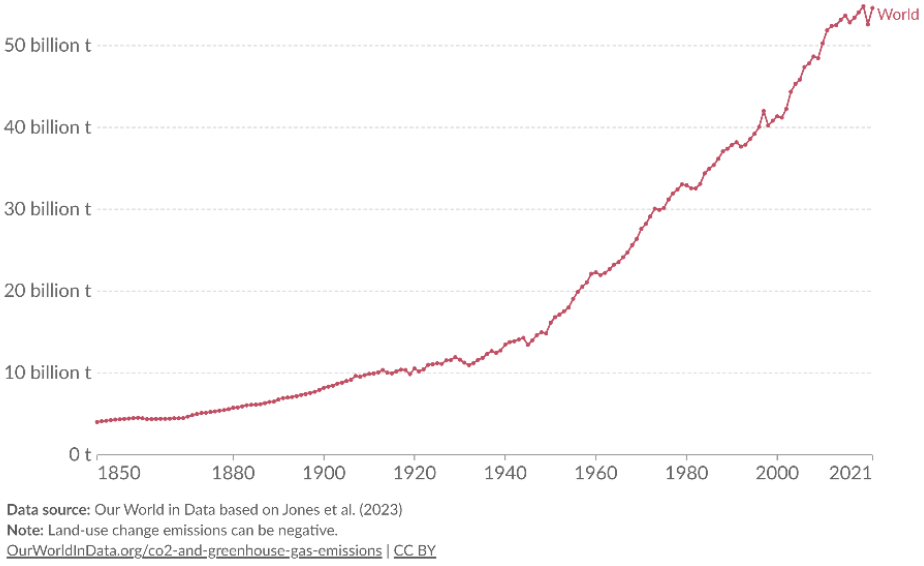

Fig. 1-1 Greenhouse gas emissions [4]

The excessive release of greenhouse gas will lead to various environmental issues including global warming, extreme weather events, sea level rise and biodiversity loss. While, the use of fossil fuels will also cause serious environmental issues, like air and water pollutions, which can cause respiratory problem and pose threats to human health. To prevent the reverse consequences and achieve sustainable development, it is imperative to reduce energy consumption and greenhouse gas emissions. In the meanwhile, clean energy derived from renewable resources like sunlight, wind, water, and geothermal heat is also being noticed for its environmental benefits. There is a need to increase the proportion of non-fossil energy in the energy mix and promote the clean and efficient use of fossil energy [5-6].

It is widely accepted that a zero-emission society should be achieved worldwide in the second half of the 21st century [7]. In December 2015, the Paris Agreement [8] was adopted by 196 Parties to establish a global goal on climate change to ensure sustainable development. The greenhouse gas emission must be peak before 2025 at the latest and reduced by 45% from 2019 levels by 2030. There is also an expectation to achieve net zero emissions by 2050. The Asia-Pacific Economic Cooperation (APEC) [9], consisting of 21 country members, aims to reduce energy intensity by 45% from 2005 levels by 2035 and double the share of renewable energy in the energy mix between 2010 and 2030. Table 1-1 [10] summarizes the 2030 and 2050 targets for GHG emissions published by

some major economies.

Table 1-1 2030 and 2050 targets for GHG emissions

Country/region	2030 Emission reduction target	2050 Net zero target
Japan	-46% from 2013	Expressed
Korea	-24.4% from 2017	Expressed
China	(1) Strive to reach the peak of CO_2 emissions by 2030. (2) Lower CO_2 emissions per unit of GDP by over 65% from 2005.	Net zero CO_2 by 2060
Canada	-40% to -45% from 2005	Expressed
EU, France, Germany, Italy	At least -55% from 1990	Expressed
UK	At least -68% from 1990	Expressed
USA	-50% to -52% from 2005	Expressed

1.1.2 Zero energy building (ZEB)

Currently, buildings are a major primary energy consumer, costing approximately 34% of the total energy consumption and 37% of energy-related greenhouse gas emissions worldwide [11], as shown in Fig. 1-2 and Fig. 1-3. Thus, promoting the concept of zero energy building (ZEB) was considered the most efficient way to respond to the goal in the building sector. Zero energy building (ZEB) or net zero energy building (nZEB) [12,13], and some derived concepts, such as zero energy emission building, zero energy cost building, and zero carbon building have been proposed. These aim to reduce more overall release of greenhouse gas emissions into the atmosphere than similar non-zero energy buildings [14]. The defining scope and assessment index of ZEB (nZEB) is still open to discussion, considering different goals, which include equal energy generation, usage, energy costs equal to zero, or net zero greenhouse gas emissions [15]. Moreover, depending on different climatic and geographic characteristics as well as different building functions (residential or commercial), each country has its classification, initiatives, and national ZEB policies [16]. Fig. 1-4 [17] provides an overview of the ZEB certification system in each country, including certification organizations, start year, and number of recent projects.

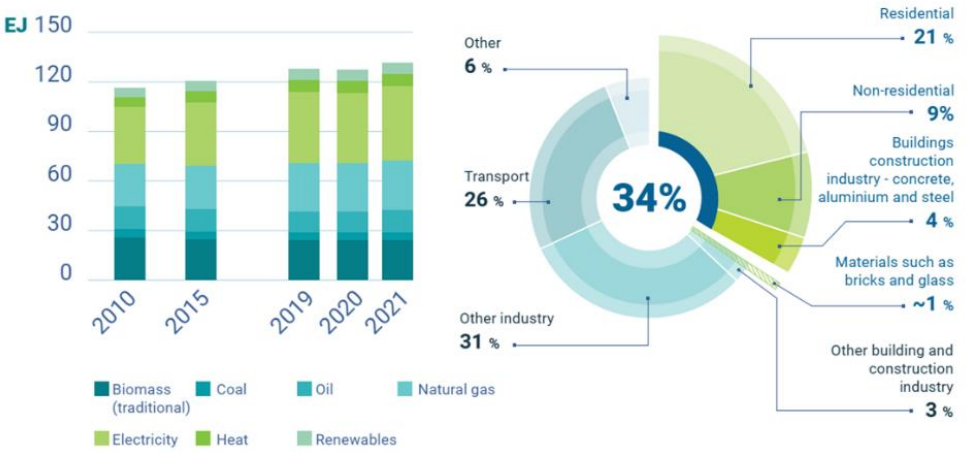

Fig. 1- 2 Share of buildings in total final energy consumption in 2021 [11]

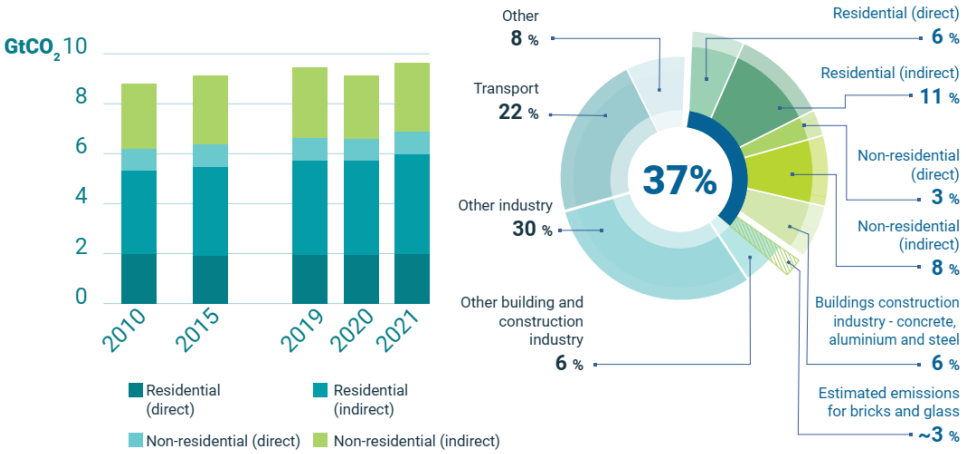

Fig. 1-3 Share of buildings in global energy and process emissions in 2021 [11]

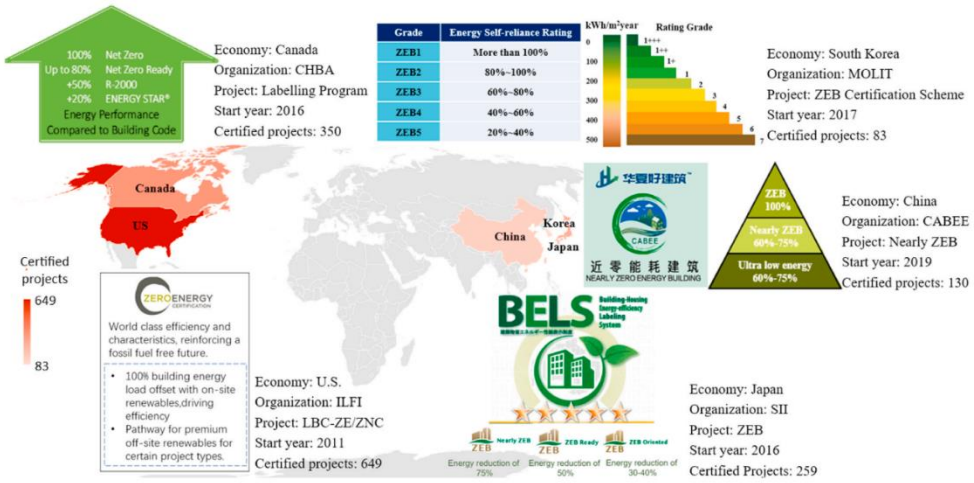

Fig. 1-4 ZEB certifications in different economies [17]

In Japan, the Society of Heating, Air-Conditioning, and Sanitary Engineers (SHASE, 空気調和衛生工学会) released the definition of ZEB and the evaluation method for ZEBs in 2015. ZEBs are defined as buildings that can reduce the annual net primary energy consumption to zero through renewable energy, highly efficient systems, and control of the building load through advanced architectural designs (Fig. 1-5). The primary energy consumption of the reference building should be calculated based on the standard given for each facility, region, and room function, according to the Japanese law on energy-saving published by the Ministry of Land, Infrastructure, and Transport (MLIT, 国土交通省) [18]. The Ministry of Economy, Trade, and Industry (METI, 経済産業省) issued a national definition of ZEB in four stages to promote its widespread use: ZEB (100% decrease in primary energy consumption), nearly ZEB (75% decrease), ZEB ready (50% decrease), and ZEB oriented (40% or 30% decrease) [17,19].

The basic requirement of a ZEB is a high-performance building envelope that can maintain indoor thermal comfort, irrespective of extreme conditions in the external environment [20]. On the other hand, the heating, ventilation, and air conditioning (HVAC) systems account for approximately half of the total energy consumed by buildings. Therefore, several advanced technologies for HVAC systems have been developed to achieve the use of ZEBs and the future goal of a zero-emission society [21]. Renewable technologies exhibit strong regional characteristics [22]. For example, the air heat recovery systems, the radiant heating and cooling (RHC) systems, and the ceiling fans are popular HVAC related technologies worldwide. The displacement ventilation and the independent temperature and humidity control systems have been applied primarily in China and the US, while the evaporative cooling and the chilled beams are preferred in the EU.

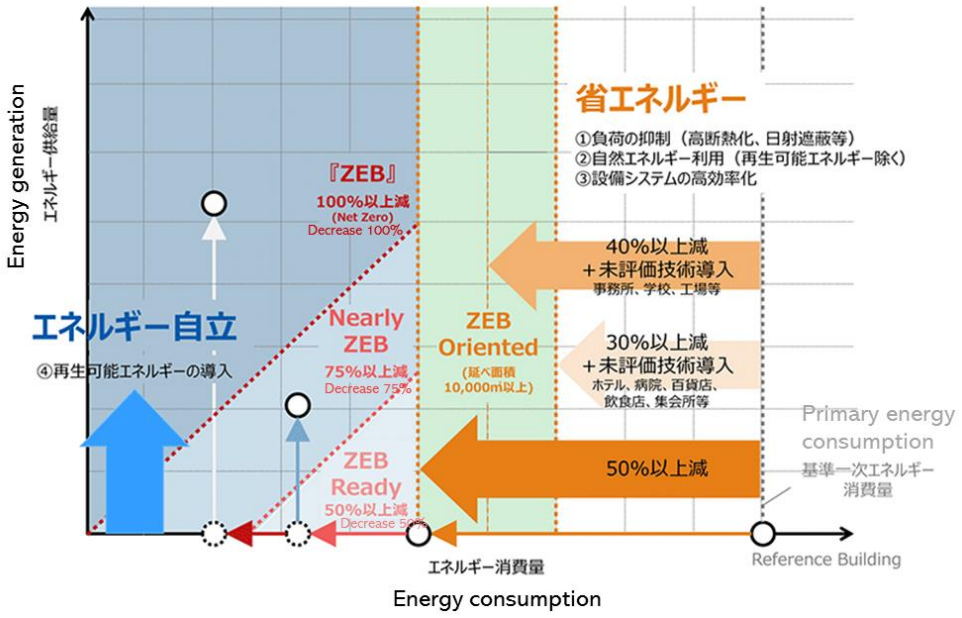

Fig. 1-5 Definition of ZEB in Japan

1.1.3 Radiant heating and cooling (RHC) system

As mentioned in *Section 1.1.2*, the radiant heating and cooling (RHC) systems are typically used to achieve ZEB and are accepted worldwide. The modern radiant system has been developed during the few last decades since the 1900s, started by the British professor A.H.barker [23]. This system mainly exchange heat through radiation within

a conditioned space [24]. In this system, thermal mediums (such as water) are heated or cooled and circulated through a network of pipes embedded in building structure (such as floors, walls, or ceilings) or radiant panels. The surfaces are heated or cooled accordingly as the medium flows through the envelope or panels. Then the heat is exchanged with objects and other surfaces within a space based on their surface temperature difference.

Compared to conventional methods that rely on the distribution of heated or chilled air, the radiant system may provide equal or better comfort and has higher energy efficiency concluded by the experimental and simulation studies [25–27]. First, the radiant systems can create a more consistent temperature profile and eliminate noise during operation. Second, the characteristic of low-temperature heating and high-temperature cooling has the potential to reduce energy consumption. Moreover, the utilization of water as the thermal media in RHC systems provides the advantage of direct utilization or integration with renewable energy technologies, such as geothermal systems. Hence nowadays the RHC system has gained popularity in diverse building types [28] and space [29], even including the airports [30], as an effective strategy for low-energy consumption [31].

The RHC system can be classified into different types based on four main factors: (1) the position (ceiling, floor, or building structure); (2) the operation mode (heating, cooling, or both); (3) water pipe position and (4) whether insulation is included.

Many comprehensive literature reviews on various aspects of the RHC system have been published to describe this system. Rhee made a significant overview of the RHC system from the published papers through 50 years 2 and strengthened the important research issues [24], covering almost all the research methods, topics, and trends of this system. The determination of the heat transfer coefficient [32] and cooling load calculation methods [33] of the radiant system were suggested for design and simulation usage. The practical projects for various purposes 6 and diverse advanced RHC systems [34–36] were elaborated regarding the system feasibility, properties, heating and cooling performance, and existing application problems. The hot points in the research on the RHC system, such as the actual thermal comfort sensation of occupants [37], integrated ventilation system configuration [38,39], condensation prevention for radiant cooling [40], and incorporated phase change materials [41] also have been discussed. In this sense, the review articles highlight the current state, key focus areas, and limitations of the RHC systems and subsequently figure out future research directions.

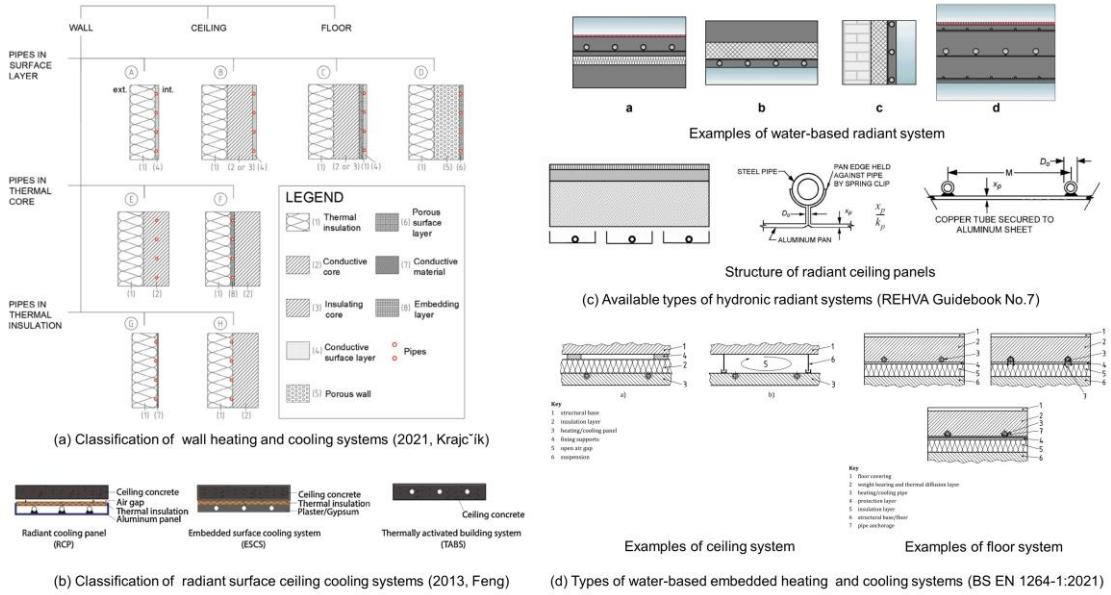

Fig. 1-6 Classification of RHC system in literatures

However, the adoption of the RHC system still has been limited, and this can be attributed to several factors:

- ***High initial cost***

The installation and implementation of RHC systems often involve higher upfront costs compared to conventional heating and cooling systems.

- ***Risk of dew condensation in summer and requirement for humidity control***

In summer, humidity control is necessary to prevent the risk of dew condensation when the surface temperature of the RHC system is below the dew point temperature. In addition, the RHC system only handles the sensible heat load. The air handling unit or ventilation system is required to deal with the latent heat load and provide outdoor air to maintain indoor air quality.

- ***Lack of capability to handle extreme heating loads and adverse effect on building envelopes***

Currently, the cooling and heating capacity of the RHC system is limited due to considerations of the condensation risk and the ability of water to transport heat. The limitation makes it unsuitable for applications with high thermal loads. Consequently, the system design and planning become necessary when apply the RHC system in space with high heat load densities, or even in the areas around windows with high solar radiation loads.

- ***Long thermal response time***

The RHC system typically exhibits a longer response time for heating and cooling compared to the conventional systems mainly based on convective heat transfer [42]. Recently, the phase change materials (PCM) is used to integrated with some RHC systems to offset and reduce the peak load. It is also crucial to consider the thermal response in such cases.

- ***Lack of knowledge about system design and operation control***

The integration of the RHC system with ventilation and heat sources requires a sophisticated design and control method that considers both indoor thermal comfort and energy efficiency. The new improvement strategies for the RHC system also pose a challenge in adapting suitable operational methods.

1.1.4 Design and control optimization of building energy system

As states in Section 1.1.2, the buildings are responsible for approximately 40% of total energy use. Thus, it is highly required to reduce the building energy consumption and achieve green cities. The building energy system (BES) are defined as the system which are responsible for consumption of energy in buildings [43]. It usually consists of many sub-systems and components, making it difficult to coordinate their operation and ensure that all the components are running efficiently. Also, the desire for energy reduction and high thermal comfort often conflicts. Therefore, the design and control optimization of building energy systems play a significant role to obtain the optimal performance. The previous studies show that the optimization can lead to approximately 20%-50% energy savings, which can be generalized to achieve ZEB [44]. Table 1-2 summarized the benefits for optimization of BES.

Table 1-2 Summary of the benefits for optimization of building energy systems

Building types	Optimized BES	Benefits
Office building [45]	Chilled water setpoints and supply inlet temperature of RHC system	Annual energy saving of 54%
Mixed-mode office building [46]	Dynamic mixed mode window controls and ventilation supply air fans	Annual cooling energy savings of 40%
University building [47]	Nighttime precooling of multiple HVAC system supply components	Annual energy saving of 29%

The optimization of the BES includes three steps in design optimization and two steps in control optimization [48], as shown in Fig. 1-7. It aims to aims to make BES operate with a high efficiency under different conditions. The optimization contains (1) Optimize the capacity of BES to avoid being both oversized and undersized system. (2) Optimize the component selection and system configurations such as chilled water network systems (3) Optimize the selection of advanced technologies with higher efficiency. (4) Optimize the design of BES considering the uncertainties, possible deviations, failures, or unpredicted changes. (5) Optimize the control strategies of BES, particularly under partial cooling or heating load.

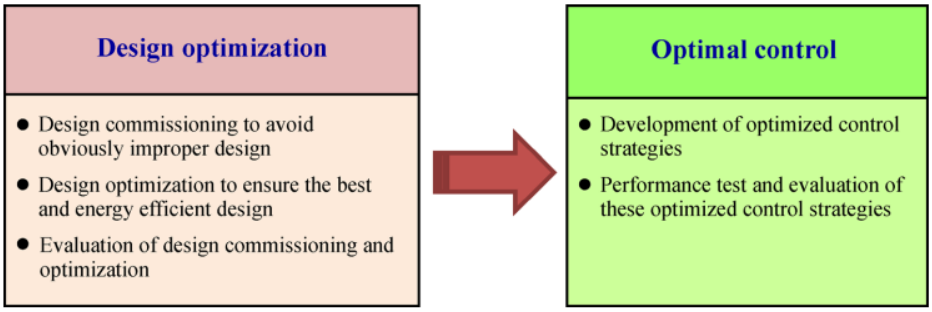

Fig. 1-7 Steps for design and control optimization [48]

As illustrated in Fig. 1-8, the HVAC systems are the main sources of energy consumption, occupies about 40% of total energy use in building sector. Therefore, works on the optimization of heating, ventilation, and air-conditioning (HVAC) systems have been done the most extensively [49,50].

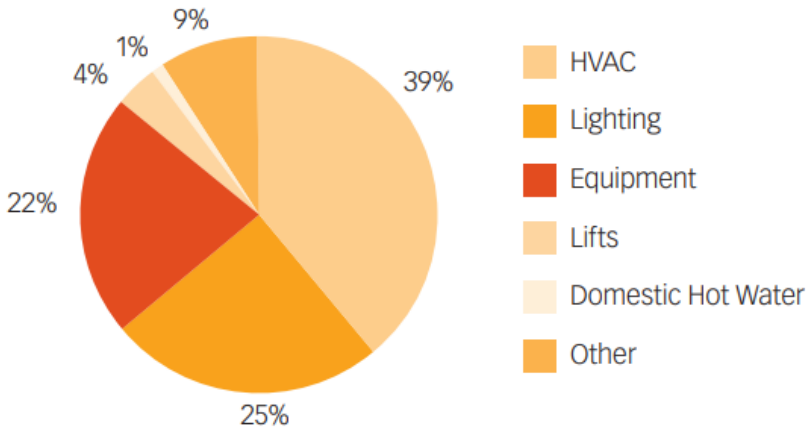

Fig. 1-8 Typical energy consumption breakdown in an office building [51]

The optimization of HVAC contains:

- ***HVAC operation parameters optimization***

Determining suitable operational parameter settings is crucial before system operation, which is closely related to the specifications of the HVAC system. In the conventional HVAC system (Fig. 1-9 (a)), the optimized operational parameters can be outdoor air flowrate, supply chilled water temperature, supply cooling water temperature setpoint, and static pressure in the duct system. While for the RHC system (Fig. 1-9(b)), the optimized operational parameters can be supply water temperature, supply water flowrate, and supply air flowrate.

- ***HVAC controller optimization***

The control optimization of the HVAC system is effective to prevent overheating and overcooling and avoid unnecessary energy waste. With the development of the artificial intelligence (AI) technologies, modern intelligent controllers are becoming commonplace in the building industry, including model predicted control (MPC), adaptive fuzzy controllers, and artificial neural network (ANN). The implementation of better controllers usually requires accurate modeling approach of the system.

- ***HVAC building design optimization***

The HVAC system energy consumption in buildings can also be reduced indirectly based on the design optimization of the building envelopes, such as the wall thickness, wall materials, window width, window materials and types of window blinds used.

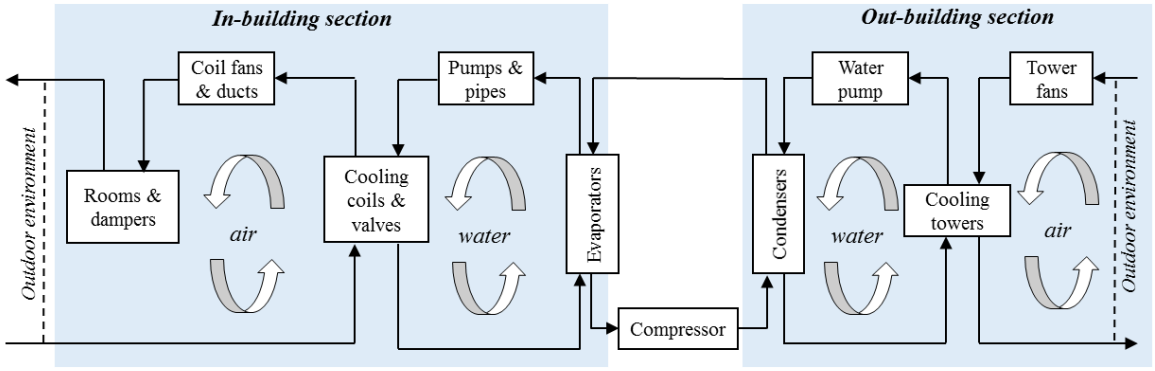

(a) A typical conventional HVAC system

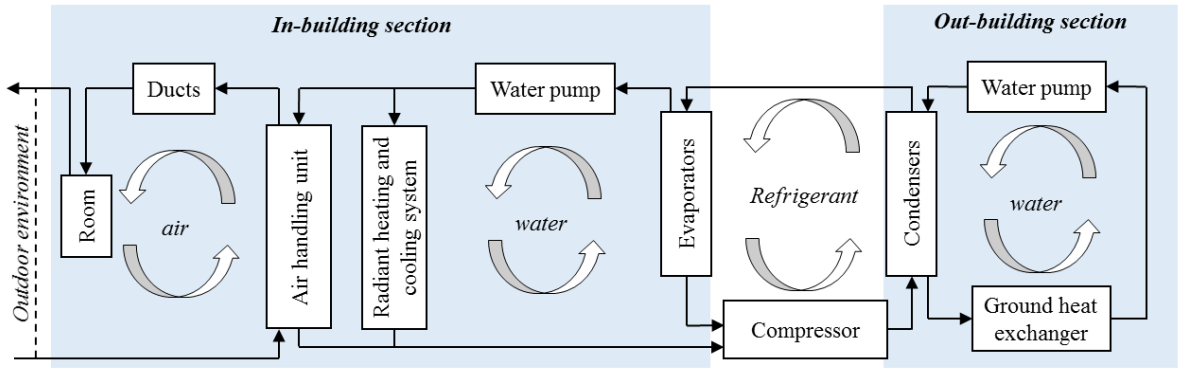

(b) Integrated RHC and ventilation system

Fig. 1-9 Schematic of a typical conventional HVAC system and RHC system

1.2 Research objectives and originality

A novel open-type radiant ceiling panel (RCP) with curved and segmented structure was proposed to enhance convective heat transfer, aiming to improve the system efficiency. It is essential to practically investigate the thermal performance of the proposed system and demonstrate its priority in terms of the energy efficiency and thermal comfort. Design and control optimization of this system are necessary to expand its application and guide its usage.

- ***Performance analysis of the novel open-type radiant ceiling panel system***

The research objectives:

1. Analyze the thermal performance of the novel open-type radiant ceiling panel system.
2. Figure out the thermal comfort when applying this system in enclosed space.
3. Calculate the annual energy consumption of the integrated RCP and groundwater heat pump (GWHP) system.

The originalities:

1. The system performance of the open-type RCP system is examined under different operating conditions and compared with other panel types.
2. The indoor thermal comfort and energy efficiency of the system are examined in a real building simultaneously.
3. The continuous and intermittent operation methods are compared in winter.

- ***Design optimization of the panel shape and integrated system with wall-attached ventilation through CFD simulation and sensitivity analysis***

The research objectives:

1. Develop a CFD simulation model for the open-type RCP system.
2. Optimize the panel shape and panel arrangement of the open-type RCP and find out the optimal panel shape.
3. Optimize the integrated of the open-type RCP and wall-attached ventilation (WAV) system.

The originalities:

1. The CFD simulation and sensitivity analysis are applied together for the design optimization of the RCP system.
2. The effect of panel design parameters on the cooling capacity is investigated and different shapes of panels are compared after normalization.
3. The integrated RCP and WAV system is investigated to reduce the effect of window. The operation conditions and system arrangement are optimized considering both air temperature uniformity and system efficiency.

- ***Control optimization of the system operation based on a grey-box model***

The research objectives:

1. Develop a simplified RC-network model for the open-type RCP system.
2. Optimize the system operation of the RCP system based on multi-objective optimization method.

The originalities:

1. Carry out the optimization on a new simplified grey-box model with high accuracy.
2. Discuss the building envelope thermal insulation and panel coverage area in terms of indoor temperature, energy consumption and cost.

1.3 Thesis structure

The structure of this thesis is demonstrated in Fig. 1-. The arrow shows the flow and dependencies of this research. The thesis is a total of 6 chapters, and followings are brief description on each chapter.

In **Chapter 1**, the introduction presents the research background and presented the research purpose.

In **Chapter 2**, brief overviews of radiant heating and cooling system and the radiant ceiling panel (RCP) system are presented. The author highlights the research hotspots and development trends of the RCP system, along with a review of previous studies focusing on the optimization of the panel structure, panel arrangement, integrated systems with ventilation and energy systems, as well as system control strategies. Finally, this chapter introduces the basic theory of the proposed novel open-type RCP system and the methodologies used in this thesis.

Chapter 3-Chapter 5 are the main content of this thesis. In **Chapter 3**, the thermal performance of the novel open-type RCP with curved and segmented structure are investigated based on a chamber test in laboratory and a field study in an office building. The heat capacity and heat transfer coefficient are calculated under different operation conditions in the chamber test and subsequently compared with those of other panel types. The practical indoor thermal condition and energy consumption by using the RCP system are investigated in field study. Several operational issues of the RCP system are appeared in the experiments.

In **Chapter 4**, the panel shape and the integrated RCP and wall-attached ventilation (WAV) system are optimized using CFD simulation and sensitivity analysis. A three-dimensional CFD model is developed based on the experimental results of chamber test introduced in Chapter 3. The panel shape is optimized to maximize the cooling capacity and the effect of six panel design parameters are examined through one-at-a-time (OAT) approach. The WAV system is integrated to eliminate the influence of the warm air stream from the window. The surface response and sensitivity analysis are carried out to optimize the operation of the integrated system.

In **Chapter 5**, a simplified dynamic thermal resistance and capacity (RC) network model is developed for the open-type RCP system. The model is validated with the field measurements results introduced in Chapter 3. The system operation is optimized based on the model through multi-objective optimization method for the energy efficient and thermal comfort. Life cycle cost (LCC) is carried out to analysis the economic benefit of the optimization. Then, the building envelope thermal insulation strategies and panel coverage area setting are discussed, taking into account the reduction of the investment cost.

Finally, **Chapter 6** summarizes and discusses the brief findings obtained in this research, and finally describes some future subjects.

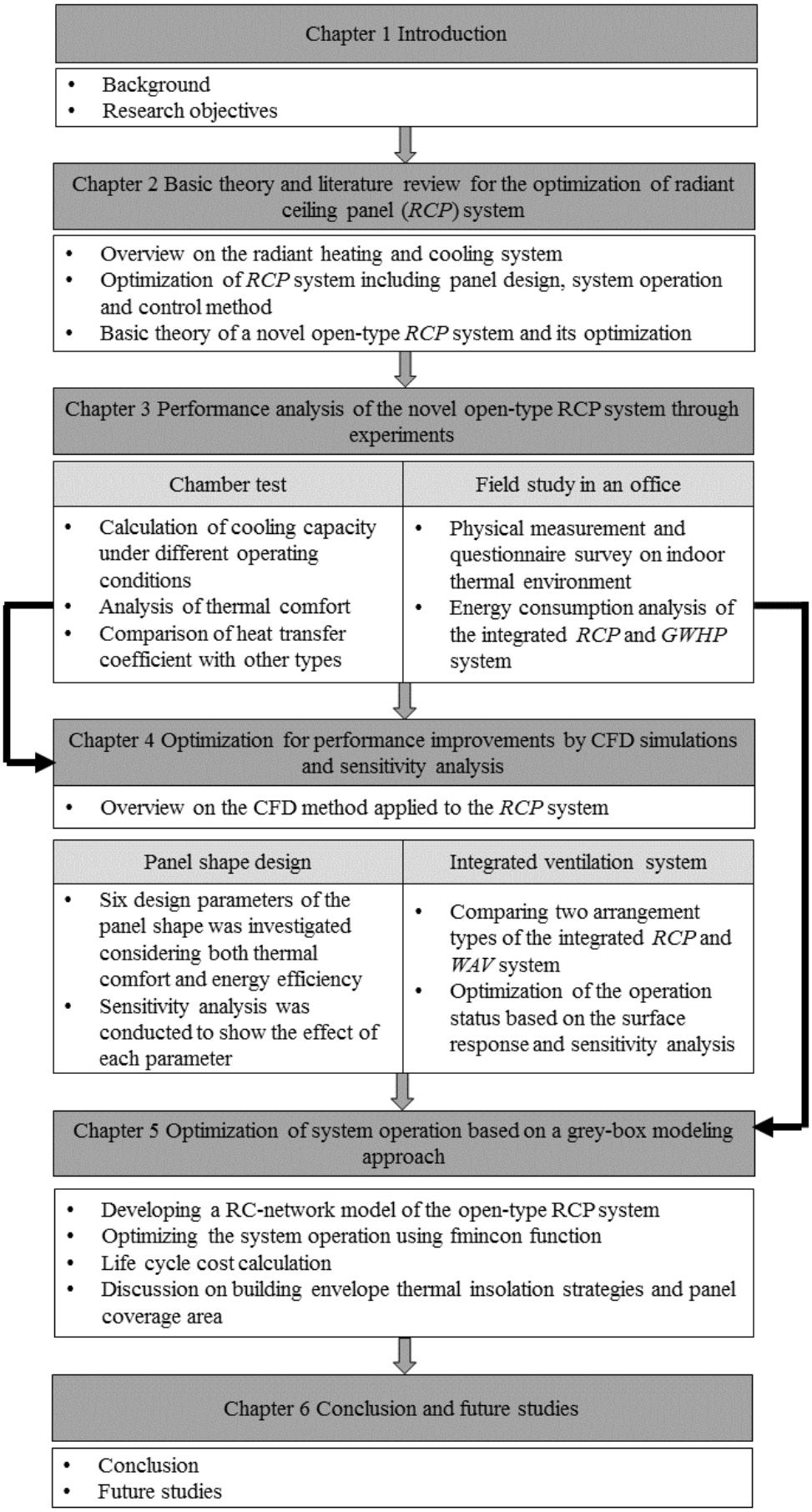

Fig. 1-10 Structure sketch of the thesis

Reference

[1] S.R. Behera, D.P. Dash, The effect of urbanization, energy consumption, and foreign direct investment on the carbon dioxide emission in the SSEA (South and Southeast Asian) region, Renew. Sustain. Energy Rev. 70 (2017) 96–106. https://doi.org/10.1016/j.rser.2016.11.201.

[2] B. Muhammad, Energy consumption, CO2 emissions and economic growth in developed, emerging and Middle East and North Africa countries, Energy. 179 (2019) 232–245. https://doi.org/10.1016/j.energy.2019.03.126.

[3] N. Antonakakis, I. Chatziantoniou, G. Filis, Energy consumption, CO2 emissions, and economic growth: An ethical dilemma, Renew. Sustain. Energy Rev. 68 (2017) 808–824. https://doi.org/10.1016/j.rser.2016.09.105.

[4] Hannah Ritchie, Pablo Rosado and Max Roser, Greenhouse gas emissions (2020) https://ourworldindata.org/greenhouse-gas-emissions.

[5] E. Dogan, F. Seker, The influence of real output, renewable and non-renewable energy, trade and financial development on carbon emissions in the top renewable energy countries, Renew. Sustain. Energy Rev. 60 (2016) 1074–1085. https://doi.org/10.1016/j.rser.2016.02.006.

[6] S. Guo, Q. Liu, J. Sun, H. Jin, A review on the utilization of hybrid renewable energy, Renew. Sustain. Energy Rev. 91 (2018) 1121–1147. https://doi.org/10.1016/j.rser.2018.04.105.

[7] A. Hesaraki, N. Huda, A comparative review on the application of radiant low-temperature heating and high-temperature cooling for energy, thermal comfort, indoor air quality, design and control, Sustainable Energy Technologies and Assessments. 49 (2022). https://doi.org/10.1016/j.seta.2021.101661.

[8] Adoption of the Paris agreement (Decision 1/CP.17), Available at, https://unfccc.int/resource/docs/2015/cop21/eng/l09r01.pdf

[9] Asia-Pacific Economic Cooperation (APEC), APEC's commitment to improving energy efficiency (Last page update: September 2021), Available at, https://www.apec.org/about-us/about-apec/fact-sheets/energy

[10] 外務省, Intended Nationally Determined Contributions (INDC): Greenhouse Gas Emission Reduction Target in FY2030, Available at, https://www.mofa.go.jp/ic/ch/page1we_000104.html

[11] United Nations Environment Programme (2022). 2022 Global Status Report for Buildings and Construction: Towards a Zero-emission, Efficient and Resilient Buildings and Construction Sector. Nairobi. ISBN No: 978-92-807-3984-8.

[12] A.J. Marszal, P. Heiselberg, J.S. Bourrelle, E. Musall, K. Voss, I. Sartori, A. Napolitano, Zero Energy Building - a review of definitions and calculation methodologies, Energy Build. 43 (2011) 971–979, https://doi.org/10.1016/j.enbuild.2010.12.022.

[13] W. Overgen, Zero-net-energy homes: here today, affordable tomorrow, Electr. J. 28 (2015) 3–4, https://doi.org/10.1016/j.tej.2015.05.013.

[14] E. Ohene, A.P.C. Chan, A. Darko, Review of global research advances towards net-zero emissions buildings, Energy Build. 266 (2022), 112142, https://doi.org/10.1016/j.enbuild.2022.112142.

[15] L. Wells, B. Rismanchi, L. Aye, A review of net zero energy buildings with reflections on the Australian context, Energy Build. 158 (2018) 616–628, https://doi.org/10.1016/j.enbuild.2017.10.055.

[16] M. Panagiotidou, R.J. Fuller, Progress in ZEBs-A review of definitions, policies and construction activity, Energy Pol. 62 (2013) 196–206, https://doi.org/10.1016/j.enpol.2013.06.099.

[17] S. Zhang, K. Wang, W. Xu, U. Iyer-Raniga, A. Athienitis, H. Ge, D. woo Cho, W. Feng, M. Okumiya, G. Yoon, E. Mazria, Y. Lyu, Policy recommendations for the zero energy building promotion towards carbon neutral in Asia-Pacific Region, Energy Policy. 159 (2021) 112661. https://doi.org/10.1016/j.enpol.2021.112661.
[18] 国土交通省, 建築物省エネ法について （最終更新日：令和 5 年 9 月 25 日 https://www.mlit.go.jp/jutakukentiku/jutakukentiku_house_tk4_000103.html. (日本語)
[19] G. Yoon, H. Niwa, G. Onishi, Current Situation and Actions for ZEB in Japan, REHVA J., 2018, p. 32. –37, https://researchmap.jp/yoonlab/published_papers/16155309/attachment_file.pdf.
[20] Y. Lin, L. Zhao, W. Yang, X. Hao, C.Q. Li, A review on research and development of passive building in China, J. Build. Eng. 42 (2021), 102509, https://doi.org/10.1016/j.jobe.2021.102509.
[21] X. Cao, X. Dai, J. Liu, Building energy-consumption status worldwide and the state-of-the-art technologies for zero-energy buildings during the past decade, Energy Build. 128 (2016) 198–213, https://doi.org/10.1016/j.enbuild.2016.06.089.
[22] R. Wang, W. Feng, L. Wang, S. Lu, A comprehensive evaluation of zero energy buildings in cold regions: actual performance and key technologies of cases from China, the US, and the European Union, Energy 215 (2021), 118992, https://doi.org/10.1016/j.energy.2020.118992.
[23] R. Bean, B. Olesen, K. Kim, History of Radiant Heating and Cooling, 2010. www.ashrae.org.
[24] K.-N. Rhee, K.W. Kim, A 50 year review of basic and applied research in radiant heating and cooling systems for the built environment, Build Environ. 91 (2015) 166–190. https://doi.org/10.1016/j.buildenv.2015.03.040.
[25] H.E. Feustel, C. Stetiu, Hydronic radiant cooling-preliminary assessment *, 1995.
[26] T. Imanari, T. Omori, K. Bogaki, Thermal comfort and energy consumption of the radiant ceiling panel system. Comparison with the conventional all-air system, 1999.
[27] C. Karmann, S. Schiavon, F. Bauman, Thermal comfort in buildings using radiant vs. all-air systems: A critical literature review, Build Environ. (2017). https://doi.org/10.1016/J.BUILDENV.2016.10.020.
[28] R. Hu, J.L. Niu, A review of the application of radiant cooling & heating systems in Mainland China, Energy Build. 52 (2012) 11–19. https://doi.org/10.1016/j.enbuild.2012.05.030.
[29] W. Liao, Y. Luo, J. Peng, D. Wang, C. Yuan, R. Yin, N. Li, Experimental study on energy consumption and thermal environment of radiant ceiling heating system for different types of rooms, Energy. 244 (2022). https://doi.org/10.1016/j.energy.2021.122555.
[30] K. Zhao, X.H. Liu, Y. Jiang, On-site measured performance of a radiant floor cooling/heating system in Xi'an Xianyang International Airport, Solar Energy. 108 (2014) 274–286. https://doi.org/10.1016/j.solener.2014.07.012.
[31] R. Wang, W. Feng, L. Wang, S. Lu, A comprehensive evaluation of zero energy buildings in cold regions: Actual performance and key technologies of cases from China, the US, and the European Union, Energy. 215 (2021). https://doi.org/10.1016/j.energy.2020.118992.
[32] K.-N. Rhee, B.W. Olesen, K.W. Kim, Ten questions about radiant heating and cooling systems, Build Environ. 112 (2017) 367–381. https://doi.org/10.1016/j.buildenv.2016.11.030.
[33] J. Shinoda, O.B. Kazanci, S. ichi Tanabe, B.W. Olesen, A review of the surface heat transfer coefficients of radiant heating and cooling systems, Build Environ. 159 (2019). https://doi.org/10.1016/j.buildenv.2019.05.034.

[34] J. Feng, S. Schiavon, F. Bauman, Cooling load differences between radiant and air systems, Energy Build. 65 (2013) 310–321. https://doi.org/10.1016/j.enbuild.2013.06.009.

[35] K. Zhao, X.H. Liu, Y. Jiang, Application of radiant floor cooling in large space buildings - A review, Renewable and Sustainable Energy Reviews. 55 (2016) 1083–1096. https://doi.org/10.1016/j.rser.2015.11.028.

[36] M. Krajčík, M. Arıcı, O. Šikula, M. Šimko, Review of water-based wall systems: Heating, cooling, and thermal barriers, Energy Build. 253 (2021). https://doi.org/10.1016/j.enbuild.2021.111476.

[37] K. Dharmasastha, Z. Zhong, J. Niu, H. Liang, A comprehensive review of cover-shield-assisted radiant cooling system, Energy Build. 291 (2023). https://doi.org/10.1016/j.enbuild.2023.113121.

[38] A. Novoselac, J. Srebric, A critical review on the performance and design of combined cooled ceiling and displacement ventilation systems, 2002.

[39] C. Zhang, M. Pomianowski, P.K. Heiselberg, T. Yu, A review of integrated radiant heating/cooling with ventilation systems- Thermal comfort and indoor air quality, Energy Build. 223 (2020). https://doi.org/10.1016/j.enbuild.2020.110094.

[40] D. Xing, N. Li, C. Zhang, P. Heiselberg, A critical review of passive condensation prevention for radiant cooling, Build Environ. 205 (2021). https://doi.org/10.1016/j.buildenv.2021.108230.

[41] M. Moreira, J. Dias-de-Oliveira, C. Amaral, F. Neto, T. Silva, Outline of the incorporation of phase change materials in radiant systems, J Energy Storage. 57 (2023). https://doi.org/10.1016/j.est.2022.106307.

[42] J. Romaní, A. De Gracia, L.F. Cabeza, Simulation and control of thermally activated building systems (TABS), Energy Build. 127 (2016) 22–42. https://doi.org/10.1016/j.enbuild.2016.05.057.

[43] V.S.K.V. Harish, A. Kumar, A review on modeling and simulation of building energy systems, Renew. Sustain. Energy Rev. 56 (2016) 1272–1292. https://doi.org/10.1016/j.rser.2015.12.040.

[44] K.A. Barber, M. Krarti, A review of optimization based tools for design and control of building energy systems, Renew. Sustain. Energy Rev. 160 (2022) 112359. https://doi.org/10.1016/j.rser.2022.112359.

[45] Corbin Charles D, Henze Gregor P, May-Ostendorp Peter. A model predictive control optimization environment for real-time commercial building application. J Build Perform Simulat 2013;6(3):159–74. https://doi.org/10.1080/19401493.2011.648343.

[46] May-Ostendorp Peter, Henze Gregor P, Corbin Charles D, Rajagopalan Balaji, Felsmann Clemens. Model-predictive control of mixed-mode buildings with rule extraction. Build Environ 2011;46(2):428–37. https://doi.org/10.1016/j. buildenv.2010.08.004.

[47] Hilliard Trent, Swan Lukas, Zheng Qin. Experimental implementation of whole building MPC with zone based thermal comfort adjustments. Build Environ 2017; 125:326–38. https://doi.org/10.1016/j.buildenv.2017.09.003.

[48] S. WANG, W. GANG, Design and control optimization of energy systems of smart buildings today and in the near future, Front. Eng. Manag. 4 (2017) 58. https://doi.org/10.15302/j-fem-2017005.

[49] L. Lu, W. Cai, L. Xie, S. Li, Y.C. Soh, HVAC system optimization - In-building section, Energy Build. 37 (2005) 11–22. https://doi.org/10.1016/j.enbuild.2003.12.007.

[50] H. Selamat, M.F. Haniff, Z.M. Sharif, S.M. Attaran, F.M. Sakri, M. Al'Hapis Bin Abdul Razak, Review on HVAC system optimization towards energy saving building operation, Int. Energy J. 20 (2020) 345–357.

[51] Guide to Best Practice Maintenance and Operation of HVAC Systems for Energy Efficiency (January 2012),

Pages 36–37 http://ee.ret.gov.au/energy-efficiency/non-residential-buildings/heating-ventilation-and-air-conditioning-hvac

Chapter 2

Basic theory and literature review for the radiant ceiling panel (RCP) system and its optimization

2.1 Introduction

This chapter briefly summarized the basic theory and methodologies used in the design and control optimization of the open-type radiant ceiling panel (RCP) system. In *Section 2.2*, an introduction to the radiant ceiling panel system is provided, along with an overview of the research hotspots in this field. In *Section 2.3*, a summary of the optimization of the RCP system is presented, covering aspects such as panel structure and arrangement, integrated system design, and control strategies. A novel open-type RCP system with curved and segmented structure used in this study is introduced in *Section 2.4*. The introduction of the optimization methods, including CFD simulation, grey-box modeling, sensitivity analysis and multi-objective optimization is presented in *Section 2.5*.

2.2 Radiant ceiling panel system

2.2.1 Overview on the radiant ceiling panel system

The radiant heating and cooling (RHC) system are generally classified in to embedded surface system, thermally activated building system (TABS), and radiant panel system [1]. The radiant panel system is separate from the building structure, making it easier to install and renovate compared to other types of RHC systems. The radiant ceiling panel (RCP) system is one of the radiant panel systems that is fixed to the ceiling. The system commonly consists of a metal panel, a water pipe directly or indirectly touching the panel, and insulation on the top of the panel surface [2,3]. There are four types of radiant ceiling panel systems shown in Fig. 2-1.

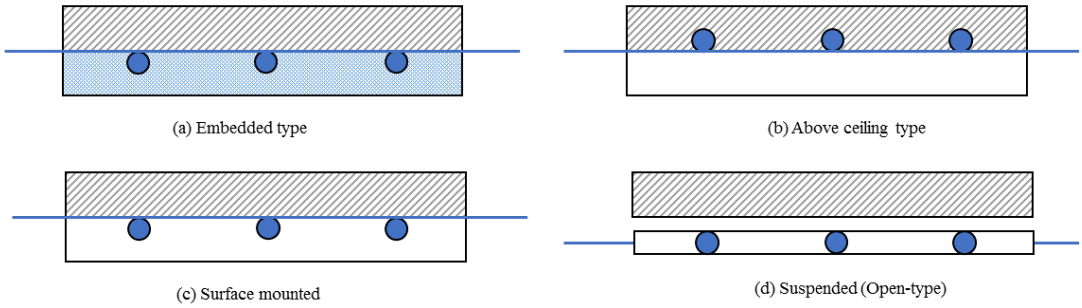

Fig. 2-1 Four types of radiant ceiling panel systems

Installing the radiant panels on the ceiling can be wall space free for other uses besides cooling or heating units, avoid disturbing the human activities and provide a larger functional area. Therefore, the system have been a matter of great concern in recent decades [4]. This system has already been commercialized and produced by many companies, as shown in Fig. 2-2, and applied in various building types, such as high-volume halls (e.g., vehicle repair shops and markets) [5], office buildings [6,7], schools [8], hospitals [9], and residential buildings [10].

When designing radiant ceiling panel systems, the heating and cooling capacity determines the area of the panel as expressed from Eq. (2-1).

$$Q = A\alpha\Delta T = A\alpha|T_{air} - T_s| \qquad (2-1)$$

Where Q is the heating or cooling capacity (W), A is the area of panel (m^2), α is the heat transfer coefficient between panel surface ($W/(m^2 \cdot K)$) and air. T_{air} is indoor air temperature (°C). T_s is surface temperature of panel (°C).

The panel surface temperature is closely related to the supply water temperature. It is suggested to be higher than 16 °C to prevent condensation in summer. The heat transfer coefficient is determined by the specification of the panel, which is related to panel material and panel structure. Shinoda et al. [11] reports a literature review of the heat transfer coefficients for radiant heating and cooling system. As shown in Fig. 2-3, in ceiling cooling, the radiant heat flux has a liner correlation with ΔT, which is around 5.5 W/(m^2·K). The convective heat transfer coefficients, on the other hand, are different for different panels, ranging from 2 to 6 W/(m^2·K). The total heat transfer coefficients are consequently vary from 8 to 14 W/(m^2·K).

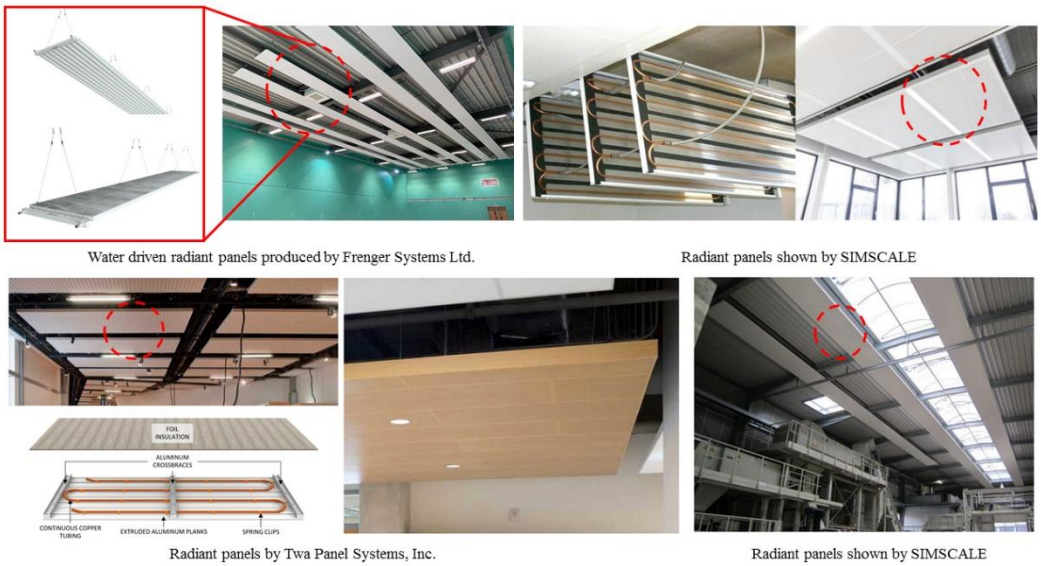

Fig. 2-2 Commercialized radiant ceiling panels

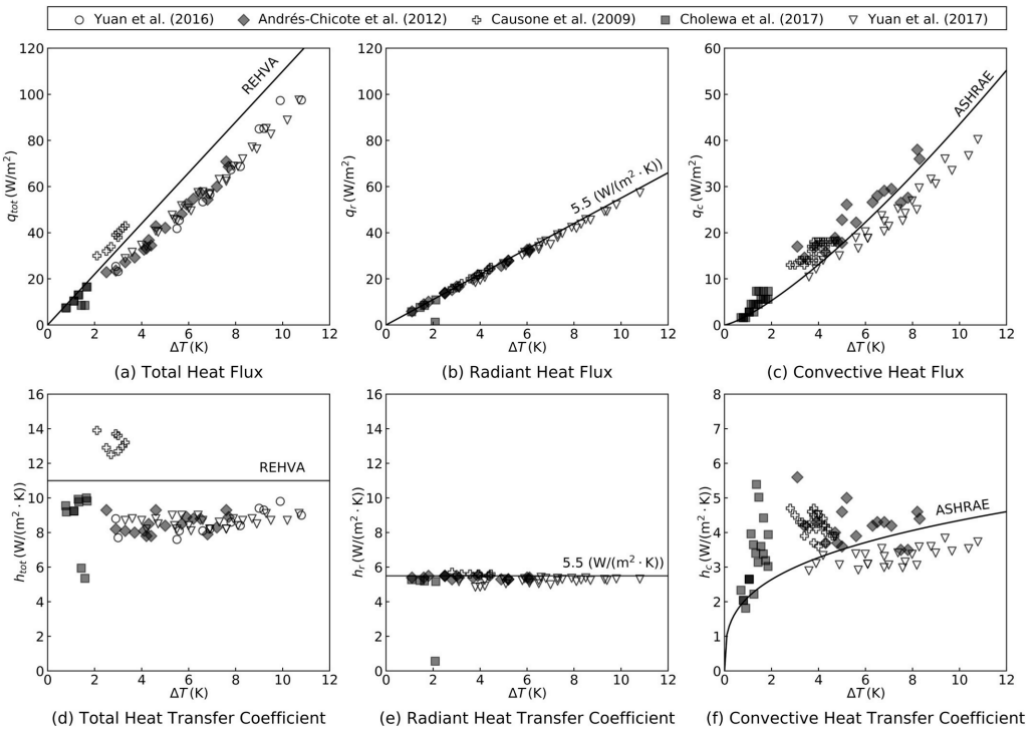

Fig. 2-3 Measured heat flux and heat transfer coefficients of ceiling cooling [11]

Fig. 2-4 illustrates the heat transfer coefficients for ceiling heating systems. The radiant heat flux is linearly related to ΔT, resulting in a constant radiant heat transfer coefficient equal to the ceiling cooling. In contrast to ceiling cooling, ceiling heating resulted in minimal convective heat transfer, with the majority of heat transfer occurring through radiation. Thus, the total heat transfer coefficient of ceiling heating is generally ranged between 6 to 8 W/(m^2 ·K).

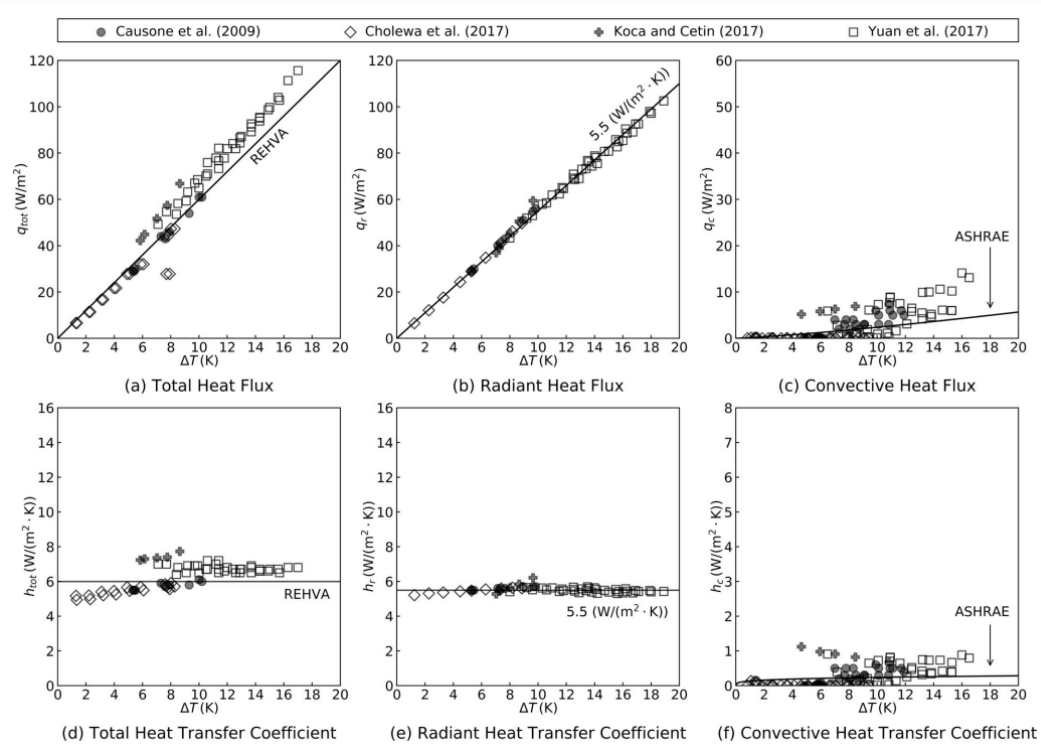

Fig. 2-4 Measured heat flux and heat transfer coefficients of ceiling heating

The design and usage of the radiant ceiling panel system also have been guided by many standards including ASHRAE Handbook [12], ISO 18566-3 [13], and REHVA Guidebook [14]. In ASHRAE Handbook, the radiant heat transfer of the RCP system can be approximated based on the panel and envelope surface temperature as expressed in Eq. (2-2), while the convective heat transfer coefficient differs between ceiling heating and ceiling cooling as shown in Eq. (2-3) and Eq. (2-4), separately.

$$q_r = 5 \times 10^{-8}[(T_s + 273.15)^4 - (AUST + 273.15)^4] \quad (2-2)$$

Ceiling heating equation:

$$q_c = 0.87(T_s - T_a)^{0.25}(T_s - T_a) \quad (2-3)$$

Ceiling cooling equation:

$$q_c = 2.13|T_s - T_a|^{0.32}(T_s - T_a) \quad (2-4)$$

Where T_s is the effective temperature of panel surface (°C), T_a is the dry-bulb indoor air temperature (°C), *AUST* is the area-weighted temperature of all indoor surfaces of walls, ceiling, floor, windows, doors, etc. (°C).

2.2.2 Research hotspots and development trends of radiant ceiling panel system

From 2020 to the writing of this paper, numerous articles discussing the radiant ceiling panel system have been published, with a predominant focus on the following aspects. The current research on the RCP system focuses on improvement and smart control. The research is mostly aimed at the widespread application of the RCP system, given that this system has already been commercialized.

- ***Heating and cooling capacity improvement***

As mentioned in *Section 2.2.1*, the heating or cooling capacity is influenced by the panel surface temperature and the specification of the panel itself. Subsequently, it may have an impact on both thermal comfort and energy consumption. Many studies aim to enhance the radiant and convective heat transfer to improve the efficiency of the panel and prevent the surface condensation through various approaches and possibly to prevent the surface. Labat et al. (2020) [15] focused on the panel arrangement and varied the size and number of the suspended RCP to highlight influence of the distribution on the radiant temperature field. Jin et al. (2020) [16] investigated the dynamic change of surface temperature in regulating the supply water flow. The study found that when the chilled water supply is closed, the condensation on the radiant ceiling panel surface can be effectively prevented. Zhong et al. (2022) [17] investigated the condensation heat transfer of ceiling superhydrophobic surfaces and assess the potential enhancement of the total heat flux of RCP with superhydrophobic treatment. Hassan and Kaood (2022) [18] proposed a passive enhancement approach to enhance the cooling capacity and improve the temperature uniformity of the RCP by internally finning the copper tubes. Shinacka and Mroz (2023) [19] studied a novel heating and cooling panel with a U-groove surface and aluminium monolithic structure that increases heat exchange between the heating–cooling medium and the panel through both experimental measurements and numerical simulations.

- ***Ventilation integration***

As described in *Section 1.1.3*, the radiant heating and cooling systems lack the capability to handle the latent heat and maintain a good indoor air quality. The RCP system is no exception and requires integration with a ventilation system for practice use. Recently, some studies evaluated the performance of an integrated RCP and ventilation system as summarized in Table 2-2. These studies mapped the heat transfer of the integrated system, calculated the radiant and convective heat transfer coefficient, and investigated various scenarios of system operations. Some examples for the sketch of the integrated system are shown in Fig. 2-5.

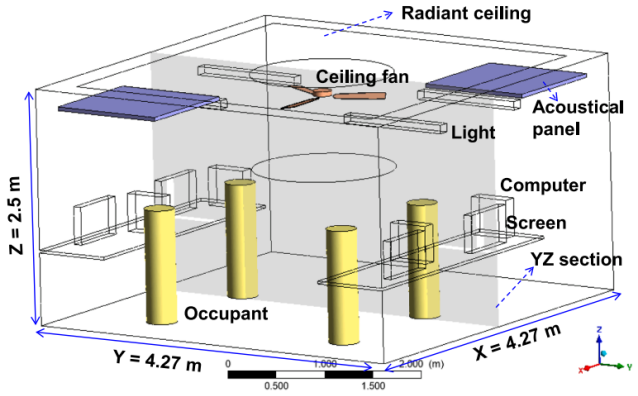

(a) Guo et al. (2023) [21]

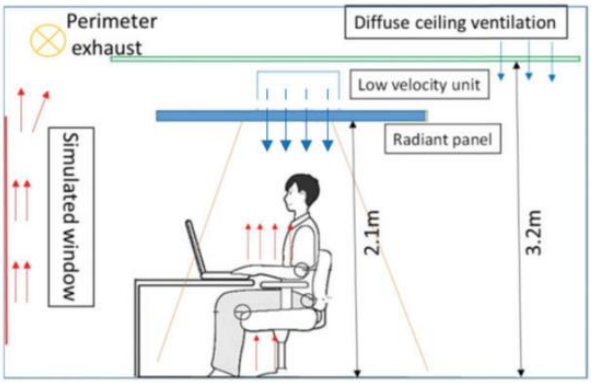

(b) Zhao et al. (2020) [23]

Fig. 2-5 Sketch of the integrated RCP and ventilation system

Table 2-2 Literatures of the integrated RCP and ventilation system

Literature	Ventilation system	Methodology	Research target
Krusaa and Hviid (2021) [20]	Diffuse ceiling ventilation	Reduced-scale experiment	Map the heat transfer from the perforated radiant ceiling panel at different ventilation rates.
Guo et al. (2023) [21]	Upward-directed ceiling fan	CFD simulation	Provide generalizable knowledge for design, and optimization of the coupling operation parameters of ceiling-fan integrated radiant ceiling cooling systems.
Choi et al. (2023) [22]	Fan	Experiment and CFD simulation	Develop a fan-assisted ceiling radiant cooling panel system to minimize the modification of architectural or mechanical elements
Zhao et al. (2020) [23]	Diffuse ceiling ventilation systems	Experiment	Introduce and analyze the performance of new ventilation and cooling systems where local micro-environment is created
Jahanbin and Semprini (2022) [24]	Up-supply and down-supply ventilations.	CFD simulation	Investigates the integrated effects of the ceiling radiant cooling and ventilation on dispersion and deposition of indoor airborne particles.
Ning et al. (2020) [25]	Dedicated outdoor air system	Numerical model	Explore the cooling load dynamics and

develop a simplified calculation method for the integrated system.

- ***Phase change material integration***

Recently, the phase change materials (PCM), have also been explored for integration with the radiant ceiling panel (RCP) system as shown in Fig. 2-6.

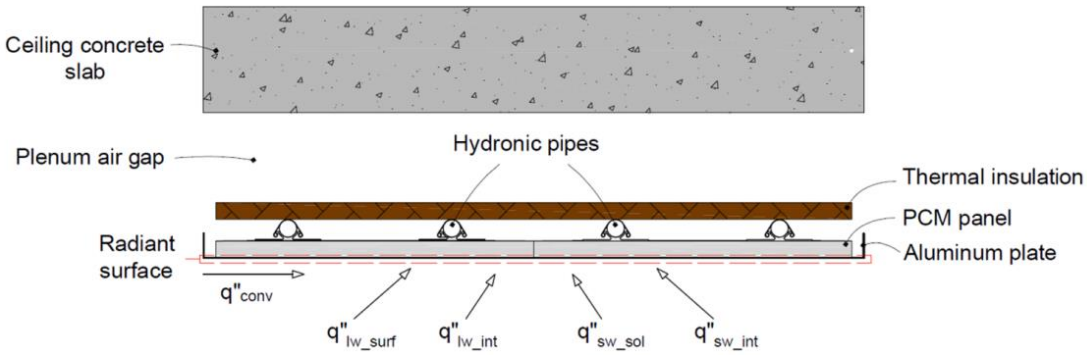

Fig. 2-6 Schematic of the PCM radiant ceiling panel (PCM-RCP) [26]

Incorporating the PCM in the embedded type radiant ceiling panel (RCP) system can provide thermal energy storage capacity to the system instead of using the thermal mass of the building structure. It takes advantages to reduce peak cooling loads or shift peak cooling loads to off-peak hours by regenerating the PCM during unoccupied periods. Table 2-3 lists the literatures for this novel integrated system.

Table 2-3 Literatures of the integrated RCP and thermal energy storage

Literature	TES	Methodology	Research target
Gallardo and Berardi (2021) [26]	PCM determined using the standard ASTM C1784-20	Numerical simulation by EnergyPlus v.9.4	Provide criteria to design, size, and control radiant ceiling panels with integrated RCP-PCM for space cooling in office buildings
Mousavi et al. (2023) [27]	Organic-based shape-stabilised PCM boards	Experiment	Comprehend the potentials and challenges of the PCM-RCC technologies in load shifting and energy savings
Bogatu et al. (2021) [28]	A novel macro-encapsulated PCM panel (MEP)	Experiment	The novel macro-encapsulated PCM ceiling panel construction was investigated and compared experimentally to commercially available ceiling cooling systems.

- ***Modeling and measuring method development***

Modeling and measuring the radiant ceiling panel system is another research hotspot, as it serves as the foundation for the further system development and the realization of smart system control. Jin et al. (2023) [29] developed a novel cooling capacity prediction model for the open-type cooling radiant ceiling panel systems (O-CRCP) using a multi-regression method. Ning and Chen (2021) [30] defined radiant and convective time series (RTS and CTS) factors to quantify the cooling load conversion process for radiant ceiling panel (RCP) system. Shinoda et al. (2022) [31] proposed a cooling capacity measurement methodology with controlled room and plenum temperatures. An empirical approach for estimating the heat extraction at both sides of the panel was then proposed as well and the developed model was validated through field measurements. Joe and Park (2023) [32] proposed thermal conditions for radiant ceiling heating panels that can be applied to perimeter zones, ensuring both comfort and the ability to handle the heating load. A heat transfer model [3] was used to derive the factors affecting the cooling capacity of the RCP and each factor was simulated and verified through this model.

2.3 Optimization of radiant ceiling panel system

2.3.1 Panel structure and arrangement

As demonstrated by Shinoda et al. [11], the heat transfer coefficient of the radiant ceiling panel system varies depending on the specifications of the panel itself. Improving the panel structure and arrangement is possibly to increase the heat transfer efficiency. Table 2-4 lists the previous studies that aimed to enhance the heating and cooling capacity of panels by panel design. The designs of panels included (1) the water tube/water channel configuration design, (2) panel configuration design, (3) panel distribution arrangement design, and (4) panel material design. It is showed that the cooling capacity or even the uniformity of the indoor air temperature field can be substantially improved by applying novel design strategies.

Table 2-4 Literature of the optimization of the panel structure and arrangement

Literature	Methodology	Design Strategies	Improvement Results
Mosa et al. [33,34]	Numerical simulation	Serpentine and dendritic flow channel design	The dendritic architecture allows for a significant improvement in the cooling panel performance.
Hassan and Kaood [18]	CFD simulation	Application of internal longitudinal fins	The presented balanced design enhances the cooling capacity and cooling rate by 1.54 and 17.7%, respectively.
Radzai et al. [35]	CFD simulations	New RCP serpentine-based flow configuration	The proposed designs have the potential to improve the overall efficiency of RCP in terms of temperature distribution, cooling capacity, and pressure.
Labat et al. [15]	Genetic algorithm	Arrangement of multiple panels on the ceiling	The uniformity of the temperature field can be significantly improved by using 10 panels or more compared with using a single panel.
Shin et al. [36]	Experiments and CFD simulation	Open-type CRCP installed with void areas between adjacent ceiling panels	The open-type CRCP can provide 54–80% higher nominal cooling capacity than a conventional closed-type CRCP.
Radwan et al. [37]	CFD simulation	New multisegmented mini-channel-based CRCP	The design can accomplish the same cooling capacity and identical indoor air temperature by using a higher panel surface temperature.
Zhang et al. [38]	Experiments	A new type of CRCP with inclined aluminum fins	The cooling capacity of the CRCP with inclined fins is about 19% higher than that of a suspended panel.
Lv et al. [39]	Experiments	A novel grooved radiant ceiling panel filled with heat transfer liquid	The cooling capacity of this radiant panel was 18–25% higher than that of traditional metal radiant panels.
Ning et al. [40]	CFD simulation	CRCP with a thin air layer	The cooling capacities are increased by 43–46% compared to the original CRCP.
Xing and Li [41]	Experiments	Replacement of the radiation shield with a convection shield	The improved inbuilt air gap has a better synergy in improving cooling capacity and anticondensation ability.

2.3.2 Integrated systems

The integrated radiant ceiling panel (RCP) and ventilation system attracted attention to replace the conventional HVAC system in the building for its potential for energy savings while providing high indoor air quality and thermal comfort. Table 2-5 summarizes the studies focusing on the integrated RCP and ventilation system. It is shown that the displacement ventilation system is most commonly used ventilation system combined to the RCP system. Fig. 2-7 shows a layout of an integrated RCP and under floor displacement ventilation system in an office of the HELILON building in Europe [42]. It was concluded that the integrated system provided cooling by both radiant and convective transmission, and therefore produced better thermal comfort and air quality than other air conditioning systems that provided purely convective cooling.

Table 2-5 Literature of the optimization of the integrated RCP and ventilation system

Literature	Ventilation system	Studied parameters	Methodology
Chiang et al. [43]	Mechanical ventilation	Diffuser position in the mechanical ventilation system	Experiments and CFD simulations
Corgnati et al. [44]	Mixing ventilation	Main supply jet properties (throw and penetration length)	Experiments and CFD simulations
Liu et al. [45]	Displacement ventilation system	Thermal performance of the integrated system	Experiments
Schiavon et al. [46]	Displacement ventilation system	(1) The ratio of cooling load removed by RCP over the total cooling load (2) The percentage of RCP affects the room air stratification.	Experiments
Yu et al. [47]	Natural ventilation with diffuse ceiling inlet	Thermal performance of the integrated system	Experiments
Zhao et al. [48]	Low velocity unit and personalized ventilation system	Human response to the proposed integrated system	Experiments

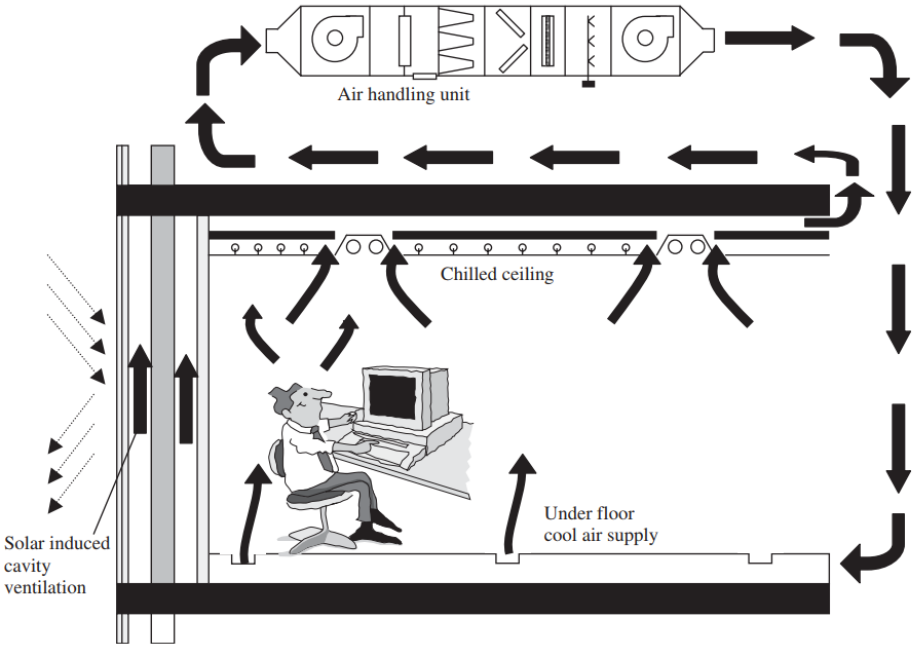

Fig. 2-7 Schematic diagram showing the layout of an integrated RCP and under floor displacement ventilation system [42]

Except for the ventilation system, Ranzato et al. [49] studied the integrated system consisting of radiant ceiling panels, mechanical ventilation system with energy recovery and a well-water-cooled electric heat pump. A simplified physical model of the system was built to calculate its annual efficiency, the energy consumption of each component and its life cycle costs. When combined with the energy system, more attention is paid to the system control. Arghand et al. [50] investigated the performance of two control methods for the RCP and groundwater system. The control methods were implemented through three types of indoor feedback controllers: 1) an on/off controller, 2) an on/off controller with a dead band and 3) P controller regarding room temperature stability and pump energy use. The control optimization are detailly summarized in *Section 2.3.3*.

2.3.3 Control strategies and advanced control methods

The optimization and control of the radiant ceiling panel system have relatively rare publications due to a lack of knowledge about its operational status. Therefore, the optimization control strategies for the radiant heating and cooling (RHC) system are discussed and summarized in this section instead of only the RCP system. The control optimization of the RHC or RCP systems is crucially related to both energy consumption patterns and comfort levels within the buildings.

Building energy system control has been brought to the fore with the rapid rise of using the centralized building management system [51]. As a general type of HVAC system, the RHC system is not an exception that should be emphasized in terms of its control. On the one hand, the importance of controlling the supplied chilled water temperature and making temperature regulations to assist in condensation prevention of radiant cooling systems was pointed out many times for decades [4]. However, the simple temperature limitation control has a risk of insufficient cooling capacity [52] and reduces the performance of energy efficiency [53]. A more sophisticated

control is needed considering the system operation enhancement, indoor operative temperature, and other parameters such as return water temperature [54]. On the other hand, the advanced control strategies are required to mitigate under-heating or over-hearing issues caused by the system response delays [1], and over-cooling affected by furniture [55].

The system integration with PCM [56, 57] and ventilation [58] also complicate the control due to the increasing number of setpoints and impact variables, in terms of the storage capacity of PCM and the requirement of dehumidification for the ventilation system. Different ventilation configurations contribute to the variation of the suitable control strategy according to the system characteristics [59]. Remaní et al. summarized [60] the control logic of the TABS systems and discussed seven different controls employed in TABS systems. The author finally concluded that while the simple strategies are suitable for meeting comfort demands, the strategies taking into account the system properties are superior in terms of energy reduction and the utilization of renewable energy.

2.4 A novel open-type radiant ceiling panel system

The insulation layer above the panel is expected to insulate the heat transfer between the panel and the ceiling to activate heat transfer on the bottom surface towards the conditioned space. Some researchers have focused on improving the insulation layer to reduce the heat flux to increase the cooling capacity of the RCP system due to the upward heat loss is inevitable [41].

The open-type RCP, also called a suspended radiant ceiling panel (SRCP) [15] or suspended ceiling radiant panel (CRP) [38] has recently come to public attention. Unlike the top-insulated type, an open-type RCP is installed separately from the ceiling, excluding insulation between the panel top and ceiling. Due to the characteristic of convenient and flexible installation, this type is also widely used in existing or new buildings in practice [61]. A novel open-type radiant ceiling panel system with curved and segmented structure (Fig. 2-7) was proposed [62] and produced by SANKEN SETSUBI KOGYO CO., LTD. Fig. 2-8 shows the sketch and detailed measurement of the novel panel.

Fig. 2-7 Image shown by SANKEN SETSUBI KOGYO CO., LTD.

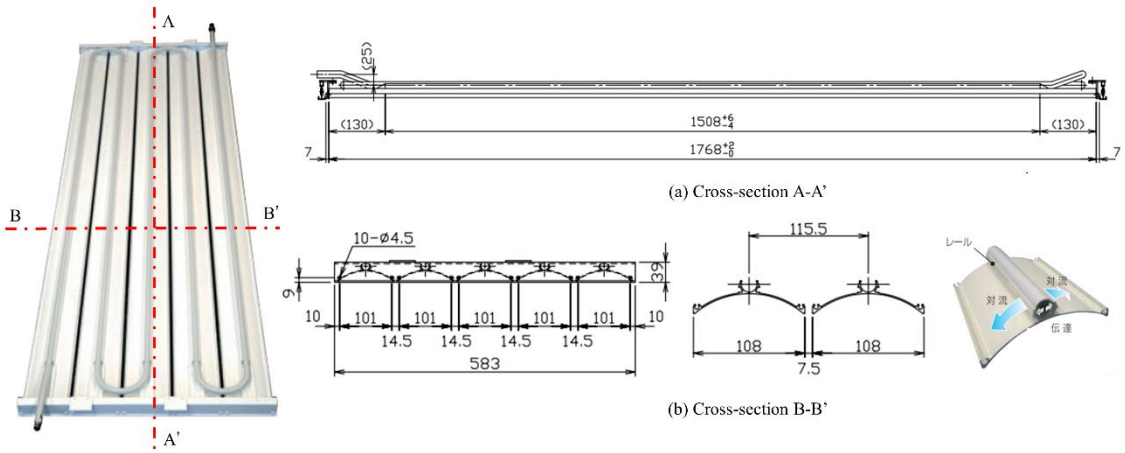

Fig. 2-8 Sketch of a novel open-type radiant ceiling panel system with curved and segmented structure

Nomenclature

List of symbols

Q	Heating and cooling capacity (W)
A	Area of panel (m^2)
T_{air}	Indoor air temperature (°C)
T_s	Panel surface temperature (°C)

Greek symbol

α	Heat transfer coefficient ($W/(m^2 \cdot K)$)

Abbreviations

RCP	Radiant ceiling panel
CRCP	Ceiling radiant cooling panel
TABS	Thermally activated building system
RHC	Radiant heating and cooling system
ASHRAE	American Society of Heating, Refrigerating and Air-Conditioning Engineers
ISO	International Organization for Standardization
REHVA	Federation of European Heating, Ventilation and Air Conditioning Associations
PCM	Phase change material
HVAC	Heating, Ventilation and Air Conditioning

Reference

[1] K.N. Rhee, B.W. Olesen, K.W. Kim, Ten questions about radiant heating and cooling systems, Build. Environ. 112 (2017) 367–381, https://doi.org/10.1016/j.buildenv.2016.11.030.

[2] J. Feng, F. Bauman, S. Schiavon, Experimental comparison of zone cooling load between radiant and air systems, Energy Build. 84 (2014) 152–159. https://doi.org/10.1016/j.enbuild.2014.07.080.

[3] S.H. Park, D.W. Kim, G.S. Joe, S.R. Ryu, M.S. Yeo, K.W. Kim, Establishing boundary conditions considering influence factors of the room equipped with a ceiling radiant cooling panel, Energies. 13 (2020) 1–21. https://doi.org/10.3390/en13071684.

[4] K.N. Rhee, K.W. Kim, A 50 year review of basic and applied research in radiant heating and cooling systems for the built environment, Build. Environ. 91 (2015)166–190, https://doi.org/10.1016/j.buildenv.2015.03.040.

[5] E. Dudkiewicz, P. Jadwiszczak, J. Jeżowiecki, Examination of operational dynamics of radiant ceiling panel, Cent. Eur. J. Eng. 1 (2011) 159–167. https://doi.org/10.2478/s13531-011-0016-7.

[6] J. Miriel, L. Serres, A. Trombe, Radiant ceiling panel heating-cooling systems: Experimental and simulated study of the performances, thermal comfort and energy consumptions, Appl. Therm. Eng. 22 (2002) 1861–1873. https://doi.org/10.1016/S1359-4311(02)00087-X.

[7] M. Ye, K. Nagano, A.A. Serageldin, H. Sato, Field studies on the energy consumption and thermal comfort of a nZEB using radiant ceiling panel and open-loop groundwater heat pump system in a cold region, J. Build. Eng. 67 (2023) 105999. https://doi.org/10.1016/j.jobe.2023.105999.

[8] R.A. Memon, S. Chirarattananon, P. Vangtook, Thermal comfort assessment and application of radiant cooling: A case study, Build. Environ. 43 (2008) 1185–1196. https://doi.org/10.1016/j.buildenv.2006.04.025.

[9] P. Valdiserri, S. Cesari, M. Coccagna, P. Romio, S. Mazzacane, Experimental data and simulations of performance and thermal comfort in a patient room equipped with radiant ceiling panels, Buildings. 10 (2020) 1–18. https://doi.org/10.3390/buildings10120235.

[10] M. Tye-Gingras, L. Gosselin, Comfort and energy consumption of hydronic heating radiant ceilings and walls based on CFD analysis, Build. Environ. 54 (2012) 1–13. https://doi.org/10.1016/j.buildenv.2012.01.019.

[11] J. Shinoda, O.B. Kazanci, S. ichi Tanabe, B.W. Olesen, A review of the surface heat transfer coefficients of radiant heating and cooling systems, Build. Environ. 159 (2019) 106156. https://doi.org/10.1016/j.buildenv.2019.05.034.

[12] ASHRAE, ASHRAE Handbook-HVAC Systems and Equipment, (2012).

[13] ISO 18566-3: 2017, Building Environment Design-Design, test methods and control of hydronic radiant heating and cooling panel system Part 3: Design of ceiling mounted radiant panels, (2017).

[14] J. Babiak, B.W. Olesen, D Petras, Low temperature heating and high temperature cooling, REHVA Guidebook no.7, (2009).

[15] M. Labat, S. Lorente, M. Mosa, Influence of the arrangement of multiple radiant ceiling panels on the radiant temperature field, Int. J. Therm. Sci. 149 (2020) 106184. https://doi.org/10.1016/j.ijthermalsci.2019.106184.

[16] W. Jin, J. Jing, L. Jia, Z. Wang, The dynamic effect of supply water flow regulation on surface temperature changes of radiant ceiling panel for cooling operation, Sustain. Cities Soc. 52 (2020). https://doi.org/10.1016/j.scs.2019.101765.

[17] Z. Zhong, W. Ma, S. Yao, X. Xu, J. Niu, Enhancing the cooling capacity of radiant ceiling panels by latent heat transfer of superhydrophobic surfaces, Energy Build. 263 (2022) 112036. https://doi.org/10.1016/j.enbuild.2022.112036.

[18] M.A. Hassan, A. Kaood, Multi-criteria assessment of enhanced radiant ceiling panels using internal longitudinal fins, Build. Environ. 224 (2022) 109554. https://doi.org/10.1016/j.buildenv.2022.109554.

[19] J. Sinacka, T. Mróz, Novel radiant heating and cooling panel with a monolithic aluminium structure and U-groove surface – Experimental investigation and numerical model, Appl. Therm. Eng. 229 (2023). https://doi.org/10.1016/j.applthermaleng.2023.120611.

[20] M.R. Krusaa, C.A. Hviid, Reduced-scale experiments of heat transfer from integrated radiant ceiling panel and diffuse ceiling ventilation, Appl. Therm. Eng. 197 (2021) 117348. https://doi.org/10.1016/j.applthermaleng.2021.117348.

[21] X. Guo, S. Wan, W. Chen, H. Zhang, E. Arens, Y. Cheng, W. Pasut, Numerical simulation of cooling performance of radiant ceiling system interacting with a ceiling fan, Energy Build. 297 (2023) 113492. https://doi.org/10.1016/j.enbuild.2023.113492.

[22] J.S. Choi, G.J. Jung, K.N. Rhee, Cooling performance evaluation of a fan-assisted ceiling radiant cooling panel system, Energy Build. 281 (2023) 112760. https://doi.org/10.1016/j.enbuild.2022.112760.

[23] W. Zhao, S. Kilpeläinen, R. Kosonen, J. Jokisalo, Experimental comparison of local low velocity unit combined with radiant panel and diffuse ceiling ventilation systems, Indoor Built Environ. 29 (2020) 895–914. https://doi.org/10.1177/1420326X20918398.

[24] A. Jahanbin, G. Semprini, Combined impacts of the ceiling radiant cooling and ventilation on dispersion and deposition of indoor airborne particles, Therm. Sci. Eng. Prog. 34 (2022) 101438. https://doi.org/10.1016/j.tsep.2022.101438.

[25] B. Ning, Y. Chen, H. Jia, Cooling load dynamics and simplified calculation method for radiant ceiling panel and dedicated outdoor air system, Energy Build. 207 (2020). https://doi.org/10.1016/j.enbuild.2019.109631.

[26] A. Gallardo, U. Berardi, Design and control of radiant ceiling panels incorporating phase change materials for cooling applications, Appl. Energy. 304 (2021) 117736. https://doi.org/10.1016/j.apenergy.2021.117736.

[27] S. Mousavi, B. Rismanchi, S. Brey, L. Aye, Thermal and energy performance evaluation of a full-scale test cabin equipped with PCM embedded radiant chilled ceiling, Build. Environ. 237 (2023) 110348. https://doi.org/10.1016/j.buildenv.2023.110348.

[28] D.I. Bogatu, O.B. Kazanci, B.W. Olesen, An experimental study of the active cooling performance of a novel radiant ceiling panel containing phase change material (PCM), Energy Build. 243 (2021) 110981. https://doi.org/10.1016/j.enbuild.2021.110981.

[29] W. Jin, Y. Wang, C. Wang, L. Jia, D. Moon, S. Song, A novel cooling capacity prediction model for open-type cooling radiant ceiling, J. Build. Eng. 74 (2023) 106846. https://doi.org/10.1016/j.jobe.2023.106846.

[30] B. Ning, Y. Chen, A radiant and convective time series method for cooling load calculation of radiant ceiling panel system, Build. Environ. 188 (2021) 107411. https://doi.org/10.1016/j.buildenv.2020.107411.

[31] J. Shinoda, O.B. Kazanci, K. Hidari, H. Watanabe, Y. Takahashi, S. ichi Tanabe, Improvements to the cooling capacity measurements of suspended radiant ceiling panels to prevent under-sizing, J. Build. Eng. 51 (2022) 104242. https://doi.org/10.1016/j.jobe.2022.104242.

[32] G. Joe, S. Park, A Study on Establishing Thermal Output Conditions of Radiant Ceiling Heating Panels for Improving Thermal Comfort of Perimeter Zone in Buildings, Appl. Sci. 13 (2023). https://doi.org/10.3390/app13116744.

[33] M. Mosa, M. Labat, S. Lorente, Role of flow architectures on the design of radiant cooling panels, a constructal approach, Appl Therm Eng. 150 (2019) 1345–1352. https://doi.org/10.1016/j.applthermaleng.2018.12.107.

[34] M. Mosa, M. Labat, S. Lorente, Constructal design of flow channels for radiant cooling panels, International Journal of Thermal Sciences. 145 (2019). https://doi.org/10.1016/j.ijthermalsci.2019.106052.

[35] M.H.M. Radzai, C.T. Yaw, C.W. Lim, S.P. Koh, N.A. Ahmad, Numerical analysis on the performance of a radiant cooling panel with serpentine-based design, Energies (Basel). 14 (2021). https://doi.org/10.3390/en14164744.

[36] M.S. Shin, K.N. Rhee, S.H. Park, M.S. Yeo, K.W. Kim, Enhancement of cooling capacity through open-type installation of cooling radiant ceiling panel systems, Build Environ. 148 (2019) 417–432. https://doi.org/10.1016/j.buildenv.2018.11.005.

[37] A. Radwan, T. Katsura, L. Ding, A.A. Serageldin, A.I. EL-Seesy, K. Nagano, Design and thermal analysis of a new multi-segmented mini channel based radiant ceiling cooling panel, Journal of Building Engineering. 40 (2021). https://doi.org/10.1016/j.jobe.2021.102330.

[38] L. Zhang, X.H. Liu, Y. Jiang, Experimental evaluation of a suspended metal ceiling radiant panel with inclined fins, Energy Build. 62 (2013) 522–529. https://doi.org/10.1016/j.enbuild.2013.03.044.

[39] G. Lv, C. Shen, Z. Han, W. Liao, D. Chen, Experimental investigation on the cooling performance of a novel grooved radiant panel filled with heat transfer liquid, Sustain Cities Soc. 50 (2019). https://doi.org/10.1016/j.scs.2019.101638.

[40] B. Ning, Y. Chen, H. Liu, S. Zhang, Cooling capacity improvement for a radiant ceiling panel with uniform surface temperature distribution, Build Environ. 102 (2016) 64–72. https://doi.org/10.1016/j.buildenv.2016.03.009.

[41] D. Xing, N. Li, Thermal performance improvement for the ceiling radiant cooling panel with an inbuilt air gap by the convection shield, Sustainable Energy Technologies and Assessments. 44 (2021). https://doi.org/10.1016/j.seta.2021.101012.

[42] S.B. Riffat, X. Zhao, P.S. Doherty, Review of research into and application of chilled ceilings and displacement ventilation systems in Europe, Int. J. Energy Res. 28 (2004) 257–286. https://doi.org/10.1002/er.964.

[43] W.H. Chiang, C.Y. Wang, J.S. Huang, Evaluation of cooling ceiling and mechanical ventilation systems on thermal comfort using CFD study in an office for subtropical region, Build. Environ. 48 (2012) 113–127. https://doi.org/10.1016/j.buildenv.2011.09.002.

[44] S.P. Corgnati, M. Perino, G. V. Fracastoro, P. V. Nielsen, Experimental and numerical analysis of air and radiant cooling systems in offices, Build. Environ. 44 (2009) 801–806. https://doi.org/10.1016/j.buildenv.2008.05.022.

[45] Z. Liu, L. Zhang, G. Gong, Experimental evaluation of a solar thermoelectric cooled ceiling combined with displacement ventilation system, Energy Convers. Manag. 87 (2014) 559–565. https://doi.org/10.1016/j.enconman.2014.07.051.

[46] S. Schiavon, F. Bauman, B. Tully, J. Rimmer, Room air stratification in combined chilled ceiling and displacement ventilation systems, HVAC R Res. 18 (2012) 147–159. https://doi.org/10.1080/10789669.2011.592105.

[47] T. Yu, P. Heiselberg, B. Lei, M. Pomianowski, C. Zhang, R. Jensen, Experimental investigation of cooling performance of a novel HVAC system combining natural ventilation with diffuse ceiling inlet and TABS, Energy Build. 105 (2015) 165–177. https://doi.org/10.1016/j.enbuild.2015.07.039.

[48] W. Zhao, S. Kilpeläinen, R. Kosonen, J. Jokisalo, S. Lestinen, Y. Wu, P. Mustakallio, Human response to thermal environment and perceived air quality in an office with individually controlled convective and radiant cooling systems, Build. Environ. 195 (2021). https://doi.org/10.1016/j.buildenv.2021.107736.

[49] G. Ranzato, M. Grisot, L. Cecchinato, A. Gastaldello, An innovative system based on water-water heat pump with radiant panels and a ventilation energy recovery system for residential air-conditioning and tap water production, Int. J. Low Carbon Technol. 2 (2007) 300–311. https://doi.org/10.1093/ijlct/2.3.300.

[50] T. Arghand, S. Javed, A. Trüschel, J.O. Dalenbäck, Control methods for a direct-ground cooling system: An experimental study on office cooling with ground-coupled ceiling cooling panels, Energy Build. 197 (2019) 47–56. https://doi.org/10.1016/j.enbuild.2019.05.049.

[51] P.H. Shaikh, N.B.M. Nor, P. Nallagownden, I. Elamvazuthi, T. Ibrahim, A review on optimized control systems for building energy and comfort management of smart sustainable buildings, Renewable and Sustainable Energy Reviews. 34 (2014) 409–429. https://doi.org/10.1016/j.rser.2014.03.027.

[52] D. Xing, N. Li, C. Zhang, P. Heiselberg, A critical review of passive condensation prevention for radiant cooling, Build Environ. 205 (2021). https://doi.org/10.1016/j.buildenv.2021.108230.

[53] F. Zhang, H.A. Guo, Z. Liu, G. Zhang, A critical review of the research about radiant cooling systems in China, Energy Build. 235 (2021). https://doi.org/10.1016/j.enbuild.2021.110756.

[54] A. Hesaraki, N. Huda, A comparative review on the application of radiant low-temperature heating and high-temperature cooling for energy, thermal comfort, indoor air quality, design and control, Sustainable Energy Technologies and Assessments. 49 (2022). https://doi.org/10.1016/j.seta.2021.101661.

[55] K. Zhao, X.H. Liu, Y. Jiang, Application of radiant floor cooling in large space buildings - A review, Renewable and Sustainable Energy Reviews. 55 (2016) 1083–1096. https://doi.org/10.1016/j.rser.2015.11.028.

[56] S. Mousavi, B. Rismanchi, S. Brey, L. Aye, PCM embedded radiant chilled ceiling: A state-of-the-art review, Renewable & Sustainable Energy Reviews. (2021). https://doi.org/10.1016/J.RSER.2021.111601.

[57] M. Moreira, J. Dias-de-Oliveira, C. Amaral, F. Neto, T. Silva, Outline of the incorporation of phase change materials in radiant systems, J Energy Storage. 57 (2023). https://doi.org/10.1016/j.est.2022.106307.

[58] A. Novoselac, J. Srebric, A critical review on the performance and design of combined cooled ceiling and displacement ventilation systems, 2002.

[59] C. Zhang, M. Pomianowski, P.K. Heiselberg, T. Yu, A review of integrated radiant heating/cooling with ventilation systems- Thermal comfort and indoor air quality, Energy Build. 223 (2020). https://doi.org/10.1016/j.enbuild.2020.110094.

[60] J. Romaní, A. De Gracia, L.F. Cabeza, Simulation and control of thermally activated building systems (TABS), Energy Build. 127 (2016) 22–42. https://doi.org/10.1016/j.enbuild.2016.05.057.

[61] S. Jordan, J. Hafner, T.E. Kuhn, A. Legat, M. Zbašnik-Senegačnik, Indoor environment in retrofitted offices

equipped with radiant ceiling panels, Gradjevinar. 68 (2016) 125–134. https://doi.org/10.14256/jce.1289.2015.
[62] 塩谷正樹（2014年3月）; スリットを有する天井放射パネルユニットの制御法及び汎用熱計算法に関する研究，宇都宮大学大学院工学研究科博士論文

Chapter 3

Performance analysis of the novel open-type RCP system through experiments

3.1 Introduction

A novel open-type radiant ceiling panel (RCP) system with a segmented and concave surface had been proposed to improve thermal efficiency and reduce the risk of dew condensation. However, it is still unclear whether the system performs well in the field, as the previous laboratory test [1] was conducted in ideal conditions excluding the effects of outdoor climate conditions and occupant activities. The performance may change when exposed to a dynamic environment. It is also expected to identify ignored issues during long-term system operation that will guide the future design and optimization.

The methods for designing and testing RCP systems are provided in international design standards, such as EN 14240 [2], EN 14037-1 [3], and ANSI/ASHRAE Standard 138 [4]. While, to study the new proposed RCP system, it is essential to carry out the experimental tests in the laboratory to investigate its heating and cooling performance. Zhang et al. [5] conducted a study on a novel open-type RCP with inclined aluminum fins through the experiments carried out in two test rooms. The heat flux was assessed through measurements of the indoor thermal conditions and the water supply parameters. Subsequently, the results were compared with those from other RCP systems. Zhong et al. [6] proposed a RCP using superhydrophobic surface materials to prevent dew condensation and experimentally investigate the condensation heat transfer. The empirical method and heat and mass transfer analogy were verified based on the experimental results. Jin et al. [7] carried out experiments to investigate the surface temperature change of the RCP. Then, the effect of supply water temperature was studied by numerical simulations based on the experiments. Ning et al. [8] experimentally and numerically investigated the performance of a novel RCP with uniform surface temperature distribution by adding an air layer between the pipes and metal plates. This modification increased the cooling capacity by 43 %–46 % relative to the original RCP. Wojtkowiak and Amanowicz [9] investigated a RCP with a triangular corrugation shape through experiment and theoretical analysis. They studied the impact of the corrugation length and angle on the cooling capacity. The results show that cooling capacity of this new RCP increased by 15 %–20 % compared to the traditional flat shape.

Conducting experiments is also a valuable approach to gain insights into the performance of the integrated system that combines the RCP with other technologies. Ree and Haves [10] studied the characteristics of displacement ventilation and chilled ceiling panel system through chamber tests over a range of operating parameters typical of office applications. Bogatu et al. [11] investigated the operation and performance of a novel macro-encapsulated PCM panel with embedded pipe as an active ceiling cooling component compared to commercially available radiant ceiling system. Krussa and Hviid [12] studied a RCP with diffuse ventilation in a reduced-scale experiment. The heat transfer coefficients of this system were calculated and compared to the values presented in the previous studies.

Experimental measurements can also serve to validate the simulation model, enabling the authors to make adjustments to the operational parameters as needed. Su et al. [13] carried out an experiment on a concrete ceiling radiant cooling panel system and developed a two-dimensional mathematical model by using finite difference method. The heat transfer and cooling characteristics of the system were then numerically investigated under different conditions. Shin et al. [14] introduced an open-type cooling RCP system and evaluated its radiant and convective heat transfer by using a simulation model validated against the mock-up experiment. Yu et al. [15] developed a simplified model for top insulated metal ceiling radiant cooling panels with serpentine tube

arrangement based on the experiments conducted for two kinds of panels.

On the other hand, the field study is an effective method for evaluating system performance and thermal comfort. Direct measurement evaluation is undoubtedly more accurate than other simulation methods. Aryal et al. [16] conducted full-scale experiments to investigate the radiant ceiling cooling in office building in a tropical hot humid climate, considering indoor thermal conditions and the envelope heat gain.

The discrepancies have been found between the calculated predicted value and actual sensation of thermal comfort when apply the RCP systems. Tian et al. [17] detected occupant thermal comfort in an office using an RCP and an overhead dedicated outdoor air system. The results showed that the actual dissatisfaction rate was lower than the calculated values because the radiant system could obtain a uniform vertical temperature distribution and a low draft rate. He et al. [18] conducted a field survey combining environmental measurements and questionnaires in offices with cooling ceilings in Zhuhai, China. The results showed that local thermal sensations differ greatly for different body parts depending on factors such as clothing and adaptive behaviors. As a result, it is difficult to assess the accuracy of predicted thermal comfort calculations based on environmental measurements, because only a few field studies on radiant ceiling systems have been conducted. Therefore, in-situ studies are necessary for radiant ceiling systems to investigate realistic thermal comfort.

Given these points, the experiments in this study conducted both in the laboratory and in a sample office building to study the performance of the novel open-type RCP system with a segmented and concave surface. In *Section 3.2*, a series of laboratory experiments under different operating conditions were carried out to investigate the cooling performance of this novel RCP system. The effects of the flow rates and fluid inlet temperatures were extensively examined. In the experiments, the air temperature, mean radiant temperature, humidity, and air velocity in the test room were recorded. The convective and radiant heat transfer were calculated accordingly, and the radiant and convective heat transfer coefficients were also calculated for each case and compared with other RCPs. In *Section 3.3*, a field study was conducted in an office building to examine this novel RCP system in practice in terms of both thermal condition and energy consumption. Physical measurements and subjective survey questionnaires were conducted for one week in summer and two weeks in winter. The indoor air temperature, panel surface temperature, indoor humidity, and CO_2 concentration were measured at three locations in the office. The panel surface temperature distributions and variations were recorded using an infrared camera, and the energy performance was recorded during the measurement period. Finally, intermittent and continuous operation methods were compared during winter.

3.2 Cooling capacity analysis through laboratory tests

3.2.1 Experimental set-up

The experiments are operated in two identical walk-in environmental chambers (ESPEC E, ESPEC Corporation) with autonomous control. Each room had an internal length, width, and height of 2.7 m × 2.7 m × 2 m, and the two chambers shared a wall with a double-glazed window. The two glass layers had a thickness of 3 mm with a 14 mm air gap between them. This window was also fitted with a rubber seal around the four edges to prevent any infiltration between the test cells, resulting in an overall heat transfer coefficient of 1.85 W/(m^2·K).

The temperature of the left chamber was adjusted to 40 °C to mimic the outdoor environmental temperature during summer. Simultaneously, the room on the right was the test cell, and was equipped with four radiant ceiling panels (RCPs). A constant-temperature water bath chiller and a circulating pump provide the chilled water for circulating. The fluid temperature and flow rate were adjusted according to the predefined conditions. The test cell was internally heated by four cylindrical dummies. The heat generated from each cylinder was set as 43.2 W to represent the energy generated from the human sitting at rest. Fig. 3-1 depicts the overall arrangement of the panels, internal loads, and measurement devices.

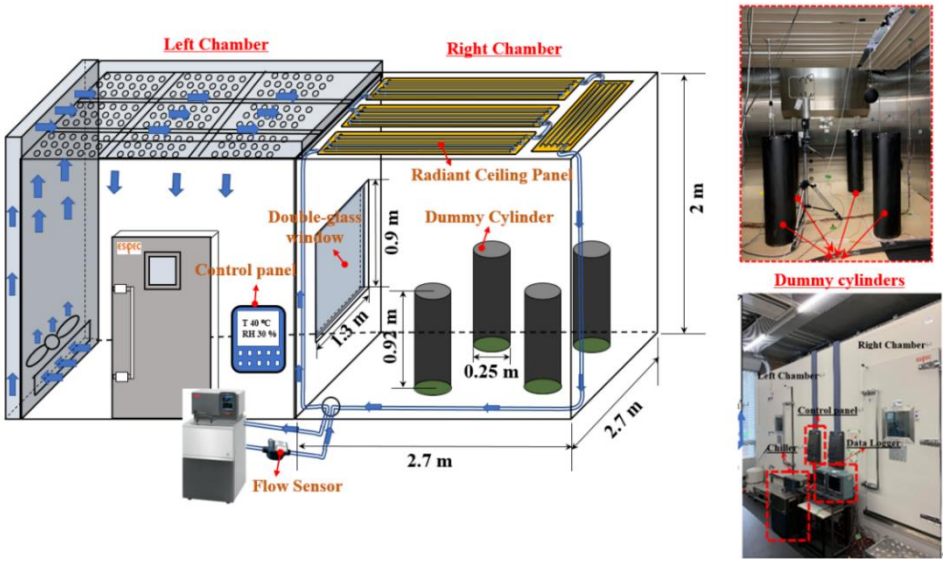

Fig. 3-1 Schematic diagram of the experimental set-up and arrangement

The open-type radiant ceiling panel (RCP) prototypes used in this study were manufactured and developed by SANKEN SETSUBI Co., LTD. The panels are formed from aluminum sheets with a thickness of 1 mm, and the pipes are made from aluminum tubes coated with polyethylene resin. Each panel has five segments, with each segment comprising a concave surface with a width of 108 mm and height 89 mm. Between each adjacent segment there is a void space of 6 mm, as shown in Fig. 3-2. The concave panel has a larger surface area than the flat panel, with a surface area (A_s) of 1.38 m^2 for the top surface and 1.03 m^2 for the bottom surface; therefore, the total surface area of each panel is 2.41 m^2. The projected area (A_p) of the panel is 1.04 m^2 for both the bottom and top surfaces. The ratio of the surface area to the projected area was 1.15:1.

Four RCPs were connected in series mode in the test chamber, and water was supplied through a closed-cycle

cooling circuit. The circulating fluid was cooled using a refrigeration bath circulator (*Huber CC-415*), where the fluid temperature and flow rate were controlled. 16 experiments were conducted under the operating conditions listed in Table 3-1. The water flow rate was varied from 2 to 8 L/min and the inlet water temperature was varied from 15 ℃ to 24 ℃.

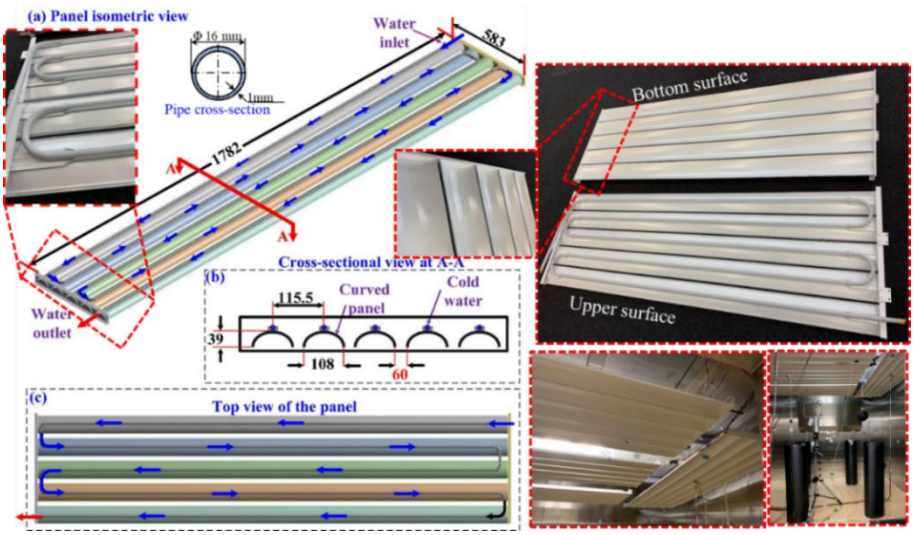

Fig. 3-2 Detailed drawing and photos of the RCP used in this study

Table 3-1 The operating conditions for the experiment

Case	Flow rate (L/min)	Inlet water temperature (°C)
Case1-1	2	15
Case1-2		18
Case1-3		21
Case1-4		24
Case2-1	4	15
Case2-2		18
Case2-3		21
Case2-4		24
Case3-1	6	15
Case3-2		18
Case3-3		21
Case3-4		24
Case4-1	8	15
Case4-2		18
Case4-3		21
Case4-4		24

3.2.2 Measurement methods

In these experiments, the envelope surface temperature, indoor air temperature, air velocity, relative humidity, and globe temperature were simultaneously measured and recorded. Three type-K thermocouples were used to measure the temperature of the inner window surface, in line with the window centerline, and two thermocouples were used to measure the outer window surface temperature, as shown in Fig. 3-3 (a). Six thermocouples were used to measure the wall, ceiling, and roof surface temperatures. The indoor air temperature was measured using 33 type-k thermocouples, which were distributed in three lines. Each line contained 11 thermocouples at a vertical spacing of 20 cm. The globe temperature was measured using a 38 mm globe thermometer, suspended near Line 2.

Two different types of heat flow meter were used to measure the heat flux of each wall to determine the energy balance. A portable heat flow meter (HFM-201) was used for the window and connected to a computer. The heat flow of the walls, floor, and ceiling was measured using heat flux sensors (MF-180) connected to a datalogger. The relative humidity of the indoor air was measured using three relative humidity sensors (NOVALYNX, 220-HMP155D), which were suspended along the middle line. Furthermore, the air velocity was measured at a local point using a three-dimensional ultrasonic anemometer (YOUNG-81000). The sensor was fixed at the midpoint below the panel.

The temperatures of the upper and lower panel surfaces were measured using thermocouples attached directly to the surface. Each surface of a panel had three measurement points, as shown in Fig. 3-3 (b). A compact electromagnetic flowmeter measured the flow rate (VN10R, Aichi Tokei Denki Co.,), and the inlet and outlet water temperatures were measured using PT100.

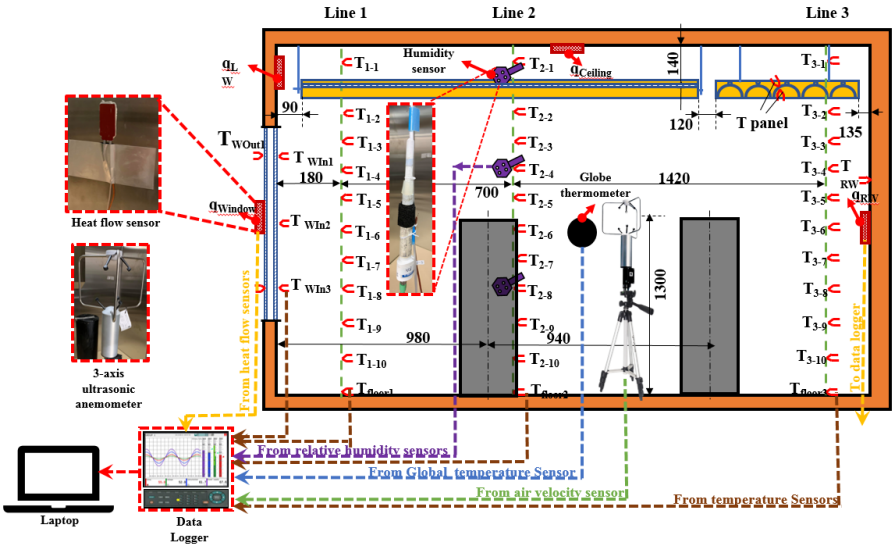

(a)

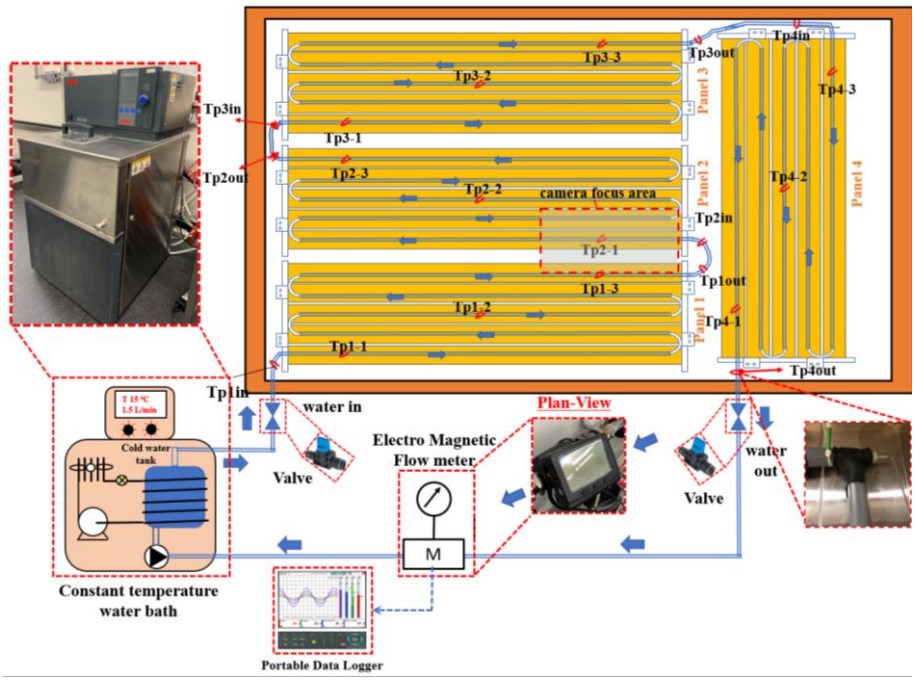

(b)

Fig. 3-3 Schematic diagram of the front view and photos of instruments

The primary variable of this study was the measured temperature, so the temperature sensors were calibrated against a standard thermometer measurement before they were fixed to the experimental setup. The absolute and relative error values of the measurement devices are listed in Table 3-2.

Table 3-2 Error of instruments

Experimental measurements	Device	Error
T_a, T_s, T_{op}	Thermocouple	0.2
T_{in}, T_{out}	PT100	0.19
Air velocity (v)	3-axis ultrasonic anemometer	1.00 %
Flow rate (G)	Flow sensor	0.5 %
Heat flux (q)	Heat flow meter	0.03/0.01
Current (I)/ Voltage (V)	Digital multimeter	0.09 %

3.2.3 Temperature measurement results

Fig. 3-4 shows a sample of the variation in panel surface temperature over time, which was recorded using an infrared thermal camera. After circulating cold water through the radiant panel, the panel surface temperature decreased significantly within the first 10 min, from 31.1 °C to 25.6 °C. After 20 min, the surface temperature stabilized at approximately 24.5 °C. Except for the small gap between each panel, there was a uniform temperature distribution pattern across the bottom surface of each panel.

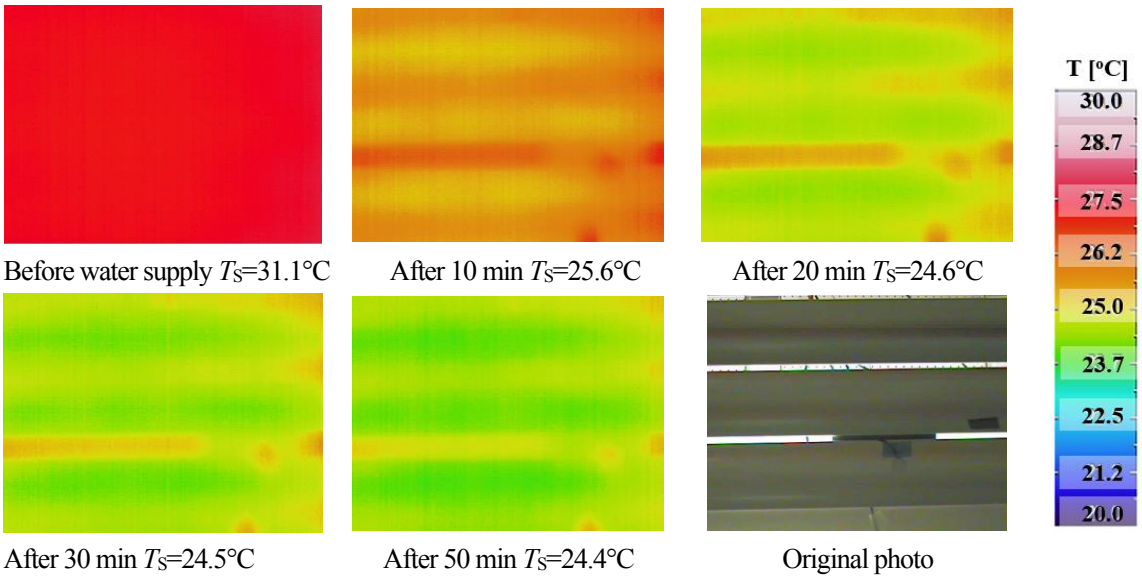

Fig. 3-4 Infrared images of the panel surface temperature distribution

Fig. 3-5 illustrates the indoor air temperature distribution. All the experimental cases resulted in a uniform temperature distribution in the chamber, and the temperature difference between the foot (Y=0.1 m) and head (Y=1.5 m) was approximately 0.3 K. When the flow rate was increased from 4 L/min to 8 L/min, the average air temperature merely decreased by approximately 0.6 °C. Reducing the inlet water temperature from 21 °C to 18 °C, lowered the average air temperature by approximately 1.5 °C.

Although the double glass had a low overall heat transfer coefficient (1.85 W/(m·K)), the indoor air temperature near the window was approximately 0.6 K higher than the average indoor air temperature, and 1 K higher than the temperature along line 3. The radiant ceiling panels could not prevent the hot air near the window from diffusing into the environment. Therefore, the RCP system needs to be optimized or integrated with other forced ventilation methods to eliminate the impact of the building envelope.

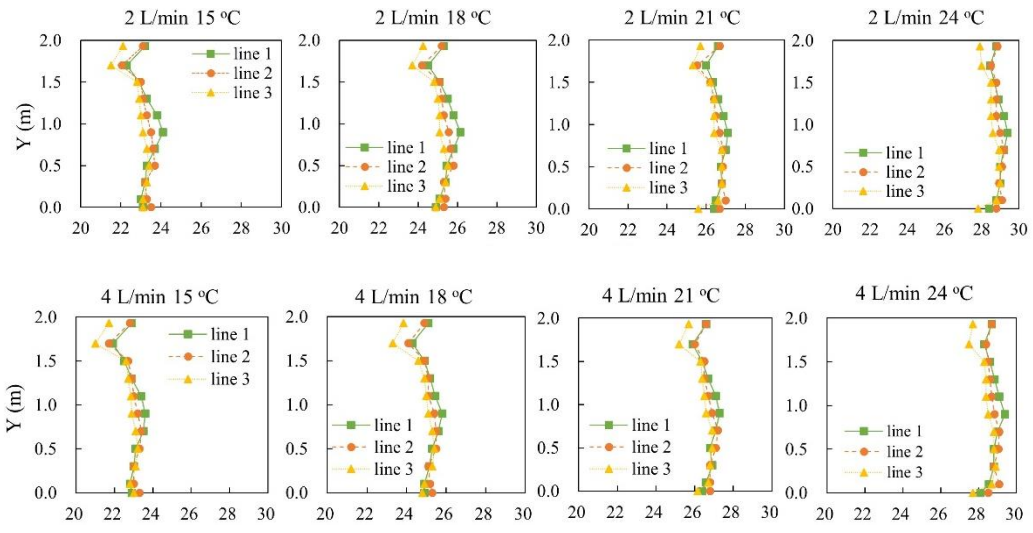

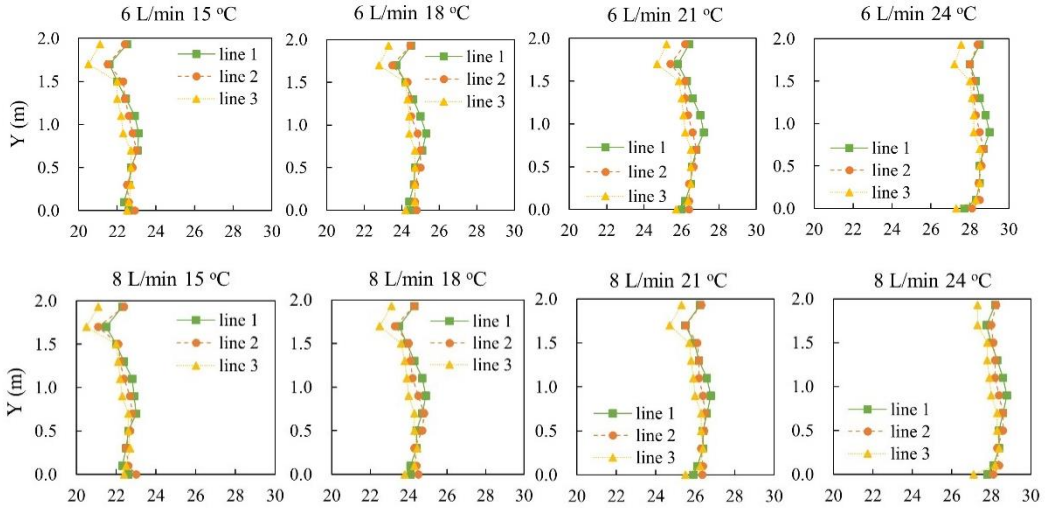

Fig. 3-5 Indoor air temperature variation in the Y-direction

3.2.4 Heat transfer analysis

The heat flux of the RCPs (q_{tot}) was calculated as the total heat flux through both the top and bottom of the panel surface, which was calculated using Eq. (3-1).

$$q_{tot} = \frac{Q_{tot}}{A_p} = \frac{C_p G \rho |T_{in} - T_{out}|}{A_p} \quad (3-1)$$

C_p is the specific heat of water (kJ/(kg·K)), G is the water flow rate (m^3/s), ρ is the density of water (kg/m^3), T_{in} and T_{out} are the inlet and outlet temperatures of the water flowing through the radiant panel tubes, and A_p is the projected area of the radiant panel (m^2).

The total cooling load is given by Eq. (3-2)

$$Q_{cl} = Q_{human} + Q_{window} + Q_{left\ wall} - Q_{other\ wall} \quad (3-2)$$

Q_{wall} is the overall rate of heat transfer through the surrounding walls, as measured by the heat flux sensors.

The heat absorbed by the radiant panel, calculated using Eq. (3-1), must be balanced with the net heat energy, calculated using Eq. (3-2). When the difference between these two values is very small or within an acceptable error value, the energy balance can be confirmed.

On the other hand, the total heat flux (q_{tot}) consists of the convective heat flux (q_c) and radiant heat flux (q_r). The q_r was calculated using the view factor ($F_{s\text{-}j}$) and radiation interchange factors ($F_{\varepsilon s\text{-}j}$) as well as the surface emissivity, according to Eq. (3-3).

$$q_r = \delta \sum_{j=1}^{n} \left((T_j + 273.15)^4 - (T_s + 273.15)^4 \right) \quad (3-3)$$

$F_{\varepsilon s\text{-}j}$ is the radiation interchange factor, which was calculated using Eq. (3-4). The view factor $F_{s\text{-}j}$ depends on the orientation of the surface, view angle, surface geometry, and distance between the surfaces. The resulting radiation interchange factors are listed in Table 3-3.

$$F_{\varepsilon_{s-j}} = \frac{1}{\frac{(1-\varepsilon_s)}{\varepsilon_s} + \frac{1}{F_{s-j}} + \frac{A_s}{A_j}\frac{(1-\varepsilon_j)}{\varepsilon_j}} \quad (3-4)$$

Table 3-3 The radiation interchange factors

$F_{\varepsilon s\text{-}j}$	$P_{1bottom}$	P_{1up}	$P_{2bottom}$	P_{2up}	$P_{3bottom}$	P_{3up}	$P_{4bottom}$	P_{4up}
Back wall	0.061	0.002	0.110	0.004	0.211	0.018	0.115	0.006
Front wall	0.240	0.024	0.134	0.005	0.076	0.002	0.135	0.007
Floor	0.273	0.000	0.296	0.000	0.269	0.000	0.250	0.000
Left wall	0.105	0.022	0.077	0.022	0.109	0.023	0.318	0.002
Right wall	0.099	0.003	0.108	0.003	0.101	0.003	0.101	0.063
Ceiling	0.000	0.891	0.000	0.902	0.000	0.896	0.000	0.867
Window	0.059	0.000	0.070	0.000	0.053	0.000	0.015	0.000

The surface emissivity (ε) of the walls, ceiling, floor, and panel surface is essential for calculating the radiant heat transfer coefficient and consequently the convective heat transfer coefficient. Therefore, an infrared camera (InfReC R550, *Nippon Electronics Co.,* Japan) was used to measure the emissivity of each surface. The stored emissivity value in this camera was changed iteratively until the measured surface temperature matched that measured with the thermocouple, for each surface. The values of surface emissivity are listed in Table 3-4.

Table 3-4 The results of surface emissivity

	Back wall	Front wall	Ground wall	Left wall	Right wall	Roof wall	Window	Panel surface
ε	0.94	0.94	0.94	0.94	0.94	0.94	0.94	0.96

The convective heat flux (q_c) was calculated as the difference between the q_{tot} and the q_r, as described by Eq. (3-5).

$$q_c = q_{tot} - q_r \quad (3-5)$$

After calculating the radiant and convective heat fluxes, the radiant heat flux coefficient (h_r) and convective heat flux coefficient (h_c) were calculated using Eq. (3-6) and Eq. (3-7).

$$h_r = \frac{q_r}{(AUST - T_s)} \quad (3-6)$$

$$h_c = \frac{q_c}{(T_a - T_s)}\frac{A_p}{A_s} \quad (3-7)$$

T_s is the panel surface temperature (°C) and T_a is the average air temperature (°C). *AUST* is the average unheated surface temperature (°C), and A_s is the surface area of the panel (m^2).

The analysis began with checking the energy balance between the cooling load inside the room and the cooling capacity absorbed by the fluid circulating through the tubes of the radiant ceiling panels. The analysis was carried out under steady-state conditions, so the energy stored within the indoor air space was negligible. The test room was also assumed to be well insulated without any external ventilation, and all openings and doors were well sealed, which prevented any possible infiltration. The energy balance was checked by calculating the cooling capacity and cooling load, including the heat of the window and cylindrical heat-generating dummies, to ensure experimental accuracy.

A comparison between the cooling load and cooling capacity is shown in Fig. 3-6. In all cases, the difference between the cooling load and cooling capacity was within 15 %. The cooling capacity changed significantly with variations in the inlet water temperature, while changing the flow rate had less of an impact. When the inlet water temperature was less than 21 °C, the flow rate significantly affected the cooling capacity. On the contrast, when the inlet water temperature was greater than 21 °C, the cooling capacity remained the same. The cooling capacity and flow rate did not exhibit a simple linear relationship, such as the relationship with inlet water temperature. The largest cooling capacity was obtained with a flow rate of 4 L/min.

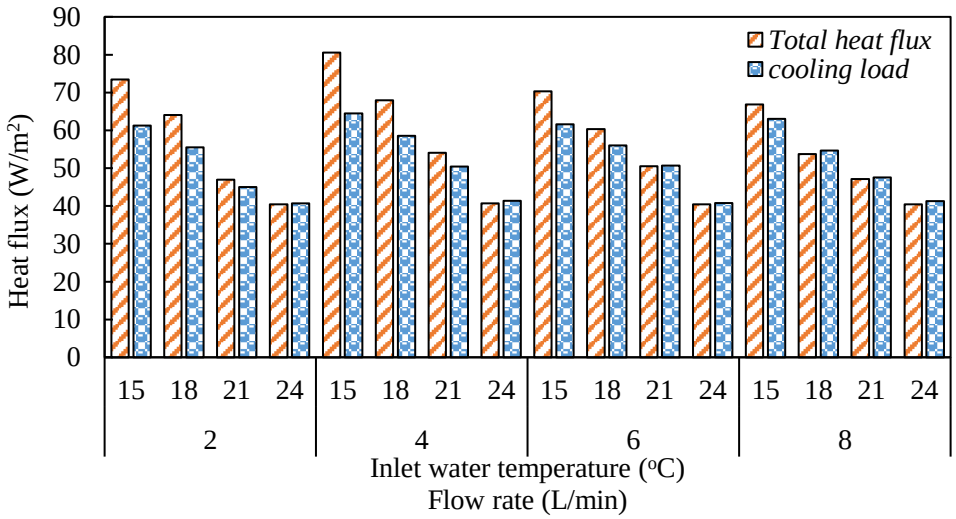

Fig. 3-6 Total heat flux and cooling load of the RCP under different operating conditions

The average temperature of the unheated surfaces (*AUST*) can also be calculated using the view factor, as shown in Eq. (3-8).

$$AUST = \sqrt[4]{\sum_{j=1}^{n} \left(F_{s-j} T_j^{\,4}\right)} \qquad (3-8)$$

The operative temperature T_{op} is roughly the average of the air and the *AUST*. It can also be calculated mathematically using Eq. (3-9).

$$T_{op} = \frac{h_c T_a + h_r AUST}{h_c + h_r} \qquad (3-9)$$

Fig. 3-7 shows the operative temperature (T_{op}), globe temperature (*GT)*, average air temperature, panel surface

temperature, and dew point temperature (*DPT*) in each case. The operative temperature was calculated using Eq. (3-9), while the globe temperature was measured with a globe thermometer hanging in the right chamber. The difference between the operative temperature and globe temperature was less than 0.67 K, so the error between these two temperatures can be ignored.

The average panel surface temperature increased with increasing inlet temperature and decreased with increasing flow rate. Therefore, the difference between the operative and panels' surface temperature decreased with increasing inlet temperature, from 4.2 K to 2.1 K. In addition, the panel surface temperature was always approximately 3.7 K, and the supply water temperature was 0.8 K higher than the dew point temperature. Therefore, there was no risk of dew condensation occurring during the experiments.

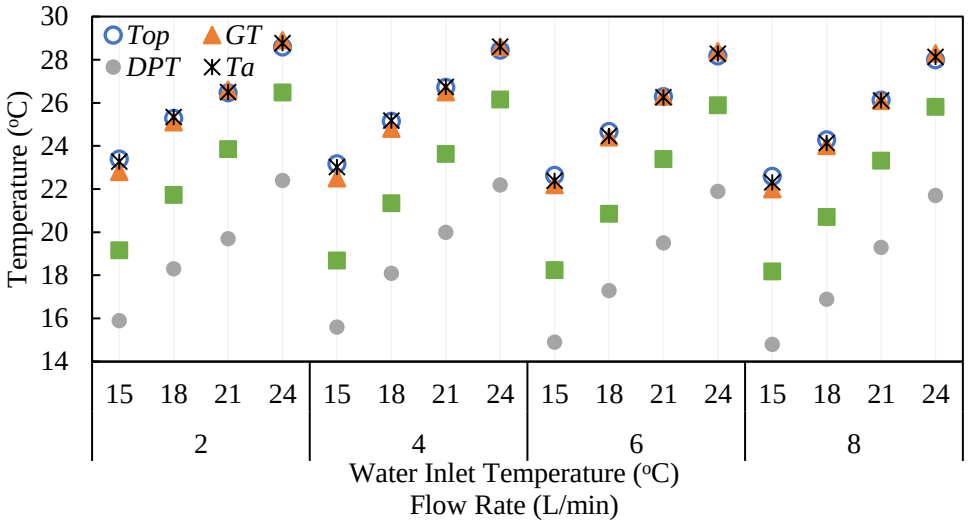

Fig. 3-7 The results of operative temperature, globe temperature and dewpoint temperature

Fig. 3-8 presents the convective and radiant heat fluxes transferred to the upper and lower panel surfaces under different operating conditions. Except in Case 1, the radiant heat flux accounted for more than half of the total heat flux. The ratio of the radiant heat flux increased by 10 % from 2 L/min to 8 L/min. In addition, the ratio of radiation was almost the same under the same flow rate.

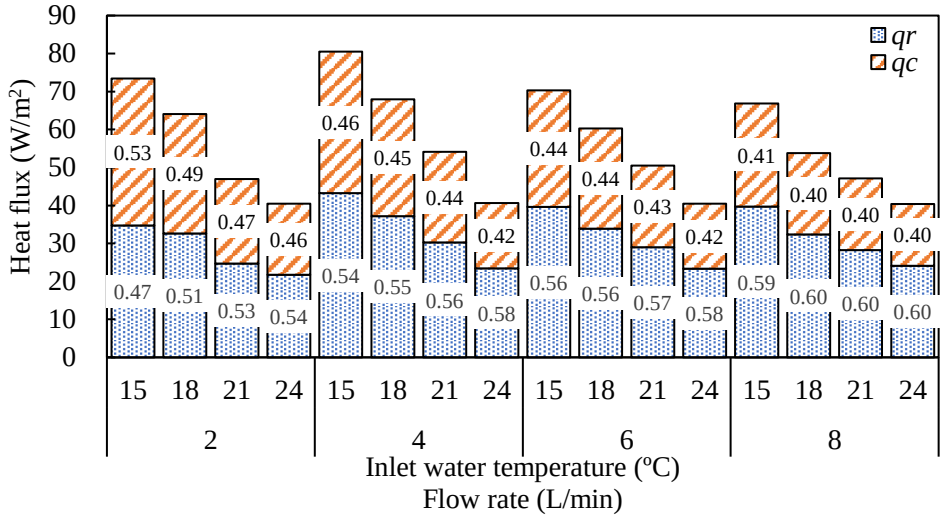

Fig. 3-8 Radiant and convective heat flux under different operating conditions

The results of radiant and convective heat transfer coefficients are shown in Fig. 3-9. The average h_r was 4.95 W/m^2·K and the average h_c value was 3.33 W/m^2·K. When the flow rate increased from 4 to 8 L/min, the average h_r and h_c decreased by 14 %. On the other hand, the h_r and h_c increased by 17 % with decreasing the inlet water temperature, when the flow rate was less than 4 L/min.

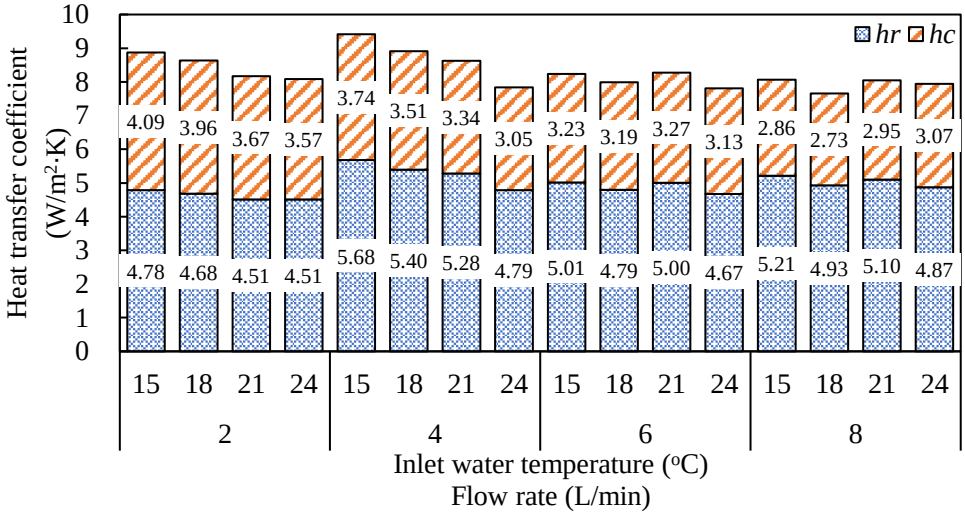

Fig. 3-9 Radiant and convective heat transfer coefficients under different operating conditions

The time constant, based on the indoor air temperature, is defined as the time required to change 63% of the total difference between its initial and final temperatures as shown in Fig. 3-10. The time constants for all the cases are summarized in Table 3-5. The cases with a higher flow rate and lower inlet water temperature always had higher time constant values.

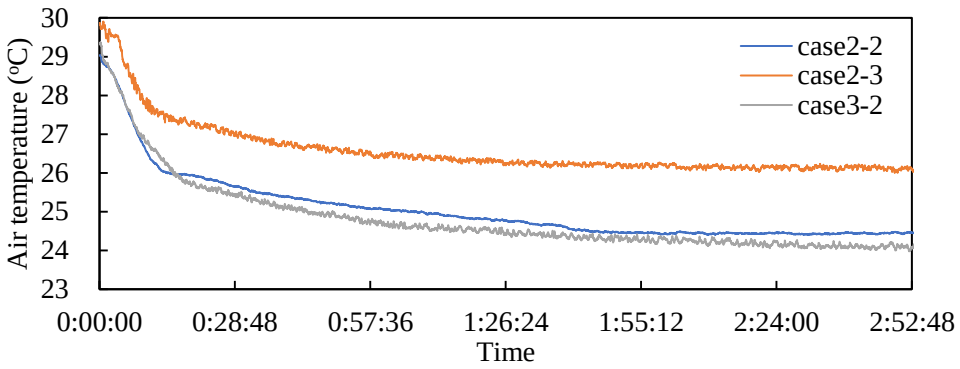

Fig. 3-10 Transient indoor air temperature

Table 3-5 Time constant under different operating conditions

G	T_{in}	Case	Time constant	G	T_{in}	Case	Time constant
2 L/min	15	1-1	15’01”	6 L/min	15	3-1	16’06”
	18	1-2	10’47”		18	3-2	15’21”
	21	1-3	10’33”		21	3-3	14’56”
	24	1-4	4’34”		24	3-4	4’20”
4 L/min	15	2-1	15’54”	8 L/min	15	4-1	17’03”
	18	2-2	12’33”		18	4-2	10’35”
	21	2-3	11’04”		21	4-3	07’55”
	24	2-4	4’11”		24	4-4	4’59”

Fig. 3-11 shows the relationship between the heat fluxes and the temperature difference. The radiant heat flux is linearly related to the temperature difference between the *AUST* and panel surface temperature, whereas the convective heat flux has an exponential relationship with the temperature difference between the indoor air temperature and panel surface temperature.

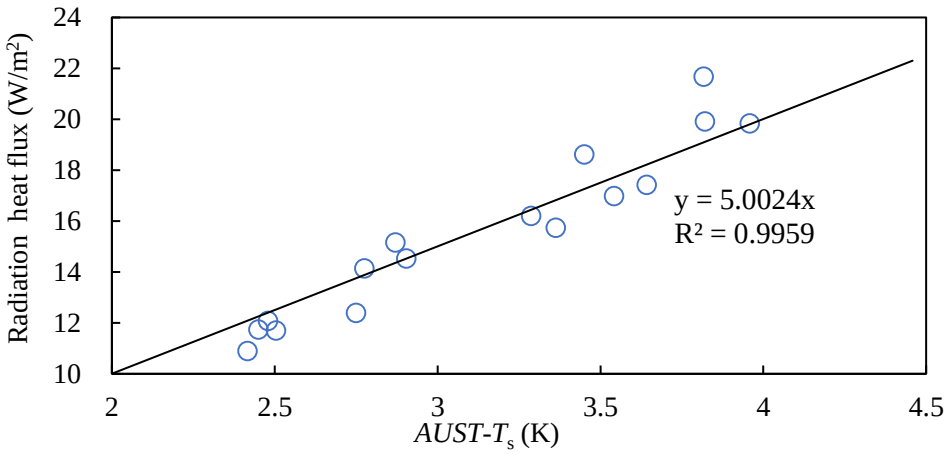

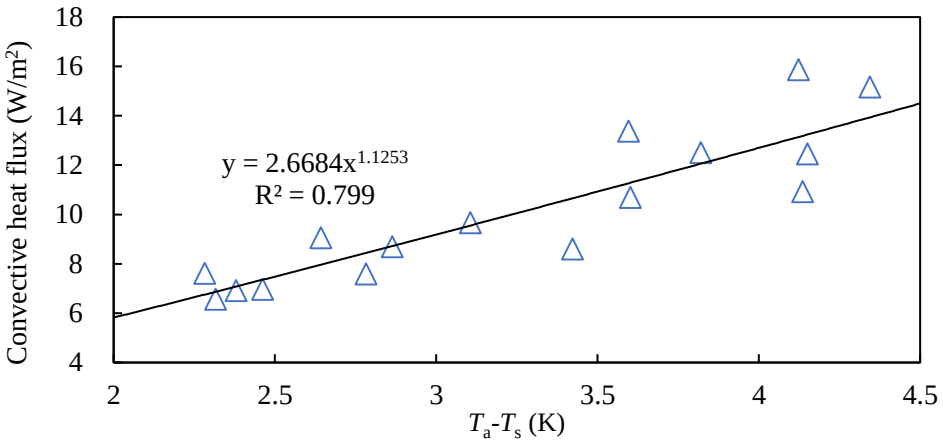

Fig. 3-11 Heat fluxes and their regression equations

Thus, the radiant and convective heat transfer coefficients can be determined from the regression equations in Fig. 3-11, as follows:

$$h_r = 5.0024 \quad (3-10)$$

$$h_c = 2.6684|T_a - T_s|^{0.1253} \quad (3-11)$$

3.2.5 Comparison with other open-type RCPs

After calculating the heat fluxes, the ratio of convection and radiation were compared with data from an open-type RCP with a flat surface and an open-type RCP with inclined fins. Fig. 3-12 presents a comparison of these ratios with data from the other studies. The open-type RCP with a segmented and concave surface proposed in this study resulted in the ratio of convection that was 21 % higher than that of the flat surface and 9 % higher than that of the inclined fins.

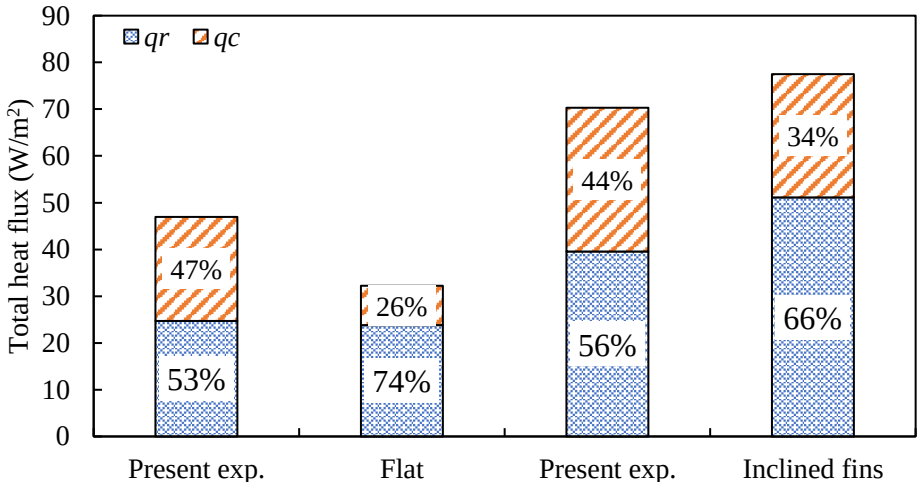

Fig. 3-12 Comparison of the total heat fluxes obtained with the curved and flat panels [14] and the panel with inclined fins [5]

Table 3-6 shows the heat flux of each panel. The RCP in this study resulted in a heat flux of 46.97 W/m^2 with a temperature difference of 2.7 K, which is 14.7 W/m^2 greater than the heat flux achieved with the RCP with flat surface. In the second group of comparison, the total heat flux is 70.06 W/m^2, which is close to that of the panel with inclined fins (77.51 W/m^2). However, the ratio between the surface area and the projected area of RCP in this study was 1.15:1, which was lower than that of the panel with inclined fins. This means that the concave shape allows the use of a smaller surface area to achieve the same improvement obtained with the RCP with inclined fins. Also, comparison on the heat flux clearly shows that the concave shape can enhance both the radiation and convection. The advantages of this panel have been confirmed.

Table 3-6 Comparison of radiant and convective heat transfer data in other studies

	Exp.	Flat [14]	Exp.	Inclined fins [5]
T_a-T_s (K)	2.7	2.7	4.1	4.1
q_r (W/m^2)	24.73	23.83	39.59	51.1
q_c (W/m^2)	22.24	8.43	30.74	26.41
q_{tot} (W/m^2)	46.97	32.26	70.33	77.51
h_c (W/m^2·k)	3.67	3.1	3.27	2.3
A_s/A_p	1.15:1	1:1	1.15:1	1.4:1

3.3. Field studies in an NZEB office building

3.3.1 Description of building and indoor space

The field studies were undertaken in a newly constructed office building (Fig.3-13), located in Sapporo, Hokkaido, Japan. The floor area of this building is 1949.58 m^2. Eight strings of 112 photovoltaic polycrystalline modules are installed between the south windows on the south wall to provide electricity to the lighting system. To reduce heat loss, the building envelopes are well insulated and covered with polystyrene foam plates. Table 3-7 summarizes the structure and heat transmission coefficients of each element. The windows use pairs of Low-E pair glass with argon gas. The area ratio of the window to the wall is 0.09 for the south and east, 0.04 for the west, and 0.02 for the north.

Fig.3-13 South view of the office building

Table 3-7 Heat conductivity and heat transmission coefficient of the building envelop

Elements	Material	Thickness (mm)	Heat conductivity λ (W/(m·K))	Heat transmission coefficient U (W/(m^2·K))
Exterior wall	Galvalume	0.4	45	0.24
	Polystyrene foam	110	0.028	
	Concrete	170	1.6	
Roof	Concrete	80	1.6	0.36
	Polystyrene foam	100	0.028	
	Concrete	170	1.6	
	Air layer	/	/	
Floor	Rock wool sound-absorbing board	12	0.17	0.40
	PVC floor tile	3	0.19	
	Concrete	15	1.6	
	Polystyrene foam	50	0.028	
	Air layer	/	/	
	Concrete	310	1.6	
	Base (Rocks)	150	1	
Window	Low-E glass	26	/	1.40

Fig. 3-14 illustrates the heating and cooling system used in this building, including open-loop groundwater heat pump (GWHP) system, open-type RCP system, and outdoor-air handling units. The groundwater is pumped through the two heat exchangers, which are maintained at approximately 12 °C at this site in the Sapporo region. During summer, a passive free-cooling mode is activated: the heat exchanger directly exchanges heat between the groundwater, RCP, outdoor-air handling units without using the refrigeration machine. In winter, the heat exchanger and heat pump chiller (MCRV-P450E; Mitsubishi Electric) are operated simultaneously. Because a single use of the heat exchanger cannot supply hot water at sufficiently high temperatures. The heat pump chiller is used to boost the cycle and further process the heat.

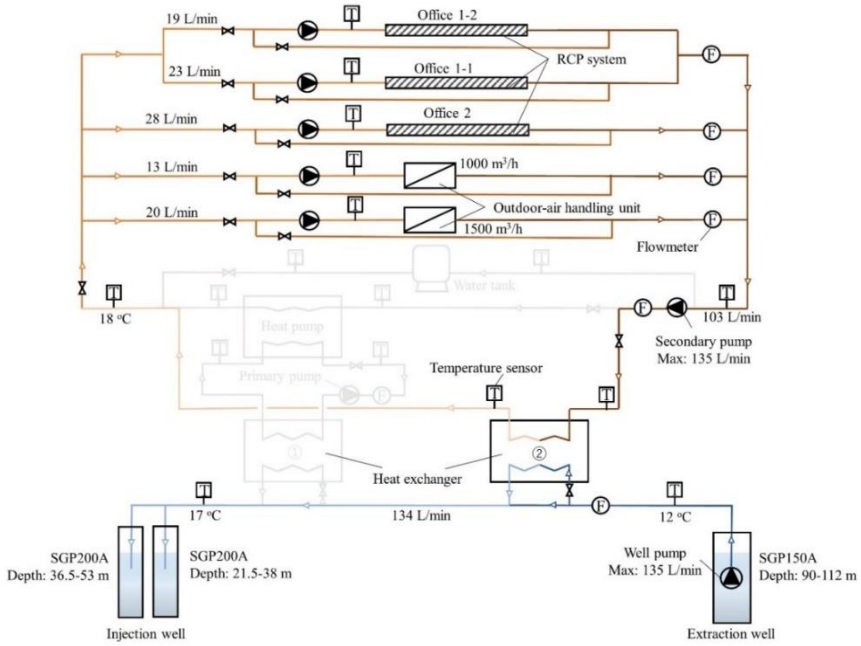

(a) summer

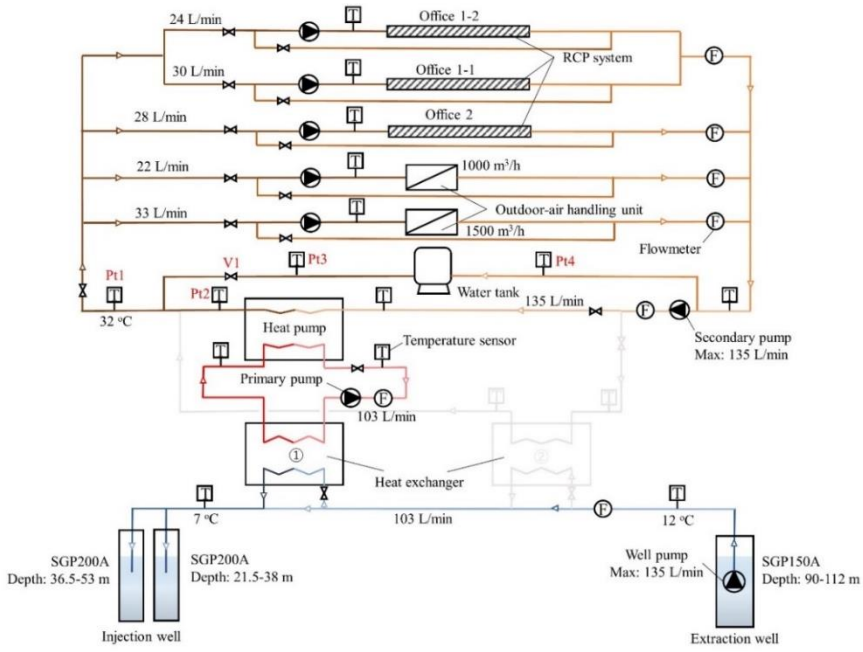

(b) winter

Fig.3-14 Schematic diagram of the heating and cooling system (a) summer (b) winter

In addition, all these systems are controlled via the Building Energy Management System (BEMS). It controls and monitors all the system's components and records a total of 167 variables every second. A schematic of the system control for each part is shown in Fig.3-15.

As shown in Fig.3-15 (a), the open-type RCP system comprised a supplying water loop and a circulating water loop, which were controlled by Valves 1 and 2, respectively. The operative temperature (T_{op}) is the average of the indoor air and wall temperatures. Ratio control was applied to valves to maintain the calculated T_{op} at 24 °C. For example, if the T_{op} exceeded 26 °C in summer, Valve 2 would be closed, and Valve 1 would be fully opened. As the T_{op} decreases, the open ratio of Valve 1 also decreases and that of Valve 2 increases. When the T_{op} reaches 22 °C, Valve 1 would be closed, and Valve 2 would be fully opened. According to these adjustments, the indoor temperature fluctuated at approximately 24 °C.

Fig.3-15 (b) and (c) illustrate the control of the GWHP system. In summer, the extraction well pump was adjusted to change the water flow rate and to maintain the outlet temperature of the heat exchanger at 18 °C. In winter, the groundwater was pumped via another loop, including a heat pump chiller and a water tank. The water tank was added to store and supply hot water to keep the temperature of the water supplied (Pt1) at 32 °C, under the condition that the heat pump outlet temperature (Pt2) be lower than 40 °C and the water tank outlet temperature (Pt4) was lower than 36 °C. This control aims to keep the heat pump operating under safe and highly efficient conditions. Otherwise, the heat pump outlet temperature would increase without control and cause system overload error.

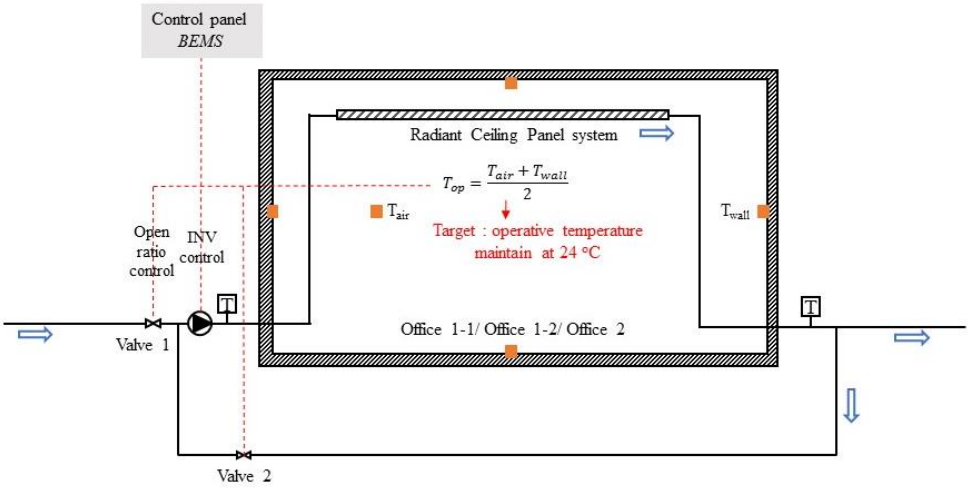

(a) RCP system

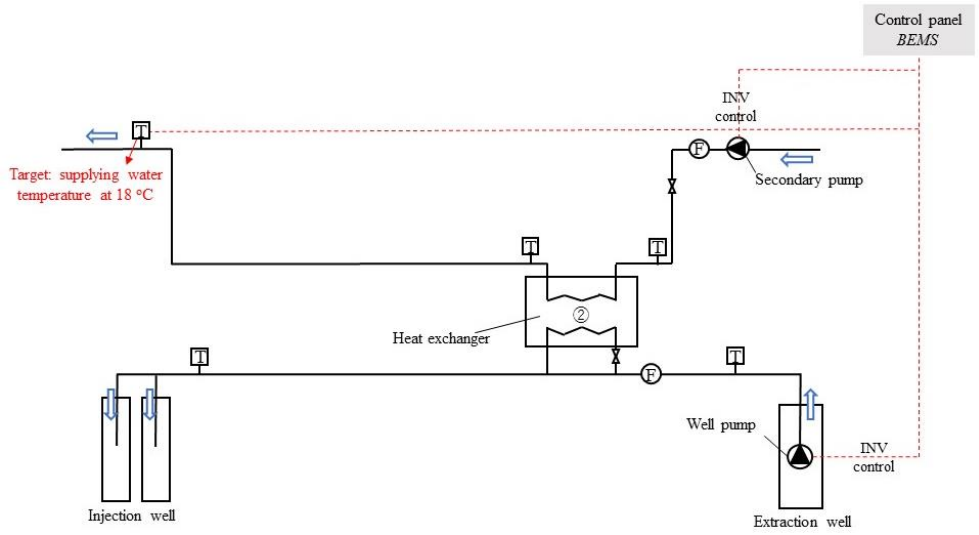

(b) GWHP system in summer

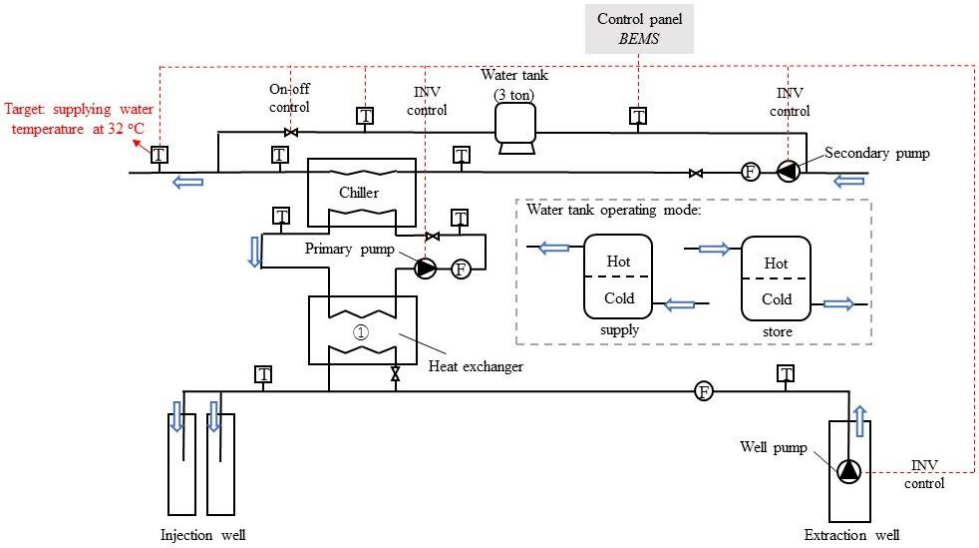

(c) GWHP system in winter

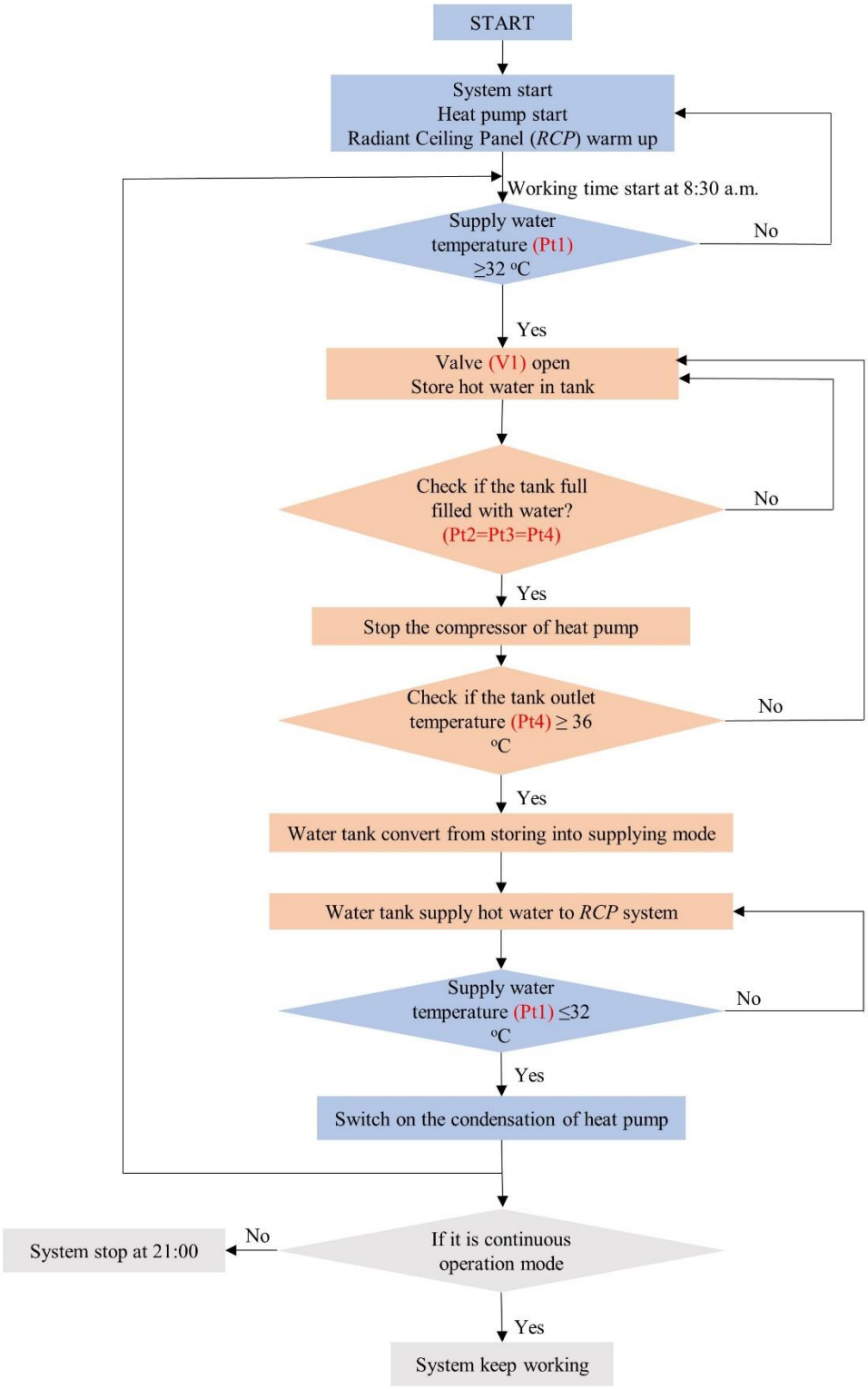

(d) Control process in winter

Fig.3-15 Schematic of the control of RCP and GWHP system

In this study, in situ thermal comfort measurements were conducted in an office (457.39 m^2) in the building. The office was equipped with the novel open-type RCP and displacement ventilation systems. As shown in Fig.3-16 (a), the panels were freely suspended 1.4 m beneath the ceiling and 2.7 m above the floor. They occupied over 200 m^2 of the ceiling area. The system was divided into two parts which were independently controlled using different water supply circuits. Fig.3-16 (b) shows the position and layout of the supply air and exhaust air diffuser. The displacement ventilation system delivers fresh air provided by the outdoor-air handling unit through the ceiling/floor supply air diffusers and extracts air from the ceiling exhaust air diffuser.

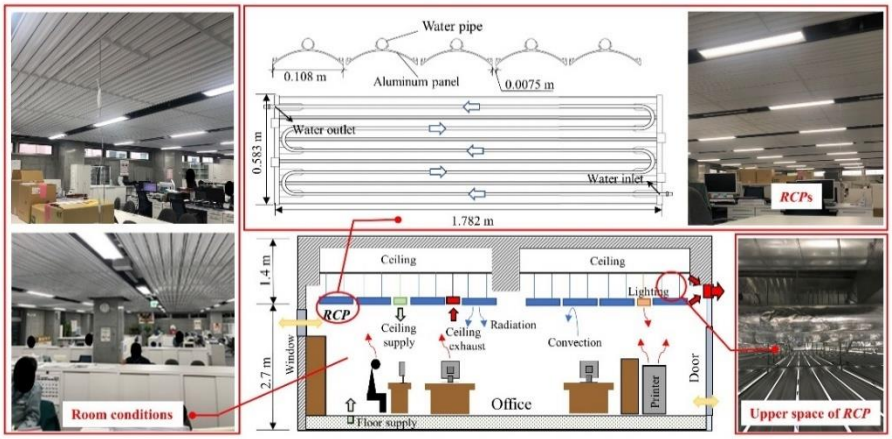

(a) Elevation view

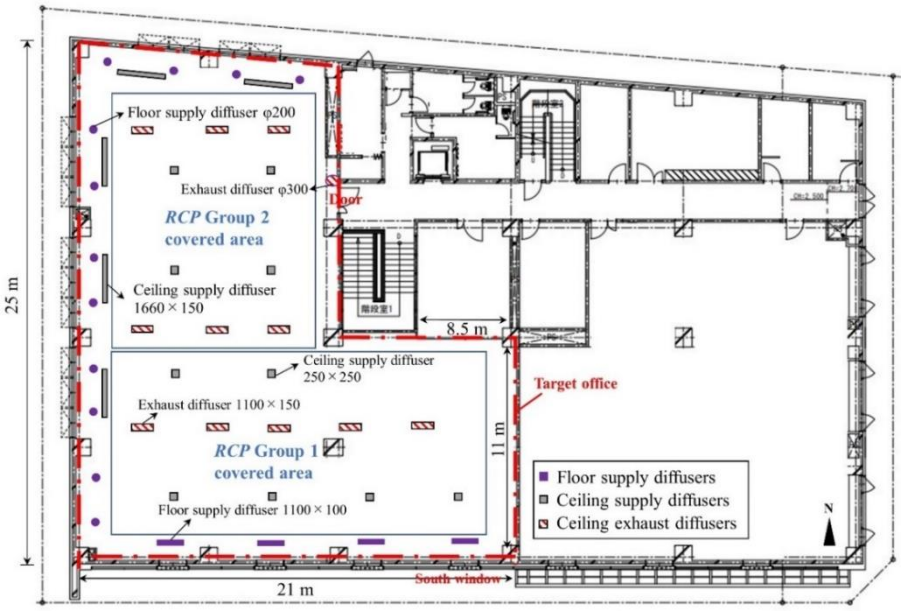

(b) Plan view

Fig.3-16 Elevation and plan view of the target office

The heating and cooling systems typically operate intermittently. They operate from 7:00 a.m. to 20:00 p.m. on workdays. This study verified the indoor thermal conditions of the usual intermittent operating mode during summer and winter. Moreover, a continuous operating mode was added during the winter season for comparison. The

operating methods and dates are summarized in Table 3-8.

Table 3-8 The operating method and dates

Operating method	Date
Intermittent	08/17–08/21/2020
Continuous	01/12–01/15/2021
Intermittent	01/18–01/20/2021

3.3.2 Research methods

In this study, physical measurements of the surrounding environmental conditions were conducted to evaluate indoor thermal comfort under the operation of the open-type RCP system. The experimental measurements of the indoor thermal conditions were recorded on 08/17–08/21/2020 and 01/12–01/20/2021. Simultaneously, staff members working in the office were invited to answer questions on thermal sensation and thermal comfort based on their experiences during the day.

The indoor air temperature was measured using 12 temperature sensors, which were hung in three lines fixed in the north, west, and middle of the office room, as shown in Fig.3-17. Two temperature sensors were attached to the top and bottom surfaces of the panel to measure the temperature of the panel surfaces. Two different colored globe thermometers were positioned at the height of a seated person (1.2 m) in the South and West Lines near the south and west windows. To accurately record the mean radiant temperature (*MRT*), a white solid globe thermometer was hung in the South Line, and a black solid globe thermometer was hung in the West Line. All temperature sensors were connected to data loggers (YOKOGAWA XL100) to record the temperature at 30 min intervals. In addition, the temperature data loggers were directly adhered to the surface of each wall, ground, and ceiling to measure the wall surface temperature and check the insulation effect on the envelope.

The uniform distribution of the panel surface temperature was also tested using an infrared camera (NEC TN9100) fixed on a stand (height 0.8 m) positioned near the south window. The camera was set on 08/19/2020, and it automatically took photos every hour from 8:30 a.m. to 5:30 p.m. CO_2 concentration in this office was measured using two CO_2 sensors hanging in the South and West Lines. The relative humidity sensors measured the indoor humidity at a height of 1.1 m in the three measurement lines.

Furthermore, Table 3-9 lists the error values of the temperature, flow rate, heat flux, CO_2 concentration, and humidity mentioned in the instrument's technical manual.

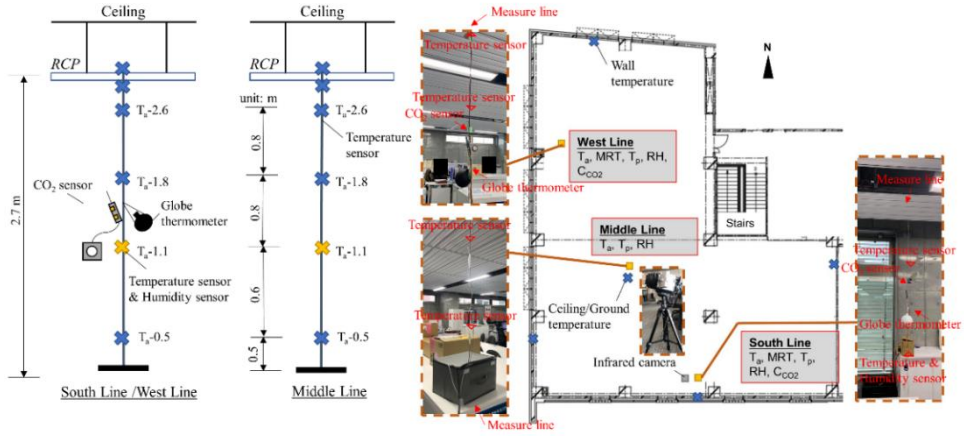

Fig.3-17 Schematic and photos of the physical measurements

Table 3-9 Error in the instruments used in this study

Experimental measurements	Device	Range	Error
T_{air}, T_s, MRT	T-type Thermocouple	-200–200 °C	±0.75%
T_{wall}	T&D TR51A	-40–80 °C	±0.5 °C
Wall heat flux	MF-180	Use condition: -20–120 °C	±2%
CO_2 concentration	GMP222 CO2 sensor	0–5000 ppm	±3.5%
Relative humidity	NOVALYNX 220-HMP155D	0–100 %RH	±1%
T_{in}, T_{out}	PT100	-50 -250 °C	±0.12%
Flow rate (G)	Electronic flowmeter	0.3 – 20 m/s	±0.5%

On the other hand, the surveys questionnaires were issued to analyze the thermal responses of the staff working in this office. The questionnaire comprised two sections to record subjective and objective measurements as follows:

(1) Section 1- Personal information: Staff members were requested to answer this section only once in advance. It included personal information, such as gender, age, physical characteristics, and working information (e.g., job characteristics, work clothing habits). In addition, the participants were asked to circle their working positions due to the separation of the RCP system.

(2) Section 2-Thermal perceptions of occupants: This section records the thermal perceptions of occupants, including thermal sensation votes (TSV) and thermal comfort votes (TCV), as shown in Fig.3-18. If they felt uncomfortable, or even slightly uncomfortable, they were invited to provide the exact reason for their response and the specific time when they felt uncomfortable.

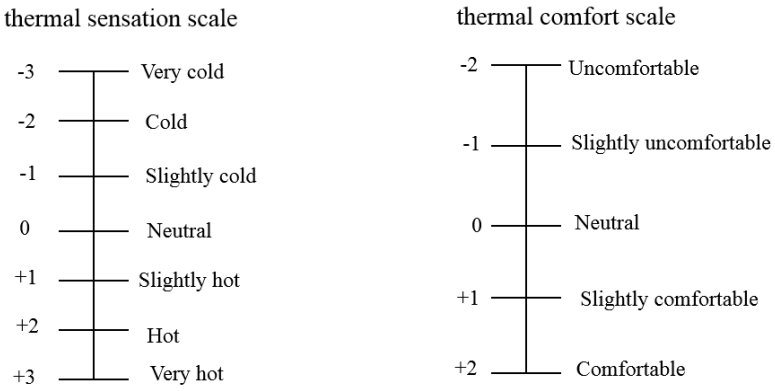

Fig.3-18 Scale of thermal sensation votes and thermal comfort votes

Part1: Personal question

Age: ☐20-30 ☐30-40 ☐40-50 ☐over 50
Gender: ☐Male ☐Female
Height: _____ kg
Weight: _____ cm

Part2: Questions for working style

Habit for clothing:
Top: ☐Short-sleeved shirt ☐Long-sleeved shirt ☐Suit ☐Other:_____
Under: ☐Lone-pants ☐Skirt ☐Other:_____
Frequency of going outside: ☐Never ☐Sometimes ☐Usually
The position of your desk: (*please circle your position on the figure*)

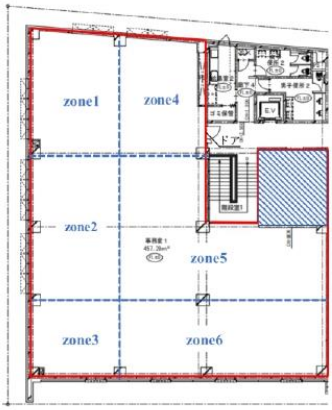

Are you sit near the walls: ☐Yes ☐ No
Are you sit near a window: ☐Yes ☐ No

Part3: Feelings about the panel

Satisfaction of the aesthetics of the novel radiant ceiling panel: ☐Like it ☐Hate it ☐Neutral
Recommend for the aesthetics of the panel:(*if you have any recommendation for the* aesthetics *of the panel, please write here*)

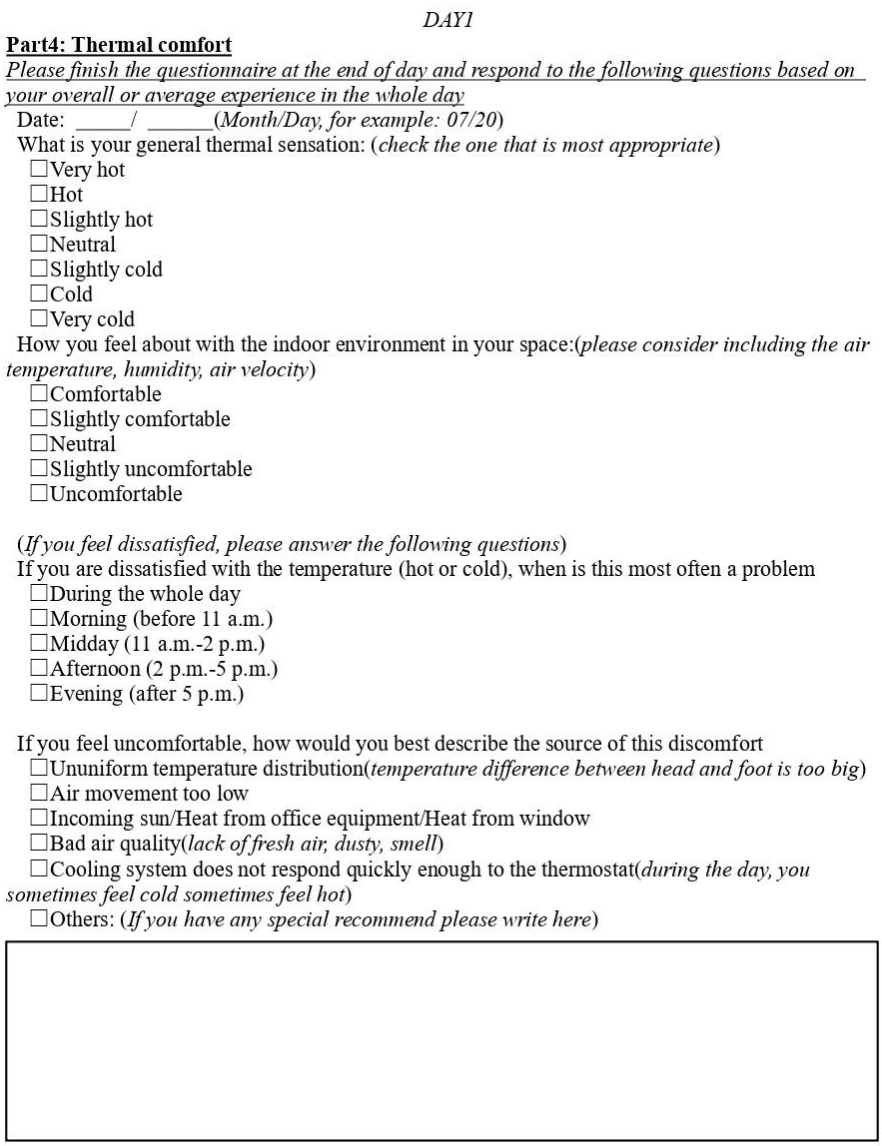

DAY1

Part4: Thermal comfort

Please finish the questionnaire at the end of day and respond to the following questions based on your overall or average experience in the whole day

Date: _____/ _____(*Month/Day, for example: 07/20*)

What is your general thermal sensation: (*check the one that is most appropriate*)

☐Very hot
☐Hot
☐Slightly hot
☐Neutral
☐Slightly cold
☐Cold
☐Very cold

How you feel about with the indoor environment in your space:(*please consider including the air temperature, humidity, air velocity*)

☐Comfortable
☐Slightly comfortable
☐Neutral
☐Slightly uncomfortable
☐Uncomfortable

(*If you feel dissatisfied, please answer the following questions*)

If you are dissatisfied with the temperature (hot or cold), when is this most often a problem

☐During the whole day
☐Morning (before 11 a.m.)
☐Midday (11 a.m.-2 p.m.)
☐Afternoon (2 p.m.-5 p.m.)
☐Evening (after 5 p.m.)

If you feel uncomfortable, how would you best describe the source of this discomfort

☐Ununiform temperature distribution(*temperature difference between head and foot is too big*)
☐Air movement too low
☐Incoming sun/Heat from office equipment/Heat from window
☐Bad air quality(*lack of fresh air, dusty, smell*)
☐Cooling system does not respond quickly enough to the thermostat(*during the day, you sometimes feel cold sometimes feel hot*)
☐Others: (*If you have any special recommend please write here*)

Fig. 3-19 Sample of questionnaires (English translated version)

In the end, after considering the accuracy and continuity of the answers, approximately 24 valid questionnaires were obtained and used for further analysis, and each answer was valid for at least 4 days. Personal information statistics are presented in Table 3-10.

Table 3-10 Statistics of age, height, weight, and insulation of participants

Gender		Age		Height (cm)	Weight (kg)	clo	
		20–40	Over 40			Summer	Winter
Male	20	6	14	168.6	66.2	0.51	0.68
Female	4	3	1	166.0	61.8	0.48	0.73
All	24	9	15	168.6	66.3	0.50	0.70

3.3.3 Measurement results

Fig.3-20 shows the overall average vertical indoor air temperature profiles of all the study days at the measurement positions - South, Middle, and West Lines. The grey lines represent the daily average of each study day. The maximum vertical temperature difference in the occupancy area (<1.8 m) is approximately 0.5 K in summer and 1.5 K in winter.

In the winter season, the air temperature in the South Line was approximately 2 K lower than that in the Middle and West Lines, as shown in Fig.3-20 (b), because the South and Middle Lines were in the area conditioned by the north loop group, and the West Line was in the area conditioned by the south loop group. The indoor temperature in blind areas of the office, such as the South Line, deviated by 2 K from the set value.

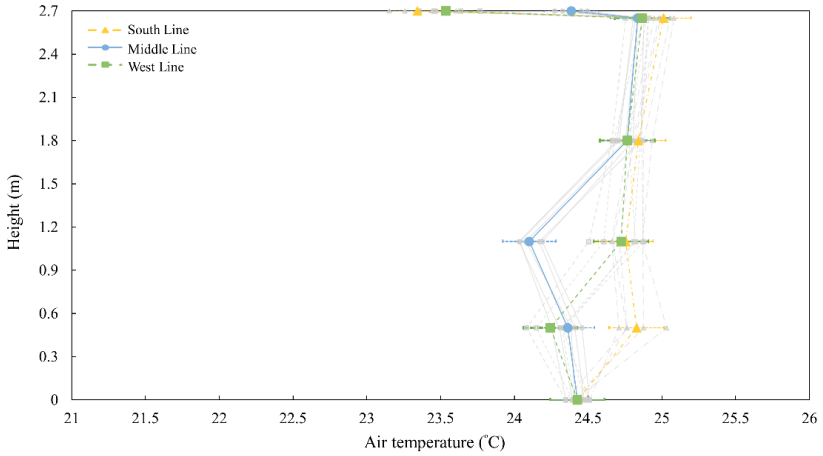

(a) summer

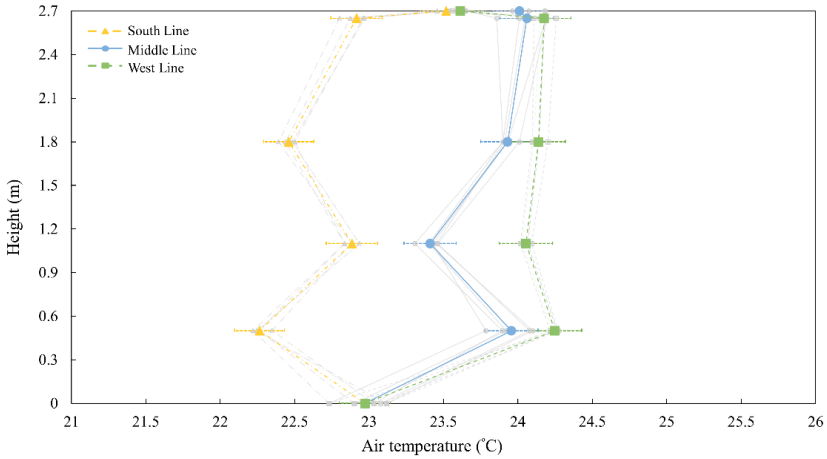

(b) winter

Fig.3-20 Vertical temperature distribution in the office

Real-time indoor and outdoor air temperatures are shown in Fig.3-21. The South, Middle, and West Line represents the average indoor air temperature at each measurement position, and the *MRT* is the temperature measured using globe thermometers. In summer, the indoor air temperature remained stable and varied around 24±1 °C. In winter, the system kept the indoor temperature stable at 23 °C±1 °C during the day. However, the indoor

air temperature significantly declines at night when the RCP system is turned off. This leads to a lower air temperature in the morning, owing to the system response delay. The *MRT* is merely 0.5 °C higher (black globe thermometer) or lower (white globe thermometer) than the air temperature due to the well-insulated envelope and slow indoor air movement.

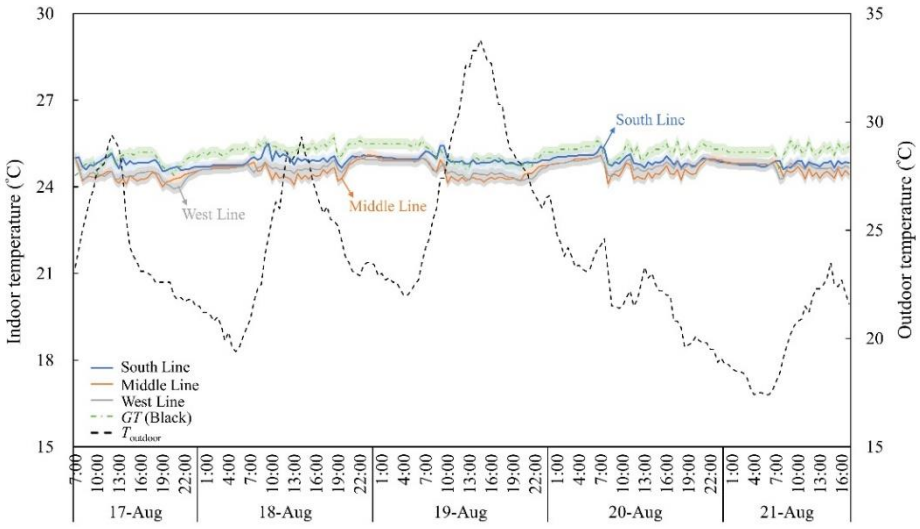

(a) summer, intermittent operation

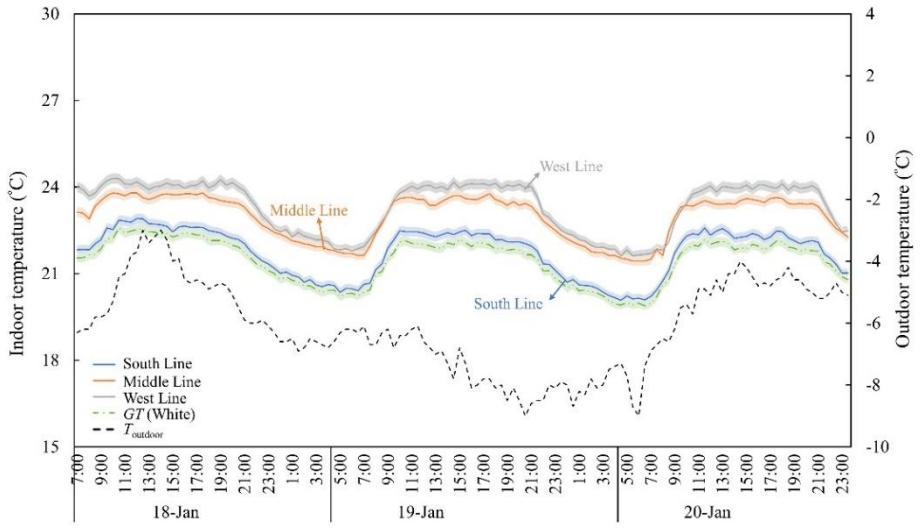

(b) winter, intermittent operation

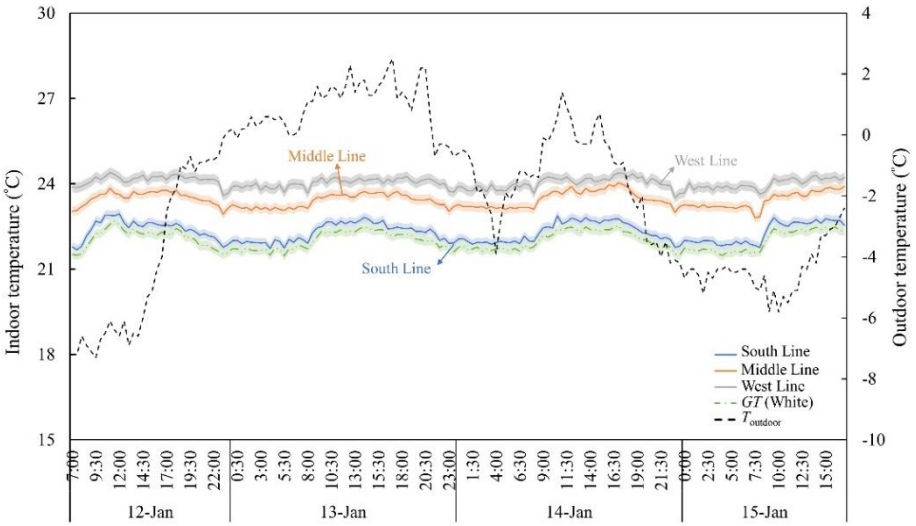

(c) winter, continuous operation

Fig.3-21 Variation in indoor air temperature with time in the office

Fig. 3-22 show the panel surface temperature at three measurement positions, two measurements recorded using BEMS, and the heat flux calculated based on the inlet/outlet water temperature and flow rate by Eq. (3-12).

$$q = \frac{\rho C_p G(T_{out} - T_{in})}{A} \qquad (3-12)$$

C_p is the specific heat of water (kJ/kg·K); G is the water flow rate (m^3/s); ρ is the density of water (kg/m^3); T_{in} and T_{out} are the inlet and outlet temperatures, respectively, of the water flowing through the tubes; and A_p is the projected area of the radiant panel (m^2).

In the RCP system, the panel surface temperature varied depending on the supply water flow rate, supply water temperature, and ambient conditions. In summer, the panel surface temperature was approximately 24 °C. However, in winter, the temperature varied in different measurement lines, where it was 23 °C in the South Line, 24 °C in the Middle Line, and 25.5 °C in the West Line. $BEMS_{Group1}$ and $BEMS_{Group2}$ are the BEMS's panel temperature measurement points that are located in the covered areas for different panel groups. The results show that the panel surface temperature for each panel group loop had a difference of 1.5 K. The possible explanation for this is that the RCP operation was independently controlled according to the indoor temperature measurements in each group zone. Notably, the panel surface temperature in the same panel group, also showed a difference of 1 K.

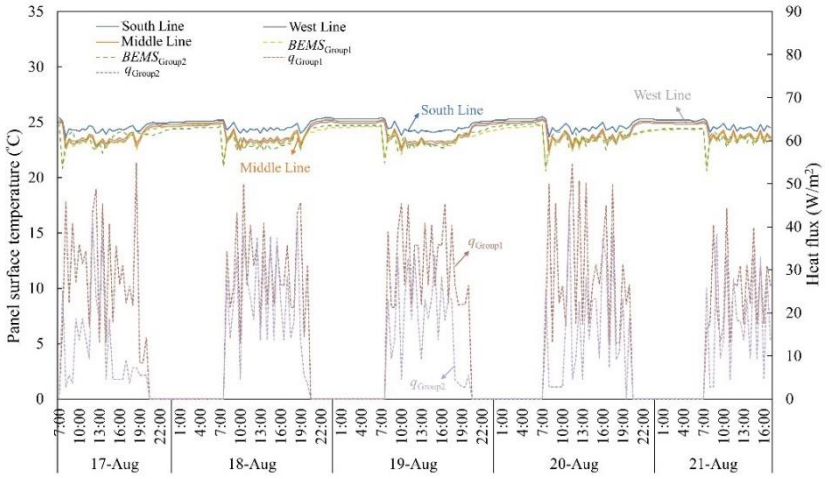

(a) summer, intermittent operation

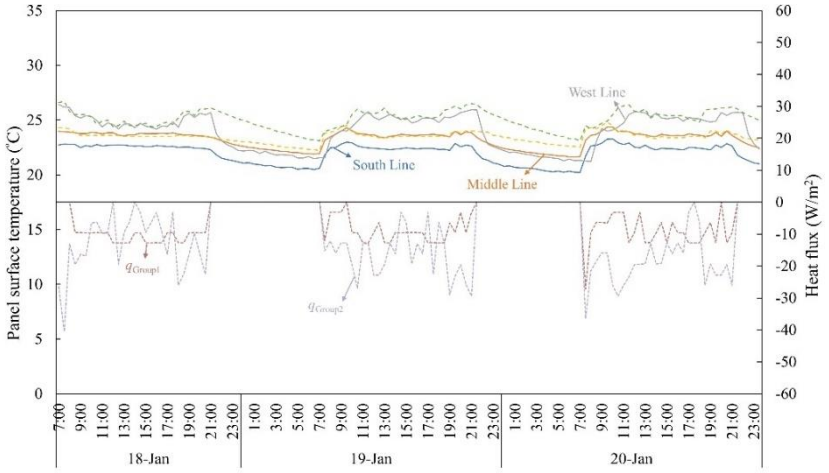

(b) winter, intermittent operation

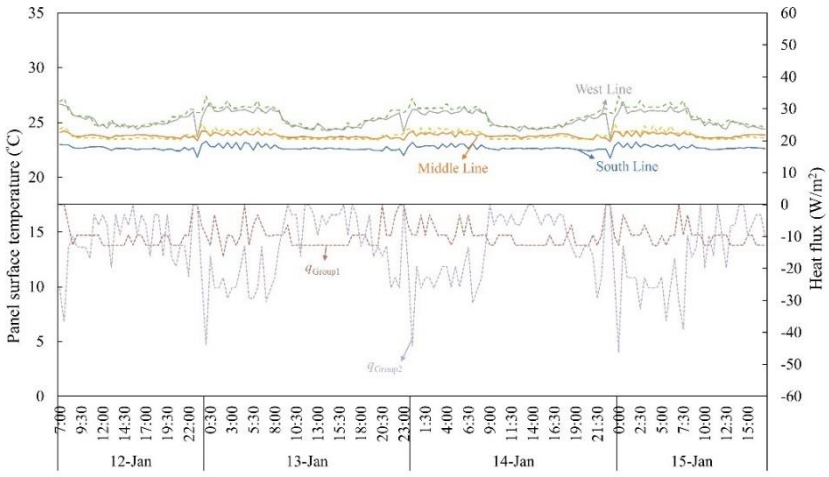

(c) winter, continuous operation

Fig.3-22 Panel surface temperature and heat flux in the office

Fig.3-23 shows the infrared images of the ceiling panel from 9:00 to 17:00 on Aug 19, 2020, during the summer. The light temperature was significantly higher than the surface temperature of the surrounding panel. Thus, the temperature difference was analyzed within area "*A*" without the effect of light. The minimum temperature was close to the measured panel surface temperature, whereas the maximum temperature originated from the gap between the panels. The difference between the maximum and minimum temperatures was less than 2 K because the panels were arranged tightly. It was concluded that the RCP system in the office could achieve a uniform surface temperature distribution. However, there was a significant temperature discrepancy between the two RCP system groups in the image at 10:00 a.m. because they were independent water supply systems, and the temperature difference between the two groups then disappeared with time.

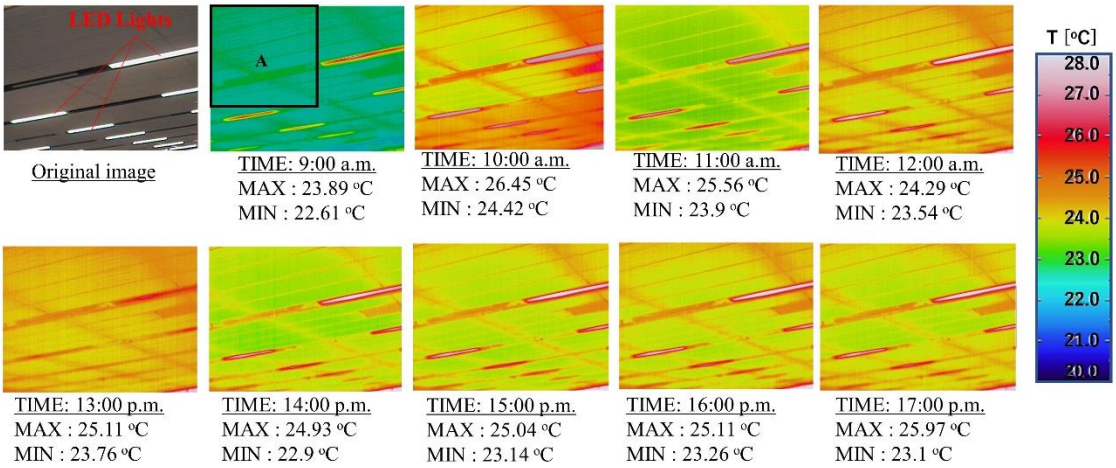

Fig.3-23 Infrared image of the *RCP* system

The box plot illustrates the variations in indoor and outdoor relative humidity during the study period (night data were also included). The indoor humidity in Fig.16 summarizes the average indoor humidity measured in the office. The indoor humidity was primarily controlled by the air processing unit and occasionally by natural ventilation in summer, as the RCP system could not remove latent heat. The outside humidity varied from 50% to approximately 95% in both summer and winter. However, the indoor humidity was stable at 55% in summer and 30% in winter. Compared with intermittent operation, continuous operation could maintain humidity within a narrow range. Nonetheless, the intermittent operation could satisfy the comfortable environment requirement range of 30–60%.

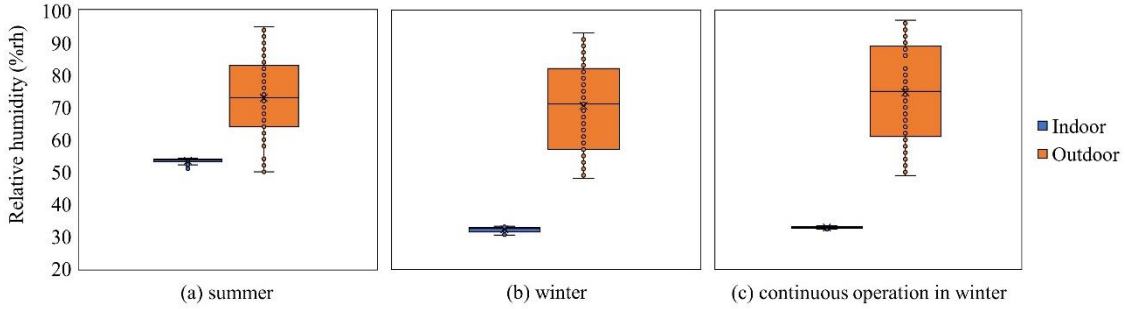

Fig.3-24 Boxplot of indoor and outdoor humidity

Fig.3-25 shows the variations in indoor and outdoor humidity in the summer. On sunny days in summer, the staff typically opens windows inside the office, as well as the clerestory windows of the penthouse on the top of the building. This might cause fluctuations in the indoor humidity measurements.

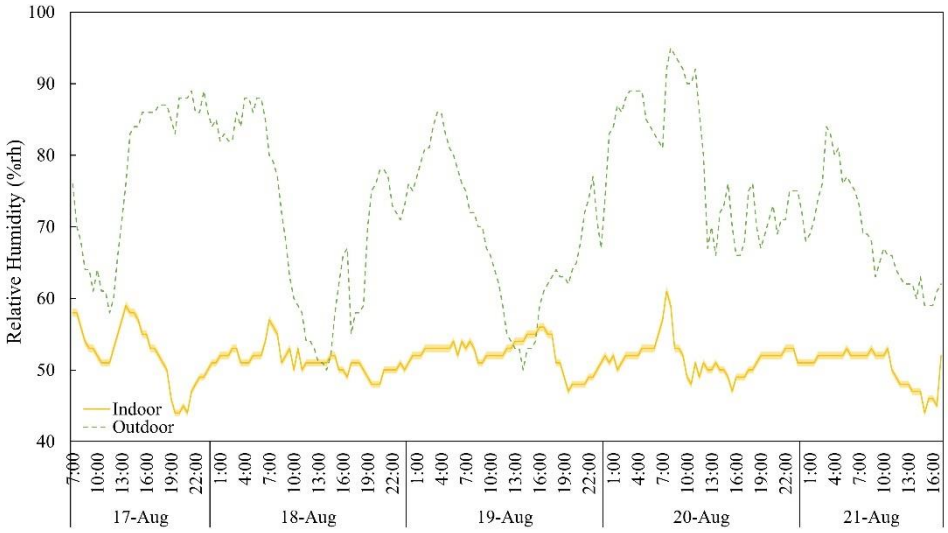

Fig.3-25 Humidity variations with time in summer

Fig.3-26 show the results of the CO_2 concentration measurement in the South and West Lines. Because the West Line was closer to the office desks, the CO_2 concentration there was always higher than that on the South Line. The CO_2 concentration was maintained below 1000 ppm to meet the required indoor air quality. The concentration gradually increased after 8:00 a.m. when the office staff enter and decreased after working hours. On winter and rainy days in summer, similar to what was seen on Aug 20, the windows were closed, and the usage of natural ventilation was kept at the lowest level. Thus, the concentration was higher than on days when natural ventilation was used (Aug 17–19). In addition, the CO_2 concentration always increased slightly around 15:00 p.m. in winter because it is the time when staff return to the office from the site. According to the results, it is recommended to adjust the ventilation system depending on the occupancy schedule and weather, rather than using a constant supply air flow rate.

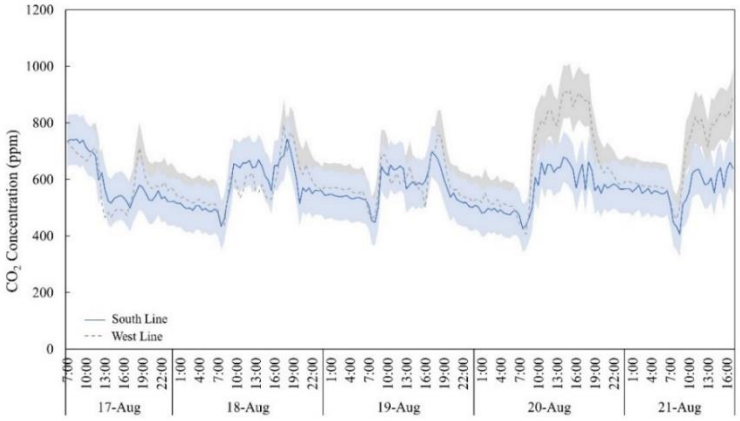

(a) summer, intermittent operation

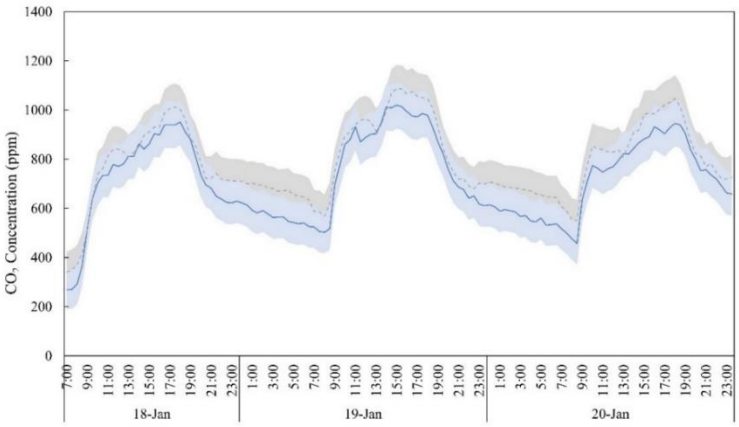

(b) winter, intermittent operation

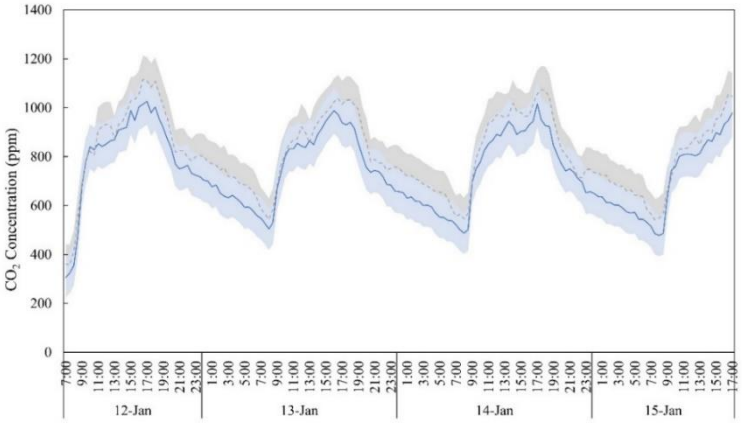

(c) winter, continuous operation

Fig.3-26 CO_2 concentration in the office

Fig.3-27 shows the results of the TSVs and TCVs from the survey questionnaire. The mean TSV was calculated as 0.15 in summer, -0.36 in winter and -0.16 during the period of continuous operation. According to the TCVs, it can be concluded that the RCP system can achieve the required comfortable indoor thermal condition in the office. Compared with the intermittent operation methods, continuous operation likely makes people feel slightly more comfortable, as the TSVs of the continuous operation were closer to zero.

However, 50% of the staff felt slightly hot, and 20% of the staff answered that they felt slightly uncomfortable with the indoor environment on August 19. The time at which the staff felt uncomfortable was primarily from 2:00–5:00 p.m. Briefly, 60% of the staff who felt slightly uncomfortable stated that high humidity was the major reason why they felt uncomfortable, while the other 10% blamed low air velocity as the major reason. When comparing the humidity with the recommendation from the standard and the former results of the other 4 days (Fig.3-25), the value was within the comfort range and was the same as on the other days. A possible explanation for this phenomenon might be that the slow air movement of the radiant system does not favor the efficient evaporation of sweat, which leads to a hot sensation and suffocating feeling. Thus, the uncomfortable feeling might be reduced by increasing the ventilation rate when the weather is hot.

In addition, the thermal comfort in the covered areas of different RCP groups was compared because of the

independent control strategy. Thus, it is also recommended to apply an advanced local control strategy to the RCP system rather than using the same and constant temperature setting.

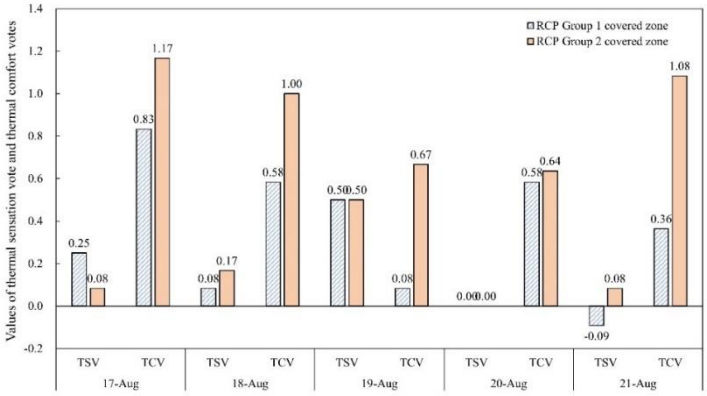

(a) summer

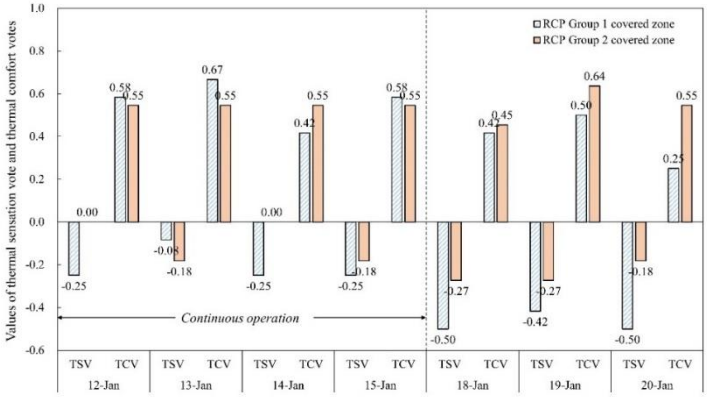

(b) winter

Fig.3-27 The results of *TSV* and *TCV* in the office

3.3.4 Analysis of the time constant

The thermal time constant (τ) of the building envelope was calculated using a simplified method [19][20] from the heat storage capacity of the storage mass (C_m, J/K), and the coupling thermal conductance coefficient of internal thermal mass (H_m, W/K), using the following simplified equation:

$$\tau = \frac{C_m}{3600 H_m} \qquad (3-13)$$

The heat storage capacity C_m was calculated by summing the heat capacities x_j (J/(m^3·K)) of all structural elements in direct thermal contact with the air inside the analyzed area. This is done using Eq. (3-13).

$$C_m = \sum x_j \cdot A_j \cdot d_j \qquad (3-14)$$

where A_j is the area of the elements (m^2) and d_j is the thickness of the elements (m).

The coupling thermal coefficient of the internal thermal mass H_m was calculated using the following equation:

$$H_m = H_{tr} + H_{ve} \qquad (3-15)$$

where H_{tr} is the thermal conductance from transmission, and H_{ve} is the thermal conductance from ventilation. In addition, H_{tr} is the thermal conductance from transmission, which is a specific characteristic of the building envelope, and can be represented by the thermal transmission coefficient U-value (W/(m^2·K)). H_{ve} is the thermal conductance from the ventilation, which is evaluated using the following equation:

$$H_{ve} = \rho_a \cdot C_a \cdot q_{ve} \quad (3-16)$$

where ρ_a·Ca is the heat capacity of the air volume, which is equal to 1200 J/(m^3·K), and q_{ve} is the flow of air in the conditioned space (m^3/s).

Finally, Table 3-11 summarizes the characteristics of the envelope of the target office, and the parameters calculated using Eq. (3-13) - Eq. (3-16).

Table 3-11 Thermal time constant of the target office

	Exterior wall	Roof	Target office
A (m^2)	141.36	457.39	
C_m (kJ/K)	49081	214224	263305
U (W/(m^2·K))	0.24	0.36	
H_{tr} (W/K)			198.6
H_{ve} (W/K)			616.7
H_m (W/K)			815.3
τ			89.7

The time constants of the indoor air and panel surface temperatures were calculated based on the measurements. Table 3-12 presents the calculated results of the time constant (τ) of the indoor air at each measurement position after the system started operating on August 19 and January 19. The time constant was given as a requirement to change 63% of the total difference between the initial and final temperatures. The average time constant of the indoor air temperature was 56 min in the summer and 1 h 52 min in the winter.

Table 3-12 Time constant of the indoor air temperature

		Start temperature (°C)	End temperature (°C)	τ
Summer	South Line	25.2	24.9	1:04
	Middle Line	24.9	24.5	0:52
	West Line	25.0	24.5	0:54
Winter	South Line	20.6	22.5	1:59
	Middle Line	21.6	23.6	1:44
	West Line	21.9	23.8	1:54

Table 3-13 shows the time constant of the panel surface temperature when the system started at 7:00 a.m. on August 19 and January 19. The average time constant of the indoor air temperature was 51 min in summer and 1 h 13 min in winter.

Table 3-13 Time constant of the panel surface temperature

		Start temperature (°C)	End temperature (°C)	τ
Summer	South Line	25.4	24.5	0:50
	Middle Line	25.1	23.5	0:50
	West Line	25.2	23.7	0:53
Winter	South Line	20.6	22.9	1:08
	Middle Line	21.9	24.0	0:57
	West Line	21.5	24.4	1:35

3.3.5 Analysis of the energy consumption

Table 3-14 summarizes the system performance and energy consumption of the RCP system and GWHP system in winter to compare the intermittent and continuous operation methods. The total electric power consumption was 160 kWh/day in intermittent operation, which was lower, by approximately 19 kWh, than that under continuous operation. However, the heat pump performance was better when using the continuous operation mode because the COP was higher than the intermittent operation mode. The COP and SCOP were calculated using the following equations:

$$COP = \frac{\sum Q_{out}}{\sum E_{HP}} \quad (3-17)$$

$$SCOP = \frac{\sum Q_{out}}{\sum \left(E_{HP} + E_{WP} + E_{cp1} + E_{cp2} + E_{RCP} \right)} \quad (3-18)$$

According to the law of the Carnot cycle, the ideal COP can be expressed by dividing the condensing temperature by the difference between the condensing and evaporating temperatures. Thus, the heat pump efficiency generally increases with increasing evaporation temperature. Consequently, the COP during continuous operation increased by approximately 10% as the evaporating temperature increased.

The comparison between continuous and intermittent operations shows that different operation methods lead to different performances. A suitable operation mode has great potential to save more energy while maintaining indoor thermal conditions in a more comfortable zone. Therefore, it is necessary to optimize the operating conditions and control methods in future studies.

Table 3-14 Comparison between continuous and intermittent operations in winter

		Continuous operation	Intermittent operation
Date		2021.01.12-01.15	2021.01.18-01.20
Total heating time (h)		87.8	46.9
Heat transfer amount (kWh)		2196.3	1404.4
Heating capacity (kW)		25.0	29.9
Energy consumption	Heat pump (kWh)	525.5	364.1
	Well pump (kWh)	51.8	31.9
	Primary pump (kWh)	12.7	8.0

Secondary pump (kWh)	9.9	6.3
Water circulating pump (kWh)	79.3	42.9
Total electric power consumption (kWh)	714.9	480.10
COP	4.18	3.86
SCOP	3.07	2.93
Indoor air temperature in target office (°C)	23.4	23.2
Condensation outlet temperature (°C)	34.2	33.0
Evaporator outlet temperature (°C)	6.5	4.8
Well backwater temperature (°C)	9.0	8.6
Secondary circulating flow rate (L/min)	85.5	93.5
Primary circulating flow rate (L/min)	84.1	84.1
RCP system circulating flow rate (L/min)	111.1/85.4	110.8/84.9
Well pumping flow rate [L/min]	77.1	82.7

Fig.3-28 illustrates the monthly average indoor air temperature and electric energy consumption of each part, including air conditioning, ventilation, lighting, hot water, elevator, and power generated by solar PV during 2019 and 2020. The energy consumption of the heating and cooling system accounted for 48% of the total annual energy consumed, and more than 60% of that from December to March. This also results in an evident increase in total energy consumption during winter. However, the energy consumption was lowest in May and June, as the outside temperature was neither hot nor cold, thus the air-conditioning system was used less. Moreover, the energy consumption of ventilation had almost doubled from 1,256 kWh (2019) to 2,189 kWh (2020) owing to the impact of the COVID-19 epidemic.

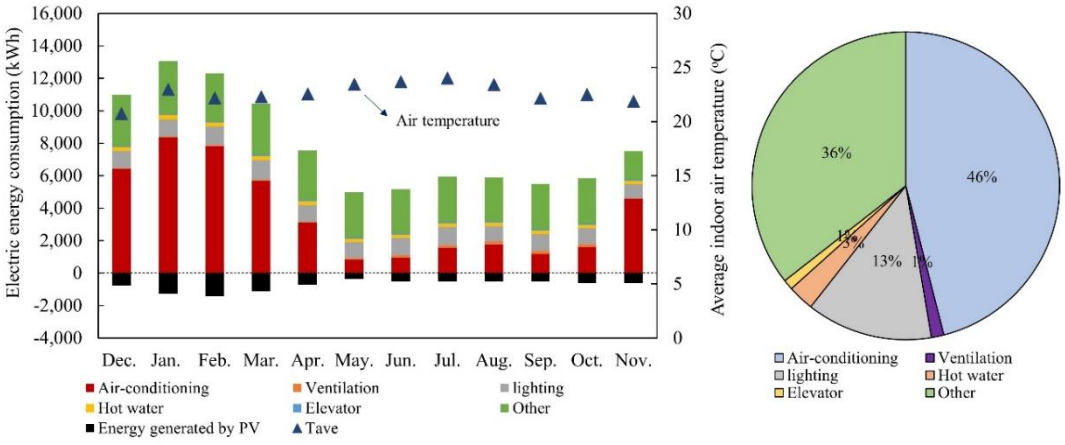

(a)

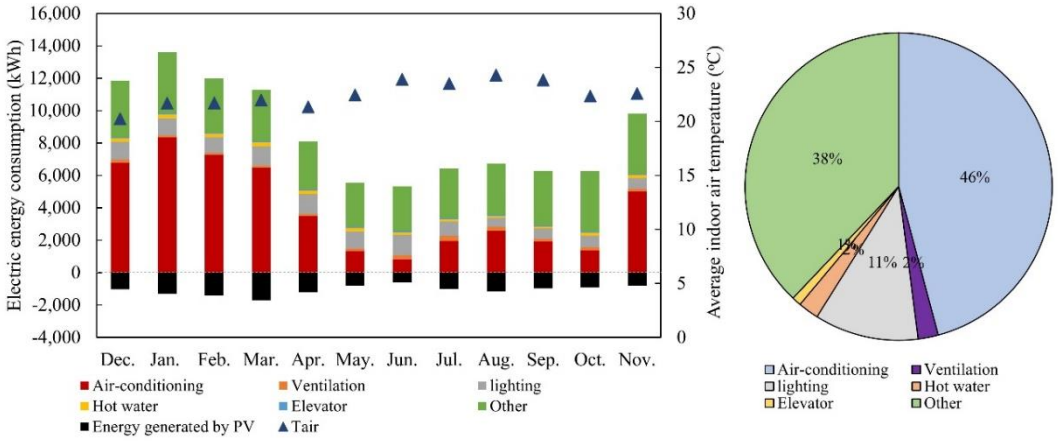

(b)

Fig.3-28 Annual electrical energy consumption of the office building in (a)2019 and (b)2020

Table 3-15 summarizes the primary energy consumption during 2019 and 2020, which was calculated based on the total electrical energy consumption. The conversion between electric energy and primary energy in energy-saving standards was 9,970 kJ/kWh during the day and 9,280 kJ/kWh at night in Japan. The results were then compared with the primary energy consumption of the reference according to the 'ZEB definition' [21] in Japan, and with the primary energy consumption estimated at the design stage. The standard calculation methods of the primary energy consumption for the reference and design were prescribed according to the Japanese law published in 2016 [22]. The primary energy consumption of the reference building EST (GJ/year) is calculated by the following equation:

$$E_{ST} = (E_{SAC} + E_{SV} + E_{SL} + E_{SHW} + E_{SEV} + E_m) \times 10^{-3} \quad (3-19)$$

where E_{SAC}, E_{SV}, E_{SL}, E_{SHW}, E_{SEV}, and E_m are the reference primary energy consumptions of air conditioning, ventilation, lighting, hot water, elevator, and others respectively. The calculation was mainly based on the proposed standard values in the law.

Taking E_{SAC} (MJ/year) as an example, the primary energy consumption of the air conditioning E_{SAC} is calculated using Eq. (3-20).

$$E_{SAC} = \sum_{r=1}^{n} (a_{SAC,r} \times A_r) \quad (3-20)$$

where A_r is the room area (m^2) and $a_{SAC,r}$ is the standard primary energy consumption per floor area ($MJ/m^2 \cdot year$) proposed depending on the region, zone, and room type. In addition, the reference building located in Region No.2 in Japan is assumed to use the traditional air source heat pump with COP of 3.24 in summer and 2.74 in winter.

Table 3-15 Regional classification in Japan

Region No.	Total heat loss U_a [W/(m^2·K)]	Solar heat gain coefficient η_{AC} [-]
1 2	0.46	-

3	0.56	
4	0.75	
5		3.0
6	0.87	2.8
7		2.7
8	-	3.2

The primary energy consumption of the building at the design stage E_T (GJ/year) was calculated using Eq. (3-21).

$$E_T = (E_{AC} + E_v + E_L + E_{HW} + E_{EV} - E_{PV} - E_{CGS} + E_m) \times 10^{-3} \quad (3-21)$$

Where E_{AC}, E_V, E_L, E_{HW}, E_{EV}, and E_m are the primary energy consumptions of air conditioning, ventilation, lighting, hot water, elevator, and others, respectively, at the design stage. E_{PV} is the reduction in primary energy consumption using solar energy equipment. E_{CGS} is the reduction in primary energy consumption using cogeneration systems.

Each part of the energy consumption was calculated based on the building design itself. The following calculation flowchart shows the calculation of the primary energy consumption of air conditioning at the design stage E_{AC}.

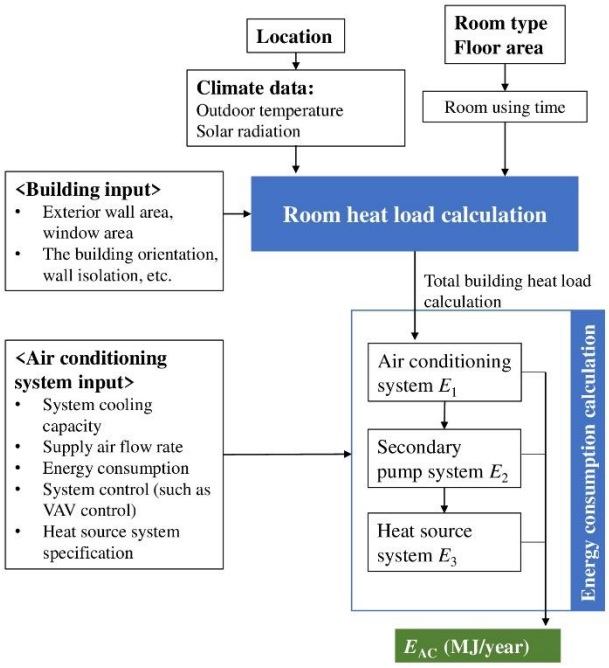

Fig. 3-29 The primary energy consumption calculation flow chart of air conditioning E_{AC}

The calculations were conducted based on the specifications of each part of the system. For example, at the design stage, the specified cooling capacity and electric consumption of the heat pump chiller (MCRV-P450E, Mitsubishi Electric Corporation) were 45 kW and 11.1 kW, respectively.

As a result, the total consumption decreased by 69% in the first year and 66% in the second year, compared with the reference. Nevertheless, the energy consumption, particularly that of the air-conditioning system, should be

further reduced and targeted to achieve the next level of being nearly-ZEB.

Table 3-16 Primary energy consumption

	Reference (GJ/year)	Design (GJ/year)	2019 (GJ/year)	2020 (GJ/year)
Air-conditioning	1249	528	427	462
Ventilation	65	53	12	21
lighting	574	138	123	110
Hot water	23	37	26	22
Elevator	24	21	10	10
Solar energy		-141	-86	-126
Other	368	368	330	382

3.3.6 Economic study and discussion of building envelope

The building energy system was also examined financially in terms of cost-effectiveness, by calculating simple payback period according to the following equations.

$$Payback\ period = \frac{Initial\ investment}{Cash\ inflow\ per\ period} \qquad (3-22)$$

The initial investment is summarized in Table 3-17. The useful life of the RCP system refers to 15-20 years so that the maintenance and operating costs are considered as zero. The cash inflow per period considers the yearly net profits from the energy saving and CO_2 emission reduction as Eq. (3-23).

$$Cash\ inflow\ \left(\frac{JPY}{year}\right) = energy\ saving\ \left(\frac{kWh}{year}\right) \times Electricity\ traiff\ \left(\frac{JPY}{year}\right)$$
$$+CO_2\ emission\ reduction\ \left(\frac{ton}{year}\right) \times CO_2\ price\ \left(\frac{JPY}{year}\right) \qquad (3-23)$$

The amount of energy saving has been evaluated in *Section 3.3.5*. Electricity tariff is approximately 25 JPY/kWh for commercial buildings in Japan [23], while CO_2 price according to state and trend in Japan is about 285 JPY/CO_2e ton [24]. The CO_2 emission reduction is roughly estimated by the amount of energy saving and CO_2 emission coefficient, which is 0.442 (kg CO_2/kWh) [25]. As a result, the simple payback period using the RCP system is 13.2 years. Although the design of the groundwater heating and cooling system in this study is complicated, the system can be simplified with lower initial costs for general application in the pre-design stage. The system designs including the panel number and arrangement are supposed to be optimized. Moreover, it is recommended to apply multi-renewable energy sources for heating and cooling for further energy saving to achieve more financial benefits.

Table 3-17 Initial cost and simple payback period of this office building

		Price (JPY)
Initial investment	Well drilling	10,000,000
	GWHP system (including heat pump chiller, pumps)	6,000,000
	RCP system	22,000,000
	Piping system	10,000,000
	Total initial cost	48,000,000
Maintenance and Operating costs		
Electric saving cost		3,614,600
Carbon saving cost		18,419
Simple payback period (Year)		13.2

Finally, Table 3-18 presents the temperature measurement results for each external wall and floor. This illustrates that the surface temperature remained almost constant even when the outdoor temperature varied significantly because the envelope of this building had a high thermal capacity. A well-insulated envelope can maintain the fluctuation of indoor air temperature within a narrow range. Thus, it is necessary to further analyze the trade-off between a high thermal insulation envelope and highly efficient HVAC systems based on life cycle cost (LCC). The thermal performance of the integrated system should be tested under low thermal insulation conditions.

Table 3-18 Indoor side envelope surface temperature

		Summer		Winter (continuous)		Winter (intermittent)	
		Max	Min	Max	Min	Max	Min
Outdoor temperature (°C)		33.8	17.4	2.5	-7.3	-3.0	-9.0
Wall temperature (°C)	North	26.0	24.8	22.4	21.9	22.4	19.7
	South	25.4	24.1	21.8	21.3	21.8	20.3
	West	25.0	24.7	23.1	22.8	23.3	21.5
Floor Temperature (°C)		24.8	24.2	23.3	22.5	23.4	21.5

3.4 Conclusions

This study investigated the thermal performance of a novel open-type radiant ceiling panel (RCP) system by experiments in a laboratory test room and an nZEB office building.

The heat flux of the RCP changed significantly with variations in the inlet water temperature. However, changing the flow rate had a smaller impact on the cooling capacity. The radiant heat transfer coefficient was constant at 5 W/(m^2·K), and the convective heat transfer coefficient exhibited an exponential relationship with the temperature difference between the indoor air and panel surface. The curved panel shape enhanced both radiation and convection. The convective heat transfer coefficient obtained with this panel was larger than other open-type RCPs.

Through the application of the open-type RCP system and displacement ventilation system, a comfortable indoor thermal environment can be achieved. More than 70% of the staff selected the neutral level in the TSVs, and the uncomfortable rate was lower than 10%. Measuring the thermal condition in the target office showed that the indoor air temperature was approximately 24.5 °C in summer and 23 °C in winter. The indoor humidity was maintained at 55% in summer and 30% in winter. The CO_2 concentration was always within the acceptable level (≤ 1000 ppm).

The RCP can achieve a uniform indoor air distribution. The maximum vertical temperature difference in the occupancy zone was approximately 0.5 K in summer and 1.5 K in winter, which is lower than the standard requirement. Concerns about heterogenous vertical temperature distribution can be eliminated.

Compared with intermittent operation, the continuous operation could improve both the system performance and indoor thermal comfort as the COP of the heat pump increased and the TSV was closer to zero.

The novel open-type RCP allows the use of a lower fluid flow rate to achieve a comfortable room environment, which shows a potential for saving energy. However, the experimental results reveal several weak points on system operation:

(1) It is still challenging to prevent effects resulting from the building envelope.

(2) When the RCP is applied in a large area, there are some blind areas and the horizontal temperature distribution is nonuniform.

(3) The system shows a response delay during intermittent operation in winter.

(4) The electrical energy consumption of continuous operation with better indoor thermal comfort costs more than that of intermittent operation mode.

(5) The trade-off between a high thermal insulation envelope and highly efficient HVAC systems should be analyzed in terms of cost reduction.

Therefore, by refining the system design and control methods, it has the potential to further improve the use of this open-type RCP system.

Nomenclature

List of symbols

A_s	Panel surface area (m^2)
A_p	Projected area of panel (m^2)
AUST	Average Unheated Surface Temperature (ºC)
MRT	Mean radiant temperature (ºC)
T_{op}	The operative temperature (ºC)
T_a	Indoor air temperature (ºC)
T_s	Panel surface temperature (ºC)
T_{in}	Fluid inlet temperature (ºC)
T_{out}	Fluid outlet temperature (ºC)
T_{wall}	Wall surface temperature (ºC)
v	Air velocity (m/s)
G	The water flow rate (m^3/s)
q	Heat flux (W/m^2)
Q	Heat amount (W)
C_p	The specific heat of water (kJ/(kg·K))
$F_{s\text{-}j}$	View factor
$F_{\varepsilon s\text{-}j}$	Radiation interchange factor
U	Heat transmission coefficient ($W/(m^2 \cdot K)$)
TSV	Thermal sensation vote
TCV	Thermal comfort vote
COP	Coefficient of performance
SCOP	System coefficient of performance
E	Energy consumption (kWh)

Greek symbol

σ	Stefan-Boltzmann constants ($W/m^2 \cdot K^4$)
λ	Heat conductivity (W/(m·K))
ε	Surface emissivity
ρ	Density (kg/m^3)

Abbreviations

RCP	Radiant ceiling panel
GWHP	Groundwater heat pump
EN	European Norm
ANSI	American national standards institute
ASHRAE	American Society of Heating, Refrigerating and Air-Conditioning Engineers
PCM	Phase change material

BEMS	Building energy management system
ZEB	Zero energy building
Subscripts	
cl	Cooling load
r	Radiation
c	Convection
tot	Total
HP	Heat pump
WP	Well pump
CP1	Primary pump
CP2	Secondary pump

Reference

[1] 塩谷正樹（2014 年 3 月）；スリットを有する天井放射パネルユニットの制御法及び汎用熱計算法に関する研究，宇都宮大学大学院工学研究科博士論文

[2] EN 14240:2004; Ventilation for buildings–Chilled ceilings–Testing and rating.

[3] DIN EN 14037-1:2016; Free hanging heating and cooling surfaces for water with a temperature below 120 ºC – Part 1: Prefabricated ceiling mounted radiant panels for space heating – Technical specifications and requirements.

[4] J.-H. Lim, K.-W. Kim, ISO 11855 - The international Standard on the Design, dimensioning, installation and control of embedded radiant heating and cooling systems, REHVA J. 01 (2016) 46–53.

[5] L. Zhang, X.H. Liu, Y. Jiang, Experimental evaluation of a suspended metal ceiling radiant panel with inclined fins, Energy Build. 62 (2013) 522–529. https://doi.org/10.1016/j.enbuild.2013.03.044.

[6] Z. Zhong, W. Ma, S. Yao, X. Xu, J. Niu, Enhancing the cooling capacity of radiant ceiling panels by latent heat transfer of superhydrophobic surfaces, Energy Build. 263 (2022) 112036. https://doi.org/10.1016/j.enbuild.2022.112036.

[7] W. Jin, J. Ma, L. Jia, Z. Wang, Dynamic variation of surface temperatures on the radiant ceiling cooling panel based on the different supply water temperature adjustments, Sustain. Cities Soc. 52 (2020) 101805. https://doi.org/10.1016/j.scs.2019.101805.

[8] B. Ning, Y. Chen, H. Liu, S. Zhang, Cooling capacity improvement for a radiant ceiling panel with uniform surface temperature distribution, Build. Environ. 102 (2016) 64–72. https://doi.org/10.1016/j.buildenv.2016.03.009.

[9] J. Wojtkowiak, Ł. Amanowicz, Effect of surface corrugation on cooling capacity of ceiling panel, Therm. Sci. Eng. Prog. 19 (2020). https://doi.org/10.1016/j.tsep.2020.100572.

[10] S.J. Rees, P. Haves, An experimental study of air flow and temperature distribution in a room with displacement ventilation and a chilled ceiling, Build. Environ. 59 (2013) 358–368. https://doi.org/10.1016/j.buildenv.2012.09.001.

[11] D.I. Bogatu, O.B. Kazanci, B.W. Olesen, An experimental study of the active cooling performance of a novel radiant ceiling panel containing phase change material (PCM), Energy Build. 243 (2021) 110981. https://doi.org/10.1016/j.enbuild.2021.110981.

[12] M.R. Krusaa, C.A. Hviid, Reduced-scale experiments of heat transfer from integrated radiant ceiling panel and diffuse ceiling ventilation, Appl. Therm. Eng. 197 (2021) 117348. https://doi.org/10.1016/j.applthermaleng.2021.117348.

[13] L. Su, N. Li, X. Zhang, Y. Sun, J. Qian, Heat transfer and cooling characteristics of concrete ceiling radiant cooling panel, Appl. Therm. Eng. 84 (2015) 170–179. https://doi.org/10.1016/j.applthermaleng.2015.03.045.

[14] M.S. Shin, K.N. Rhee, S.H. Park, M.S. Yeo, K.W. Kim, Enhancement of cooling capacity through open-type installation of cooling radiant ceiling panel systems, Build. Environ. 148 (2019) 417–432. https://doi.org/10.1016/j.buildenv.2018.11.005.

[15] G. Yu, L. Xiong, C. Du, H. Chen, Simplified model and performance analysis for top insulated metal ceiling radiant cooling panels with serpentine tube arrangement, Case Stud. Therm. Eng. 11 (2018) 35–42.

https://doi.org/10.1016/j.csite.2017.12.006.

[16] A. Aryal, P. Chaiwiwatworakul, S. Chirarattananon, An experimental study of thermal performance of the radiant ceiling cooling in office building in Thailand, Energy Build. 283 (2023) 112849. https://doi.org/10.1016/j.enbuild.2023.112849.

[17] Z. Tian, L. Yang, X. Wu, Z. Guan, A field study of occupant thermal comfort with radiant ceiling cooling and overhead air distribution system, Energy Build. 223 (2020) 109949. https://doi.org/10.1016/j.enbuild.2020.109949.

[18] Y. He, N. Li, Q. Huang, A field study on thermal environment and occupant local thermal sensation in offices with cooling ceiling in Zhuhai, China, Energy Build. 102 (2015) 277–283. https://doi.org/10.1016/j.enbuild.2015.05.058.

[19] S.I.F. Elena, M. Ion, Determining the time constant of buildings; advances in automatic control, Model. Simulat., 202-206; ISBN: 978-1-61804-189-0

[20] Johan Hedbrant, On the thermal inertia and time constant of single-family houses, Linkoping Studies in Science and Technology Thesis No 887, 2001. ISBN: 91-7373 -045-9.

[21] 経済産業省資源エネルギー庁「ZEB ロードマップフォローアップ委員会とりまとめ」（平成 31 年 3 月）

[22] 国土交通省「建築物省エネ法について」 https://www.mlit.go.jp/jutakukentiku/jutakukentiku_house_tk4_000103.html

[23] 北海道電力株式会社「電気料金のご案内」https://www.hepco.co.jp/business/price/price.html

[24] OECD, Key findings for carbon pricing in Japan; https://www.oecd.org/tax/tax-policy/carbon-pricing-japan.pdf

[25] Tokyo Electic Power Company Holdings, CO_2 Emissions, CO_2 Emission Intensity and Electricity Sales; https://www.tepco.co.jp/en/corpinfo/illustrated/environment/emissions-co2-e.html

Chapter 4

Optimization for performance improvements by CFD simulation and sensitivity analysis

4.1 Introduction

Some issues of the novel open-type radiant ceiling panel (RCP) system in practical usage are revealed in *Section 3*. In this section, improvements to the RCP system are explored through changes in the panel structure and integration of ventilation systems to address the following problems:

(1) Enhancing the thermal capacity of the RCP system to reduce the energy consumption.

(2) Preventing the occurrence of airflow caused by temperature differences between indoor air and envelopes to maintain a uniform temperature distribution.

To optimize the system, it is essential to understand the operation behavior of the system and the impact of its parameters. This section mainly focuses on optimizing the RCP system at the design stage, where the use of experimental methods is both costly and time-consuming. Therefore, an optimization method combining numerical modeling with sensitivity analysis was employed, which is a highly effective approach for optimizing the system performance and system control. The numerical simulation can offer flexibility to adjust the operation conditions and investigate the behavior of the system, while the sensitivity analysis can provide a quantitative numerical analysis of the impact of various parameters on its performance.

Many researchers have applied this method to optimize the radiant heating and cooling system while considering novel proposals. Tang et al. [1] propose a novel pulsed flow control method (PFM) for radiant slab (radiant floor) system. A 3D finite difference model of the radiant slab was developed to capture the dynamic behavior of the PFM. Then, a screening-based sensitivity analysis was used to identify the most important parameters in relation to energy performance in order to design and optimize the PFM. Talami and Jakubiec [2] studied three radiant system technologies applied to a parametric office building in the tropical climate of Singapore based on EnergyPlus simulation models. Morris sensitivity analysis was conducted to analyses the impact of 13 different building and system design parameters on comfort, system and energy performances for 3 radiant systems typologies. Pieska et al. [3] compared the performance of radiant cooling systems with and without dehumidification supplied by geothermal energy by building energy models. A sensitivity analysis is also conducted to assess the influence of selected input parameters on the simulation output. The authors [4] then studied a life-cycle assessment (LCA) of the radiant cooling system for a retrofit project of a small office building based on the building energy models in IDA-ICE 4.8. A sensitivity analysis was also conducted and revealed that the radiant system's environmental impact is mainly dependent on the manufacturing process. Chen and Li [5] proposed an optimal control strategy for radiant floor heating systems based on a thermal response time prediction model by applying the gaussian process regression (GPR) algorithm. A sensitivity analysis of the response performance of the seven explanatory variables was conducted and a theoretical explanation was provided. Le Dreau and Heiselberg [6] investigated four different radiant terminals (active chilled beam, radiant floor, wall and ceiling) through steady-state simulations of a typical office room. Subsequently, a sensitivity analysis has been conducted to determine the parameters influencing their thermal performance the most.

In this study, the Computational Fluid Dynamics (CFD) simulations were firstly carried out in enclosed spaces to analyze the thermal conditions and heat transfer efficiency for the proposed schemes. However, the desire for higher thermal comfort always conflicts with the goals of energy and cost reduction. The sensitivity analysis was then conducted to investigate the impact of each designable input parameter on the thermal performance of the RCP

system. The optimal panel structure and integration method were suggested based on the analysis results, considering factors such as cooling capacity, panel surface temperature, and indoor temperature distribution.

The overview of the CFD method of the RCP system was first introduced in *Section 4.2*. This section describes the numerical models and simulation setup methods employed in the CFD analysis. In *Section 4.3*, the design of the novel open-type RCP with curved and segmented structure was optimized to maximize the cooling capacity. A three-dimensional CFD model was developed to investigate the cooling capacity and heat transfer coefficient of the RCPs installed inside a single enclosed room. Panel structure was determined based on four dependent parameters: the panel curvature width (L, m), the panel curvature radius (r, m), the void distance (d, m), and the panel coverage area (A_c, m^2). The panel surface area (A_s, m^2) and the ratio of panel curvature width to radius (L/r) were also examined. A total of 35 designs were compared under 7 different cooling load conditions. The sensitivity analysis was conducted based on the simulations and concluded that void distance plays the most crucial role in influencing cooling performance. In *Section 4.4*, a heating and cooling system integrating the novel open-type RCP with a wall-attached ventilation (WAV) system was proposed to prevent the warm air stream that floats from the window, unfavorable influencing indoor thermal conditions. A three-dimensional CFD model of the RCP system was validated with the experimental results in the previous chamber test. Then, two WAV systems (ceiling inlet/ceiling outlet; ceiling inlet/floor outlet) are examined under various operating conditions. The result indicated that applying the ventilation system with a ceiling inlet and ceiling outlet is more effective than installing a ceiling inlet and a floor outlet. Finally, the surface response and sensitivity analysis of the operating condition are carried out to optimize the integrated system. The optimization objectives are to maximize the cooling capacity of the RCP system and minimize the flow rate and supply air temperature of the WAV system.

4.2 Overview on the CFD method applied to the RCP system

The Computational Fluid Dynamics (CFD) method is generally used to simulate the thermal process of the RCP system used in an enclosed space. Firstly, some assumptions are applied before simulations in the CFD model as follows:

1. The heat transfer is calculated under a steady state condition.
2. The air density difference is ignored, and only the gravitational force effect is considered.
3. The heat transfer between the water pipe and the panel surface is ignored, and the panel surface temperature is considered uniform.
4. The emissivity is constant and a property of the surface, which is independent of wavelength.
5. The surface is opaque and diffuse, and only the transferred radiation between two surfaces is considered.

When modelling the RCP systems, it is common to assume that the panel surface temperature is constant under reasonable conditions. The temperature difference among the panel surface is far smaller than the difference between the panel and the surrounding area. The following table lists some studies which apply assumption in their simulations.

Table 4-1 Examples of the boundary setting of the RCPs in CFD simulation

Literature	Objective	Boundary setting of the panels
Zhang et al. [7]	Radiant ceiling	A uniform surface temperature, and the temperature decay along the pipe was assumed to be negligible
Chiang et al. [8]	Cooling ceiling and mechanical ventilation system	Two radiant cooling surface temperature settings: T_s=18 °C; T_s=22 °C
Najafi and Haghighi [9]	Radiant cooling panel system	It is assumed that the whole ceiling area is covered by radiant cooling panels. The boundary condition of the ceiling is considered as constant temperature.

When the simulations carry out, the computational domain is discretized into difference grids. The governing equations [10] are solved iteratively at each node of the grid until the convergence of residuals is achieved, describing the fundamental principles of fluid flow and heat transfer. In this study, the simulations were carried out in a steady state, and the equation are indicated as shown in Eq. (4-1) to Eq. (4-4).

(a) Mass conservation:

$$\nabla \cdot (\rho \vec{v}) = 0 \qquad (4-1)$$

(b) Momentum conservation:

$$\nabla \cdot (\rho \vec{v} \vec{v}) = -\nabla p + \nabla \cdot (\bar{\bar{\tau}}) + \rho \vec{g} \qquad (4-2)$$

where the surface stress tensor ($\bar{\bar{\tau}}$, N/m^2) is given by the following equation:

$$\bar{\bar{\tau}} = \mu \left[(\nabla \vec{v} + \nabla \vec{v}^T) - \frac{2}{3} \nabla \cdot \vec{v} I \right] \qquad (4-3)$$

(c) Energy conservation:

$$\nabla \cdot \left(\rho C_p \vec{v} T_f\right) = \nabla \cdot \left(k_f \nabla T_f\right) \quad (4-4)$$

ρ is the fluid density (kg/m^3), v is the velocity vector (m/s), p is the static pressure (N/m^2), ρg is the gravitational body force (N/m^3), μ is the molecular viscosity (kg/m·s), I is the unit tensor, C_p is the specific heat capacity (J/kg·K), T_f is the fluid temperature (K), and k_f is the fluid thermal conductivity (W/m·k).

The turbulence model should also be included because it can accurately to solve the air movement problem and predict forced, natural, and mixed convection for indoor air flow. The two-equation model is commonly used to solve the problems related to radiant systems installed in an enclosed room, such as the standard k–ε model [11-13], RNG k–ε model [14], realizable k–ε model [15-16] or even SST k-ω [17]. Based on the model validation and comparison [18], the standard k–ε model proposed by Launder and Spalding (1972) was ultimately chosen in this study. The equations for turbulent kinetic energy k (m^2/s^2) and the turbulent dissipation rate ε (m^2/s^3) are expressed as Eq. (4-5) and Eq. (4-6), respectively:

$$\frac{\partial}{\partial t}(\rho k) + \frac{\partial}{\partial x_i}(\rho k u) = \frac{\partial}{\partial x_j}\left[\left(\mu + \frac{\mu_t}{\sigma_k}\right)\frac{\partial k}{\partial x_j}\right] + G_k + G_b - \rho\varepsilon - \Upsilon_M + S_k \quad (4-5)$$

$$\frac{\partial}{\partial t}(\rho \varepsilon) + \frac{\partial}{\partial x_i}(\rho \varepsilon I) = \frac{\partial}{\partial x_j}\left[\left(\mu + \frac{\mu_t}{\sigma_\varepsilon}\right)\frac{\partial \varepsilon}{\partial x_j}\right] + C_{1\varepsilon}\frac{\varepsilon}{k}(G_k + C_{3\varepsilon}G_b) - C_{2\varepsilon}\rho\frac{\varepsilon^2}{k} + S_\varepsilon \quad (4-6)$$

μ_t is the turbulent viscosity (kg/m·s), as follows.

$$\mu_t = \rho C_\mu \frac{k^2}{\varepsilon} \quad (4-7)$$

u_i is the velocity, G_k is the turbulence kinetic energy generated by the mean velocity gradients, G_b is the turbulence kinetic energy generated by buoyancy, and Y_M is the dilatation dissipation term. C_μ, σ_ε, σ_k, $C_{1\varepsilon}$, and $C_{2\varepsilon}$ are empirical constants with the following default values: $C_\mu = 0.09$, $\sigma_\varepsilon = 1.2$, $\sigma_k = 1$, $C_{1\varepsilon} = 1.44$, and $C_{2\varepsilon} = 1.92$. S_k and S_ε are the user-defined source terms.

Additionally, radiative heat transfer accounts for a significant portion of total heat transfer in the RCP systems. Therefore, the surface-to-surface (S2S) radiation model are always used in the simulations to account for radiative heat transfer between the RCPs and other surfaces within the domain. In this model, the radiation of a surface (k) is composed of both emission and reflection.

$$q_{k,out} = \varepsilon_k \sigma {T_k}^4 + \rho_k q_{k,in} \quad (4-8)$$

ε_k is the emissivity, σ is Boltzmann's constant, and $q_{k,in}$ is the energy incident on the surface (k) from the surroundings, which is represented as a summation of radiation from the surrounding surface (j), as shown in Eq. (4-9).

$$A_k q_{k,in} = \sum_{j=1}^{N} A_j F_{jk} q_{j,out} \quad (4-9)$$

A_k and A_j are the area of surface k and surface j (m^2), respectively; F_{jk} is the view factor between surface j and surface k; and $q_{j,out}$ is the radiative heat flux of the surface j (W/m^2).

On the other hand, the Boussinesq model is employed to model the natural convection in the closed space driven by buoyancy force. The model performs with the fluid density as a function of the temperature gradient as follows.

$$(\rho - \rho_0)g \approx -\rho_0\beta(T - T_0)g \qquad (4-10)$$

ρ_0 is the specified constant density of the flow, T_0 is the operating temperature, and β is the thermal expansion coefficient.

4.3 Optimizing the shape of open-type RCP

4.3.1 Parameter design of open-type RCP with curved and segmented structure

The aim of this study is to explore the inter-relationship between panel design (including curved structure and panel distribution designs) and cooling performance. It was urgently required to determine the optimal design, which can balance contradictory goals in terms of enhancing cooling capacity and maintaining thermal comfort. Therefore, four independent parameters were used to determine the panel shape, as shown in Fig. 4-1: the panel curvature width L (m), the curvature radius r (m), the void distance between each panel or panel segment d (m), and the panel coverage area A_c (m^2). Two dependent parameters were also investigated: the ratio of panel curvature width to radius L/r and panel surface area A_s (m^2). The L/r ratio is a parameter affecting the curvature shape of the panel. The curvature of the panel increases with an increase in the value of L/r. The panel surface area A_s is a parameter depending on all four independent parameters and calculated according to Eq. (4-10). It closely relates to the manufacturing cost. Therefore, it is preferred to minimize the panel surface area in the de-sign stage.

$$A_s = \frac{2sin^{-1}\left(\frac{L}{2r}\right)}{180}\pi r \cdot l \cdot n \qquad (4-10)$$

Where l is the panel length (m), and n is the panel number related to the panel curvature width L, void distance d, and panel coverage area A_c.

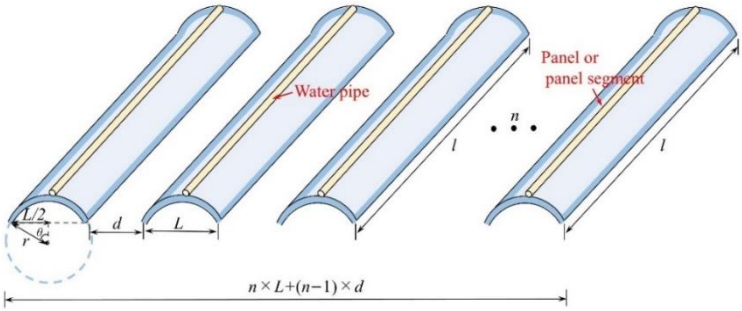

Fig.4-1 Schematic diagram of the panel and design parameters

Thirty-five designs were created and compared to show the effect of each parameter. The values of each parameter in each case are summarized in Table 4-2. The panel curvature width L was altered from 0.03 to 0.12 m, the panel curvature radius r was altered from 0.03 m to 0.3 m, the void distance d was altered from 0 m to 0.33 m, and the panel cover area A_c was altered from 7.58 m^2 to 12.96 m^2. Accordingly, the L/r ratio varied from 0 to 2, and the panel surface area A_s varied from 2.51 m^2 to 16.90 m^2. When the effect of one independent parameter was examined individually, the other three parameters were held constant. Two dependent parameters—L/r ratio and A_s—were investigated with different panel width and curvature radius values, while the coverage area and void distance were the same. Additionally, four replenished designs were proposed for optimization and verification.

Table 4-2 Design of parameters

Design	*L* (m)	*r* (m)	*d* (m)	*L*/*r*	A_c (m^2)	A_s (m^2)
1	0.03	0.06	0.03	0.5	12.96	8.18
2	0.06	0.06	0.03	1	12.96	10.28
3	0.09	0.06	0.03	1.5	12.96	11.72
4	0.12	0.06	0.03	2	12.96	16.90
5	0.06	0.03	0.03	2	12.96	14.90
6	0.06	0.09	0.03	0.7	12.96	10.06
7	0.06	0.15	0.03	0.4	12.96	9.96
8	0.06	0.2	0.03	0.3	12.96	9.93
9	0.06	0.3	0.03	0.2	12.96	9.91
10	0.06	0.06	0	1	12.96	13.58
11	0.06	0.06	0.01	1	12.96	13.05
12	0.06	0.06	0.03	1	12.96	10.03
13	0.06	0.06	0.06	1	12.96	7.53
14	0.06	0.06	0.1	1	12.96	5.77
15	0.06	0.06	0.14	1	12.96	4.51
16	0.06	0.06	0.21	1	12.96	3.51
17	0.06	0.06	0.33	1	12.96	2.51
18	0.06	0.06	0.03	1	11.43	9.05
19	0.06	0.06	0.03	1	10.80	8.53
20	0.06	0.06	0.03	1	10.15	8.02
21	0.06	0.06	0.03	1	8.86	7.02
22	0.06	0.06	0.03	1	7.58	5.77
23	0.1	0.09	0.03	1.1	12.96	11.18
24	0.15	0.2	0.03	0.75	12.96	11.17
25	0.2	0.4	0.03	0.5	12.96	10.85
26	0.3	1	0.03	0.3	12.96	10.80
27	0.16	-	0.03	0	12.96	10.84
28	0.045	0.03	0.03	1.5	12.96	10.09
29	0.135	0.09	0.03	1.5	12.96	12.65
30	0.225	0.15	0.03	1.5	12.96	13.19
31	0.3	0.2	0.03	1.5	12.96	13.73
32	0.03	0.06	0.05	0.5	12.96	6.04
33	0.03	0.06	0.1	0.5	12.96	3.62
34	0.03	0.06	0.05	0.5	11.43	5.38
35	0.03	0.06	0.1	0.5	11.43	3.35

4.3.2 CFD simulation set-up

ANSYS 2020 R2 Fluent commercial software was used to perform the CFD simulations. A three-dimensional finite-volume model was developed to determine the heat transfer and temperature field. The enclosed room is 4 m (L) × 4 m (W) × 2.9 m (H), which has same dimensions and arrangement as the room model for a suspended flat panel validated by Shin et al. [15]. Twelve cylindrical occupant dummies with dimensions of 0.3 m (D) × 1.1 m (H) are deployed symmetrically in the room to mimic human bodies, generating energy dissipation in the space and representing a cooling load. The panels are suspended 0.3 m beneath the ceiling and arranged along the central line. In the validated case, the panel is one flat, solid panel with dimensions of 3.6 m (L) × 3.6 m (W) × 0.03 m (H), while in other cases with curved and segmented type panels, four independent panel design parameters (L, r, d, and A_c) are set using the design values listed in Table 4-2. Instead of directly inputting the coverage area A_c, the number of panels n is employed in the geometric drawing, which can be determined according to Eq. (4-11):

$$n = \frac{1}{(L+d)} \cdot \left(\frac{A_c}{l} + d\right) \qquad (4-11)$$

Moreover, the symmetry boundary condition was applied to the middle plane to simplify the modeling and accelerate the simulation speed due to the completely symmetrical characteristic of the room. In this study, all the simulations were conducted in half of the space, as shown in Fig. 4-2.

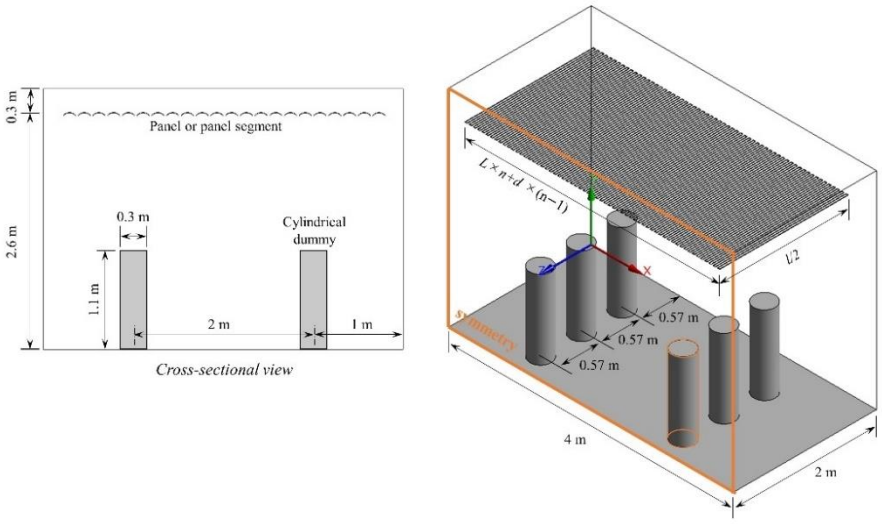

Fig. 4-2 The geometry of the model and a cross-sectional view at the middle plane

The mesh was generated by the ANSYS Meshing tool using tetrahedron mesh and inflation layers near the cylinder surface (Fig. 4-3 (a)). The grid around the wall, panel, and dummy cylinder surface was refined to address the expected high gradient of temperature by adding an inflation layer with 0.001 m first-layer thickness and a growth rate of 1.2. Mesh-independent analysis was carried out for one curved panel design to minimize the impact of element size on the simulation accuracy. Seven different element numbers were selected: (1) 216,283 (2) 597,963, (3) 927,073, (4) 1,432,275, (5) 2,191,931, (6) 2,616,270 and (7) 3,578,974. The total heat flux and indoor air temperature varied with an increasing number of elements, as shown in Fig. 4-3 (b). There-fore, the preferred number of elements was 1,432,275 in the present study, as the results demonstrated a change in heat flux of only 0.17% and a change in average air temperature of only 0.81% compared with the finer mesh.

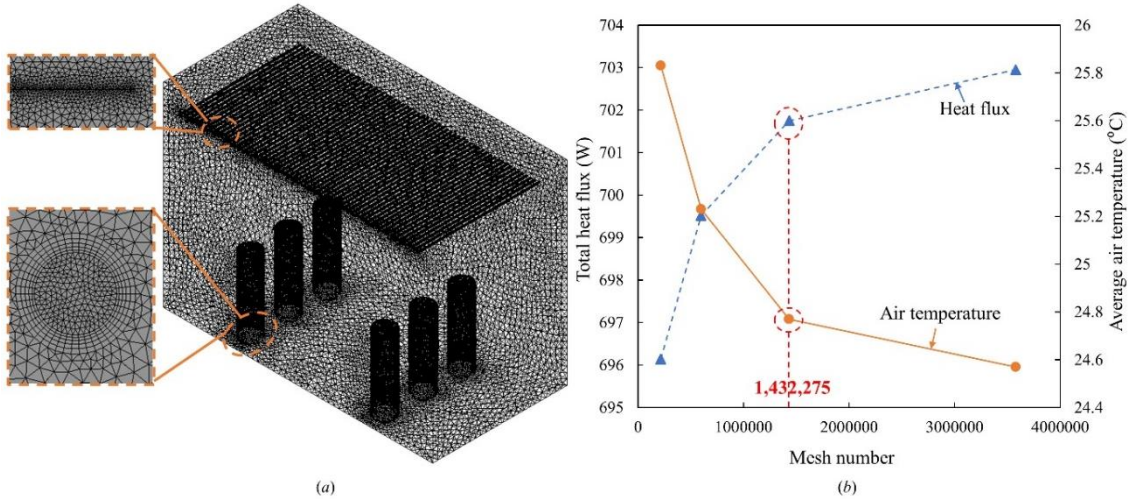

Fig. 4-3 (a) Computational mesh used in the present study (b) Results of mesh-independent analysis

The governing equations are iteratively solved at each control volume in the computational domain until convergence is achieved. The Semi-Implicit Method for Pressure Linked Equations (SIMPLE) algorithm was applied for coupling pressure and momentum. The first-order upwind discretization scheme was chosen for turbulent kinetic energy and turbulent dissipation rate. The second-order upwind discretization scheme was used for the pressure, momentum, and energy. Enhanced wall treatment was selected as a wall treatment. The convergence criteria are 10^{-5} for all equations, with the exception of 10−6 for the energy equation.

Table 4-3 lists the boundary conditions and emissivity. The room is assumed to be well-insulated without heat transfer so that the envelope is assigned to the adiabatic condition. The non-uniform temperature distribution on the panel surface always occurs from the rise of chilled water or pipe arrangement. However, the temperature difference on the panel surface has less effect than the large difference between the air and the panel. Our study mainly focuses on optimizing the panel shape design based on heat transfer performance to improve the cooling capacity and indoor thermal condition. Therefore, the panel surface temperature is set constant at 15.83 ℃, which is the experimentally measured value given by Shin et al. [15]. Each panel design was investigated under seven different cooling load conditions (621.69 W, 746.03 W, 870.37 W, 994.71 W, 1119.04 W, 1243.38 W, and 1405.02 W), owing to differences in heat flux emitted from cylindrical dummies. In summary, 245 cases were simulated for analysis.

Table 4-3 Boundary condition and emissivity of each surface

	Condition	Temperature (°C)	Heat Flux (W/m^2)	Emissivity
Wall/ceiling	adiabatic	-	0	0.82
Floor	adiabatic	-	0	0.95
Middle_plane	symmetry	-	-	-
Panel_surface	T = constant	15.83	-	0.92
Cylinder_outer	q = constant	-	50/60/70/80/90/100/113	0.92
Cylinder_upper	adiabatic	-	0	0.92

4.3.3 Simulation results

The CFD model was validated with the experimental results for a flat panel presented by Shin et al. [15]. Fig. 4-4 shows the air temperature distribution of the vertical measured line in three validation cases in which the cooling load was adjusted from 469.92 W to 1409.76 W. The simulated temperature showed marginal differences, with an average error of 1.01% in Case 1, 0.89% in Case 2, and 0.86% in Case 3, indicating that the CFD model agrees with the experimental measurements conducted for the freely suspended panel under different cooling load conditions.

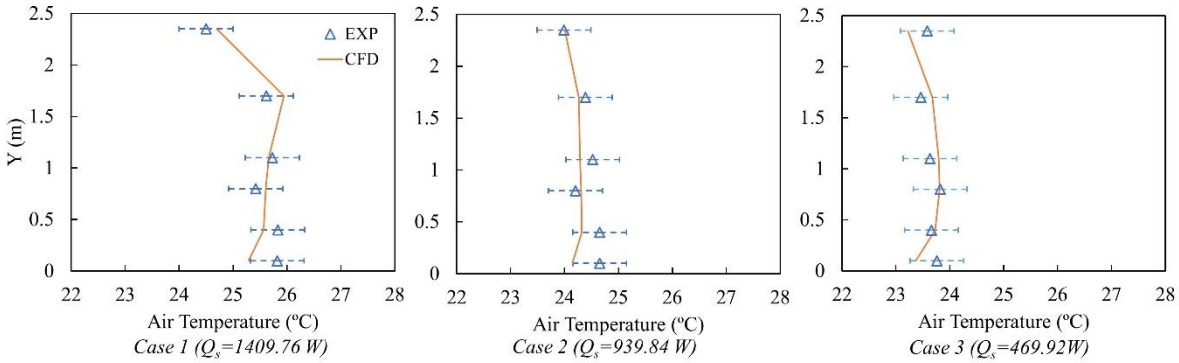

Fig. 4-4 Comparison between *CFD* and experimental results reported by Shin et al.

Different ceiling radiant cooling panels can be compared and evaluated using the cooling capacity curve present in the standard [19], which is represented by the cooling capacity and the difference between the operative and panel surface temperature (Eq. (17)). Previous studies [15][18] reported the curves under different cooling load conditions, adjusting the panel surface temperature to ensure that the indoor air temperature was within a comfort range. Nevertheless, in this study, the panel surface temperature was maintained at 15.83 °C in each case, with the cooling load increasing from 621.69 W to 1405.02 W.

Fig. 4-5 compares the results of heat flux, heat transfer coefficient, average indoor air temperature, and the difference between operative and panel surface temperature, which were obtained under different panel surface temperature conditions. The panel surface temperature was set from 14.83 °C to 19.83 °C with an interval of 1 °C according to the design guidelines presented in [20]. Except for indoor air temperature increasing with the panel surface temperature increase, the heat flux and temperature difference were almost the same, with the difference maintained within 5%, indicating that different panel surface temperature settings only affect indoor thermal conditions but not the panel cooling performance. The amount of heat transferred from the panel is related to the load and the panel itself rather than the surface temperature. Therefore, the boundary setting of this study was simplified.

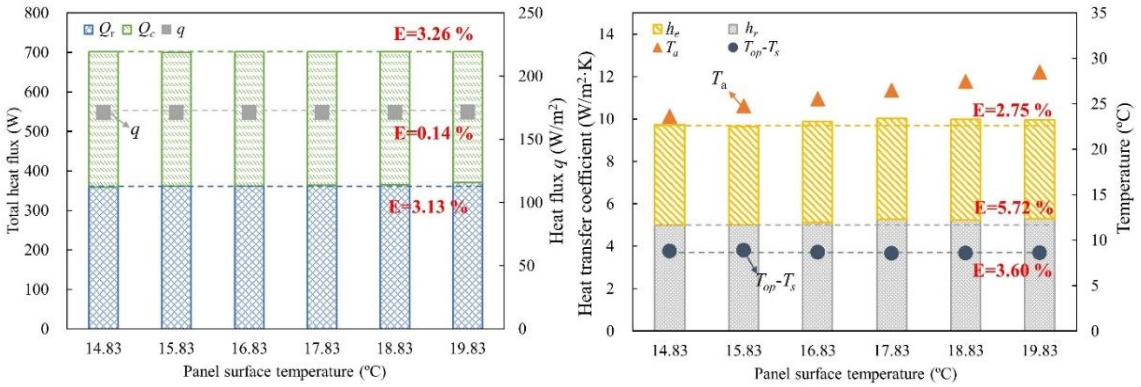

Fig. 4-5 Calculation results under different panel surface temperatures

In this study, the total heat flux q_{tot} (W/m^2) is defined as the total heat transfer rate through all the panel surfaces divided by the panel surface area A_s (m^2).

$$q_{tot} = \frac{Q_{tot}}{A_s} \tag{4-12}$$

The radiation and convection heat transfer coefficient are then calculated based on the following equations.

$$h_r = \frac{Q_r}{A_s(AUST - T_s)} \tag{4-13}$$

$$h_c = \frac{Q_c}{A_s(T_a - T_s)} \tag{4-14}$$

where $AUST$ is the area-weighted uncooled temperature of the surfaces excluding the panel surface (°C), T_a is the air temperature (°C), and T_s is the panel surface temperature (°C). Then, the operative temperature T_{op} (°C) can be roughly determined by Eq. (4-15).

$$T_{op} = \frac{h_c T_a + h_r AUST}{h_c + h_r} \tag{4-15}$$

The cooling capacity of RCPs is influenced by multiple factors—not only the panel design but also the cooling load, indoor condition, and panel surface temperature—making it difficult to evaluate and compare directly. Therefore, the cooling performance should be compared between different panel designs under a generalized operation condition. In this study, the cooling capacity was analyzed using power regression, which is in a functional relationship with the temperature difference between the operative and panel surface temperature as follows:

$$q = k\left(T_{op} - T_s\right)^n \tag{4-16}$$

The nominal cooling capacity was obtained when the temperature difference was 8 K (T_{op}–T_s = 8 K). All the designs were compared with a closed-type RCP proposed in the European Standard [20], named 'Standard', and an open-type flat RCP with a distributed layout proposed by Shin et al. [19], named 'A-d' in the following figures.

The effect of panel curvature width is shown by comparing the results of Design No.1–No.4. The curvature width L of Design 1, Design 2, Design 3, and Design 4 is 0.03 m, 0.06 m, 0.09 m, and 0.12 m, respectively. While the curvature radius is maintained at 0.06 m, and the void distance is maintained at 0.03 m. As shown in Fig. 4-6, the cooling capacity and heat transfer coefficient decrease dramatically with increasing L. With a decrease in L from 0.12 m to 0.03 m, the nominal cooling capacity increases by 35.8% from 113.89 W/m^2 to 154.64 W/m^2. Additionally,

both the h_r and h_c are improved significantly by 49.8% and 35%, respectively, under the same cooling load condition. Compared with Design 2 and Design 3, the convective heat transfer accounts for more in Design 1 and Design 4. Fig. 4-7 compares the velocity contours in Design 1 and Design 4 under the highest cooling load. It is clear that the design with a shorter width contributes to accelerating the air moving through the openings around the panel to promote heat exchange.

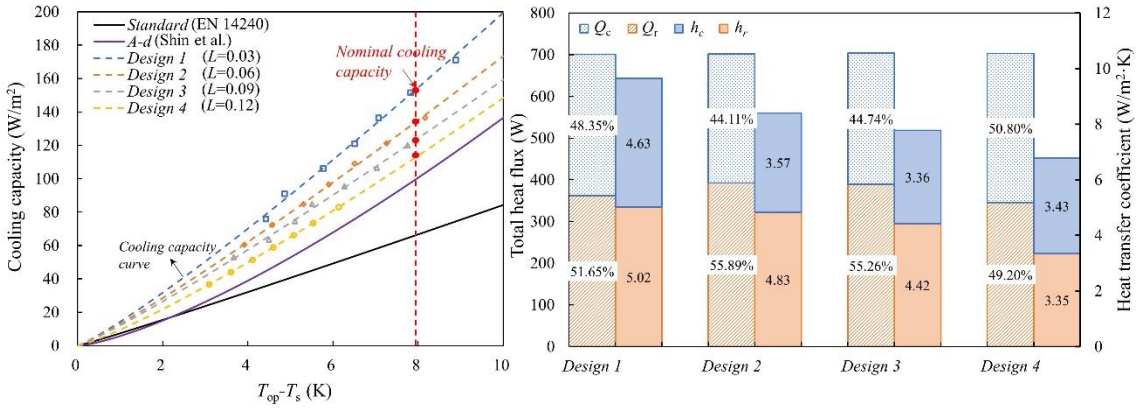

(a) (b)

Fig. 4-6 Comparison of different panel curvature lengths (a) cooling capacity curves (b) thermal performances under a cooling load of 1405.02 W

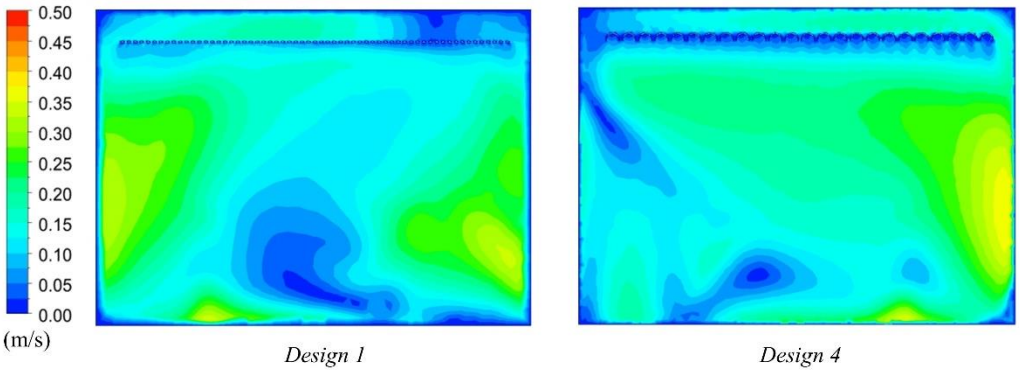

Fig. 4-7 Velocity contours in Design 1 and Design 4 under a cooling load of 1405.02 W

Fig. 4-8 compares different curvature radii using the results from Design 5, Design 2, and Design No.6–No.9, with curvature radii 0.03 m, 0.06 m, 0.09 m, 0.15 m, 0.2 m, and 0.3 m, respectively. On the other hand, the panel curvature width is constant at 0.06 m, and the void distance is constant at 0.03 m. The results show that the cooling capacity and heat transfer coefficient increase with increasing curvature radius. In particular, the nominal cooling capacity and radiation heat transfer coefficient are obviously improved by 9.1% and 36%, respectively, when r is increased from 0.03 m to 0.06 m. However, when r is larger than 0.06 m, the impact of increasing r is significantly reduced. The nominal cooling capacity and radiation heat transfer coefficient only increase by 4.2% and 3.9%, respectively, when r is increased from 0.06 m to 0.3 m.

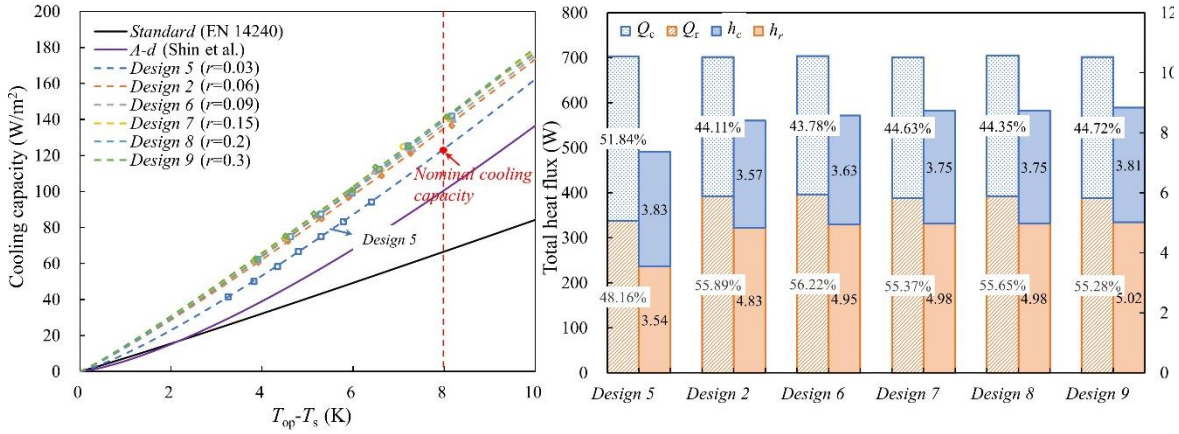

(a) (b)

Fig. 4-8 Comparison of different panel curvature radius (a) cooling capacity curves (b) thermal performances under a cooling load of 1405.02 W

Fig. 4-9 and Fig. 4-10 illustrate the effect of voids between adjacent panels or panel segments. Eight different distances were compared, varying from 0 m to 0.3 m, with L = 0.06 m and r = 0.06 m. A solid panel without an opening (Design 10) results in the same nominal cooling capacity as the RCP proposed by Shin et al. When d is expanded from 0 m to 0.03 m, the nominal cooling capacity increases significantly by 33% from 101.27 W/m^2 to 134.69 W/m^2, and the h_r and h_c are improved by 6.4% and 92.9%, respectively. Including an opening between panels or panel segments can effectively increase convection heat transfer and enhance indoor air movement, as shown in the comparison of airflow distribution between Design 10 and Design 12 in Fig. 4-10. The cooling capacity, h_r, and h_c continue to increase as the distance increases, but the growth slows when d is larger than 0.06 m. In particular, the nominal cooling capacity is highest in Design 16 when d is 0.21 m, which is 4.4% higher than that in Design 13, 13.3% higher than that in Design 12, and 50.1% higher than that in Design 10.

The indoor air temperature in Design 16 is 10 °C higher than in Design 10 and Design 12, as shown in Fig. 4-10, because the panel number in this design is too small to match the required total heat transfer amount. However, the air temperature uniformity in Design 16 is better than in the other two cases due to active air activity and sufficient heat exchange. The cooled air trapped on the top surface is allowed to move down, resulting in better cooling performance.

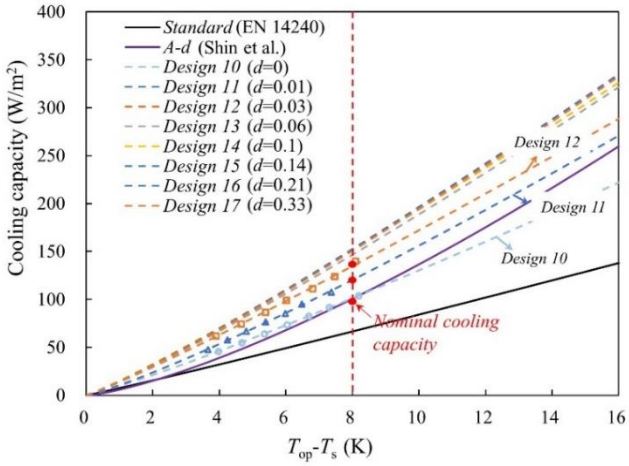

(a)

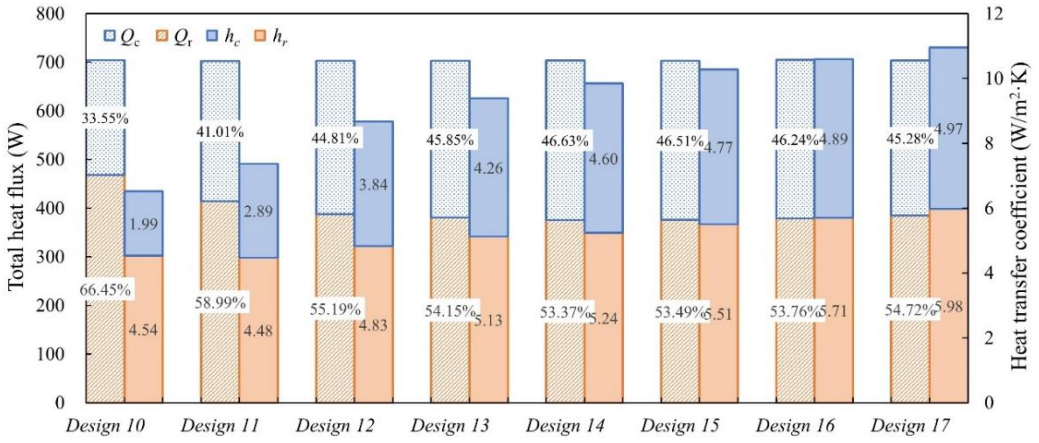

(b)

Fig. 4-9 Comparison of different void distances (a) cooling capacity curves (b) thermal performances under a cooling load of 1405.02 W

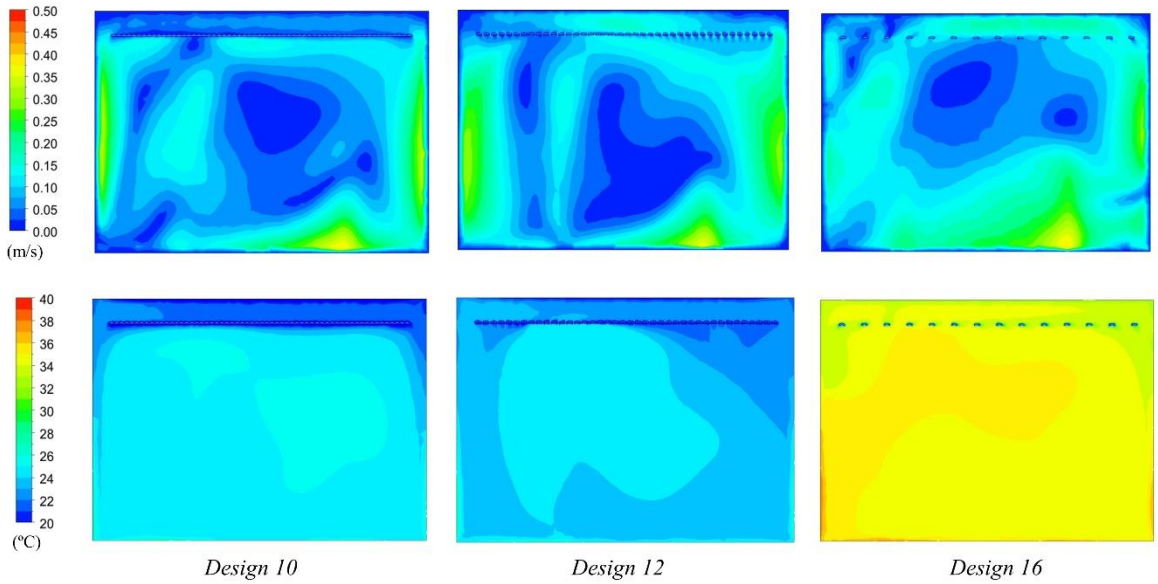

Fig. 4-10 Velocity and temperature contours in Design 10, Design 12, and Design 16

The effect of coverage area was investigated by comparing Design 2 and Design No.18–No.22, as shown in Fig. 4-11. When the coverage area is 11.43 m^2, the nominal cooling capacity is 12.8% higher than 7.58 m^2 and 5.8% higher than 12.96 m^2. The total heat transfer coefficient increases by 4.3% from 8.4 $W/m^2 \cdot K$ to 8.76 $W/m^2 \cdot K$ when the coverage area is reduced from 12.96 m^2 to 7.58 m^2. In other words, expanding the distance between the side of the panel and the wall within an appropriate range can enhance the cooling performance to the same extent as increasing the void distance between adjacent panels.

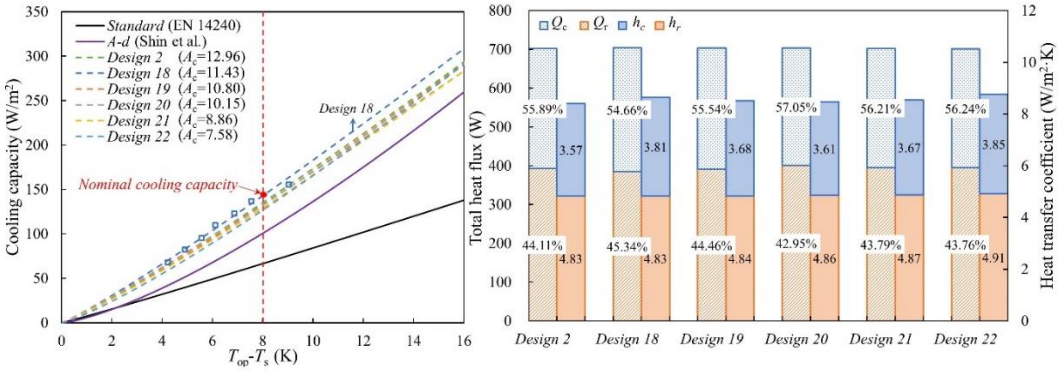

(a) (b)

Fig. 4-11 Comparison of different coverage areas (a) cooling capacity curves (b) thermal performances under a cooling load of 1405.02 W

Two dependent parameters—*L*/*r* ratio and the panel surface area (A_s)—were examined with the other parameters unchanged. The *L*/*r* ratio is discussed by comparing Design No.23–No.27, as shown in Fig. 4-12, which have the same void of 0.03 m and surface area of 11 m^2 ± 0.4 m^2. As a result, when the L/r ratio is 0.5, the nominal cooling capacity is the highest, at 129.65 W/m^2, which is about 5% higher than that of the flat design. On the other hand, the h_c decreases by 12.2% and the h_r increases by 3.6% when the *L*/*r* is decreased from 1.1 to 0, illustrating that the curved shape can effectively promote air movement over the top surface and enhance convective heat transfer because the curved structure has a streamlined shape. Notably, when comparing the optimum design of *L*/*r* = 0.5 with the flat design, the h_c is increased by 5.3%, and h_r is maintained at the same value.

The panel surface area (A_s) was considered with an *L*/*r* ratio of 1.5 for the same void distance and panel coverage area, as shown in Fig. 4-13. It should be noted that the *L* and *r* values are different in each design, as A_s is a dependent parameter related to all four independent design parameters. When A_s increases from 10.09 m^2 to 13.73 m^2, the nominal cooling capacity decreases by 15.2% from 136.11 W/m^2 to 118.20 W/m^2. The h_r and h_c in Design 28 are also 9.4% and 18.6% higher than those in Design 31, respectively. It is concluded that the short and distributed panel design with less panel surface area achieves better cooling performance than the large solid panel design.

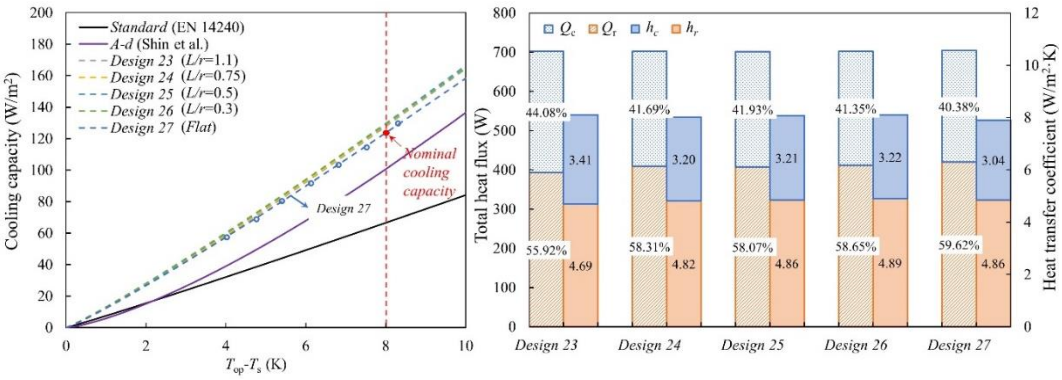

(a) (b)

Fig. 4-12 Comparison of different *L*/*r* ratios (a) cooling capacity curves (b) thermal performances under a cooling load of 1405.02 W

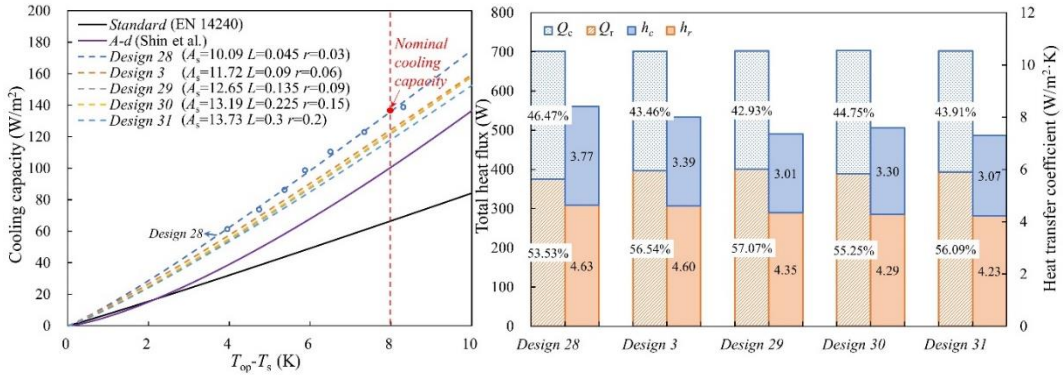

(a) (b)

Fig. 4-13 Comparison of different surface areas (a) cooling capacity curves (b) thermal performances under a cooling load of 1405.02 W

4.3.4 Sensitivity analysis and optimization

Based on the parametric analysis, the local sensitivity analysis of the effects of four independent design parameters on cooling capacity was carried out using the manual one-at-a-time (OAT) approach [21]. The sensitivities were measured by monitoring the changes in cooling capacity following the variation of one parameter while all other parameters were held constant. A linear regression equation was derived as a function of cooling capacity and each parameter. The results of sensitivity measures are summarized and compared in Fig. 4-14. Consistent with the above conclusion, the void distance *d* plays the most crucial role in influencing cooling capacity, followed by panel curvature width *L* and radius *r*. It is possible to achieve the same or even better indoor thermal conditions by applying fewer panels, demonstrating the potential for cost reduction by optimizing the panel arrangement and construction.

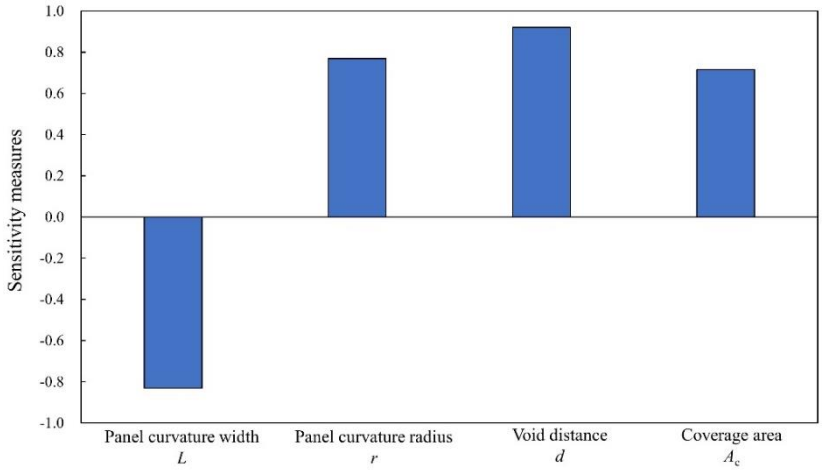

Fig. 4-14 Sensitivity analysis of four dependent design parameters

Fig. 4-15 shows the coefficient *k* and exponent *n* in Eq. (4-7) of each panel design. The coefficient *k* and exponent *n* of each design are summarized in Table 4-4. It is clear that different panel designs achieve totally different cooling performances, and that structural design is an effective way to improve the efficiency of the RCP system. All the RCP designs proposed in this study with curved and segmented shapes can achieve better cooling capacity than

those proposed in previous studies under the same condition. Moreover, four designs (Design No.32–No.35) were replenished, combining the concluded optimum panel design of L = 0.03 m and r = 0.06 m with the void distance and coverage area. Fig. 4-16 illustrates the flow and temperature fields on the symmetry plane in Design 1 and Design No.34–No.35. Design 34, with large openings between panels and between the panels and the wall, is the optimum among all the designs, if it prioritizes increasing the nominal cooling capacity. However, this design is unable to meet thermal comfort requirements under a cooling load of 1405.02 W in practice because of an insufficient number of panels. The temperature fields become more uniform in proposed Design No.34–No.35, but the average indoor temperature in Design 34 and Design 35 is about 4 K and 8 K higher than in Design 1, respectively. In regard to achieving both the thermal comfort conditions included in the ASHRAE standard [22] and maximum cooling capacity, Design 1 is the alternative optimum solution, which can maintain the indoor air temperature at 24.77 °C. Compared with Design 34, Design 1 has the same L and r values but with smaller opening areas. Therefore, (1) L = 0.03 m and r = 0.06 m represent the ideal panel shape, as concluded by comparing 35 designs in this study; (2) larger void distance and openings between panels and the wall are able to promote cooling capacity. However, preference should be given to thermal comfort and the number of required panels, which can be decided according to cooling capacity and panel surface area.

Finally, we also recommend verifying the generalization of this optimum design by applying other models or experiments in future studies. Further improvements in RCPs are also expected to be achieved through the application of advanced optimization methodology or the combination of different design strategies.

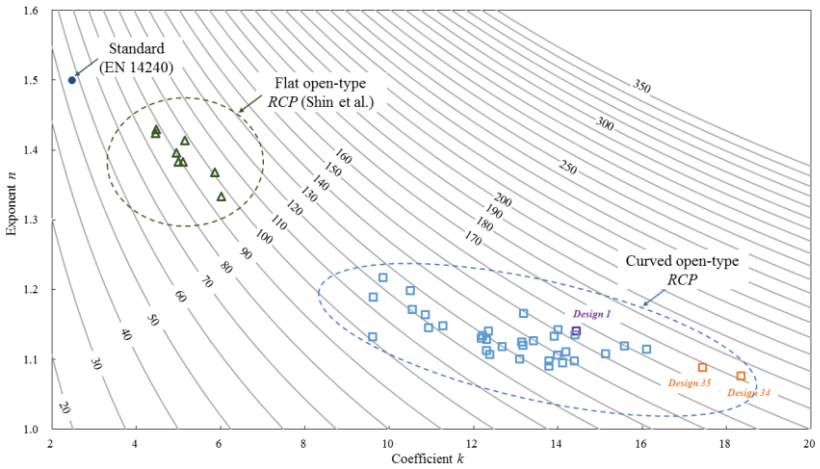

Fig. 4-15 k and n of different *RCP* design (T_{op}-T_s = 8 K)

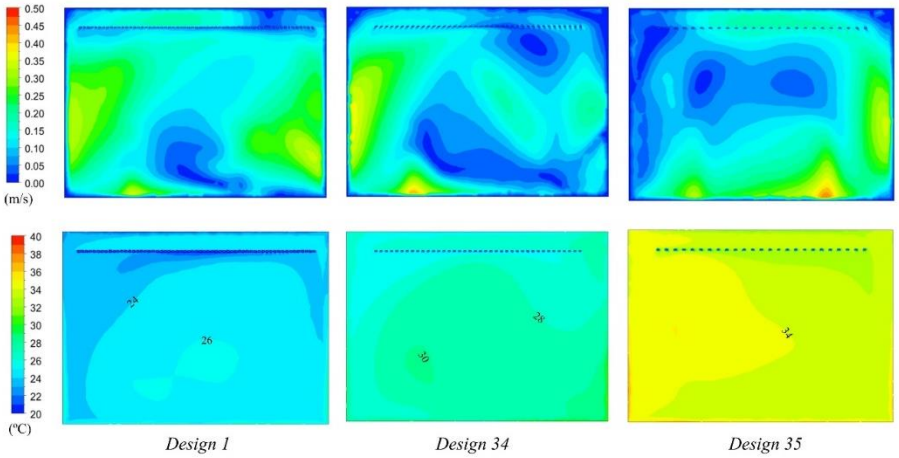

Fig. 4-16 Velocity and temperature contours in Design 1, Design 34 and Design 35

Table 4-4 Coefficient for the nominal cooling capacity equation

	k	n	R^2	$q_{(\Delta T = 8\ K)}$ (W/m^2)
Standard [19]	7.489	1.051	-	66.6
A-d [15]	5.8604	1.3674	-	100.6
Design 1	14.448	1.14	0.9949	154.64
Design 2	13.178	1.1193	0.9983	135.11
Design 3	12.321	1.1118	0.9957	124.37
Design 4	9.626	1.1882	1	113.89
Design 5	9.8661	1.2165	0.9997	123.81
Design 6	14.118	1.0942	0.9976	137.38
Design 7	13.994	1.1053	0.9974	139.36
Design 8	13.427	1.1261	0.9991	139.62
Design 9	14.392	1.0968	0.9986	140.81
Design 10	9.6204	1.132	0.9999	101.27
Design 11	10.549	1.1707	0.9984	120.35
Design 12	13.795	1.0974	0.9965	134.69
Design 13	13.927	1.1322	0.9994	146.67
Design 14	15.133	1.1075	0.9981	151.39
Design 15	13.196	1.165	0.9997	148.78
Design 16	14.418	1.1346	0.9994	152.60
Design 17	14.01	1.1421	0.9992	150.61
Design 18	14.198	1.1104	0.9843	142.90
Design 19	12.365	1.1398	0.9987	132.29
Design 20	13.795	1.0901	0.9987	133.10
Design 21	12.23	1.1338	0.9996	129.23
Design 22	10.507	1.1978	0.9978	126.82
Design 23	12.19	1.13	0.9989	127.79
Design 24	12.321	1.128	0.9979	128.63
Design 25	12.68	1.118	0.9951	129.65
Design 26	13.098	1.1004	0.9983	129.11
Design 27	12.39	1.1065	0.9989	123.69
Design 28	13.149	1.1239	0.9943	136.11
Design 29	10.864	1.1631	0.9901	122.00
Design 30	11.279	1.1475	0.9941	122.62
Design 31	10.94	1.1445	0.9998	118.20
Design 32	15.585	1.1182	0.9985	159.42
Design 33	16.117	1.1143	0.9996	163.53
Design 34	18.354	1.0754	0.9932	171.76
Design 35	17.442	1.0877	0.9997	167.45

4.3.5 Conclusions

In this study, we carried out a parametric analysis of an open-type RCP with a curved and segmented structure using CFD simulation to study the effect of panel structure on cooling capacity and heat transfer in comparison with conventional RCPs presented in the literature. Four independent and two dependent design parameters were investigated by comparing thirty-five panel designs and operating sensitivity analysis. The optimal panel design was then proposed in terms of cooling capacity, heat transfer coefficient, and airflow distribution. The results are as follows:

1. The freely suspended RCP with curved shape and void in proposed this study achieves better cooling performance than the previous reference results. The nominal cooling capacity can be improved by 157.90% compared with the transitional panel design represented in the standard.

2. The nominal cooling capacity and heat transfer coefficient increase with increasing panel curvature radius and decreasing curvature width. The nominal cooling capacity is highest when $L = 0.03$ m and $r = 0.06$ m, which is the optimal panel design among the designs proposed in this study.

3. Compared with the large solid panel design, the short and distributed panel design with less panel surface area achieves better cooling performance because it can promote air movement around the panel and assist in sufficient heat exchange.

4. The distances between adjacent panels and between the panel and the wall play the most significant role in improving the cooling performance of the panel, demonstrating the potential to simultaneously reduce costs and achieve better indoor thermal conditions by optimizing the distribution of RCPs.

5. There should be a balance between improving cooling performance and ensuring the comfort of the indoor environment in practical operations.

4.4 Optimizing the integration of the open-type RCP with a wall attached ventilation system

4.4.1 Integrated the RCP with different ventilation systems

The RCP system is unable to circulate air to remove the latent heat and reduce contaminants to achieve standard indoor air quality [23]. It cannot prevent the warm draft of the hot window singly from diffusing into the environment, which affects the indoor thermal comfort negatively [24]. Therefore, the RCP system should always be integrated with a forced ventilation system.

The ventilated air can be supplied either from the bottom or upper area, as summarized in Fig.4-17:

In the bottom supply form, the Displacement Ventilation (DV) and Underfloor Air Distribution (UFAD) are commonly used, in which the air is supplied from the floor and returned via the ceiling. In these two ventilation systems, the room's heat source generates thermal plumes that contribute to the vertical air movement and bring heated and contaminated air into the ceiling. Also, these systems can prevent downward cold draught from the window through an additional perimeter-heating system near the external walls, especially in the winter season [25,26]. Krusaa and Hviid [27] combined a radiant ceiling panel with diffuse ventilation and investigated the thermal performance and thermal comfort of the system in a building with two offices numerically. Choi et al. [28] proposed the vertical radiant panel with displacement ventilation (DV) in hospital wards through experiments.

In the upper supply form, Diffuse Ceiling Ventilation (DCV) is proposed to integrate with the radiant panel system, which is recommended for large-scale rooms and heating systems in the cold climate. In this system, the air is supplied through the gap between the ceiling panels with low air velocity [29,30]. Tian et al. [31] did a field study on the radiant ceiling cooling and overhead air distribution system (RCF). They found the RCF system can achieve better comfort conditions than conventional air conditioning at the same operative temperature range. Zhao et al. [32] studied three integrated systems-a radiant panel system combined with a low-velocity unit (LVRP), a radiant panel system combined with a personalized ventilation system (PVRP), and a radiant panel system combined with diffuse ceiling ventilation (DCV-RP). The results showed that both the LVRP and PVRP systems can satisfy the demand of the subjects and improve the perceived air quality.

In this study, the integrated system is to reduce the warm draft's effect from the window, which was detected in the experiments shown in *Section 3*. Therefore, the upper supply form- a wall attached ventilation (WAV) system [33] is selected to be used, which can deliver the air along the vertical wall as shown in Fig. 4-18.

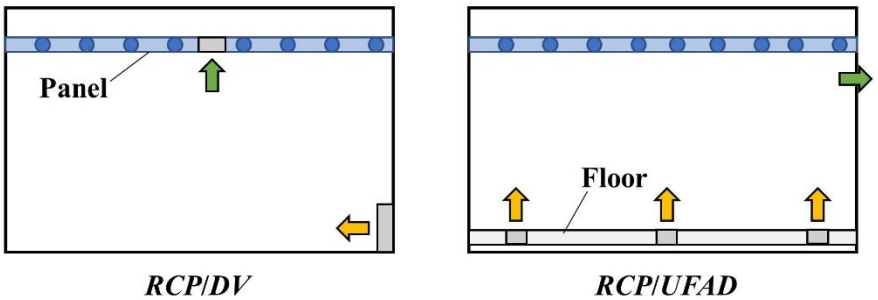

(a) Bottom supply form

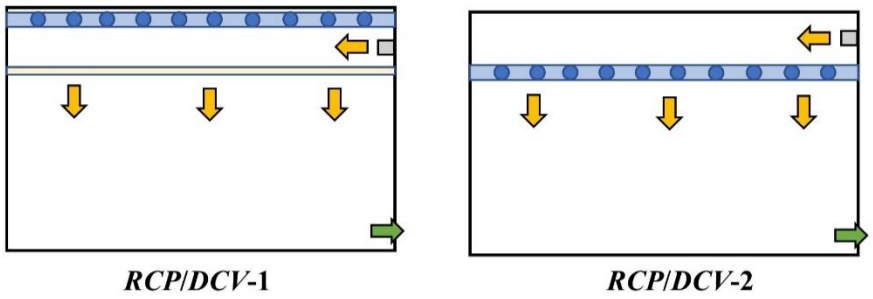

(b) Upper supply form

Fig.4-17 Different types of *RCP* system integrated with forced ventilation system

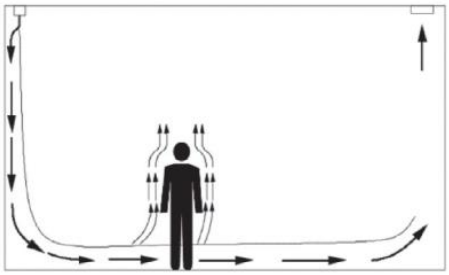

Fig. 4-18 The schematic diagram of wall attached ventilation (WAV) [33]

4.4.2 CFD simulation setup

The three-dimensional finite volume model is developed by ANSYS 2020 R2 Fluent platform for validation and comparison purposes. The basic CFD model (Case 0) has the same dimension and arrangement with the chamber and the dummy cylinders in the previous experiment introduced in *Section 3.2*. In Case 1, a wall attached ventilation (WAV) system with rectangle intake and exhaust vents are added into the model, as illustrated in Fig. 4-19 (b). The air inlet vent is located beside the window, and the air exhaust vent is on the opposite side. Both inlet and outlet have the same dimensions (1.5 m × 0.03 m × 0.19 m) and are fixed at the same level as RCP. Case 2 uses the inlet at the same position as Case 1, while the outlet is placed on the floor level with the dimension of 1.5 m × 0.03 m as shown in Fig. 4-19 (c). Besides, the middle plane is a Y-Z Plane in the middle of the X-axis (X=1.35 m).

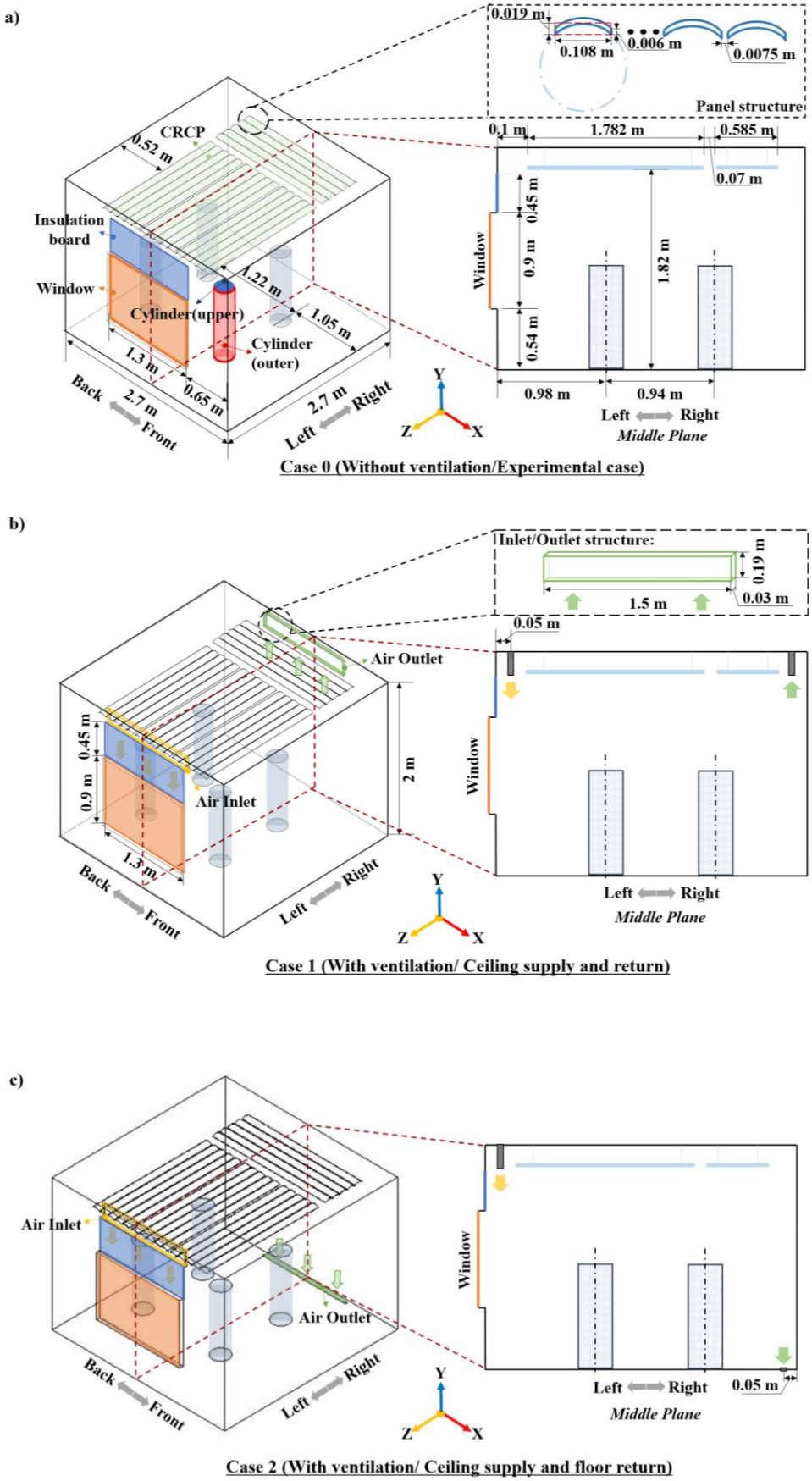

Fig. 4-19 The geometry of the chamber, RCP system and WAV system

The tetrahedron grid element is applied to discretize the space, as shown in Fig. 4-20. The inflation layers are adopted near the walls, dummy cylinder, and the RCP surfaces, the first layer thickness is 0.01 m, and the number of layers is 5 with a growth rate of 1.2 to achieve $y^+ < 10$. A mesh sensitivity test is performed on three meshes with 1,173,760; 1,402,063 and 2,018,382 elements to ensure that the mesh element size has no more impact on the solution accuracy as listed in Table 4-5.

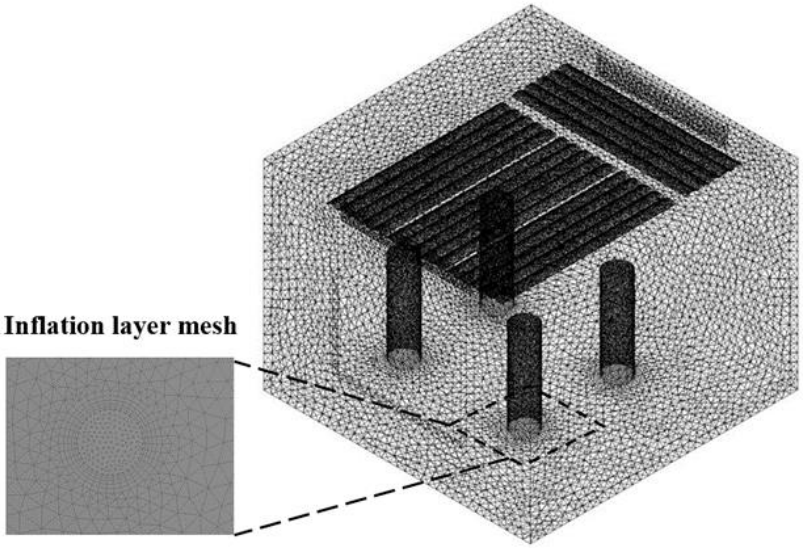

Fig.4-20 Grid of the simulation domain and the inflation layers

Table 4-5 Mesh independent solution carried out for the CFD simulation

Mesh number	1,173,760	1,402,063	2,018,382
Average air temperature (°C)	25.50	25.46	25.39
Total heat flux of RCP (W/m^2)	25.19	25.26	25.34

All the boundary conditions in Case 0 are summarized as shown in and Table 4-6. Case 1 and Case 2 have the same boundary condition as Case 0, while for the ventilation system, the inlet air temperature is set as 22.19 °C and the inlet air flow rate is 1.5 (L/m^2)/s.

Table 4-6 Boundary condition and emissivity of each surface

	Emissivity	Condition	Temperature (°C)	Heat flux (W/m^2)	Velocity (m/s)
Wall/Floor/Ceiling	0.82	adiabatic	-	0	-
Panel surface (up/ bottom)	0.92	T=constant	22.19	-	-
Cylinder (outer wall)	0.92	q=constant	-	59.5	-
Cylinder (upper wall)	1	adiabatic	-	0	-
Window	0.92	q=constant	-	42.2	-
Insulation board	0.92	q=constant	-	8.3	-

inlet	-	Velocity_inlet	22.19	-	0.2739
outlet	-	Pressure_outlet	-	-	-

A SIMPLE algorithm was applied for coupling pressure and velocity, a first-order upwind discretization scheme was chosen for turbulent kinetic energy and turbulent dissipation rate, and a second-order upwind discretization scheme was used for the rest variables. The enhanced wall treatment was selected as a wall treatment. The convergence criteria are 10^{-5} for all equations except 10^{-6} for the energy equation.

4.4.3 Simulation results

The system's performance is evaluated based on two perspectives: (1) the indoor thermal comfort. (2) the heat transfer characteristics from the radiant panel to the surrounding surfaces and indoor space. From the results of the radiation and convection heat fluxes, the radiant heat flux coefficient (h_r) and convective heat flux coefficient (h_c) can be calculated by Eq. (4-17) and Eq. (4-18).

$$h_r = \frac{q_r}{(AUST - T_s)} \quad (4-17)$$

$$h_c = \frac{q_c}{(T_a - T_s)} \quad (4-18)$$

Where T_s is the surface temperature of the radiant panel, T_a is the average air temperature in the test room, and *AUST* is the area-weighted average of the uncooled surface temperature.

In addition, the predictive mean vote (PMV) is an index that describes the thermal sensation of the human body on the 7-points scale from +3 (hot) to -3 (cold); in CFD calculation, the humidity and human indexes are assumed to be 50%rh, 1met, 0.5 clo. Thus, the PMV is simplified to be a function of both operative temperature T_{op} (℃) and relative air velocity v (m/s) with a linear relationship as follows:

$$PMV = 0.1019{T_{op}}^{1.34047} - 9.07322v^{0.04656} \quad (4-19)$$

The CFD simulation was validated with the experimental results at first. The vertical air temperature distribution along Line 2 was drawn at 0.88 m to the left wall. The total/radiant heat flux and average air temperature in three measure lines are compared, and the error value is calculated. Fig. 4-21 and Fig. 4-22 show that the CFD model had a good agreement with the experimental results in heat transfer analysis and indoor air simulation.

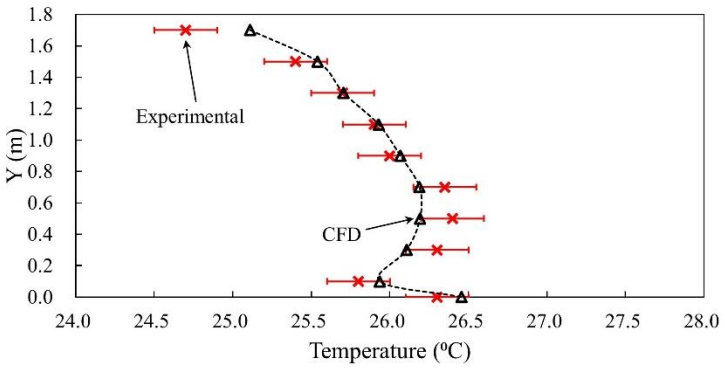

Fig. 4-21 The validation of the CFD model (Case 0) with experimental results in Line 2 (*Section 3.2*)

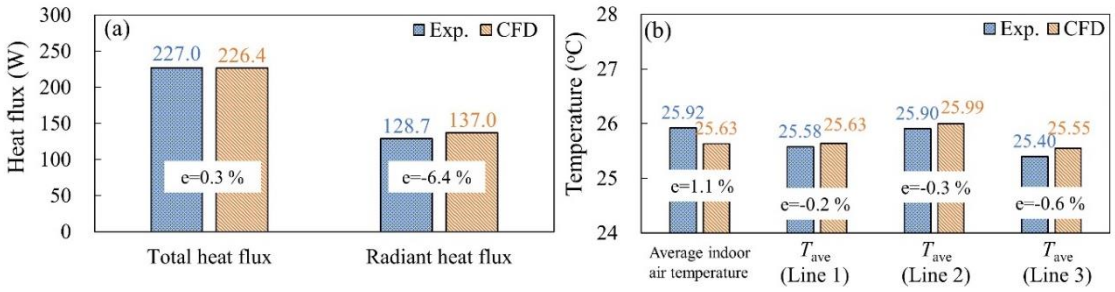

Fig. 4-22 Error between experiment and simulation results

Fig. 4-23 shows the temperature, velocity, and PMV contours of the middle plane in Cases 0 -2. It indicates that both the air temperature decreases after integrating with the forced ventilation system. The average air temperature in the middle plane dips from 25.8 ℃ to 25.3 ℃ (Case 1) and 25.5 ℃ (Case 2). The contours also illustrate that the downward cold air stream counters with the warm draft near the window. Therefore, it withstands the warm air stream tendency to buoy upward and propagate to the rest of the space. Accordingly, the ventilation system also reduces the air temperature in the middle part around dummy cylinders. When comparing Case 1 with Case 2, the air temperature in Case 1 is lower, and the ventilation system has better performance.

Conversely, the average airspeed in all the cases is less than 0.21 m/s, which is smaller than the recommended air velocity of 0.25 m/s for cooling mode [34]. Moreover, the ventilation system accelerates the air close to the bottom of the window, and therefore the air velocity at the right of the room is also decreased.

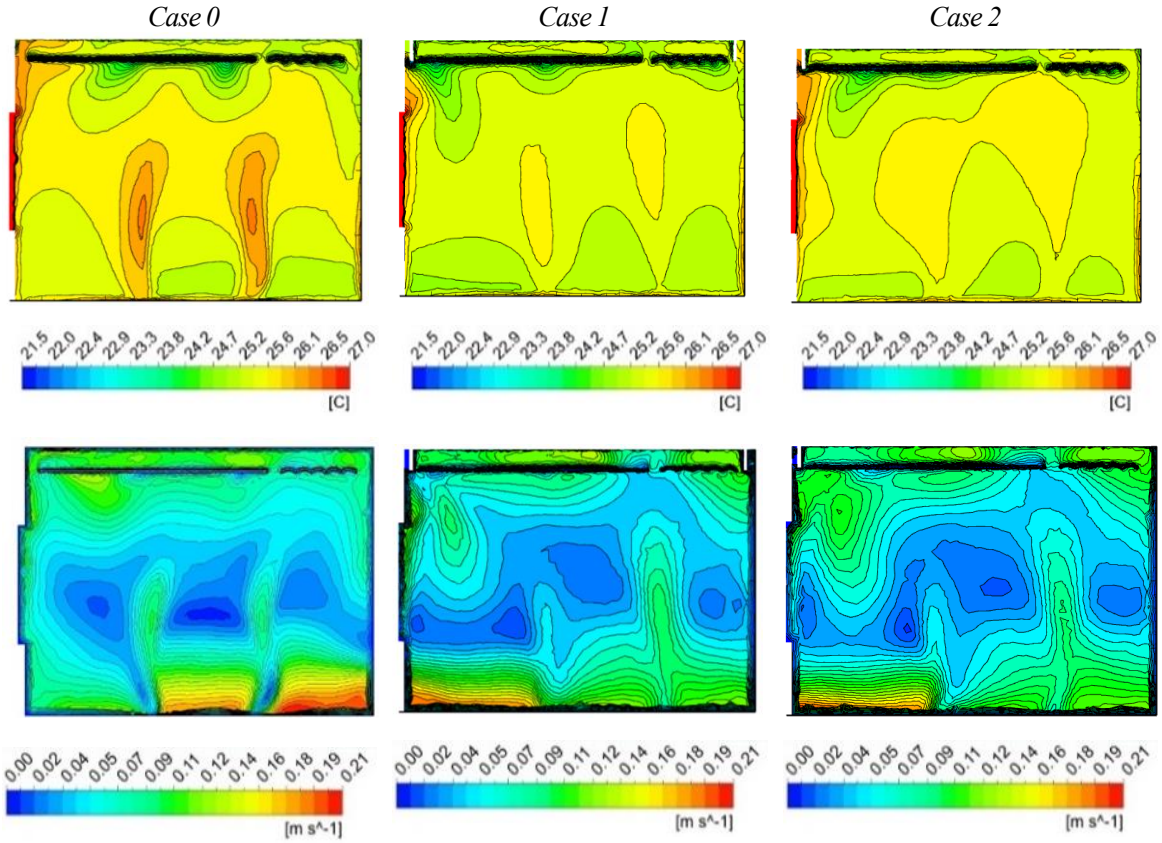

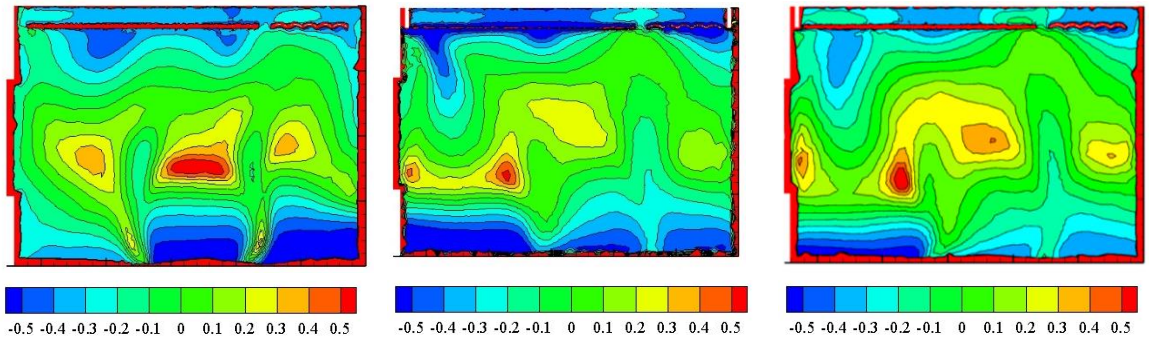

Fig. 4-23 Air temperature, PMV, and air velocity distribution in the middle plane

Heat transfer characteristics of Case 0-2 are analyzed through simulation results. As shown in Fig. 4-24 (a) and (b), after integrating with the ventilation system, the total heat flux drops from 52.55 W/m^2 to 44.48 W/m^2 (Case 1) and 51.18 W/m^2 (Case 2) since the WAV system shares some part of heat transfer through the indoor air. The convection heat transfer of CRCP reduces by 21.6 % (Case 1) and 4.9 % (Case 2), while the radiant heat transfer of RCP reduces by 11.4 % (Case 1) and 1.2 % (Case 2). Moreover, the convective heat flux ratio drops from 38.7 % to 35.8 % (Case 1) and 37.8% (Case 2). By contrast, the proportion of radiant heat flux rises from 61.3 % to 64.2 % (Case 1) and 62.2% (Case 2). Nevertheless, the convective heat transfer coefficient and the radiant heat transfer coefficient decrease by about 5 % in Case 1. While the convective heat transfer coefficient in Case 2 increases a little.

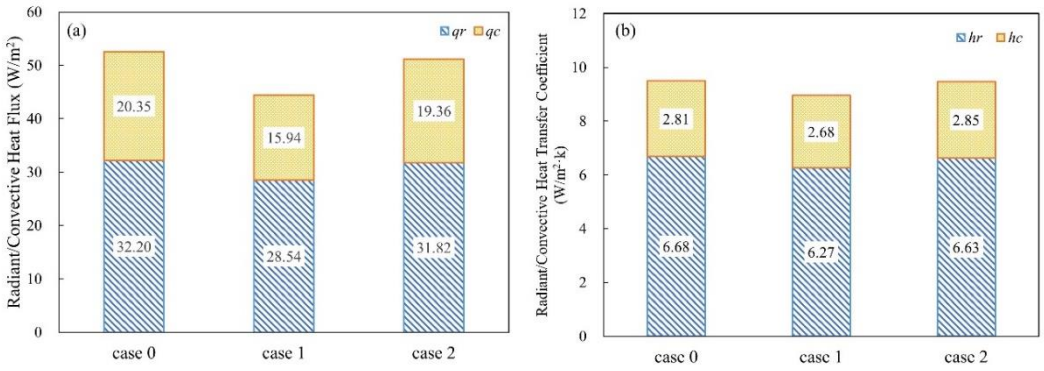

Fig.4-24 Radiant and convective heat flux and heat transfer coefficient of the RCP system

4.4.4 Sensitivity analysis and optimization

Comparing the cases with and without the ventilation system demonstrates that the ventilation system can decrease room temperature. The sensitivities analysis and optimization are carried out to select the optimum operating conditions using the ANSYS Design Explorer tool. Fig. 4-25 shows the steps and methods used in this study:

1. Three operating parameters are defined; the ventilate air flow velocity, ventilated air temperature and panel surface temperature. Seven output variables are assigned, where three of them used later for optimization purposes.
2. The Central Composite Design (CCD) algorithm available in the DOE is automatically sampled the design space. The design space's size is determined according to the number of the design parameters and its ranges.

3. Response Surface is computed from the design points to demonstrate the response of the objectives corresponding to the variation in the input parameters based on the Kriging interpolation algorithm.

4. Objectives are defined in the Gool Driven Optimization (GDO) step, and the system can provide possible optimum designs within the limits of the input parameters fulfilling the goals and constraints of the objective output parameters.

5. Finally, the thermal comfort of six optimum candidates is simulated, and compared (Case 1-1, Case 1-2, Case 1-3, Case 2-1, Case 2-2, Case 2-3)

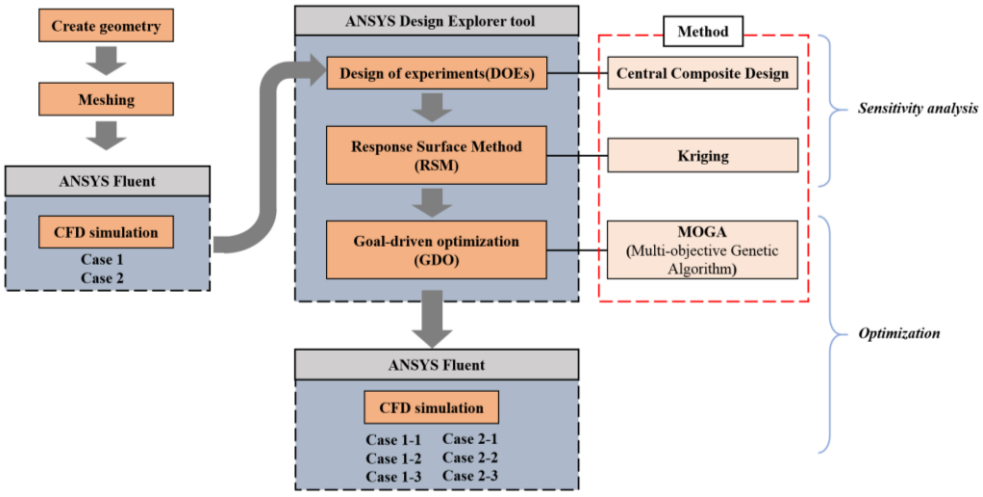

Fig. 4-25 The operating process and methods of the optimization

In this study, the analysis mainly considers three factors (two factors for ventilation, and one factor for RCP) as input parameters – (A)- inlet air velocity v, (B)- inlet air temperature T_{in}, and (C)- panel surface temperature T_s. The input/output parameters and objectives are shown in Fig. 4-26. Overall, this optimization's main objective is to increase the convective heat transfer of the RCP system and reduce the heat transfer of the WAV system as much as possible.

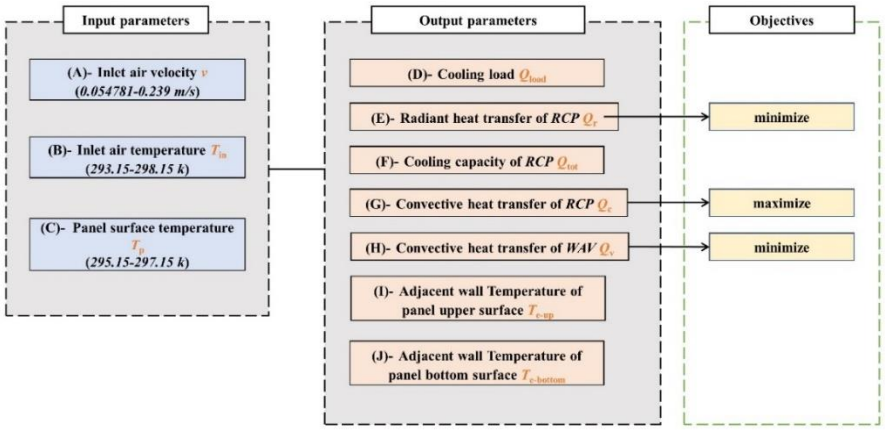

Fig. 4-26 The design of input or output parameters and objectives in the ANSYS DesignXplorer tool

Central Composite Design (CCD) is an optimal design of an experiment (DOE) algorithm that allows a minimum number of experiments, calculation with the best precision possible of each factor's effects, and interactions. The number of design space points obtained at each number of factors is given by the formula as followed [35]:

$$N = 2^n + 2n + n_o \qquad (4-20)$$

Where n is the number of process factors (n=3), n_o is the number of the center points the designer desired for (n_o=1). In this study, a total of 15 design points (including the current design) is chosen.

Response Surface Method is a mathematical and statistical method that interpolates the data generated from *DOE* using a correlation function to estimate the distribution of function value at unknown points. Kriging- one of the Response Surface is efficient in a large number of cases, suited to highly nonlinear responses, and widely used in the domain of spatial analysis and computer experiments [36]. This method. Lu et al. reviewed the Kriging model in the application of engineering optimization and discussed an advanced model [37].

Fig. 4-27 highlights the global sensitivity analysis of the impact of three input parameters: inlet air velocity, inlet air temperature, and panel surface temperature on the radiant and convective heat transfer of RCP system, and convective heat transfer of WAV system. Although the difference in value is minimal, the inlet air temperature is the most sensitive parameter affecting the cooling performance of the integrated system; followed by panel surface temperature (in Case 1) and inlet air velocity (in Case 2).

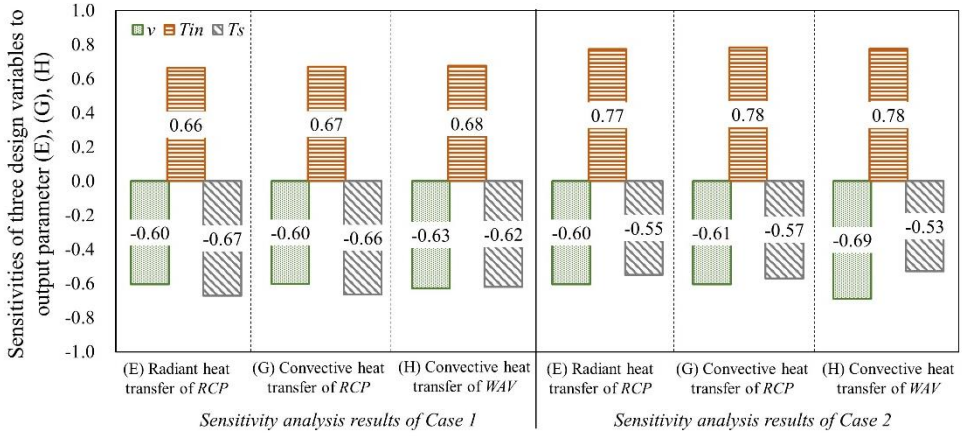

Fig. 4-27 Sensitivities analysis results of three design variables

Fig. 4-28 shows the response surfaces plot. These figures demonstrate that all response variables change almost linearly with increments or reduction. In both Case 1 and Case 2, when inlet air velocity increase, the convective and radiant heat transfer of the RCP system increase, the convective heat transfer of the WAV system decreases. In opposite, the convective and radiant heat transfer of the RCP system decreases with higher panel surface temperature and higher inlet air velocity. Consequently, sensitivity analysis can be concluded that raising the inlet air temperature is the most effective method to achieve the objectives.

Case 1 (ceiling inlet/ceiling outlet) Case 2 (ceiling inlet/floor outlet)

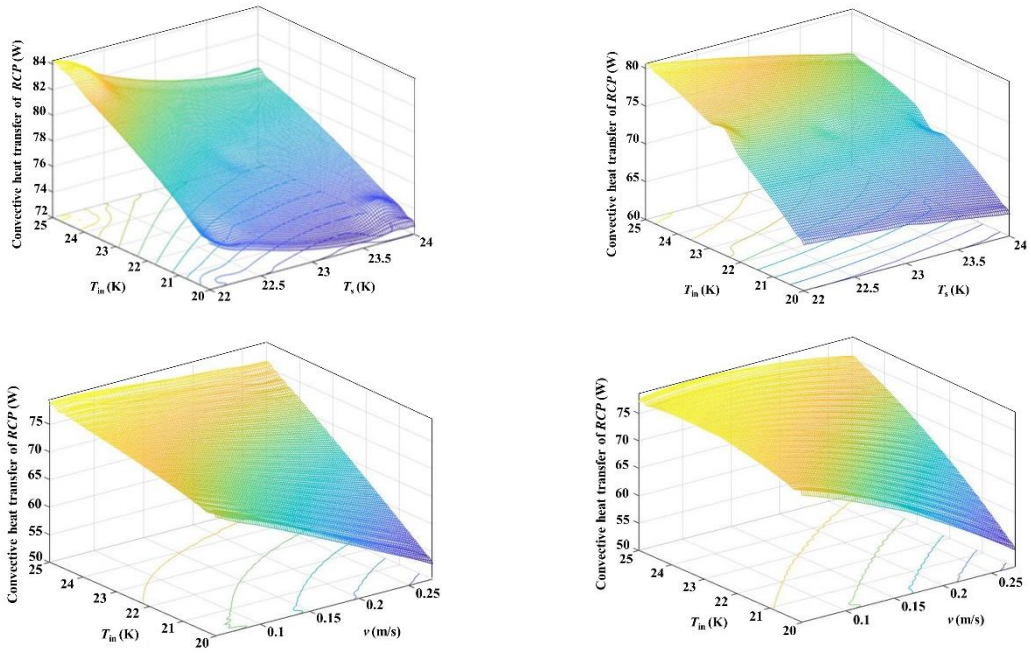

(G)-Convective heat transfer of RCP system

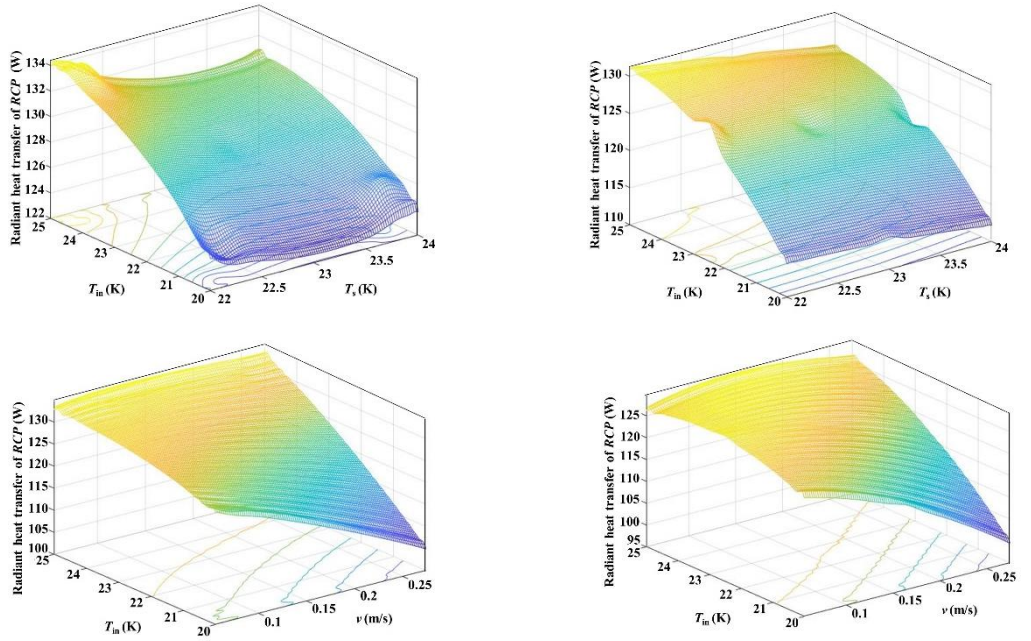

(E)-Radiant heat transfer of RCP system

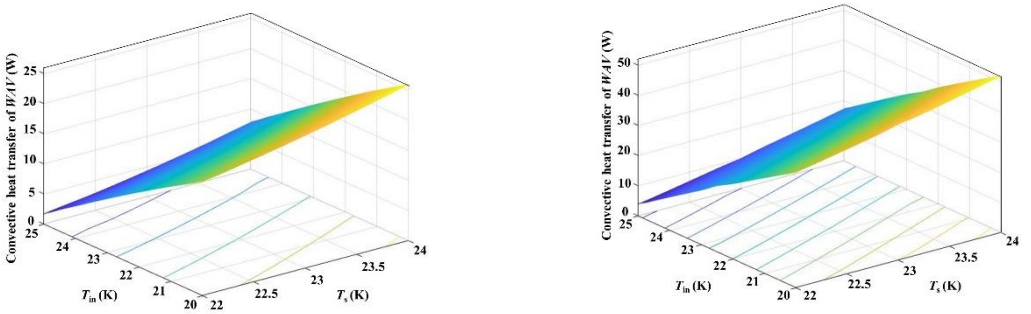

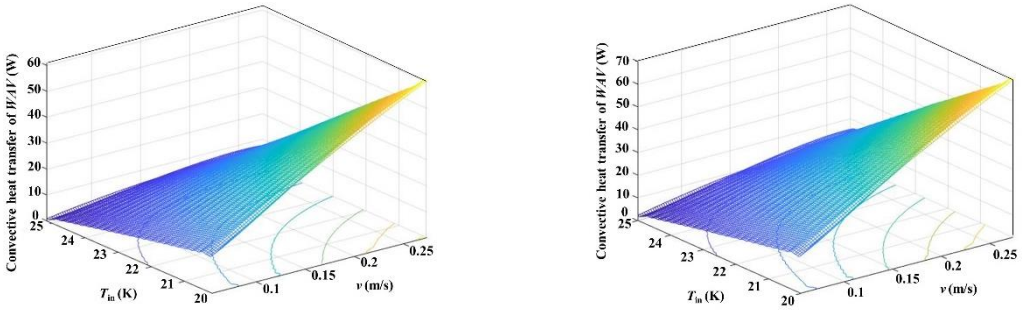

(H)-Convective heat transfer of WAV system

Fig. 4-28 Three-dimensional surface responses with three design variables

The Multi-Objective Genetic Algorithm (MOGA) used for the optimization is a hybrid variant of the popular Non-dominated Sorted Genetic Algorithm-II (NSGA-II) based on the fastnon-dominated sorting algorithm [38]. It takes the advantage of supporting all types of input parameters.

Parallel coordinate plots show the design space distributed randomly Six green lines represent the results of candidate cases as shown in Fig. 4-29.

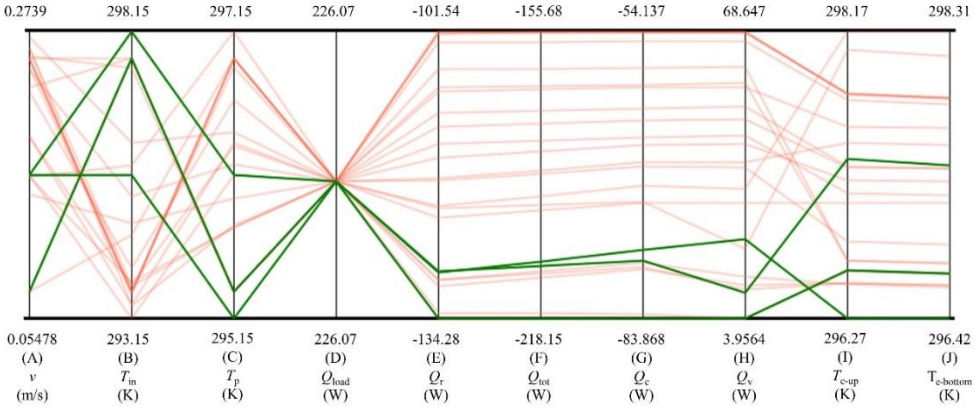

(a)

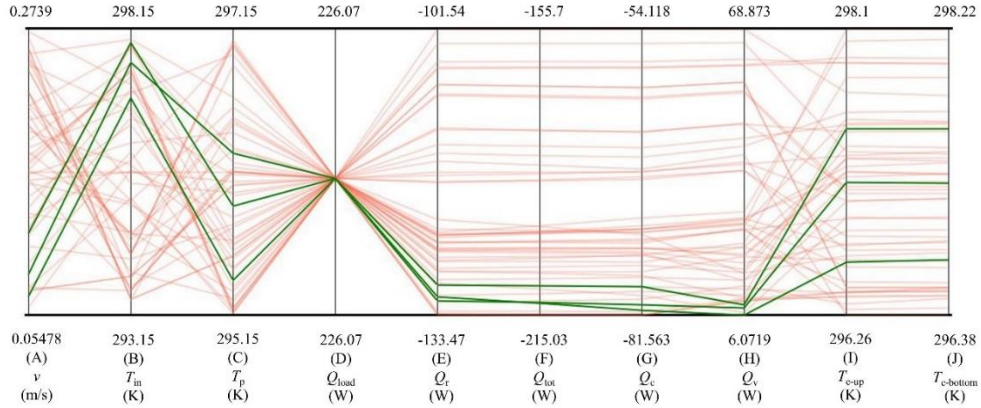

(b)

Fig.4-29 Parallel coordinate charts displaying the relationship and variability of parameters according to filtered high multi-objective design goals

Table 4-7 lists six candidate cases for possible optimum operating conditions of the integrated system. When compare Candidate #1-6 with original Case 1 and Case 2, all the candidate cases use lower inlet air velocity, a relatively higher inlet air temperature, and surface temperature, which provides the possibility for energy saving.

Two items are used to evaluate the achievement of the objectives: 1) the convective heat transfer ratio of RCP: Q_c/Q_{tot}; 2) Heat transfer of the WAV system: Q_v. Notably, all the candidates can meet the design goals that improve the convection of the radiant ceiling panel. Compared with Case 1 and Case 2, almost all candidate cases enhance the convection rate in the RCP system and decrease the heat transfer in the WAV *s*ystem. For example, in Case 1-1, the ratio of the convective heat transfer rises by 3.21 % and the heat transfer of the ventilation system descends by 89.47 % from 38.54 W to 4.06 W. Consider all these input and output parameters, Candidate -2 and Candidate -5 is the best designed respectively for optimization of Case 1 and Case 2 in terms of energy saving.

Table 4-7 Results of convection heat transfer in design candidate cases

	Operating conditions			Simulation results	
	v (m/s)	T_{in} (°C)	T_s (°C)	Q_c/Q_{tot} (%)	Q_v (W)
Case 1	0.2739	22.19	22.19	35.23	38.54
(Candidate cases for Case 1)					
Candidate -1	0.075	24.53	22.19	38.44	4.06
Candidate -2	0.164	25	23	37.67	20.87
Candidate -3	0.164	22.5	22	37.30	21.98
Case 2	0.2739	22.19	22.19	37.83	13.94
(Candidate cases for Case 2)					
Candidate -4	0.118	24.76	22.76	37.92	7.79
Candidate -5	0.086	24	23.13	37.73	8.46
Candidate -6	0.07	23.8	22.24	38.15	6.07

Fig. 4-30 illustrates the air temperature, velocity and PMV distribution in the middle plane of six candidate cases. Compared with Case 0-2, all candidate cases can get more uniform air temperature distribution and lower air velocity. The Cold air stream can prevent the warm draft from the window in all the cases except Candidate-5. In terms of energy saving, Candidate-2 and Candidate-5 are considered the energy-efficient operating condition, but the indoor temperature of the middle area exceeds 26.7 °C in Candidate-5, as shown in the temperature contour. Moreover, the temperature of Candidate 4-6 is about 1 °C higher than Candidate 1-3. After optimization, the case using ceiling inlet/ceiling outlet still performs better than ceiling inlet/floor outlet cases.

If considering both energy-saving and thermal comfort, Candidate-2 is better than other cases even the indoor temperature of this case isn't the lowest. In Candidate -2, it accessible to achieve better thermal comfort by using higher inlet and surface temperature and lower air velocity.

Candidate case for Case 1 (ceiling inlet/outlet)

Candidate -1 Candidate -2 Candidate -3

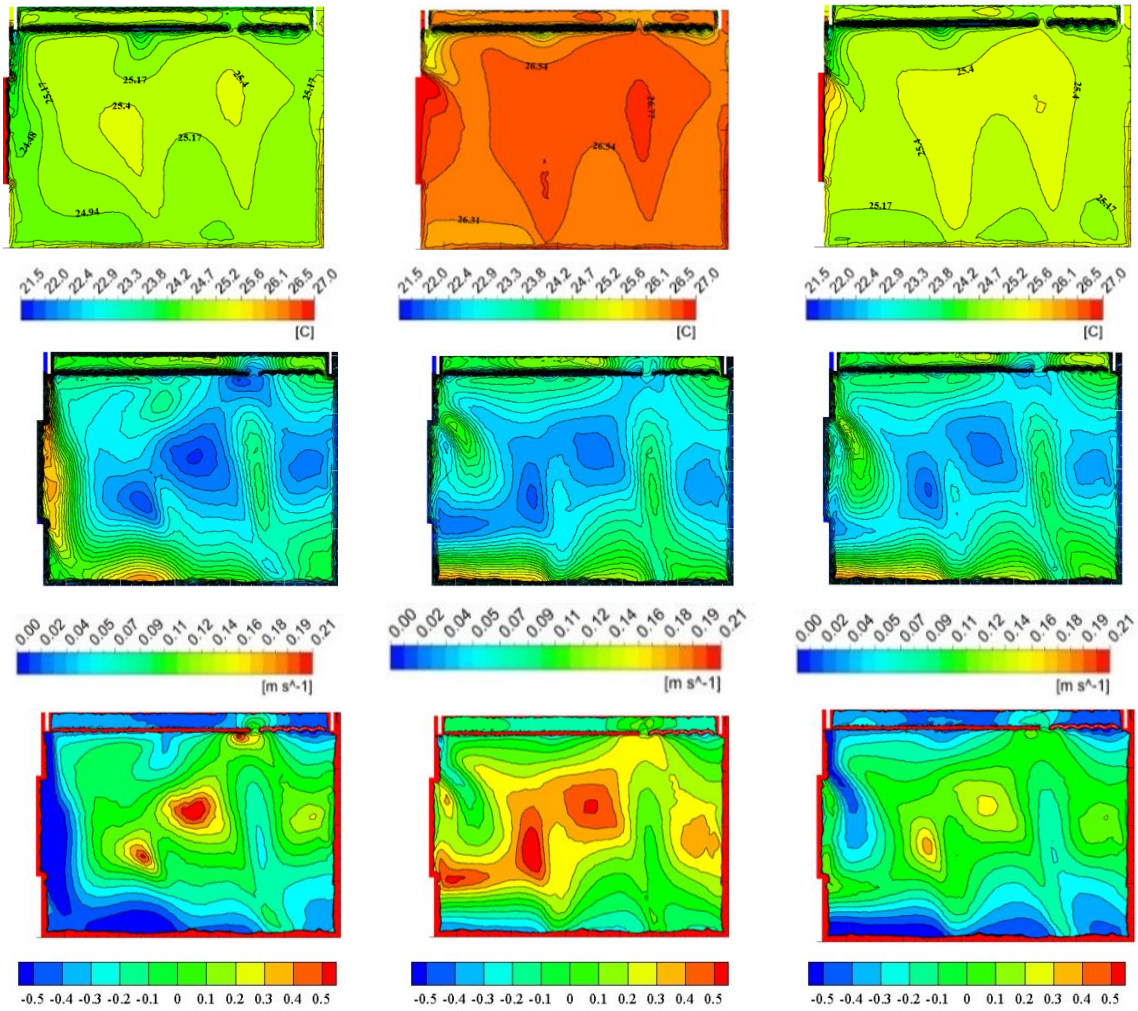

Candidate case for Case 2(ceiling inlet/floor outlet)

Candidate-4 Candidate-5 Candidate-6

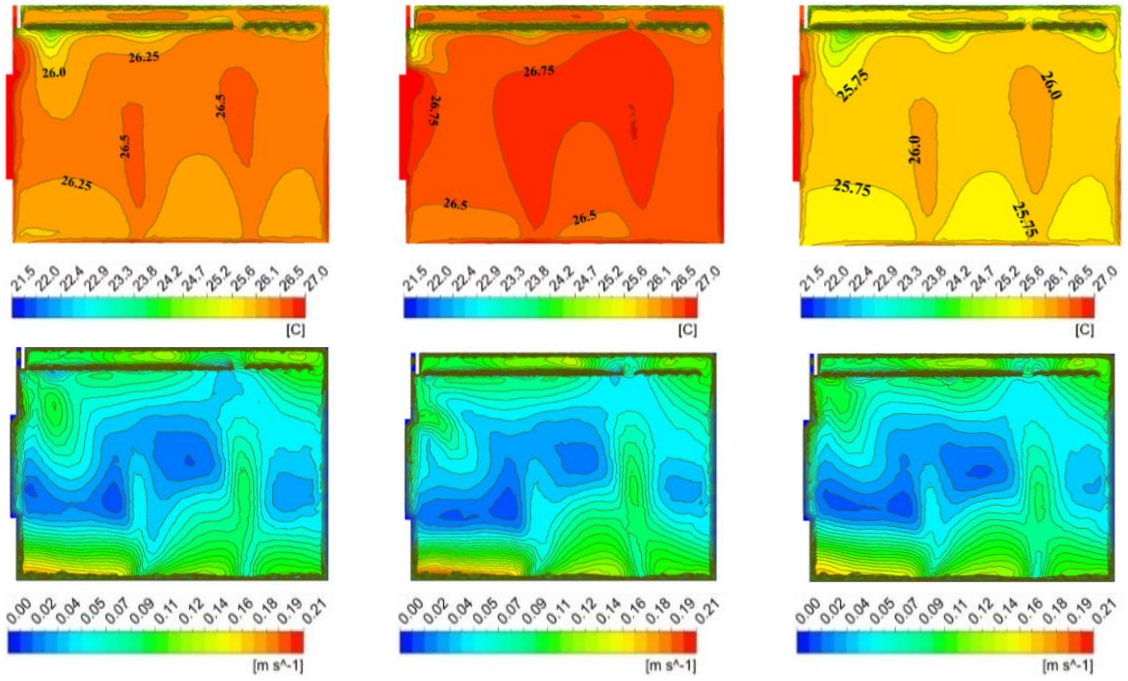

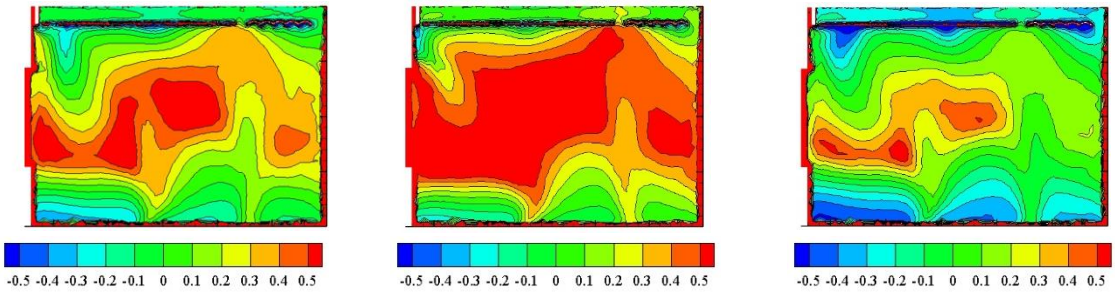

Fig. 4-30 Air temperature, velocity and PMV distribution in the middle plan of three candidate cases

4.4.5 Conclusions

This study optimizes the operating conditions of the integration system of a novel RCP with WAV system by using CFD simulation. The objectives include improve the indoor thermal conditions and save more energy. The results are concluded as follows:

1. The CFD model had a good agreement with the experimental results.

2. As a result of the sensitivity study, the inlet air temperature is the most sensitive parameter affecting the integrated system's cooling performance.

3. When inlet air velocity and inlet air temperature increase, the convective and radiant heat transfer of the RCP system increase, the convective heat transfer of the WAV system decrease.

4. The optimized operating condition in Case 1-2 allows the integrated system to operate under higher inlet and panel surface temperature (increased by 2.81 °C /0.81 °C) and lower air velocity (decreased by 0.1099m/s). Also, the PMV contours of Case 1-2 shows this case can achieve acceptable thermal comfort.

In future study, the authors are planning to optimize the cooling water temperature and flow rate, which may help save more energy consumption of this integrated system. Also, the indoor air humidity and air quality also need to discuss.

Nomenclature

List of symbols

L	Panel curvature width (m)
r	Panel curvature radius (m)
d	Void distance (m)
A_c	Panel coverage area (m^2)
A_s	Panel surface area (m^2)
$\vec{v}$	Velocity vector (m/s)
p	Static pressure (N/m^2)
I	Unit tensor
C_p	Specific heat capacity (J/kg·K)
k	Turbulent kinetic energy (m^2/s^2)
$\vec{F}$	External body force (N/m^3)
s	Energy source terms (W/m^3)
F_{jk}	View factor between surface *j* and surface *k*
A_j, A_k	Area of surface *j* and surface *k* (m^2)
q_j, q_k	Radiant heat flux of surface *j* and surface *k* (W/m^2)
S_k, S_ε	Source terms of k-equation and ε equation ($kg/m·s^3$)
C_μ, $C_{1\varepsilon}$, and $C_{2\varepsilon}$	Empirical constants
l	Panel length (m)
n	Panel number, number of factors
Q_s, Q_{tot}	Heat amount (W)
Q_r	Radiant heat transfer amount (W)
Q_c	Convective heat transfer amount (W)
q_{tot}	Total heat flux (W/m^2)
q_r	Radiant heat transfer flux (W/m^2)
q_c	Convective heat transfer flux (W/m^2)
h_r	Radiant heat transfer coefficient ($W/m^2 \cdot K$)
h_c	Convective heat transfer coefficient ($W/m^2 \cdot K$)
AUST	Uncooled surface temperature (ºC)
T_a	Indoor air temperature (ºC)
T_s	Panel surface temperature (ºC)
T_{op}	Operative temperature (ºC)
v	Inlet air velocity (m/s)
T_{in}	Inlet air temperature (ºC)
Q_v	Heat amount of ventilation system (W)
Q_{load}	Heat load (W)

e	Error
Greek symbol	
ρ	Density (kg/m^3)
ρ_0	Specific constant density of the flow (kg/m^3)
$\rho\vec{g}$	Gravitational body force (N/m^3)
$\bar{\bar{\tau}}$	Surface stress tensor (N/m^2)
ε	Turbulent dissipation rate (m^2/s^3)
ε_k	Emissivity
β	The thermal expansion coefficient (1/K)
σ_k, σ_ε	The Prandtl numbers of k and ε equations
μ_t	The eddy viscosity (kg/m·s)
σ	Stefan-Boltzmann constants (W/m^2·K^4)
Abbreviations	
RCP	Radiant ceiling panel
WAV	Wall attached ventilation
CFD	Computational fluid dynamic
ASHRAE	American Society of Heating, Refrigerating and Air-Conditioning Engineers
PMV	Predicted mean vote
DV	Displacement ventilation
UFAD	Underfloor air distribution
DCV	Diffuse ceiling ventilation
CCD	Central composite design
DOE	Design of experiment
MOGA	Multi-Objective Genetic Algorithm
NSGA-II	Non-dominated Sorted Genetic Algorithm-II

Reference

[1] H. Tang, P. Raftery, X. Liu, S. Schiavon, J. Woolley, F.S. Bauman, Performance analysis of pulsed flow control method for radiant slab system, Build. Environ. 127 (2018) 107–119. https://doi.org/10.1016/j.buildenv.2017.11.004.

[2] R. Talami, J.A. Jakubiec, Early-design sensitivity of radiant cooled office buildings in the tropics for building performance, Energy Build. 223 (2020) 110177.

[3] H. Pieskä, A. Ploskic, S. Holmberg, Q. Wang, Performance Analysis of a Geothermal Radiant Cooling System Supported by Dehumidification, Energies. 15 (2022). https://doi.org/10.3390/en15082815.

[4] H. Pieskä, A. Ploskić, Q. Wang, Life-cycle assessment of a radiant high-temperature cooling system in the Mediterranean climate, Build. Environ. 245 (2023) 110847. https://doi.org/10.1016/j.buildenv.2023.110847.

[5] Q. Chen, N. Li, Thermal response time prediction-based control strategy for radiant floor heating system based on Gaussian process regression, Energy Build. 263 (2022) 112044. https://doi.org/10.1016/j.enbuild.2022.112044.

[6] J. Le Dréau, P. Heiselberg, Sensitivity analysis of the thermal performance of radiant and convective terminals for cooling buildings, Energy Build. 82 (2014) 482–491. https://doi.org/10.1016/j.enbuild.2014.07.002.

[7] Zhang, C.; Heiselberg, P.K.; Chen, Q.; Pomianowski, M. Numerical Analysis of Diffuse Ceiling Ventilation and Its Integration with a Radiant Ceiling System. 2015, doi:10.1007/s12273-016-0318-z.

[8] Chiang, W.H.; Wang, C.Y.; Huang, J.S. Evaluation of Cooling Ceiling and Mechanical Ventilation Systems on Thermal Comfort Using CFD Study in an Office for Subtropical Region. Build. Environ. 2012, 48, 113–127, doi:10.1016/j.buildenv.2011.09.002.

[9] Najafi, N.Z.; Haghighi, A.P. Anticipating an Efficient Relative Humidity in a Room under Direct Solar Radiation and Equipped by Radiant Cooling Panel System. Int. J. Refrig. 2019, 98, 98–108, doi:10.1016/j.ijrefrig.2018.10.018.

[10] ANSYS FLUENT 12.0/12.1 Documentation.
Available online: https://www.afs.enea.it/project/neptunius/docs/fluent/index.htm

[11] Kim, T.; Kato, S.; Murakami, S.; Rho, J.W. Study on Indoor Thermal Environment of Office Space Controlled by Cooling Panel System Using Field Measurement and the Numerical Simulation. Build. Environ. 2005, 40, 301–310.

[12] Awbi, H.B.; Hatton, A. Mixed Convection from Heated Room Surfaces. Energy Build. 2000, 32, 153–166

[13] A. Radwan, T. Katsura, L. Ding, A.A. Serageldin, A.I. ELSeesy, K. Nagano, Design and thermal analysis of a new multi-segmented mini channel based radiant ceiling cooling panel, J. Build. Eng. 2021, 40, 102330.

[14] Mikeska, T.; Fan, J.; Svendsen, S. Full Scale Measurements and CFD Investigations of a Wall Radiant Cooling System Integrated in Thin Concrete Walls. Energy Build. 2017, 139, 242–253.

[15] M.S. Shin, K.N. Rhee, S.H. Park, M.S. Yeo, K.W. Kim, Enhancement of cooling capacity through open-type installation of cooling radiant ceiling panel systems, Build. Environ. 2019, 148, 417–432.

[16] A.A. Serageldin, M. Ye, A. Radwan, H. Sato, K. Nagano, Numerical investigation of the thermal performance of a radiant ceiling cooling panel with segmented concave surfaces, J. Build. Eng. 2021, 42, 102450.

[17] Tye-Gingras, M.; Gosselin, L. Comfort and Energy Consumption of Hydronic Heating Radiant Ceilings and Walls Based on CFD Analysis. Build. Environ. 2012, 54, 1–13.

[18] A.A. Serageldin, M. Ye, A. Radwan, H. Sato, K. Nagano, Numerical investigation of the thermal performance of a radiant ceiling cooling panel with segmented concave surfaces, J. Build. Eng. 42 (2021) 102450. https://doi.org/10.1016/j.jobe.2021.102450.

[19] EN 14240:2004; Ventilation for Buildings-Chilled Ceilings-Testing and Rating.

[20] ISO 11855-2:2012(E); Building Environment Design-Design, Dimensioning, Installation and Control of Embedded Radiant Heating and Cooling Systems. Part 2: Determination of the Design Heating and Cooling Capacity.

[21] E. Borgonovo, E. Plischke, Sensitivity analysis: A review of recent advances, Eur. J. Oper. Res. 248 (2016) 869–887. https://doi.org/10.1016/j.ejor.2015.06.032.

[22] ANSI/ASHRAE 55-2013; ASHRAE Standard: Thermal Environmental Conditions for Human Occupancy.

[23] C. Zhang, M. Pomianowski, P.K. Heiselberg, T. Yu, A review of integrated radiant heating/cooling with ventilation systems- Thermal comfort and indoor air quality, Energy Build. 223 (2020) 110094, https://doi.org/10.1016/j.enbuild.2020.110094.

[24] S. Antoun, N. Ghaddar, K. Ghali, Coaxial personalized ventilation system and window performance for human thermal comfort in asymmetrical environment, Energy Build. 111 (2020) 253–266, https://doi.org/10.1016/j.enbuild.2015.11.030.

[25] D. Zhang, X. Huang, D. Gao, X. Cui, N. Cai, Experimental study on control performance comparison between model predictive control and proportion-integral-derivative control for radiant ceiling cooling integrated with underfloor ventilation system, Appl. Therm. Eng. 143 (2018) 130–136, https://doi.org/10.1016/j.applthermaleng.2018.07.046.

[26] S.J. Rees, P. Haves, An experimental study of air flow and temperature distribution in a room with displacement ventilation and a chilled ceiling, Build. Environ. 59 (2013) 358–368, https://doi.org/10.1016/j.buildenv.2012.09.001.

[27] M.R. Krusaa, C.A. Hviid, Combining suspended radiant ceiling with diffuse ventilation – numerical performance analysis of low-energy office space in a temperate climate, J. Build. Eng. 38 (2021) 102161, https://doi.org/10.1016/j.jobe.2021.102161.

[28] N. Choi, T. Yamanaka, K. Sagara, Y. Momoi, T. Suzuki, Displacement ventilation with radiant panel for hospital wards: measurement and prediction of the temperature and contaminant concentration profiles, Build. Environ. 160 (2019) 106197, https://doi.org/10.1016/j.buildenv.2019.106197.

[29] C. Zhang, P.K. Heiselberg, M. Pomianowski, T. Yu, R.L. Jensen, Experimental study of diffuse ceiling ventilation coupled with a thermally activated building construction in an office room, Energy Build. 105 (2015) 60–70, https://doi.org/10.1016/j.enbuild.2015.07.048.

[30] W. Wu, N. Yoon, Z. Tong, Y. Chen, Y. Lv, T. Ærenlund, J. Benner, Diffuse ceiling ventilation for buildings: a review of fundamental theories and research methodologies, J. Clean. Prod. 211 (2019) 1600–1619, https://doi.org/10.1016/j.jclepro.2018.11.148.

[31] Z. Tian, L. Yang, X. Wu, Z. Guan, A field study of occupant thermal comfort with radiant ceiling cooling and overhead air distribution system, Energy Build. 223 (2020) 109949, https://doi.org/10.1016/j.enbuild.2020.109949.

[32] W. Zhao, S. Kilpelainen, ¨ R. Kosonen, J. Jokisalo, S. Lestinen, Y. Wu, P. Mustakallio, Human response to thermal environment and perceived air quality in an office with individually controlled convective and radiant

cooling systems, Build. Environ. 195 (2021), https://doi.org/10.1016/j.buildenv.2021.107736.

[33] B. Yang, A.K. Melikov, A. Kabanshi, C. Zhang, F.S. Bauman, G. Cao, H. Awbi, H. Wigö, J. Niu, K.W.D. Cheong, K.W. Tham, M. Sandberg, P. V. Nielsen, R. Kosonen, R. Yao, S. Kato, S.C. Sekhar, S. Schiavon, T. Karimipanah, X. Li, Z. Lin, A review of advanced air distribution methods - theory, practice, limitations and solutions, Energy Build. 202 (2019). https://doi.org/10.1016/j.enbuild.2019.109359.

[34] B.W. Olesen, International standards for the indoor environment. Where are we and do they apply worldwide? Indoor Air (2004) 18–26.

[35] B. Olawoye, A Comprehensive Handout on Central Composite Design (Ccd), 2020.

[36] E. Geology, Their most general acceptation , are concerned with the study of the distribution in space of useful values for mining engineers and such as grade , thickness , or accumulation , including a most important practical application to the problems arising 58 (1963) 1246–1266.

[37] C. Lu, Y.W. Feng, R.P. Liem, C.W. Fei, Improved Kriging with extremum response surface method for structural dynamic reliability and sensitivity analyses, Aero. Sci. Technol. 76 (2018) 164–175, https://doi.org/10.1016/j.ast.2018.02.012.

[38] M. Alizadeh, S.M. Sadrameli, Energy & Buildings Numerical modeling and optimization of thermal comfort in building: Central composite design and CFD simulation, Energy Build. 164 (2018) 187–202, https://doi.org/10.1016/j.enbuild.2018.01.006.

Chapter 5

Optimization of the system operation based on a grey-box modeling approach

5.1 Introduction

Building energy systems are defined as those which are responsible for consumption of energy in buildings, which involves physical equipment, machinery or a combination of them. Recently, many researches aim to reduce building energy consumption with focuses such as advanced controls and renewable energy applications, while modeling is the basis in advancing those building technologies [1].

In general, an energy system model is a mathematical model describing the behavior of the system. Modeling structure for any energy system is made up of input variables, output variables and the system itself. Input variables such as internal heat gains, thermostat set point settings, which can be controlled are regarded as controllable input variables. On the other hand, the weather data such as solar radiation, outdoor air temperature, wind speed are uncontrollable input variables. The variables which can describe the reaction of system to input variables, such as indoor air temperature and humidity, are considered as output variables. In certain cases, the energy consumption or energy use is also the output of the model. Mathematical equations of all the energy transfer processes are used to build the structure of the building energy system. When model a building energy system, it is required to determine any one of these three, when adequate information about the other two are available. The energy model is classified into the white-box, black-box or grey-box models. The grey-box models first formulate a physical model to represent the structure or physical configuration of the building or HVAC system, and then identifies important parameters representative of certain key and aggregated physical parameters and characteristics by statistical analysis.

The thermal resistance and capacity (RC)-network model is a commonly used grey-box model to simulate building energy system and is applied to simulated radiant heating and cooling systems. Li et al. [2] developed a simplified RC-network model for the pipe-embedded concrete radiant floors. Validation has also been conducted to demonstrate the accuracy and effectiveness of this developed simplified RC-network model in predicting the dynamic thermal performance of this multi-layer pipe-embedded concrete radiant floor. Lu et al. [3] proposed a comprehensive RC-network model in the frequency domain for lightweight radiant floor heating (RFH) coupled with envelopes under intermittent operation. Zhang et al. [4] developed a dynamic simplified RC-network model of radiant ceiling cooling integrated with underfloor ventilation (RCCUV) system. Thermal resistances, thermal capacities and convective heat transfer coefficients of RC-network model were identified by using least square method (LSM).

In *Section 5.2*, a dynamic thermal resistance and capacity (RC)-network model for the open-type radiant ceiling panel system (RCP) was developed considering the thermal capacity and heat transfer process. This section presents the development and validation of this system applied in an enclosed space based on the field measurement introduced in *Section 3.3*. A transient white-box simulation model was created in TRNSYS software to supplement the unmeasured data such as wall surface temperature, panel surface temperature, solar air temperature, transmitted radiation heat gains and heat flux from ventilation and infiltration. The Least-Square Method (LSM) is employed to identify the thermal resistance and thermal capacity of RC-network model. In *Section 5.3*, the system operation was optimized based on the developed simplified RC-network model through multi-objective optimization. In *Section 5.4*, the life cycle cost (LCC) was calculated. Three different insulation designs and panel coverage area was compared based on the system efficiency and investment cost.

5.2 Development of a RC model for the open-type RCP system

5.2.1 Building thermal model

In the open-type radiant ceiling panel (RCP) system, the panel is suspended freely below the ceiling, permitting the air to pass over the panel. The space heating and cooling are produced by the heat exchange between water and panel, and then radiation and convection between the ambient environment and both up and bottom panel surface. In this study, a thermal resistance and heat capacity (RC)-network model for a single room applying open-type radiant ceiling panel was development, its equivalent electrical circuit is shown in Fig. 5-1. The effect of the furniture in the room is neglected.

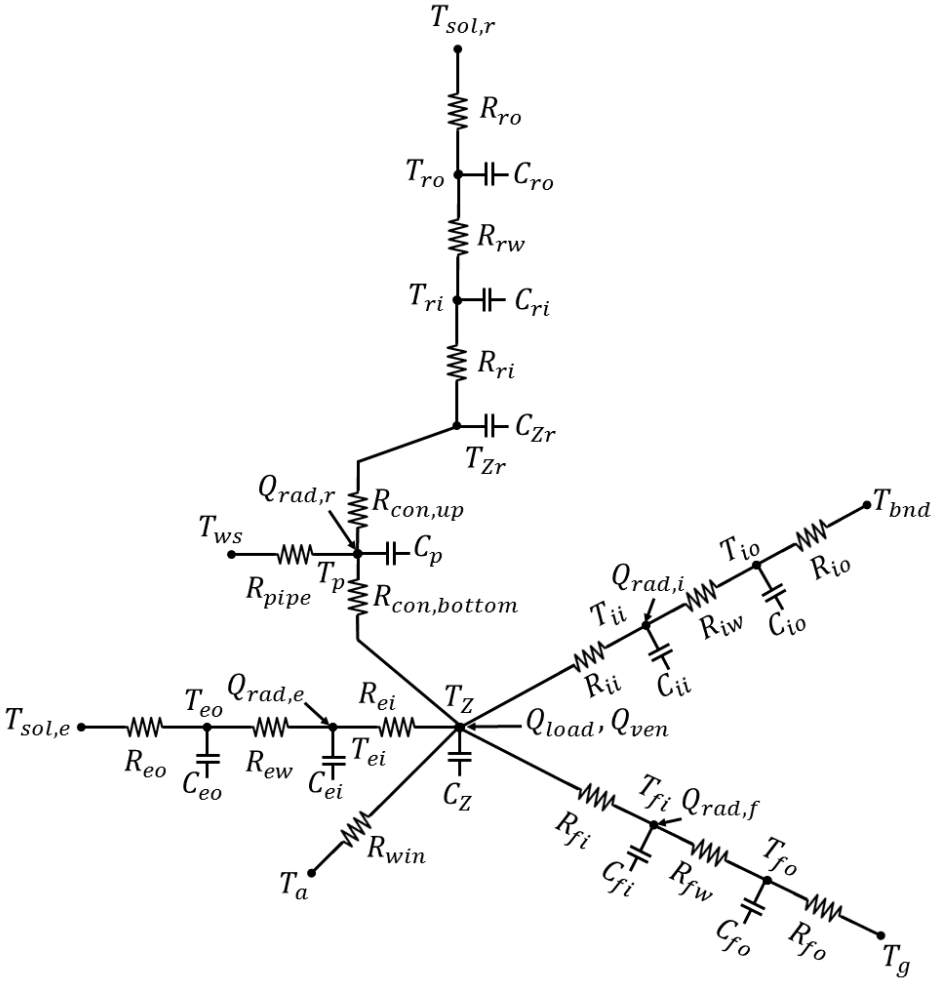

Fig. 5-1 Sketch of the model for a room applying open-type radiant ceiling panel

The external wall, internal wall, roof and floor are represented by 3R-2C network. The thermal equilibrium equations at the exterior and interior nodes of these walls can be written in the same expression. Eq. (5-1) and Eq. (5-2) present the energy balance on the surfaces of the external wall. T_{eo} and T_{ei} are the exterior and interior surface temperature of external wall, respectively. The capacitance at each node is equal to half of the thermal mass of the

wall C_{eo} and C_{ei}, while the conductive resistance is lumped into R_{ew}. R_{eo} and R_{ei} are the convective resistances between the wall and the air outside and inside. $R_{rad,e}$ is the radiant resistances between the wall and the panel. $Q_{rad,e}$ is the radiant heat flux on the interior surface of the external wall, including the short-wave solar radiation transmitted through windows and internal radiant gains from equipment and occupant.

$$C_{eo}\frac{dT_{eo}(t)}{dt} = \frac{T_{sol,e}(t) - T_{eo}(t)}{R_{eo}} + \frac{T_{ew}(t) - T_{eo}(t)}{R_{ew}} \quad (5-1)$$

$$C_{ei}\frac{dT_{ei}(t)}{dt} = \frac{T_{eo}(t) - T_{ei}(t)}{R_{ew}} + \frac{T_z(t) - T_{ei}(t)}{R_{ei}} + \frac{T_p(t) - T_{ei}(t)}{R_{rad,e}} + Q_{rad,e} \quad (5-2)$$

Solar radiation on the exterior surface of the building walls and roof will increase the surface temperature and affect the radiant heat transfer rate from the panels. Therefore, the solar air temperature (T_{sol}) is used as the boundary condition for the external wall and roof instead of the outdoor air temperature, calculated by Eq. (5-3).

$$T_{sol,e} = T_a + \frac{\alpha_e I_e}{h_{o,e}} \quad (5-3)$$

Where T_a is the outside temperature, α is solar radiation absorptivity, I is the incident solar radiation, h is the heat transfer coefficient for wind.

The variation of heat flux within the indoor air is equal to the sum of the convective heat flux from each interior surface and the panel, the conductive heat transfer from the window, the internal heat gains from equipment, occupants, and lights (Q_{load}), and the heat flux caused by ventilation and infiltration (Q_{vent}). Hence, the energy balance for the zone of indoor space is written as Eq. (5-4).

$$C_z\frac{dT_z(t)}{dt} = \frac{T_{ei}(t) - T_z(t)}{R_{ei}} + \frac{T_{ii}(t) - T_z(t)}{R_{ii}} + \frac{T_{fi}(t) - T_z(t)}{R_{fi}} + \frac{T_p(t) - T_z(t)}{R_{con,bottom}} + \frac{T_a(t) - T_z(t)}{R_{win}} + Q_{ven} + Q_{load} \quad (5-4)$$

On the other hand, the open-type radiant panel system is characterized by the presence of an open space above the panel. Therefore, the heat flux variation for this zone should be included as expressed in Eq. (5-5), which is affected by the convection from the ceiling and the panel.

$$C_{zr}\frac{dT_{zr}(t)}{dt} = \frac{T_{ri}(t) - T_{zr}(t)}{R_{ri}} + \frac{T_p(t) - T_{zr}(t)}{R_{con,up}} \quad (5-5)$$

Finally, as depicted in Eq.(5-6), the heat flux variation of the panel encompassed the conductive heat flux between the supplied water and the panel, the radiant heat flux between the interior wall and the panel surface, the convective heat flux between the panel surface and the surrounding air, and the radiant heat flux on the panel caused by transmitted solar radiation and internal radiant gains.

$$C_p\frac{dT_p(t)}{dt} = \frac{T_z(t) - T_p(t)}{R_{con,bottom}} + \frac{T_{zr}(t) - T_p(t)}{R_{con,up}} + \frac{T_{ws}(t) - T_p(t)}{R_{pi}} + \frac{T_{ri}(t) - T_p(t)}{R_{rad,r}} + \frac{T_{fi}(t) - T_p(t)}{R_{rad,f}} + \frac{T_{ii}(t) - T_p(t)}{R_{rad,i}} + \frac{T_{ei}(t) - T_p(t)}{R_{rad,e}} + Q_{rad,r} \quad (5-6)$$

5.2.2 The open-type RCP system

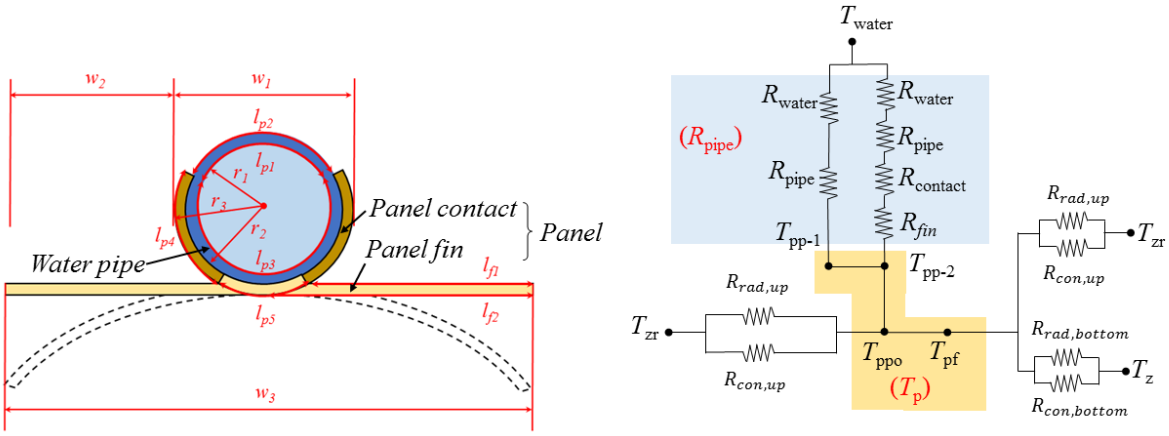

Fig. 5-2 Schematic of the mathematic model of the radiant ceiling panel

In the building thermal model, the thermal resistance between the water and the panel (R_{pipe}), the convective resistance (R_{con}), and the radiant resistance (R_{rad}) of the panel are the specific manufacturing parameters that vary according to the panel structure, panel material, panel shape and operation condition. It is important to carefully define these values as they determine the heat transfer rate of the panel. The values can be obtained from the standards, testing results or analysis by mathematical models. In this study, a numerical calculation method was employed to determine the thermal resistance of the novel proposed open-type radiant ceiling panel system, where the water pipe is directly in contact with the panel and the panel fins are flexible to be converted to any other shape, as shown in Fig. 5-2.

Each radiant panel is considered to have three components: the water pipe, the panel fin and the panel contact. The contact serves as the connection point between the water pipe and the fin to increase the heat transfer efficiency and is integrated with the fin. The temperature differences between these three components are negligible because they are much smaller than the temperature differences with the surrounding air. Therefore, their temperatures are considered equivalent and lumped into the panel surface temperature (T_p). The heat transfer between water and panel is divided into two parts, as shown in Eq. (5-7), which are the heat transfer between the water and the pipe, and the heat transfer between the water and the fin.

$$Q_p = \left(K_{p1}A_{m1} + K_{p2}A_{m2}\right)\left(T_{in} - T_p\right) \quad (5-7)$$

Where K_p (W/(m^2·K)) is the heat transfer coefficient and A_m (m^2) is the total heat transfer area

For the heat transfer between water and pipe:

$$K_{p1} = \frac{1}{\frac{1}{h_w} + \frac{r_1 - r_2}{\lambda_{pipe}}} \quad (5-8)$$

$$A_{m1} = \frac{\left(l_{p2} - l_{p1}\right)L}{In\left(\frac{l_{p2}}{l_{p1}}\right)} \quad (5-9)$$

For the heat transfer between water and fin:

$$K_{p2} = \frac{1}{\frac{1}{h_w} + \frac{r_2 - r_1}{\lambda_{pipe}} + \frac{r_3 - r_2}{\lambda_{panel}} + R} \quad (5-10)$$

$$A_{m2} = \frac{(2l_{p4} + l_{p5} - l_{p3})L}{In\left(\frac{2l_{p4} + l_{p5}}{l_{p3}}\right)} \quad (5-11)$$

h_w is the heat transfer coefficient for water flow (W/(m^2·K)), λ is the thermal conductivity coefficient (W/(m·K)), R is the thermal resistance between pipe and fin ((m^2·K)/W).

In the open-type RCP system, the inlet water temperature is always controlled as an input variable which effect the heat transfer of the system and indoor thermal condition. Nevertheless, the specific operation status of the water system is required to further evaluating the energy efficiency of the whole system and to calculate the power of circulating pump. The outlet water temperature should also be constrained within the range to operate the energy system at high efficiency.

The heat transfer from the panel to the water is equal to the heat exchange between the panel and the ambient environment according to the thermal equilibrium. Hence, the outlet water temperature (T_{wb}) can be calculated by solving simultaneous equations, Eq. (5-7) and Eq. (5-12) through Newton's method.

$$Q_p = KL\frac{T_{ws} - T_{wb}}{In\left(\frac{T_{ws} - T_{op}}{T_{wb} - T_{op}}\right)} \quad (5-12)$$

T_{op} is the operative temperature (°C), which is defined as an average of indoor air temperature and mean radiant temperature (MRT) [5], expressed as Eq. (5-13). The MRT is simply considered as a homogenous steady-state area-weighted average of the unconditioned surface temperature.

$$T_{op} = \frac{T_z + MRT}{2} \quad (5-13)$$

$$MRT = \frac{\sum A_j \times T_{i-j}}{\sum A_j} \quad (5-14)$$

A_j is the surface area of each wall j and $T_{i\text{-}j}$ is the interior surface temperature of each wall.

The total heat transfer coefficient of the panel K (W/(m·K)) is obtained by the following equations according to the mathematic model of radiant ceiling panel.

$$K = \frac{1}{\frac{1}{K_p} + \frac{1}{h_{rad,up} + h_{rad,bottom} + h_{con,up} + h_{con,bottom}}} \quad (5-15)$$

$$K_p = \frac{K_{p1}(l_{p2} - l_{p1})}{In\left(\frac{l_{p2}}{l_{p1}}\right)} + \frac{K_{p2}(2l_{p4} + l_{p5} - l_{p3})}{In\left(\frac{2l_{p4} + l_{p5}}{l_{p3}}\right)} \quad (5-16)$$

Finally, the water flow rate (G) is calculated by Eq. (5-17) based on the temperature difference between inlet and outlet water temperature.

$$G = \frac{Q_p}{C_p\rho(T_{wb} - T_{ws})} \quad (5-17)$$

5.2.3 Parameter identification

A continuous-time linear state-space model as expressed by Eq. (5-18) and Eq. (5-19), is adopted to represent the RC-network model. The differential equations introduced in *Section 2.1* are integrated into a multi-input multi-output (MIMO) system through the state space representation. The output variables are obtained by solving a single first-order matrix differential equation. The state-space model program was developed using MATLAB R2022a.

$$\frac{dx(t)}{dt} = Ax(t) + Bu(t) \qquad (5-18)$$

$$y = Cx(t) + Du(t) \qquad (5-19)$$

Where

$x(t)$ is the state vector - $x = [T_{eo}\ T_{ei}\ T_{ii}\ T_{io}\ T_{ro}\ T_{ri}\ T_{fi}\ T_{fo}\ T_z\ T_{zr}\ T_p]^T$

$u(t)$ is the input vector - $u = [T_{sol}\ \ T_{bnd}\ T_{ws}\ T_a\ T_g\ Q_{rad}\ Q_{ven}\ Q_{load}]^T$

y is the output vector, which is same as the state vector in this study. A, B, C, D are the system matrix, input matrix, output matrix, and feed-forward matrix, respectively, which describe how the input and other variables influence the evolution of the state variables within the model. The matrices are represented as follows.

$$A = \begin{bmatrix} -\frac{1}{C_{eo}}\left(\frac{1}{R_{eo}} + \frac{1}{R_{ew}}\right) & \frac{1}{C_{eo}R_{ew}} & 0 & \cdots \\ \frac{1}{C_{ei}R_{ew}} & -\frac{1}{C_{ei}}\left(\frac{1}{R_{ew}} + \frac{1}{R_{ei}} + \frac{1}{R_{rad,e}}\right) & 0 & \cdots \\ \vdots & \vdots & \vdots & \ddots \end{bmatrix}$$

$$B = \begin{bmatrix} \frac{1}{C_{eo}R_{eo}} & 0 & 0 & \cdots \\ 0 & 0 & 0 & \cdots \\ \vdots & \vdots & \vdots & \ddots \end{bmatrix}$$

$$C = \begin{bmatrix} 1 & 0 & 0 & \cdots \\ 0 & 1 & 0 & \cdots \\ \vdots & \vdots & \vdots & \ddots \end{bmatrix} \qquad D = \begin{bmatrix} 0 & 0 & 0 & \cdots \\ 0 & 0 & 0 & \cdots \\ \vdots & \vdots & \vdots & \ddots \end{bmatrix}$$

In this study, the model was validated using field measurements in an office with an open-type RCP system located in Sapporo, Hokkaido, Japan [6]. Fig. 5-3 illustrates the process of model development and validation. The indoor thermal environment in the office was measured and the operation of RCP system were control and recorded by the Building Management Energy System (BEMS). The information about the outdoor conditions is sourced from Automated Meteorological Data Acquisition System (AMeDAS), which is supported by the Japan Meteorological Agency [7]. To supplement the data not measured by the BEMS, a transient white-box simulation model was created in TRNSYS software to fill the missing measurements such as wall surface temperature, panel surface temperature, solar air temperature, transmitted radiation heat gains and heat flux from ventilation and infiltration. The Least-Square Method (LSM) is employed to identify the thermal resistance and thermal capacity of RC-network model with the data obtained from the TRNSYS simulation model. 70% of data was used for training while the remaining 30% of data was used for testing. Finally, the outlet water temperature and water flow rate of the RCP were calculated based on the results of the indoor thermal simulation.

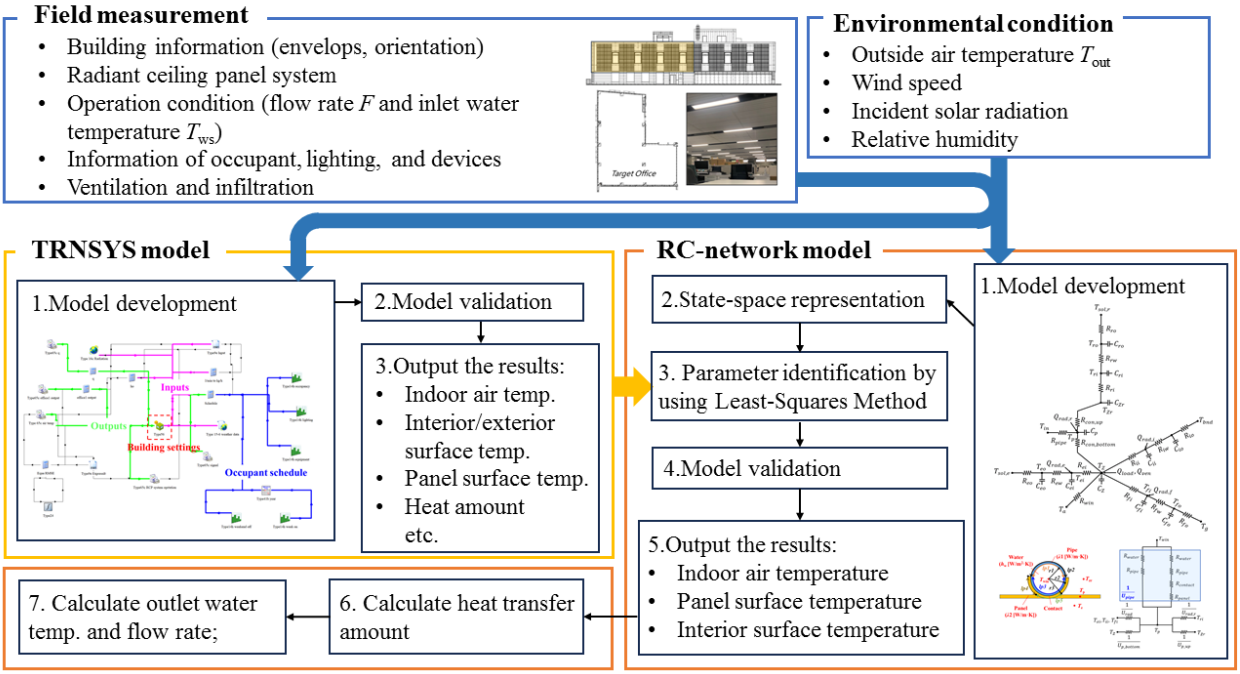

Fig. 5-3 Schematic diagram of the model development and validation

Moreover, the Root Mean Square Error (RMSE) is employed to quantify the difference between the model and the observed data, as expressed as Eq. (5-20).

$$RMSE = \sqrt{\frac{\sum_{i=1}^{N}(y_i - \hat{y}_i)^2}{N}} \qquad (5-20)$$

Where N is the number of data point. y is the measurement and $\hat{y}$ is the corresponding simulation.

The field measurements were carried out in an office (457.39 m^2) of the second floor of a newly constructed office building, situated in Sapporo, Hokkaido, Japan. Sapporo, located in the north of Japan, experiences a humid continental climate (Dfa) characterized by cold snowy winters and mild pleasant summers. The study period was from January 22 to March 14 during winter and from July 8 to August 6 during summer in 2021. The detailed description of this office and measurement set-up were provided in the previous study [6]. The office has three external walls (north, west and south), with the remaining walls serving as internal partitions connecting it to the rest of the space in the office building. The windows on three external walls use Low-E pair glass, each with a different shape, as shown in Fig. 5-4. Both the external walls and roof are well-insulated to mitigate the impact of cold temperatures from outside in winter. The floor of this office serves as the ceiling for the first floor, where the air is conditioned by a separate system. The materials of the envelops are listed in Table 5-1.

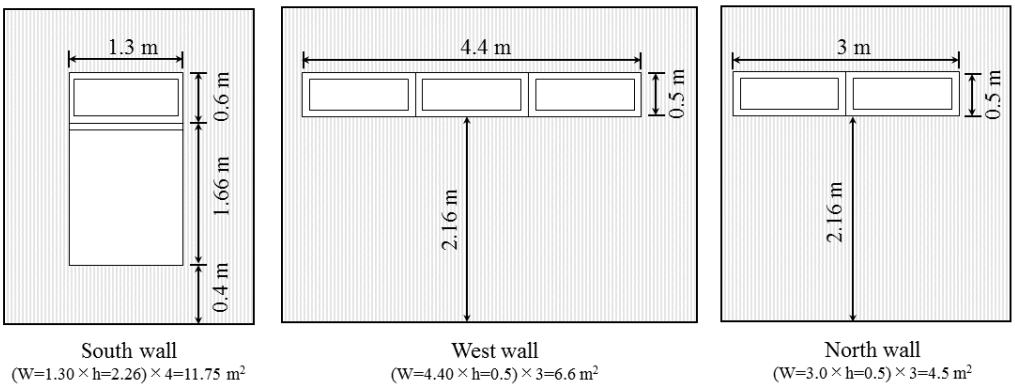

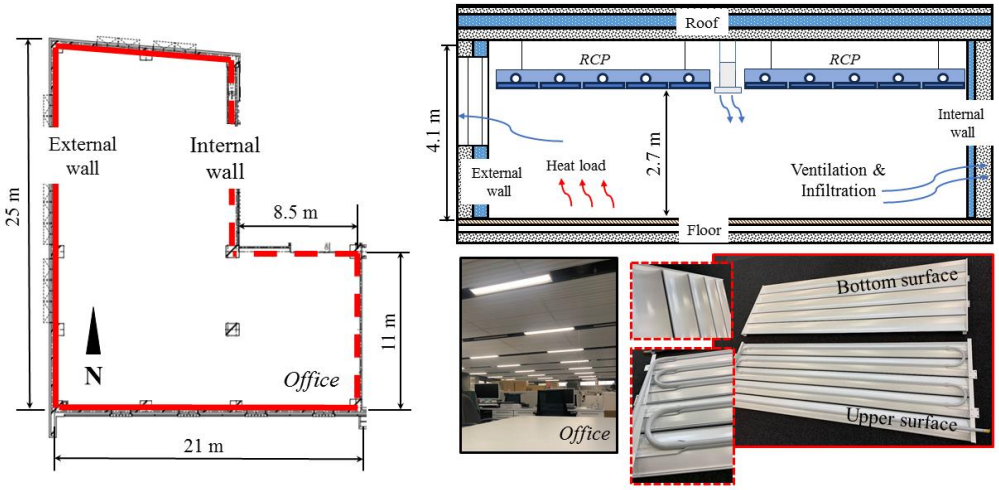

Fig. 5-4 The schematic diagram and photos of the office and the radiant ceiling panel

Table 5-1 Building envelope structure and materials

Element	Structure layer	Thickness (mm)	Thermal conductivity (W/(m·K))	Specific heat capacity (kJ/(kg·K))	Density (kg/m³)
External wall	Concrete	0.17	3.20	0.88	2400
	Polystyrene foam (PF)	0.11	0.028	1.10	1050
Internal wall	Concrete	0.17	3.20	0.88	2400
	PF	0.05	0.028	1.10	1050
Floor	Rockwool	0.006	0.17	1.03	22
			Air gap resistance: 0.04167 h·m²·K/kJ		
	Concrete	0.07	3.20	0.88	2400
Roof	Concrete	0.17	3.20	0.88	2400
	PF	0.10	0.028	1.10	1050
	Concrete	0.08	3.20	0.88	2400
Window	Low-E pair glass		U-value 1.4 W/(m²·K)		

In this office, the radiant ceiling panels are freely suspended under the ceiling at the height of 2.7 m. The RCP are featured with a curved and segmented structure. The piping is constructed using aluminum triple-layer pipes coated with polyethylene on the inner and outer surfaces. The contact and fin are made of aluminum. The values of the panel specifications shown in Fig. 5-2 are summarized in Table 5-1. The convective and radiant heat transfer coefficients of the RCP have been investigated through experiments under various conditions in a chamber test [8], as given by Eq. (5-21) and Eq. (5-22).

$$h_r = 5.0024 \tag{5-21}$$

$$h_c = 2.6684\left|T_a - T_p\right|^{0.1253} \tag{5-22}$$

The displacement ventilation system is incorporated to handle the sensible heat and bring the fresh air. Physical measurements in the office were recorded in the BEMS every minute, including indoor air temperature, panel surface temperature, and the temperature and humidity of the supplied air from the ventilation system.

Table 5-2 Specifications of the open-type radiant ceiling panel in this study

Parameter	Value	Parameter	Value	Parameter	Value
r_1	6 mm	r_2	8 mm	r_3	10 mm
l_{p1}	14 mm	l_{p2}	18 mm	l_{p3}	24 mm
l_{p4}	13 mm	l_{p5}	12 mm	L	8.9 m
λ_{pipe}	0.47 W/(m·K)	λ_{panel}	210 W/(m·K)	R	0.01 (m²·K)/W

In winter, the groundwater heat pump system provides warm water to the radiant heating system, and a water tank is used to store the hot water to ensure the efficient operation of the system. While, in summer, the RCP system directly exchanges heat with groundwater through a heat exchanger by free cooling method. The inlet and outlet water temperature and the water flow rate of the water system were also recorded.

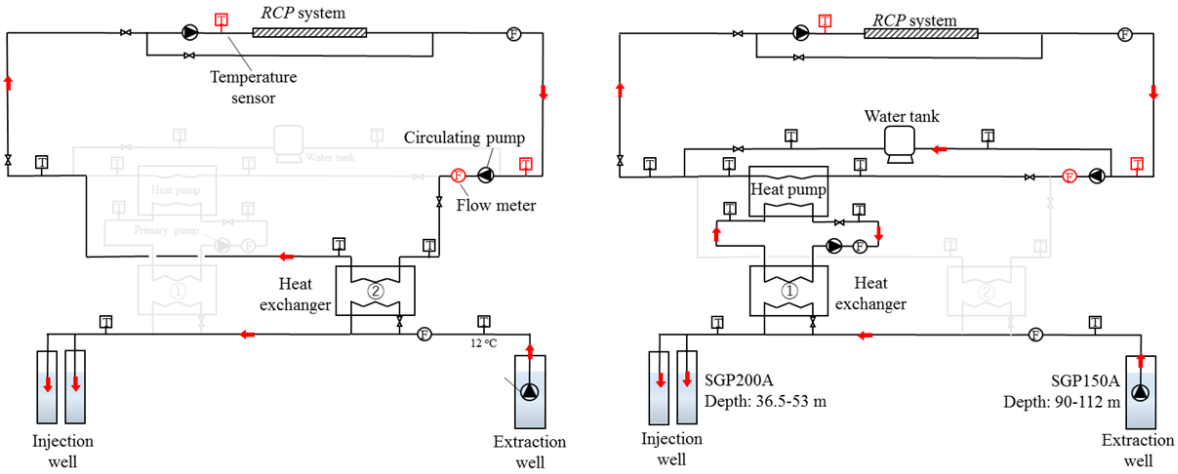

(a) summer (b) winter

Fig. 5-5 The schematic diagram of the heating and cooling system

Although the experiments have provided relevant real-time measurement data for the indoor thermal environment in the office, additional data is still required to supplement the parameter identification. Therefore, a transient simulation model of the office was created in TRNSYS 18 to simulate the dynamic thermal process in the office, as shown in Fig. 5-6. Type 56 component is linked to a graphical interface tool (TRNBuild) for creating the geometry and defining the thermal zones in building energy simulation. Within this component, the building envelopes are determined using the values provided in Fig. 5-4 and Table 5-1. An active layer, termed 'chilled ceiling' was added with an air gap between the 'chilled ceiling' and ceiling to simulate the open-type RCP system. This layer acts with user-defined specific panel heat flux and heat transfer coefficient, and the inlet water temperature and mass flow rate were entered using real-time measurement records. The ventilation system supplies air at a rate of 0.5 ACH, and the temperature and humidity of the supplied air are based on experimental data. Filtration occurs through the leakage of windows and doors is assumed to be 0.2 ACH. The internal heat gains are defined following the standard [9] as summarized in Table 5-3, which includes occupant, lighting and equipment. Type 14h and Type 41b is used to distinguish holidays and establish the hourly schedule for heat gain activities. Type 9e is a data reader used to read the climate data and the recorded operation status of the RCP and ventilation system. Type 15-6 is a weather data reader used to complement the lacking climate information such as ground reflectance and effective sky temperature, which are generated by Meteonorm. Also, Type 16c is used to estimate the incident radiation on each envelope, which is an essential factor influencing the heating and cooling performance of the RCP system, dependent on the orientation, sun position, and climate conditions. At last, Type 65c serves as the output module to display the selected output variables and save then into defined external files.

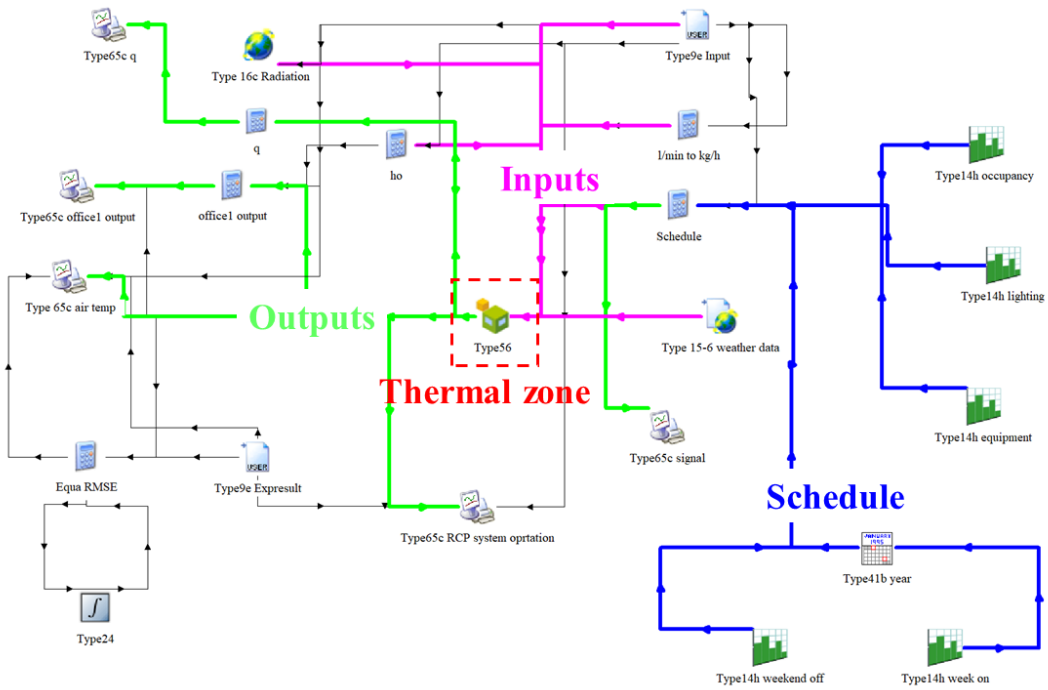

Fig. 5-6 TRNSYS transient simulation model

Table 5-3 Indoor heat gains in TRNSYS model

Internal heat gain	Setting	Schedule
Occupant	72 W (×25 person)	8:00-21:00 on weekday
Illumination	6.6 W/m^2	8:00-21:00 on weekday
Equipment	10.88 W/m^2	8:00-21:00 on weekday

5.2.4 Model validation result

Firstly, the comparison of the indoor air temperature between the experimental measurements and TRNSYS simulated results is examined as shown in Fig. 5-7, the RMSE of indoor air temperature is 0.33 in summer and 0.44 in winter. The results indicate that the TRNSYS simulation model accurately simulates transient indoor conditions in the office, and the output data were reliable to apply for parameter identification. The parameter identification was generated to determine the parameters of thermal resistance (R) and thermal capacity (C) by minimizing the difference between the predicted and observed values using trust-region-reflective (TRR) algorithm.

$$\min_x \|F(x, xdata) - ydata\|_2^2 = \min_x \sum_i (F(x, xdata_i) - ydata_i)^2 \qquad (5-23)$$

Where *xdata* refers to the input vector and *ydata* are output matrix.

In summer, the root mean square error of indoor air temperature is 0.43 for training results and 0.29 for testing results, while in winter, it is 0.60 for training results and 0.70 for testing results. The RC model is able to reproduce the observed trend at room temperature. The RC model can predict the dynamic characteristics of the open-type RCP system. However, the variation of indoor air temperature from the model is more gradual than the measurements, as it ignores some influential factors to simplify the model. When compared with the TRNSYS simulation model, the RC-network model is more sensitive to the inlet water temperature because it closely tracks the water temperature trend. On the other hand, the RMSE of other output states, such as wall, floor, roof, and panel surface temperature, are shown in Table 5-4 and Table 5-5. The values in summer are all less than 0.5. In contrast, the values become larger in winter due to larger temperature differences between day and night, but still within an acceptable range.

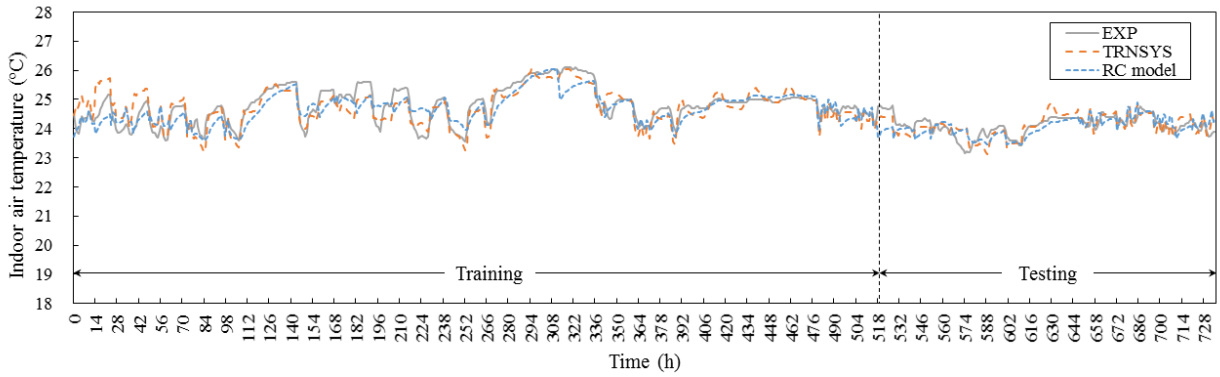

(a) Summer

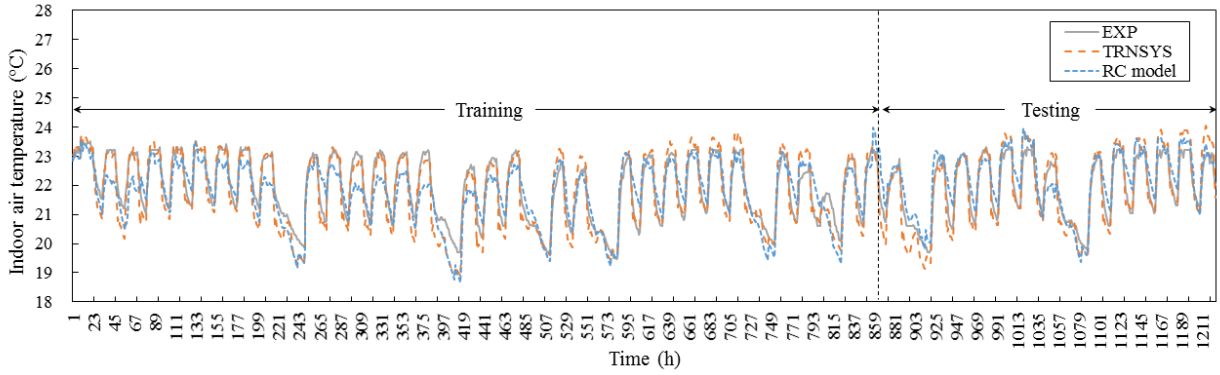

(b) Winter

Fig. 5-7 Comparison of indoor air temperature between the experimental and simulated results

Table 5-4 Root mean square error of output states of parameter identification in summer

RMSE	T_{ei_N}	T_{ei_W}	T_{ei_S}	T_{ii}	T_{aji}	T_{fi}	T_{ri}	T_z	T_{zr}	T_p
Training	0.385	0.395	0.389	0.359	0.386	0.342	0.678	0.431	0.464	0.468
Testing	0.219	0.236	0.227	0.242	0.262	0.256	0.455	0.286	0.259	0.370

Table 5-5 Root mean square error of output states of parameter identification in winter

RMSE	T_{ei_N}	T_{ei_W}	T_{ei_S}	T_{ii}	T_{aji}	T_{fi}	T_{ri}	T_z	T_{zr}	T_p
Training	0.284	0.279	0.267	0.243	0.233	0.469	0.608	0.596	0.607	0.612
Testing	0.820	0.868	0.849	0.650	0.629	0.700	0.705	0.693	0.753	0.706

The outlet water temperature and flow rate were then calculated following the equations in *Section 2.3* using the results of each surface temperature. The heat transferred by the water system is balanced with the heat exchanged from the radiant panel to the air and other surfaces in the room. The RMSE values of outlet water temperature is 0.27 in summer and 0.50 in winter. The average error of flow rate in summer is 7.7 L/min, which is around 10%. The results indicate that the calculation of water system has a good agreement with the experimental measurements. In other words, the model can also accurately predict the amount of heat in the panels for heat exchange. The developed RC-network model is reliable and parameter identification by LSM is effective to the open-type RCP system.

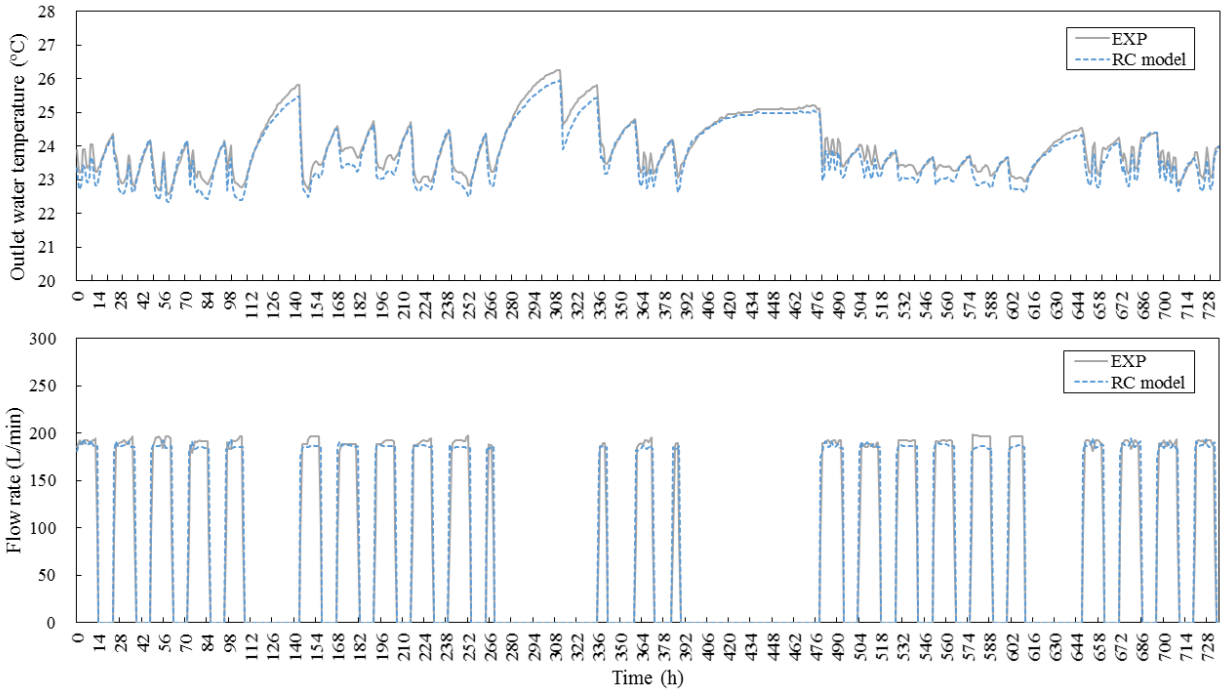

(a) Summer

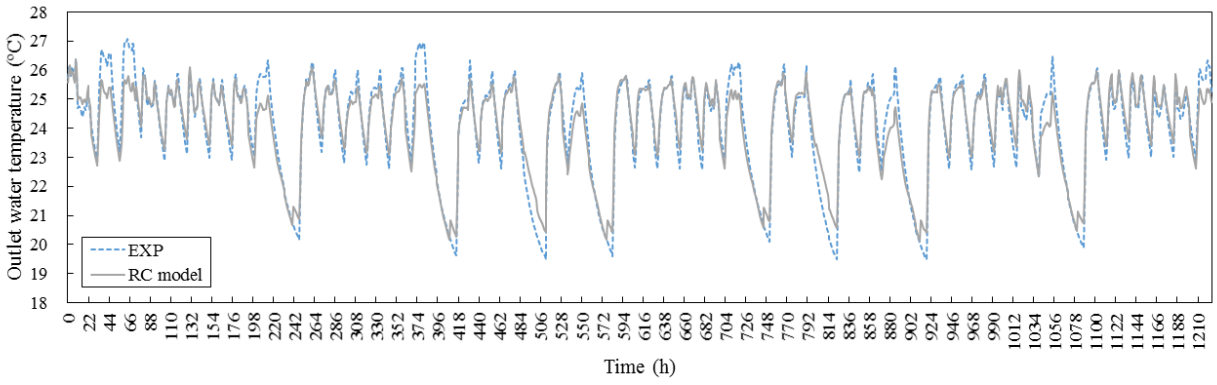

(b) Winter

Fig. 5-8 Comparison of the simulated results of water system between the experimental and simulated results

5.3 Optimization based on the RC-network model

5.3.1 Optimization methods

The optimization is performed in this office to achieve required room temperature while minimize the energy consumption based on the developed RC-network model. The inlet water temperature is constrained between 18 ℃ and 32 ℃ to prevent the risk of condensation and maintain the heat pump operating at high efficiency. The indoor air temperature is allowed to fluctuate within 0.5 ℃ during system operation. The fmincon function in MATLAB was used to solve this nonlinear constrained multi-objective optimization. Fig.5-9 shows the flowchart of the optimization.

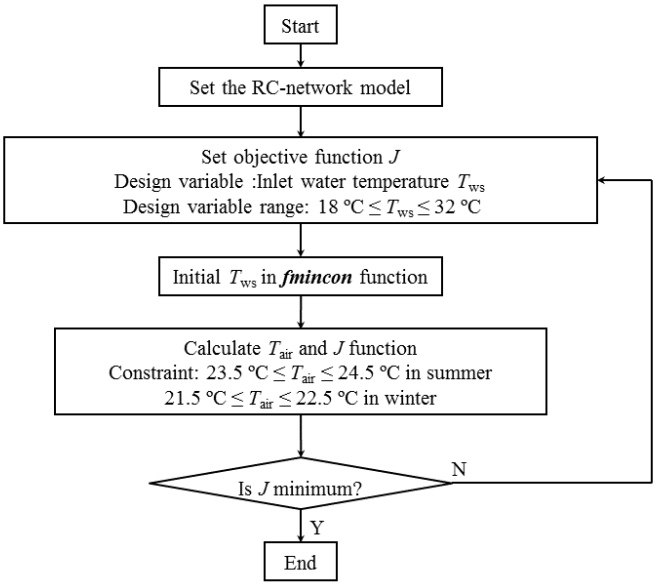

Fig. 5-9 Flow chart of the optimization

The objective function was determined based on three objectives, which are (i) maintaining the indoor air temperature at the set point, (ii) minimizing the inlet water temperature variation, and (iii) minimizing electric energy consumption as expressed in Eq. (5-24). The second term in the equation is to keep the inlet water temperature constant considering the characteristic of the control of this system. In this study, the control variable for the *RCP* system is the inlet water temperature, which is regulated by adjusting the valve opening area when using free cooling strategy in summer. Reducing the variation in the inlet water temperature aims to decrease the energy consumption caused by valve adjustments.

$$J = m\left(T_{op} - T_{set}\right)^2 + n\left(T_{ws} - T_{ws,i-1}\right)^2 + kE \qquad (5-24)$$

m, n and k are the weight coefficient, which are adjusted as 0.315, 0.06 and 0.625 in this study. T_{op} is the operative temperature calculated by Eq. (5-25). T_{set} is the set point temperature, which is 22 ℃ in winter and 24 ℃ in summer in this study. T_{ws} is the inlet water temperature and $T_{ws,i-1}$ represents the inlet water temperature in the previous step/hour. E is the electric consumption which is calculated in winter and summer separately as follows.

In summer, the supplied chilled water directly exchanges heat with groundwater through the heat exchanger. Thus, the energy consumption in summer is determined by the consumption of the circulating pump, which is calculated through circulating flow rate G, pump efficiency η and water head H.

$$E_{summer} = \frac{G}{\eta}\rho g H \quad (5-25)$$

The pump type is 32LPD5.4E, produced by EBARA Corporation. The efficiency η is estimated according to the performance curve of the pump.

$$\eta = 9 \times 10^{-6}F^3 - 0.006F^2 + 1.0637F + 2.8191 \quad (5-26)$$

In winter, the water is supplied by the heat pump, so that energy consumption is calculated from the coefficient of performance (COP) of the heat pump.

$$E_{winter} = \frac{Q_H}{COP} \quad (5-27)$$

Q_H is the supplied heat (W). The type of heat pump used in the office building in this study is MCRV-P450E, produced by Mitsubishi Electric Corporation. The COP [10] can be estimated by using a regression equation approximated based on the measurements, as shown in Eq. (5-28):

$$COP = 10.5775 - 0.258Q_H + 0.0063{Q_H}^2 - 4.25232 \times 10^{-5}{Q_H}^3 - 0.1890T_{1in} - 0.0678T_{2out} \quad (5-28)$$

Where T_{1in} is the inlet water temperature of the evaporator. T_{2out} is the outlet water temperature of the condensation.

5.3.2 Optimization results

Fig. 5-10 illustrates the optimization results of the indoor air temperature and electric consumption during the winter from January 22 to March 14. After optimization, the indoor air temperature can be maintained at 22 ℃ without overheating and overcooling. The total electric consumption decreases by 12.3% from 900.6 kWh to 789.6 kWh and the average COP increases 4.5% from 5.59 to 5.84.

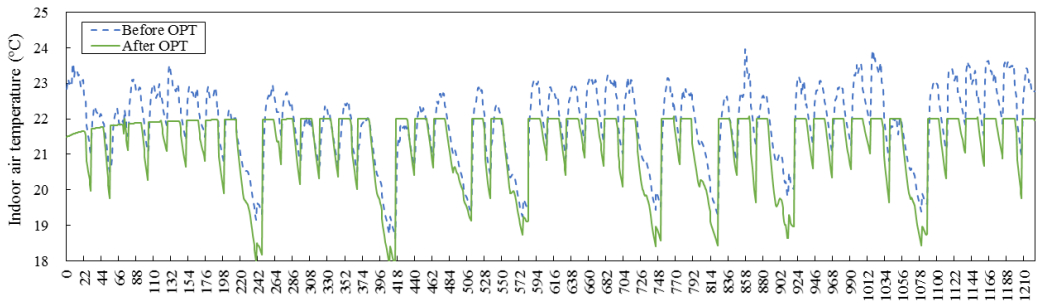

(a) Indoor air temperature

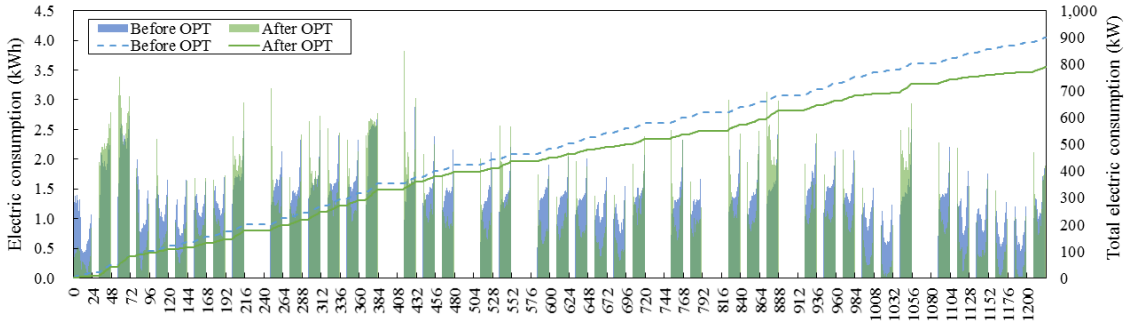

(b) Energy consumption

Fig. 5-10 Optimization results of the system operation during winter

Fig. 5-11 show the optimization results of indoor air temperature and inlet water temperature on January 24. Before optimization, the temperature is lower than the desired indoor temperature before 11 a.m. due to the time delay of the RCP system. This delay has been eliminated by increasing the supplied water temperature in the morning. In addition, the supplied water temperature in the afternoon has been adjusted when the solar radiation is strong or the outside temperature rises, which eliminates the overheating.

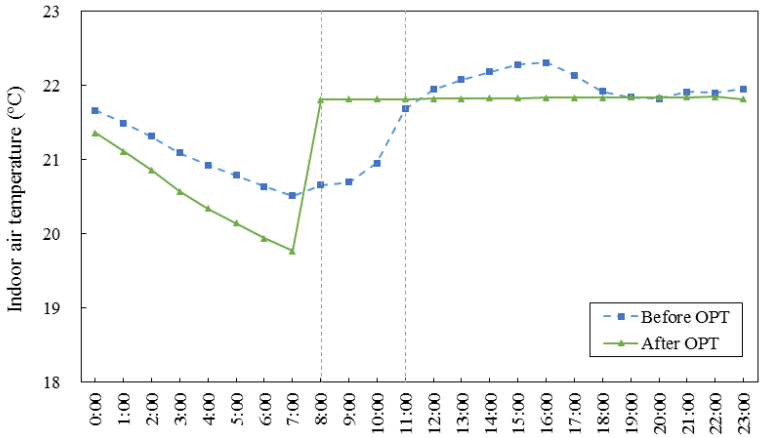

(a) Indoor air temperature

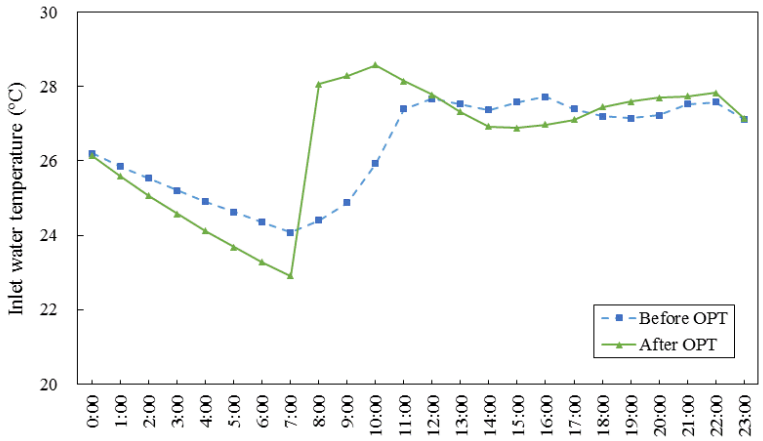

(b) Inlet water temperature

Fig. 5-11 Optimization results of the system operation on January 24

5.4 Life cycle cost (LCC) calculation

5.4.1 Calculation method

The life cycle cost (LCC) was utilized to evaluate the investment cost and the economic benefit of the optimization of the system operation. In addition, the trade-off between thick thermal insulation and large panel area are discussed based on the calculation and comparison of the LCC.

$$LCC = IC + a(re, N)EC \quad (5-1)$$

$$EC = \left(\frac{Q_H}{COP} + \frac{Q_c}{\eta}\right) \times P_{ele} \quad (5-2)$$

$$a(re, N) = \frac{1-(1+r_e)^{-N}}{r_e} \quad (5-3)$$

Where *IC* is the investment cost calculated. *EC* is the annual energy cost to maintain comfortable indoor thermal condition. *a*(*re*,*N*) is the discount factor calculated by Eq.(5-3). Q_H and Q_C are annual heating and cooling need (kWh). P_{ele} is the price of the electrical energy, which is assumed as 25 JPY/kWh. *re* is the real interest rate, which is set 3% in Japan [11]. *N* is the total of the years for study.

5.4.2 Discussion on building envelope thermal insulation strategies

In *Section 3.3*, the feedback time of the open-type RCP system was calculated, and the influence of the building envelope was suggested to be considered. In this section, three different envelope designs are discussed according to the Japanese law: Case 1-original case, Case 2- general insulation design in standard, and Case 3- light insulation design for warm area in standard. The results of investment cost of each case are summarized in Table 5-6.

Table 5-6 The investment cost of the office and the open-type RCP system

Structure layer	Area (m^2)	Case 1		Case 2		Case 3	
		Unit Price (JPY/m^2)	Total cost (JYP)	Unit Price (JPY/m^2)	Total cost (JYP)	Unit Price (JPY/m^2)	Total cost (JYP)
Interior wall							
Concrete	137.174	5,700	781,892	5,700	781,892	5,700	781,892
PF		2,180	299,039	2,180	299,039	2,180	299,039
Floor							
Rockwool	410.819	3,370	1,384,460	3,370	1,384,460	3,370	1,384,460
(Airgap)		-	-	-	-	-	-
Concrete		3,400	1,396,785	3,400	1,396,785	3,400	1,396,785
Roof							
Concrete	410.819	5,700	2,341,668	5,500	2,259,505	5,500	2,259,505
PF		4,360	1,791,171	3,270	1,343,378	2,180	895,585
Concrete		4,000	1,643,276	3,400	1,396,785	3,400	1,396,785

		Exterior wall					
Concrete	223.177	5,700	1,272,109	5,500	1,227,474	5,500	1,227,474
PF		4,360	973,052	2,180	486,526	1,090	243,263
Total investment of office envelope		11,883,452		10,575,842		9,884,787	
RCP system		11,000,000 [6]					

Table 5-7 summarized the system optimization and annual cost of three different envelope design. The heating (Q_H) and cooling capacity (Q_C) are calculated by TRNSYS. The results reveal that the COP increases in all the cases after optimization, but the reduction in electrical consumption decrease as the thickness of insulation is reduced. Fig. 5-12 illustrates the life cycle cost of the open-type RCP system. It was observed that the investment cost for case 1 and the energy cost for case 3 were the highest. Consequently, as shown in the figure, the life cycle cost of case 3 increases more rapidly and is higher than that of case 2 after 10 years, and higher than that of case 1 after 20 years.

Table 5-7 Annual cost of the operation of the open-type RCP system

	Case 1		Case 2		Case 3	
	Before OPT	After OPT	Before OPT	After OPT	Before OPT	After OPT
Q_H (kWh/year)	4177		8033		14355	
COP	5.59	5.84	4.84	5.03	4.12	4.25
Q_C (kWh/year)	5215		3979		2858	
η	40					
P_{ele} (JPY/kWh)	25					
EC (JPY)	21,940	21,140	43,980	42,413	88,890	86,225

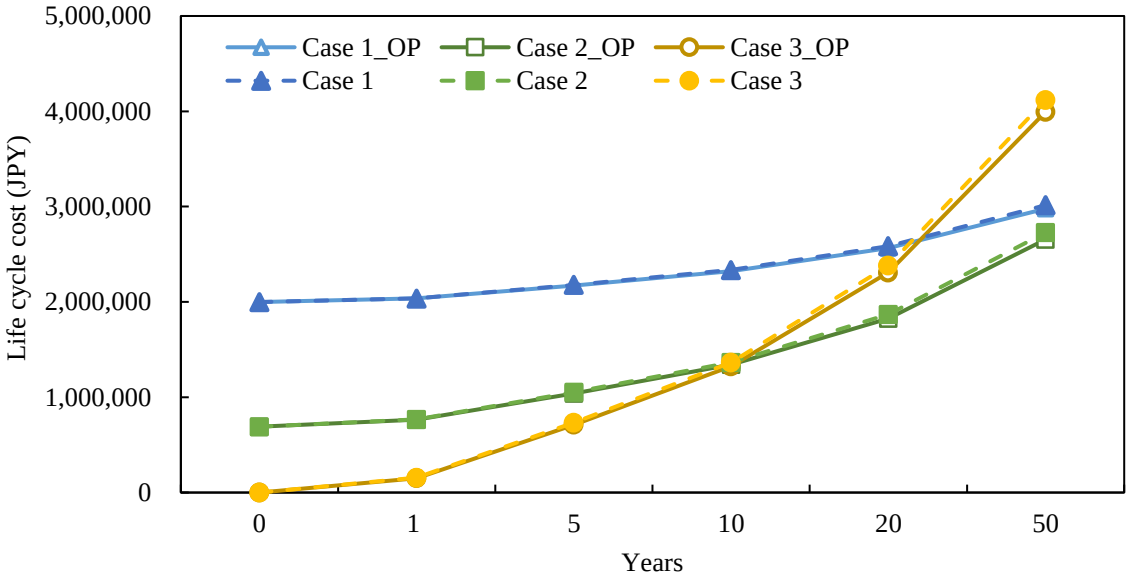

Fig. 5-12 The results of the life cycle cost of the open-type RCP system

5.5 Conclusions

The system operation of the integrated novel RCP and GWHP system was optimized based on a simplified dynamic thermal resistance and thermal capacity (RC) model and multi-objective optimization.

1. The RC model is able to reproduce the observed trend at room temperature and predict the dynamic characteristics of the open-type RCP system.

2. After optimization, the indoor air temperature can remain within the required range. The issue of the temperature not reaching the target in the morning due to time delay has been resolved, and the overheating and overcooling have been eliminated.

3. The COP increases and electrical consumption decreases in all the cases after optimization. However, the impact of optimization is diminished as the insulation is reduced.

4. The investment of the general insulation case is higher than the light insulation case, but the life cycle cost is lower after 20 years of system operation.

Nomenclature

x	State factor
y	Output factor
u	Input or control factor
A	System matrix
B	Input matrix
C	Output matrix
D	Feed forward matrix
T_{io}	Internal wall outside surface temperature (℃)
T_{ii}	Internal wall inside surface temperature (℃)
T_{eo}	External wall outside surface temperature (℃)
T_{ei}	External wall inside surface temperature (℃)
T_{ro}	roof outside surface temperature (℃)
T_{ri}	roof inside surface temperature (℃)
T_{fo}	Floor outside surface temperature (℃)
T_{fi}	Floor inside surface temperature (℃)
T_{sol}	Sol-air temperature (℃)
T_{bnd}	Boundary temperature (℃)
T_{ws}	Supply water temperature (℃)
Q_{rad}	Radiative gains, including total shortwave solar radiation transmitted through windows (W)
Q_{conv}	Internal convective gains (W)
Q_{loss}	Ventilation and infiltration heat loss (W)
R	Thermal resistance (m^2·K/W)
C	Thermal capacity (J/K)

Reference

[1] Y. Li, Z. O'Neill, L. Zhang, J. Chen, P. Im, J. DeGraw, Grey-box modeling and application for building energy simulations - A critical review, Renew. Sustain. Energy Rev. 146 (2021) 111174. https://doi.org/10.1016/j.rser.2021.111174.

[2] A. Li, Y. Sun, X. Xu, Development of a simplified resistance and capacitance (RC)-network model for pipe-embedded concrete radiant floors, Energy Build. 150 (2017) 353–375. https://doi.org/10.1016/j.enbuild.2017.06.011.

[3] L. Lu, J. Chen, T. Su, X. Liu, Y. Hu, Q. Luo, L. Luo, An RC-network model in the frequency domain for radiant floor heating coupled with envelopes, Build. Environ. 225 (2022) 109617. https://doi.org/10.1016/j.buildenv.2022.109617.

[4] D. Zhang, X. Xia, N. Cai, A dynamic simplified model of radiant ceiling cooling integrated with underfloor ventilation system, Appl. Therm. Eng. 106 (2016) 415–422. https://doi.org/10.1016/j.applthermaleng.2016.06.017.

[5] ANSI/ASHRAE Standard 55-2010 Thermal Environmental Conditions for Human Occupancy.

[6] M. Ye, K. NAGANO, A.A. Serageldin, H. Sato, Field Study on Energy Consumption and Thermal Comfort of a Nzeb Using Radiant Ceiling Panel and Open-Loop Groundwater Heat Pump System in a Cold Region, Available SSRN 4151977. 67 (2023) 105999. https://doi.org/10.1016/j.jobe.2023.105999.

[7] 国土交通省　気象庁　https://www.jma.go.jp/jma/index.html

[8] M. Ye, K. NAGANO, A.A. Serageldin, H. Sato, Field Study on Energy Consumption and Thermal Comfort of a Nzeb Using Radiant Ceiling Panel and Open-Loop Groundwater Heat Pump System in a Cold Region, Available SSRN 4151977. 67 (2023) 105999. https://doi.org/10.1016/j.jobe.2023.105999.

[9] 2001 ASHRAE Fundamentals Handbook

[10] 福岡拓真, 寒冷地における地下水熱ヒートポンプシステムを核とした ZEB に関する研究, 北海道大学　令和 2 年修士論文

[11] H. Chae, K. Nagano, T. Katsura, Y. Sakata, A.A. Serageldin, Life cycle cost analysis of ground source heat pump system based on multilayer thermal response test, Energy Build. 261 (2022) 111427. https://doi.org/10.1016/j.enbuild.2021.111427.

Chapter 6

Conclusion and future studies

6.1 General conclusions of the thesis

This thesis focuses on the design and control optimization of a novel open-type radiant ceiling panel (RCP) system in terms of both thermal comfort and energy saving. Although the RCP system is viewed as an energy-efficient alternative to conventional HVAC systems, challenges such as high initial costs, surface condensation risks, long response times, and adverse effects from windows need improvement. This study addresses these challenges by investigating the thermal performance of the novel proposed RCP system and optimizing the panel shape, integrated wall-attached ventilation (WAV) and groundwater heat pump (GWHP) system, and overall system operation, leading to the following conclusions.

- ***Laboratory analysis of the novel RCP system with curved and segmented structure.***

The thermal performance of the novel RCP system was investigated in a laboratory test room under different inlet water temperatures and flow rates.

1. The total heat flux changed significantly with variations in the inlet water temperature. However, changing the flow rate had a smaller impact on the cooling capacity.
2. The radiant heat transfer coefficient was constant at 5 W/(m^2·K), and the convective heat transfer coefficient exhibited an exponential relationship with the temperature difference between the indoor air and panel surface.
3. The RCP in this study can achieve a uniform indoor air distribution, but it is still challenging to prevent effects resulting from the building envelope. Therefore, the RCP system needs to be optimized and combined with forced ventilation methods to achieve a more comfortable indoor environment.
4. The curved panel enhanced both radiation and convection, relative to the flat panel. The convective heat transfer coefficient obtained with this panel was larger than those reported in the literature.
5. The novel curved panel allows the use of a lower fluid flow rate to achieve a comfortable room environment, which reveals its potential for saving energy.

- ***Field measurement of the novel RCP system integrated with GWHP system in an office***

The thermal and energy performances of an office building equipped with an RCP and an open-loop GWHP system were assessed. Field studies were conducted to evaluate the thermal comfort of the office, and energy consumption was analyzed based on the records of each system component.

1. Measuring the thermal conditions in the target office showed that the indoor air temperature was approximately 24.5 °C in the summer and 23 °C in the winter. The indoor humidity was maintained at 55% in the summer and 30% in the winter. The CO_2 concentration was approximately 1000 ppm. No heterogeneous vertical temperature distribution was observed. However, it is expected to reduce the temperature discrepancy caused by the independent system control and large-scale space.
2. More than 70% of the staff selected a neutral level in the TSV, and the discomfort rate was lower than 10%. However, it is recommended that the ventilation rate should be increased during hot days to eliminate hot and suffocating sensations.
3. Compared with intermittent operation, continuous operation could improve both the system performance and indoor thermal comfort as the COP of the heat pump increased from 3.86 to 4.18, and the TSV was closer to zero.

However, the electric energy consumption under continuous operation still costs more than that under the intermittent operation mode. Therefore, the control method of this system needs to be further optimized.

4. The primary energy consumption decreased by 69% during the first year and by 66% during the second year, thereby meeting the requirement of the ZEB-ready level in Japan. The energy consumption of HVAC systems accounted for 46%, making them the largest contributor to total energy consumption. Therefore, it has the potential to be further reduced by improving operation and control methods.

5. The combined RCP and GWHP system showed a good performance on energy saving and thermal comfort, but the simple payback period is 13.2 years. It is recommended to optimize the system and operating condition in the pre-design stage.

- ***Optimization of the panel curvature shape and arrangement***

A parametric analysis of the novel open-type RCP system was conducted using CFD simulation to study the effect of panel structure on cooling capacity and heat transfer in comparison with conventional RCPs presented in the literature. Four independent and two dependent design parameters were investigated by comparing thirty-five panel designs and operating sensitivity analysis.

1. The open-type RCP with curved shape and void in proposed this study achieves better cooling performance than the previous reference results. The nominal cooling capacity can be improved by 157.90% compared with the transitional panel design represented in the standard.

2. The nominal cooling capacity and heat transfer coefficient increase with increasing panel curvature radius and decreasing curvature width. The nominal cooling capacity is highest when L = 0.03 m and r = 0.06 m, which is the optimal panel design among the designs proposed in this study.

3. Compared with the large solid panel design, the short and distributed panel design with less panel surface area achieves better cooling performance because it can promote air movement around the panel and assist in sufficient heat exchange.

4. The distances between adjacent panels and between the panel and the wall play the most significant role in improving the cooling performance of the panel, demonstrating the potential to simultaneously reduce costs and achieve better indoor thermal conditions by optimizing the distribution of RCPs.

5. There should be a balance between improving cooling performance and ensuring the comfort of the indoor environment in practical operations, and total heat transfer should be accounted for based on the panel surface area and cooling capacity.

- ***Optimization of the integrated open-type RCP and WAV system***

The operating conditions of the integrated novel RCP and WAV system was optimized by using CFD simulation to improve the indoor thermal conditions and save more energy.

1. As a result of the sensitivity study, the inlet air temperature is the most sensitive parameter affecting the integrated system's cooling performance.

2. When inlet air velocity and inlet air temperature increase, the convective and radiant heat transfer of the CRCP system increase, the convective heat transfer of the WAV system decrease.

3. The optimized operating condition in Case 1-2 (v=0.164 m/s, T_{in}=25 °C, T_s=23 °C) allows the integrated system

to operate under higher inlet and panel surface temperature, which increased by 2.81 °C and 0.81 °C separately, and lower air velocity, which decreased by 0.11 m/s. Also, the PMV contours of this case shows this case can achieve acceptable thermal comfort.

- ***Optimization of the system operation of the integrated open-type RCP and GWHP system***

The system operation of the integrated novel RCP and GWHP system was optimized based on a simplified dynamic thermal resistance and thermal capacity (RC) model and multi-objective optimization.

1. The RC model is able to reproduce the observed trend at room temperature and predict the dynamic characteristics of the open-type RCP system.
2. After optimization, the indoor air temperature can remain within the required range. The issue of the temperature not reaching the target in the morning due to time delay has been resolved, and the overheating and overcooling have been eliminated.
3. The COP increases and electrical consumption decreases in all the cases after optimization. However, the impact of optimization is diminished as the insulation is reduced.
4. The investment of the general insulation case is higher than the light insulation case, but the life cycle cost is lower after 20 years of system operation.

6.2 Future studies

6.2.1 Unbalance temperature distribution

The panel surface temperature has been discussed in many studies as it highly related to indoor thermal comfort. Xie et al. proposed an index of temperature non-uniformity coefficient (TNC) σ_t to evaluate temperature profiles of ceiling panel surface as Eq. (6-1) [1].

$$\sigma_t = \frac{\sqrt{\frac{\sum_{i=1}^{N}(t_i - \bar{t})}{N}}}{\bar{t}} \qquad (6-1)$$

Where N is the temperature measurement position, t_i is the temperature value at each measurement position, $\bar{t}$ is the mean ceiling surface temperature.

The TNC was influenced by the panel structure, as indicated by Xie et al. [2], which exhibited a negatively correlated with temperature of chilled inlet water (linear correlation), water velocity, and pipe diameter, but positively correlated with tube spacing. Su et al. [3] recommended a thickness of 4.0 mm-5.0 mm for the cooling panels to achieve a uniform surface temperature distribution.

However, the non-uniform thermal load also significantly affects the surface temperature distribution which is less discussed. As shown in the measurement results in chapter 3, there was a discrepancy on panel surface temperature in office at 10:00 a.m. This temperature discrepancy exists in large-scale applications and is rare to be captured in small-scale laboratory tests. In future studies, more field measurements are required to assess the temperature balance when applying the RCP system in real-scale buildings. The topic of surface temperature distribution should be extended to the entire panel application area instead of just one panel.

6.2.2 Model predict control

In chapter 5, the system was optimized using a multi-objective optimization method. It is recommended to implement the advanced model predict control (MPC) algorithm for this system. Burak Gunay et al. [4] have proposed methodology of MPC to control the variable-air-volume (VAV) terminal unit and the hydronic ceiling radiant panel heater of a west-facing office space. It is expected that further improvements in system operation can be achieved by considering extreme climate conditions and variations in thermal load through this the implementation of the MPC method. However, the usability of MPC for the RCP system is still unknown due to the lack of research in this area.

Reference

[1] D. Xie, C. Wang, C.W. Yu, Y. Wang, H. Wang, Performance of capillary ceiling cooling panel on ceiling surface temperature and indoor thermal environment, Indoor Built Environ. 29 (2020) 881–894. https://doi.org/10.1177/1420326X20917740.

[2] D. Xie, Y. Wang, H. Wang, S. Mo, M. Liao, Numerical analysis of temperature non-uniformity and cooling capacity for capillary ceiling radiant cooling panel, Renew. Energy. 87 (2016) 1154–1161. https://doi.org/10.1016/j.renene.2015.08.029.

[3] X. Su, L. Zhang, Z. Liu, Y. Luo, J. Lian, Y. Luo, A computational model of an improved cooling radiant ceiling panel system for optimization and design, Build. Environ. 163 (2019) 106312. https://doi.org/10.1016/j.buildenv.2019.106312.

[4] H.B. Gunay, J. Bursill, B. Huchuk, W. O'Brien, I. Beausoleil-Morrison, Shortest-prediction-horizon model-based predictive control for individual offices, Build. Environ. 82 (2014) 408–419. https://doi.org/10.1016/j.buildenv.2014.09.011.

Publications

Peer-reviewed journals

1) ***Minzhi Ye***, A.A. Serageldin, K. Nagano, Numerical and Parametric Study on Open-Type Ceiling Radiant Cooling Panel with Curved and Segmented Structure, Energies 16(2023) 2705.
2) ***Minzhi Ye***, K. Nagano, A.A. Serageldin, H. Sato, Field studies on the energy consumption and thermal comfort of a nZEB using radiant ceiling panel and open-loop groundwater heat pump system in a cold region, Journal of Building Engineering 67(2023) 105999.
3) ***Minzhi Ye***, A.A. Serageldin, A. Radwan, H. Sato, K. Nagano, Thermal performance of ceiling radiant cooling panel with a segmented and concave surface: Laboratory analysis, Applied Thermal Engineering 196 (2021) 117280.
4) ***Minzhi Ye***, A.A. Serageldin, K. Nagano, Numerical optimization of a novel ceiling radiant cooling panel combined with wall attached ventilation system, Case Studies in Thermal Engineering 26 (2021) 101066.
5) A.A. Serageldin, ***Minzhi Ye***, A. Radwan, H. Sato, K. Nagano, Numerical investigation of the thermal performance of a radiant ceiling cooling panel with segmented concave surfaces, Journal of Building Engineering 42 (2021) 102450.

Conference proceedings papers

1) ***Minzhi Ye***, A.A. Serageldin, K. Nagano, Parametric analysis of the free-suspended ceiling radiant cooling panel using CFD simulation; 11th International Conference on Indoor Air Quality, Ventilation & Energy Conservation in Buildings (*IAQVEC 2023*), Tokyo Japan, 20-23 May 2023.
2) ***Minzhi Ye***, Ahmed A. Serageldin, Hideki Sato, Katsunori Nagano, Field study on indoor thermal comfort of a 'ZEB ready' office building using radiant ceiling panel coupled with open-loop ground source heat pump; 5th International conference on building energy and environment (*COBEE 2022*), Montreal Canada, 25-29 July 2022.
3) ***Minzhi Ye***, A.A. Serageldin, K. Nagano, CFD simulation on the thermal performance of a novel Radiant Ceiling Cooling Panel (RCCP) system with segmented and concave surface combined with forced ventilation; 7th International Conference on Power and Energy Systems Engineering (*CPESE 2020*), Fukuoka Japan, 26-29 September 2020.
4) ***Minzhi Ye***, K. Nagano; Development of a simplified RC network model for suspended cooling radiant ceiling panel, 令和 5 年度空気調和・衛生工学会大会（福井）, 2023 年 9 月.
5) ***Minzhi Ye***, K. Nagano, Hideki SATO; Analyzing Energy Consumption and Indoor Thermal Comfort of a 'ZEB Ready' Office Building with Suspended Radiant Ceiling Panel Heating System in Cold Region; 令和 4 年度空気調和・衛生工学会大会（神戸）, 2022 年 9 月.
6) ***叶敏之***, Serageldin Ahmed, 長野克則; CFD 解析に基づく寒冷地における放射パネルと温熱環境に関する考察; 令和元年度空気調和・衛生工学会大会（札幌）, 2019 年 9 月.

Awards

1) Best Presenter & Best Paper Award; 7th International Conference on Power and Energy Systems Engineering (*CPESE 2020*); 26-29 September 2020
2) 優秀発表奨励賞; 空気調和衛生工学会北海道支部 第 55 回学術講演会

Acknowledgements

I would like to express my gratitude to all those who helped me during the writing of this thesis.

First of all, I would like to express my sincere gratitude to my supervisor Prof. Katsunori Nagano, who leads this thesis direction, provides valuable suggestions and teaches me how to be a qualified researcher. His teachings have played a pivotal role in shaping the person I am today, and I am grateful for the numerous opportunities he has generously provided throughout my academic journey.

I would like to thank Prof. Taro MORI and Prof. Motoya HAYASHI for their service on my doctoral committee and precious comments for developing my research.

I would like to express my gratitude to the Japan Society for the Promotion of Science (JSPS) for providing a special research fellow position with fund. I would also like to thank Hokkaido University Ambitious Doctoral Fellowship (SDGs) and Hokkaido University Special Grant Program for Self-Supported International Students, which provided financial assistance during my studies.

My sincere thanks go to my tutor Dr. Ahmed A. Serageldin, who support everything throughout my research journey in the last five years. and help me grow. Words cannot fully capture my gratitude for his impactful mentorship. Being under his guidance has not only shaped my research but also transformed my character and outlook on life. This thesis is also a reflection of his invaluable contribution.

Additionally, I extend my sincere thanks to Prof. Fei Li in Nanjing Tech University, as well as Prof. Hongzhi Liu and Prof. Takao Katsura in Hokkaido University. Their support and guidance have been invaluable in both my personal and academic life.

Then, I would like to appreciate seniors and students in the Environmental System Research Laboratory, Dr. Fang He, Dr. Yutaka Shoji, Ms. Yiyang Wang, Ms. Jiayi Zhou, Ms. Lan Ding, and my friends Ms. Xi Lan in Hokkaido University.

I would like to appreciate Dr. Chao Lin. Thank you for your guidance and advice throughout my research. I also appreciate your companionship and support every day as I worked on this thesis. I have been healed since we met.

I would like to give a special shout out to my friends Ms. Kexin Tang, who encouraged me to persist my academic life when I felt confused about my future; Ms. Yuqin Xie, who pulled me out of the haze of junior high school life; Ms. Xin Xu, who has been my companion since we met in high school; and Ms. Mengqiu Xu, who not only helped my English studies as a teacher but also served as an exemplary figure.

Last but not least, I would like to express my heartfelt gratitude to my parents. I am incredibly proud to have the best parents in the world- those who have consistently shown patience, provided unwavering encourage and never give up on me.

I feel very grateful to have come to Japan, earned my Ph.D., and live a life I never imagined. I am fortunate to be living in a time when women can own property, be educated in universities, and work in the field of engineering. I appreciate all the people who have contributed to women's liberation. My wish is for every girl in this world to have the chance to pursue everything they are passionate about, to be encouraged to face difficulties in life, and to achieve their dream not as daughters, mothers, or wives but as individuals.

Finally, I would like to dedicate this thesis to my grandfather. The second year of my Ph.D. was a particularly challenging time, and it saddened me deeply to lose you during that period. I regret not being able to have our last meeting together.

2023.12

With All My Heart

Minzhi YE